IDAHO TRANSPORTATION DEPARTMENT

RESEARCH REPORT

Your Safety • Your Mobility
Your Economic Opportunity

RP 261

Development and Evaluation of Performance Measures to Augment Asphalt Mix Design in Idaho

By

Emad Kassem

Fouad Bayomy

SJ Jung

Hamza Alkuime

Fahmid Tousif

University of Idaho

Prepared for

Idaho Transportation Department

Research Program, Contracting Services

Highways Construction and Operations

August 2019

Standard Disclaimer

This document is disseminated under the sponsorship of the Idaho Transportation Department and the United States Department of Transportation in the interest of information exchange. The State of Idaho and the United States Government assume no liability of its contents or use thereof.

The contents of this report reflect the view of the authors, who are responsible for the facts and accuracy of the data presented herein. The contents do not necessarily reflect the official policies of the Idaho Transportation Department or the United States Department of Transportation.

The State of Idaho and the United States Government do not endorse products or manufacturers. Trademarks or manufacturers' names appear herein only because they are considered essential to the object of this document.

This report does not constitute a standard, specification, or regulation.

1. Report No. FHWA-ID-19-261	2. Government Accession No.	3. Recipient's Catalog No.
4. Title and Subtitle Development and Evaluation of Performance Measures to Augment Asphalt Mix Design in Idaho		5. Report Date August 2019 6. Performing Organization Code KLK581
7. Author(s) Emad Kassem, https://orcid.org/0000-0002-4331-6692 Fouad Bayomy, SJ Jung, Hamza Alkuime, and Fahmid Tousif		8. Performing Organization Report No.
9. Performing Organization Name and Address University of Idaho Department of Civil Engineering 875 Perimeter Drive MS 1022 Moscow, ID 83844-1022		10. Work Unit No. (TRAIS) 11. Contract or Grant No. UI-17-01
12. Sponsoring Agency Name and Address Idaho Transportation Department (SPR) Division of Highways, Resource Center, Research Program PO Box 7129 Boise, ID 83707-7129		13. Type of Report and Period Covered Final Report 01/01/2016 - 6/30/2018 14. Sponsoring Agency Code RP 261
15. Supplementary Notes Project performed in cooperation with the Idaho Transportation Department and the Federal Highway Administration.		

16. Abstract

The Superpave volumetric mix design should be complemented with performance criteria to evaluate the mix resistance to cracking, rutting and moisture damage. Rutting and cracking are observed in pavements that are designed using the Superpave method. With the use of new materials such as Reclaimed Asphalt Pavement (RAP) and Reclaimed Asphalt Shingles (RAS), asphalt mixes tend to get stiffer and crack prematurely if not properly designed. The main objective of this study was to develop performance thresholds to ensure adequate mix resistance to cracking and rutting in Idaho. Two rutting tests were selected and used in this study: Hamburg Wheel Tracking Test (HWTT) and Asphalt Pavement Analyzer (APA) rut test. The cracking tests included three monotonic tests (Indirect Tension (IDT) test [ASTM D6931], semi-circle bending flexibility index (SCB-FI) test [AASHTO TP 124], and semi-circle bending Jc (SCB-Jc) test [ASTM D8044]), in addition to a newly developed multi-stage semi-circle bending dynamic (MSSD) test that was presented by the research team of this study. A total number of 12 performance indicators calculated from the monotonic tests were evaluated. The Weibull-cracking resistance index ($Weibull_{CRI}$) index is a new performance indicator that was also proposed by the research team and it is calculated using the IDT test. In addition, two cracking resistance indicators were calculated from the MSSD test.

This study proposed performance thresholds to ensure adequate resistance to cracking, rutting, and moisture damage. Two cracking resistance indicators were recommended; $Weibull_{CRI}$ calculated from the IDT test and the slope (z) of the MSSD test. Good cracking resistance was associated with higher $Weibull_{CRI}$ ($Weibull_{CRI} > 4.7$) and small MSSD slope ($Z < 1.9$), while poor cracking resistance was associated with lower $Weibull_{CRI}$ ($Weibull_{CRI} < 3.57$) and higher MSSD slope ($Z > 2.9$). Thresholds for other performance indicators calculated from the monotonic tests were also proposed. In addition, this study proposed two rutting performance thresholds for the HWTT and APA rut test. A maximum rut depth of 10 mm for HWTT after 15,000 passes and 5 mm for APA rut test after 8,000 cycles are proposed to ensure good rutting resistance. The HWTT test is recommended over the APA since it can be used to evaluate both rutting and moisture damage resistance.

17. Key Words	18. Distribution Statement		
Performance measures, performance-based mix design, monotonic cracking assessment tests, SCB dynamic cracking assessments tests, rutting assessment tests, balanced mix design	Copies available from the ITD Research Program		
19. Security Classification (of this report) Unclassified	20. Security Classification (of this page) Unclassified	21. No. of Pages 218	22. Price None

FHWA Form F 1700.7

METRIC (SI*) CONVERSION FACTORS

APPROXIMATE CONVERSIONS TO SI UNITS

Symbol	When You Know	Multiply By	To Find	Symbol
		LENGTH		
in	inches	25.4	millimeters	mm
ft	Feet	0.3048	meters	m
yd	yards	0.914	meters	m
mi	miles (statute)	1.61	kilometers	km
		AREA		
in^2	square inches	645.2	millimeters squared	cm^2
ft^2	square feet	0.0929	meters squared	m^2
yd^2	square yards	0.836	meters squared	m^2
mi^2	square miles	2.59	kilometers squared	km^2
ac	Acres	0.4046	hectares	ha
		MASS (weight)		
oz	ounces (avdp)	28.35	grams	g
lb	pounds (avdp)	0.454	kilograms	kg
T	short tons (2000 lb)	0.907	megagrams	mg
		VOLUME		
fl oz	fluid ounces (US)	29.57	milliliters	mL
gal	Gallons (liq)	3.785	liters	liters
ft^3	cubic feet	0.0283	meters cubed	m^3
yd^3	cubic yards	0.765	meters cubed	m^3

Note: Volumes greater than 1000 L shall be shown in m^3

		TEMPERATURE (exact)		
°F	Fahrenheit temperature	5/9 (°F-32)	Celsius temperature	°C
		ILLUMINATION		
fc	foot-candles	10.76	lux	lx
fl	foot-lamberts	3.426	candela/m^2	cd/cm^2
		FORCE and PRESSURE or STRESS		
lbf	pound-force	4.45	newtons	N
psi	pound-force per square inch	6.89	kilopascals	kPa

APPROXIMATE CONVERSIONS FROM SI UNITS

Symbol	When You Know	Multiply By	To Find	Symbol
		LENGTH		
mm	millimeters	0.039	inches	in
m	meters	3.28	feet	ft
m	meters	1.09	yards	yd
km	kilometers	0.621	Miles (statute)	mi
		AREA		
mm^2	millimeters squared	0.0016	square inches	in^2
m^2	meters squared	10.764	square feet	ft^2
km^2	kilometers squared	0.39	square miles	mi^2
ha	hectares (10,000 m^2)	2.471	acres	ac
		MASS (weight)		
g	grams	0.0353	ounces (avdp)	oz
kg	kilograms	2.205	pounds (avdp)	lb
mg	megagrams (1000 kg)	1.103	short tons	T
		VOLUME		
mL	milliliters	0.034	fluid ounces (US)	fl oz
liters	liters	0.264	Gallons (liq)	gal
m^3	meters cubed	35.315	cubic feet	ft^3
m^3	meters cubed	1.308	cubic yards	yd^3

		TEMPERATURE (exact)		
°C	Celsius temperature	9/5 °C+32	Fahrenheit temperature	°F
		ILLUMINATION		
lx	lux	0.0929	foot-candles	fc
cd/cm^2	candela/m^2	0.2919	foot-lamberts	fl
		FORCE and PRESSURE or STRESS		
N	newtons	0.225	pound-force	lbf
kPa	kilopascals	0.145	pound-force per square inch	psi

Acknowledgments

This project is funded by Idaho Transportation Department (ITD) from SPR funds. It is performed in cooperation with ITD. The authors would like to acknowledge all members of the research project Technical Advisory Committee (TAC) for their valuable feedback and cooperation all over the project tasks. The authors would like also to acknowledge support from the National Institute for Advanced Transportation Technology (NIATT) and the Department of Civil and Environmental Engineering at the University of Idaho.

Technical Advisory Committee

Each research project is overseen by a technical advisory committee (TAC), which is led by an ITD project sponsor and project manager. The Technical Advisory Committee (TAC) is responsible for monitoring project progress, reviewing deliverables, ensuring that study objectives are met, and facilitating implementation of research recommendations, as appropriate. ITD's Research Program Manager appreciates the work of the following TAC members in guiding this research study.

Project Sponsor – John Bilderback, P.E.

Project Manager – Mike Santi, P.E.

TAC Members:

Mark Wheeler, P.E.
Chad Clawson, P.E.,
Ron Wright
Bob Engelmann

FHWA-Idaho Advisor – Kyle Holman, P.E.

Table of Contents

List of Tables

List of Figures

List of Acronyms

ALDOT	Alabama Department of Transportation
CODOT	Colorado Department of Transportation
CRI (IDT)	Cracking Resistance Index calculated from the IDT test
CRI (SCB-FI)	Cracking Resistance Index calculated from the SCB test
FHWA	Federal highway administration
FI (IDT)	Flexibility Index calculated from the IDT test
FI (SCB-FI)	Flexibility Index calculated from the SCB test
GDOT	Georgia Department of Transportation
$G_{fracture}$ (IDT)	Fracture energy calculated from the IDT test
$G_{fracture}$ [SCB]	Fracture energy calculated from the SCB test
HWTT	Hamburg Wheel-Tracking Device
IDEAL-CT_{Index}	Indirect tensile asphalt cracking test
IDOT	Illinois department of transportation
IDT	Indirect Tension Test
IDT test	Indirect Tension Test
$IDT_{Modulus}$	Ration of $IDT_{strength}$ to displacement at peak load calculated from the IDT test
$IDT_{strength}$	Indirect Tension strength calculated from the IDT test
J_c	Strain energy release rate
LADOT	Louisiana Department of Transportation
LVDTs	Linear variable displacement transducers
MNDOT	Minnesota Department of Transportation
MSSD test	Multi-Stage Semi circle bending Dynamic test
MTDOT	Montana Department of Transportation
NCHRP	National Cooperative Highway Research Program
Nflex factor	Nflex factor calculated from the IDT test
NJDOT	New Jersey Department of Transportation
SCB test	Semi-Circle Bending
TXDOT	Texas Department of Transportation
VDOT	Virginia Department of Transportation
$Weibull_{CRI}$	Weibull Cracking Resistance Index
WSDOT	Washington State Department of Transportation

Executive Summary

The Superpave volumetric mix design should be complemented with performance criteria to evaluate mix resistance to cracking, rutting and moisture damage. Asphalt pavements experience a wide range of temperatures that lead to various distresses. Rutting and cracking have been observed in pavements that were designed using the Superpave method. With the use of Reclaimed Asphalt Pavement (RAP) and Reclaimed Asphalt Shingles (RAS), asphalt mixes tend to get stiffer and crack prematurely if not properly designed. The main objective of this study was to develop performance thresholds for major pavement distresses in Idaho. These thresholds can be used to augment the current Superpave mix design by setting threshold values for performance acceptance. In addition, these values can be used for performance-based design or Balanced Mix Design (BMD) in Idaho. Cracking and rutting were found to be the major distresses in Idaho. This study examined the cracking and rutting performance of various asphalt mix specimens including field cores, Plant Mixed-Laboratory Compacted (PMLC) mixes, and Laboratory Mixed-Laboratory Compacted (LMLC) mixes.

Based on the findings of the literature review, two rutting assessment tests were selected and used in this study; Hamburg wheel-tracking test (HWTT) and Asphalt Pavement Analyzer (APA) rut test. Three rutting resistance performance indicators ($HWTT_{15000}$, $HWTT_{20000}$, and APA_{8000}) were assessed. The cracking tests included monotonic tests (Indirect Tension [IDT] test [ASTM D6931], semi-circle bending flexibility index [SCB-FI] test [AASHTO TP 124], and semi-circle bending Jc [SCB-Jc] test [ASTM D8044]), in addition to a newly developed test called Multi-Stage Semi-circle bending Dynamic (MSSD) test that was developed by the research team in this study. A total number of 12 cracking assessment performance indicators ($G_{fracture}$ [IDT], $G_{fracture}$ [SCB-FI] , CRI [IDT] , CRI [SCB-FI] , FI [IDT] , FI [SCB-FI] , IDEAL-CT_{Index}, Nflex factor, $IDT_{Strength}$, $IDT_{Modulus}$, J_c , and $Weibull_{CRI}$) calculated from the monotonic tests were evaluated. The Weibull Cracking Resistance Index ($Weibull_{CRI}$) index is a new performance indicator that was developed by the research team and it is calculated using the IDT test. In addition, two cracking resistance indicators were calculated from the MSSD test.

Based on the results of field performance and laboratory testing, this study proposed performance thresholds to ensure adequate resistance to cracking, rutting, and moisture damage. Two cracking resistance indicators were recommended; $Weibull_{CRI}$ calculated from the IDT test and the slope (*z*) of the MSSD test. Good cracking resistance was associated with higher $Weibull_{CRI}$ ($Weibull_{CRI} > 4.7$) and small MSSD slope ($z < 1.9$), while poor cracking resistance was associated with lower $Weibull_{CRI}$ ($Weibull_{CRI} < 3.57$) and higher MSSD slope ($z > 2.9$). Thresholds for other performance indicators calculated from the monotonic tests were also proposed. In addition, this study proposed two rutting performance thresholds for the HWTT and APA. A maximum rut depth of 10 mm for HWTT after 15,000 passes at 50 °C and 5 mm after 8,000 cycles for APA are proposed to ensure good rutting resistance. The HWTT test is recommended over the APA rut test since it can be used to evaluate both rutting and moisture damage resistance.

Chapter 1
Introduction

Overview

The Superpave design system was developed under the Strategic Highway Research Program (SHRP) program in the late 1990s. It aimed to produce economical asphalt mixes that have adequate asphalt content, air void content, voids in the mineral aggregate, workability, and acceptable field performance [1]. Three design levels (i.e., Level 1, Level 2, and Level 3) were proposed for the Superpave mix design. Level 1 is widely used and includes material performance specifications where mixes are designed to satisfy the volumetric requirements (e.g., AV, VMA, VFA, etc.) without evaluation of mix performance. Levels 2 and 3 include performance specifications where mixes are evaluated for rutting, fatigue cracking, and thermal cracking using laboratory tests [1]. Meanwhile, the Superpave implementation was limited to Level 1 since it requires less time and efforts.

Pavement distresses (e.g., rutting and cracking) are observed in pavements designed using the Superpave procedure. The resistance of asphalt mixes to rutting, cracking, and moisture damage is evaluated, and performance specifications are used to augment the Superpave mix design. Several transportation agencies have developed and adopted various performance-related specifications to ensure good performance in the field. These performance-related specifications may vary from state to another depending on several factors including mix design, climatic conditions, local materials used in the mix, traffic levels, etc. Various performance indicators and criteria are proposed in the literature, and thus selecting the proper indicators and criteria for Idaho should be based on a comprehensive evaluation. This study aims to assist the Idaho Transportation Department (ITD) to evaluate, develop, and adopt well-validated performance indicators and thresholds to avoid premature distresses in asphalt pavements. Also, these performance measures can allow the department to control the amount of RAP in asphalt mixtures.

Problem Statement

The Superpave volumetric mix design should be complemented with performance criteria to evaluate mix resistance to cracking, rutting and moisture damage. Asphalt pavements experience a wide range of temperatures that lead to various distresses. Rutting and cracking are observed in pavements in Idaho that are designed using the Superpave procedure. With the use of Reclaimed Asphalt Pavement (RAP) and Reclaimed Asphalt Shingles (RAS), asphalt mixes tend to get stiffer and crack prematurely if not properly designed. A previous research in Idaho (RP 213) recommended adoption of a cracking resistance criterion for mixes with RAP materials. Several state departments of transportation have already developed and implemented performance measures to evaluate the resistance of asphalt mixes to rutting, cracking, and moisture damage. Therefore, there is a need to develop and evaluate performance measures for asphalt mixes in Idaho. The proposed performance measures shall augment the current Superpave mix design method by setting threshold values for performance acceptance.

Research Objectives

The objectives of this study were to:

1. Identify performance tests and indicators used by various transportation agencies to evaluate the resistance of asphalt mixes to cracking and rutting.
2. Examine and evaluate various tests to assess the resistance of asphalt mixes to cracking and rutting and correlate the results to field performance.
3. Select the most promising performance indicators and propose new ones that are found to correlate with field performance.
4. Develop performance thresholds that can be used to evaluate the resistance of asphalt mixes to cracking and rutting.

Project Tasks

The objectives of this study were achieved by conducting the following tasks:

Task 1: Literature review

Under this task, the research team conducted a literature review to document the current tests and performance indicators used by various transportation agencies to evaluate cracking and rutting of asphalt mixes. In addition, the team reviewed the specification thresholds set by different states for these tests. The outcome of the literature review was used to identify the most promising laboratory tests that were conducted in this study to assess the performance of asphalt mixes. Many factors were considered when selecting the performance tests including their applicability to simulate field performance, simplicity of the test, applicability to Idaho conditions, availability of the equipment at ITD laboratories, and being cost- and time-effective.

Task 2: Identify and select pavement sites for evaluation

The objective of Task 2 was to select candidate pavement sites with known field performance and obtain field cores from these sites. These sites were selected with the help from ITD Material Engineers who completed a survey to identify test sites with different characteristics for evaluation. These sections selected to have different field performance with regard to cracking and rutting and they were distributed across the state of Idaho. These projects used asphalt mixes with different properties (i.e., mix design, binder content, binder grade, RAP, aggregate type, etc.).

Task 3: Conduct field performance evaluation and collect cores and virgin materials

Under this task, the research team with the help from ITD obtained field cores and collected loose materials from 10 new paving projects across the state. Field cores were extracted between the wheel path, shoulder, or turning lanes depending on the conditions of each project. The team

obtained the historical information about the performance of the selected projects and relevant mix design data (e.g., job mix design data sheet). In addition, loose asphalt materials from several new paving projects were collected. Similarly, the mix design for loose asphalt materials was obtained. Furthermore, the team collected virgin materials (asphalt and aggregates) and prepared asphalt mixture samples to evaluate the sensitivity of various performance tests and indicators to mix properties (e.g., binder type and performance grade).

Task 4: Conduct laboratory performance tests

The research team conducted several laboratory tests to evaluate the resistance of asphalt mixes to cracking and rutting. The cracking tests include monotonic cracking tests (e.g., Indirect Tension Test [IDT] [ASTM D6931], Semi-Circle Bending Flexibility Index test [SCB-FI] [AASHTO TP 124], Semi-Circle Bending Jc [SCB-Jc] test [TR 330]), in addition to Multi-Stage Semi-circle bending Dynamic test (MSSD) that was developed by the research team. Various cracking resistance performance indicators were calculated and evaluated from the cracking tests. These indicators include the Weibull-cracking resistance index ($Weibull_{CRI}$) that was also developed and proposed by the research team. The rutting tests included Hamburg Wheel Tracking Test (HWTT) and Asphalt Pavement Analyzer (APA). In addition, the HWTT test was also used to assess the moisture susceptibility of the test materials.

Task 5: Comprehensive evaluation of laboratory and field performance data

The results of the laboratory testing program conducted under Task 4 were analyzed and compared to observed field performance. Statistical analysis was used to analyze the variation of the results of the various tests and performance indicators. The research team evaluated the applicability of various performance tests to assess the resistance of the asphalt mixes to rutting and cracking. The evaluation of various test methods considered the simplicity of the test, availability of equipment, need for skilled staff, required time, and cost of the test. Based on the laboratory test results and field performance evaluation, the most promising and applicable performance assessment tests and indicators were selected and recommended.

Task 6: Develop performance-related test specifications

Based on the findings of Task 5, the research team developed specifications for selected performance indicators to ensure adequate resistance to cracking, rutting, and moisture damage. The proposed thresholds were compared to those adopted and used by other transportation agencies. These proposed performance specifications are recommended to augment the mix design in Idaho.

Report Organization

This report consists of the following seven chapters and five appendices.

Chapter 1 provides an introduction to this research project and presents the problem statement,

research objectives, research tasks, and report organization.

Chapter 2 presents a literature review of available laboratory tests used to evaluate the performance of asphalt mixes and the current performance measures developed by various transportation agencies.

Chapter 3 provides information about asphalt mixes and field projects evaluated in this study. It also discusses the current ITD specifications for hot-mix asphalt (HMA) mixes. In addition, this chapter documents the methods used by the researchers to evaluate the performance of test materials to cracking, rutting, and moisture damage.

Chapter 4 presents further information about the selected testing protocols and various performance indicators and their mathematical calculations. In addition, Chapter 4 discusses the development of the MSSD test and the $Weibull_{CRI}$ indictor used to assess the resistance of asphalt mixes to cracking.

Chapter 5 documents and presents the results for various tests used to evaluate the cracking resistance of the test materials. The tests include dynamic as well as monotonic testing. Various performance indicators were calculated, and the results were compared to field performance. The variability of the test results of different performance indicators was also studied. In addition, Chapter 5 presents the proposed performance thresholds to ensure adequate resistance to cracking.

Chapter 6 presents the results of the rutting and moisture damage tests as well the proposed thresholds to ensure adequate resistance to rutting and moisture damage.

Chapter 7 summarizes the main findings of this study and provides implementation plan for ITD to consider as well as recommendations for future studies.

Appendices provide additional information and figures that were cited and discussed in the report.

Chapter 2
Literature Review

Introduction

Various performance tests are used to evaluate the resistance of asphalt mixes to cracking and rutting, and transportation agencies develop their own performance specifications for each test and indicator. This chapter presents a literature review of available laboratory tests used to evaluate the performance of asphalt mixes and the current performance measures developed by various transportation agencies.

Rutting Tests and Previous Studies

Rutting is defined as a longitudinal surface depression in the wheel path [2]. Several causes can lead to rutting in asphalt pavements including insufficient compaction, excess binder content, improper selection of binder grade, inadequate thickness, and consolidation of base and subgrade due to repeated traffic loading. Researchers have developed standard laboratory test methods to evaluate the resistance of asphalt mixes to rutting. These tests include dynamic modulus, flow number, flow time, in addition to Hamburg Wheel Tracking Test (HWTT) and Asphalt Pavement Analyzer (APA). These tests are described in the sections that follow.

Asphalt Mixture Performance Tester (AMPT)

The AMPT is used to conduct the dynamic modulus, flow number, and flow time tests. These tests are used to evaluate the rutting resistance of asphalt mixes.

Dynamic Modulus (DM) Test

This test is conducted in accordance with AASHTO T 342 *Standard Method of Test for Determining the Dynamic Modulus of Hot-Mix Asphalt Concrete Mixes*. The dynamic modulus (DM) is the ratio between the applied stress amplitude and resulting strain amplitude. The lag between the peak stress and resulting peak strain is referred to as the phase angle. This test is conducted at five different temperatures (−10 °C, 4.4 °C, 21.1 °C, 37.8 °C, and 54.4 °C) and six loading frequencies (0.1 Hz, 0.5 Hz, 1.0 Hz, 5 Hz, 10 Hz, and 25 Hz) at each temperature. Three axial linear variable differential transformers (LVDTs) are used to measure the axial deformation during the test, as shown in Figure 1. A sinusoidal loading is applied and adjusted to obtain axial strain between 50 and 150 micro strain. Upon completion of testing, the DM master curve is constructed to describe the performance of the mix at different frequencies and temperatures. Calibrated rutting models are used to develop pass/fail criteria based on thickness of the HMA layer, design traffic level and speed, and environmental conditions. Figure 2 presents a schematic of using the DM as a mix design tool. The mixes should attain a minimum allowable DM to ensure good rutting performance. Currently, the DM is considered as one of primary inputs in AASHTO mechanistic empirical (ME) design Level 1 [3–5].

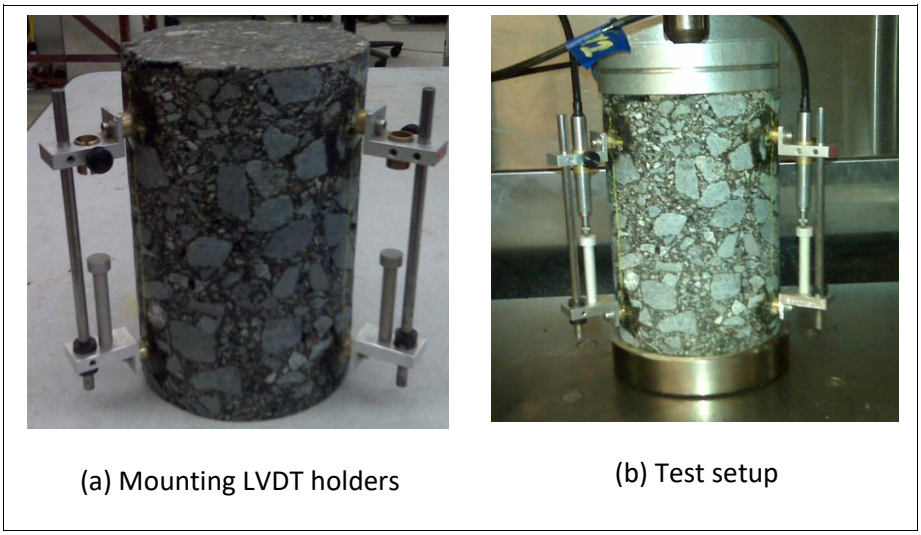

(a) Mounting LVDT holders

(b) Test setup

Figure 1 Dynamic Modulus Test Setup [6]

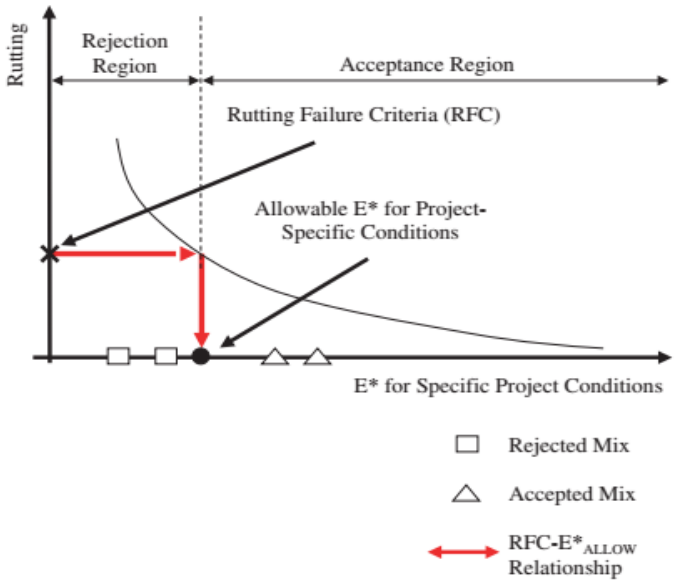

Figure 2 Using E* as Asphalt Mixture Design Tool (Pass/Fail Threshold) [3]

Flow Number Test (FN)

This test is conducted in accordance with the AASHTO T 378 *Standard Method of Test for Determining the Dynamic Modulus and Flow Number for Asphalt Mixes using the Asphalt Mixture Performance Tester (AMPT)*. In this test, a repeated haversine load is applied to a test specimen. The load consists of 0.1 second loading pulse followed by 0.9 second rest period. The cumulative permanent strain is calculated

and plotted against the loading cycles as shown in Figure 3. Three different regions or zones can be identified based on the change in the rate of cumulative permanent strain: primary, secondary, and tertiary. The rate of the cumulative permanent strain decreases in the primary zone, while it is constant in the secondary zone. The tertiary zone starts when the rate of cumulative permanent strain increases. The flow number is defined as the number of loading cycles when the tertiary flow starts [5].

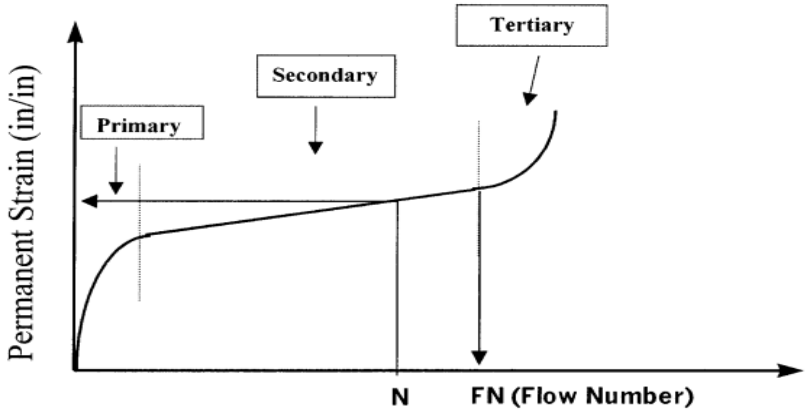

Figure 3 Number of Loading Cycles versus the Accumulated Permanent Strain [5]

Flow Time Test (FT)

In this test, an axial static load is applied. The total compliance (D[t]) is calculated as the ratio of the measured strain to the applied stress. The total compliance (D[t]) is plotted against time as shown in Figure 4. Similar to the Flow Number test, three zones are identified based on the strain rate; primary, secondary, and tertiary (Figure 4). The flow time is defined when the tertiary region starts. Figure 4 presents the recommended minimum values for the flow time and flow number tests by NCHRP Project 9-33 [5].

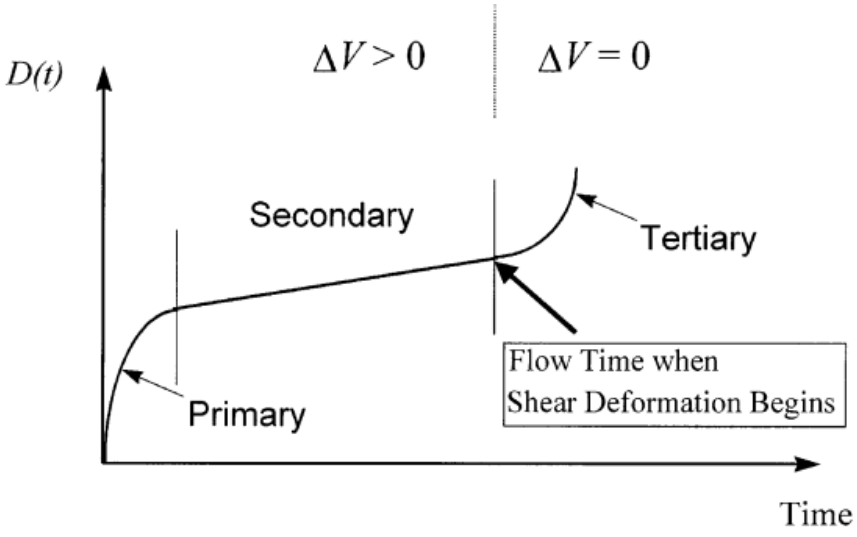

Figure 4 Flow Time Test Output [7]

Table 1 Flow Number Pass/Fail Criteria [4]

Traffic Level (Million ESALs)	Flow Number (FN) (# Load Cycles)	Flow Time (FT)
ESALs < 3	0	0
3 < ESALs < 10	200	5
10 < ESALs < 30	320	4
ESALs >30	580	3

Hamburg Wheel-Tracking Test

The Hamburg Wheel-Tracking Test (HWTT) was developed in Hamburg, Germany and is used to evaluate rutting resistance and moisture susceptibility of asphalt mixes. Figure 5 shows a Hamburg test setup. Steel wheel rollers (17 mm wide and 158 lb force) are operated backward and forward over cylindrical asphalt mixture specimens. Specimens can be tested in dry conditions or submerged in water bath at a controlled temperature. The rut depth is measured along the roller path during the test, and generally, the test is performed for 20,000 passes. The HWTT has many advantages that make it a popular test. The variation in the rut depth results is very small between two replicates [8]. In addition, researchers found this test to closely simulate the field conditions [9].

Many state department of transportations (DOTs) in the United States have adopted the Hamburg Wheel-Track Test in accordance with AASHTO T324. Table 2 presents the developed rutting performance thresholds by several state DOTs including Texas Department of Transportation (TxDOT), Washington State Department of Transportation (WSDOT), Colorado Department of Transportation (CODOT), Louisiana Department of Transportation (LADOT), and Montana Department of Transportation (MTDOT).

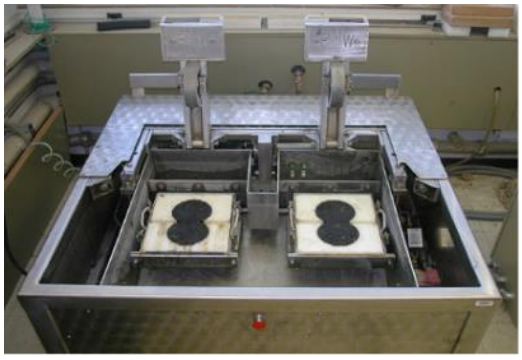

Figure 5 Hamburg Wheel Tracking Test Setup [10]

Table 2 HWTT Rutting Performance Threshold [11–17]

DOT	Test Procedure	Rutting limits for various PG grading or mixture type
TXDOT	Tex-242-F	<=PG 64; 10,000 passes @12.5mm rut depth tested at 50 °C
TXDOT	Tex-242-F	PG 70; 15,000 passes @12.5mm rut depth tested at 50 °C
TXDOT	Tex-242-F	=>PG 76; 20,000 passes @12.5mm rut depth tested at 50 °C
WSDOT	AASHTO T 324	15,000 passes @10 mm rut depth tested at 50 °C
CODOT	CP-L 5112	10,000 passes @ 4 mm rut depth tested at 50 °C
MTDOT	MT 334-14	Minimum of 10,000 passes @13 mm rut depth for mix design (for PG 58-28,64-22,64-28 and 70-28)
MTDOT	MT 334-14	Minimum of 10,000 passes @13 mm rut depth for mix design (for PG 58-28,64-22,64-28 and 70-28)
LADOT	AASHTO T 324	Incidental Paving and ATB; Design Level 1; Max rut depth at 50 °C: 10 mm @ 10,000 passes
LADOT	AASHTO T 324	Wearing and Binder Course; Design Level 1; Max rut depth at 50 °C: 10 mm @ 20,000 passes
LADOT	AASHTO T 324	Wearing and Binder Course; Design Level 2; Max rut depth at 50 °C: 6 mm @ 20,000 passes

Asphalt Pavement Analyzer (APA)

The Asphalt Pavement Analyzer (APA) is an updated version of the Georgia Loaded Wheel Tester (GLWT) that was developed by the Georgia Department of Transportation (GDOT). It is an accelerated laboratory loading equipment that simulates traffic using loaded steel wheels as shown CV 6. The APA machine can be used to perform HWTT, APA rut test, and moisture damage tests. The wheels travel along cylindrical or beam of asphalt mixes specimens. The rutting test is performed in accordance with AASHTO T340 [18]. Six to four specimens of 150 mm in diameter and 77 mm in height are used in this rutting test. Stainless steel concave wheels are used to apply the load using pressurized rubber hoses as shown Figure 6. The test specimens are then preheated before testing at a minimum of 6 hours at a temperature equivalent to the high-performance grade (PG) of the binder. The rut depth is recorded after each cycle and the average rut depth is reported after 8,000 cycles. The APA rut test was found to correlate and simulate the field performance [19,20]. Several states developed rutting performance thresholds for the APA rut test as listed in Table 3.

Figure 6 APA Rut Test Setup

Cracking Tests and Previous Studies

Fatigue cracking occurs commonly in the wheel path because it is subjected to repeated traffic loading and starts as a series of interconnected cracks before it develops in many-sided, sharp-angled pieces [2]. Several causes may lead to fatigue cracking including inadequate structural support, inadequate structural design, overloading, poor construction, and poor drainage.

Fatigue cracking is often classified into three levels of severity: high, moderate, and low. The cracks that are mainly perpendicular to the pavement centerline are referred to as thermal or transverse cracks. These cracks are often caused by shrinkage of asphalt layer due to daily temperature cycling, binder

hardening, and/or reflective cracking from underlying layers. The thermal cracks are also classified into three levels: low, moderate, and high based on the depth of the cracks. There are several testing methods and protocols that have been proposed to assess cracking resistance of asphalt mixes. The most common tests are discussed in this section.

Table 3 APA Rutting Test Pass/Fail Criteria [21–27]

DOT	Test procedure	Performance threshold (maximum rut depth @ 8,000 loading cycles)
ITD	AASHTO T340	5.0 mm
GDOT	GDT 115	7.0 mm for mix design level A
GDOT	GDT 115	6.0 mm for mix design level B
GDOT	GDT 115	5.0 mm for mix design level C and D
ALDOT	ALDOT -401	4.5 mm For ESAL range "E" mixes ($1E10^7$ < ESALs < $3E10^7$)
NJDOT	AASHTO T340	7.0 mm for high RAP, PG 64-22, surface and intermediate course,
NJDOT	AASHTO T340	6.0 mm for binder-rich intermediate course
NJDOT	AASHTO T340	5.0 mm for bottom-rich base course
NJDOT	AASHTO T340	4.0 mm for high RAP, PG 76-22, surface and intermediate course,
NJDOT	AASHTO T340	3.0 mm for bridge deck waterproofing surface course
VDOT	VTM-110	7.0 mm for mix designation A
VDOT	VTM-110	5.5 mm for mix designation D
VDOT	VTM-110	3.5 mm for mix designation E

Semicircular Bending (SCB) Test

The semi-circular bending (SCB) test was initially used to test rock specimens. Recently, however, it has been used to study the fracture behavior of asphalt mixes where an SCB test specimen is loaded in compression to measure the fracture properties [28]. Figure 7 shows the SCB test specimen that is loaded at three points. The load and displacement are then measured during the test. The SCB test is often performed at three different notch depths (i.e., 25.4 mm, 31.8 mm and 38 mm). The fracture parameter (J-integral, J_c) developed by Rice (1968)[29], is used to analyze the load-deflection relationship. The J_c represents the slope of strain energy per unit depth versus notch depth. The J_c is calculated using Figure 8. Several researchers have adopted and used the SCB test to study the fracture resistance of asphalt mixture [30–32]. Some transportation agencies have adopted the SCB-J_c test to evaluate the cracking resistance of asphalt mixes. The Louisiana Department of Transportation and Development (LaDOTD) specified minimum values for the J_c of 0.5 kJ/m^2 and 0.6 kJ/m^2 for level 1 and level 2 mix design, respectively [15]. The test is performed in accordance with standard test method TR – 330-14 [33]. A previous ITD research study (RP 181) investigated the SCB-J_C to evaluate the performance of Superpave mix design in Idaho [34].

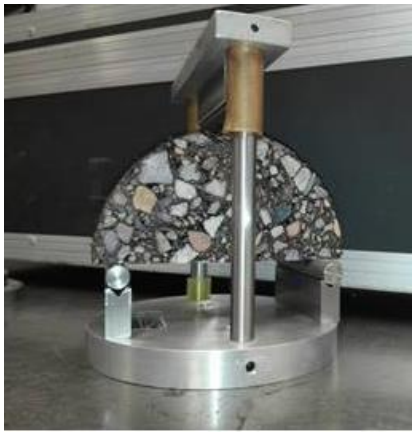

Figure 7 SCB Specimen and Testing Fixture

$$J_c = -\left(\frac{1}{t}\right)\frac{dU}{da}$$

Figure 8 J_c Calculation Equation

where:

J_c = Strain energy release rate (kJ/m^2)

U = Strain energy to failure (kJ)

t = Specimen thickness (mm)

a = Specimen notch depth (mm)

dU/da = Variation of strain energy with notch depth (kJ/mm)

The Illinois Department of Transportation (IDOT) proposed and developed a performance indicator called Illinois flexibility index (FI) to evaluate the resistance of asphalt mixes to cracking [35]. In the Flexibility Index (FI) test, a SCB specimen is tested at only one notch depth. The Flexibility Index (FI) is conducted in accordance with AASHTO TP 124-16 [36]. The FI is calculated using the equation presented in Figure 9. Higher values of FI indicate better cracking resistance. The IDOT is in the process of developing pass/fail criteria [37].

$$\mathrm{FI} = 0.01 * \frac{G_{Fracture}^{Total}}{\left|m_{\mathrm{Inflection}}^{Post-peak}\right|}$$

Figure 9 Flexibility Index Calculation Formula

where:

FI = Flexibility Index

$G_{Fracture}^{Total}$ = Total fracture energy (J/m^2)

$m_{\text{Inflection}}^{Post-peak}$ = Post-peak inflection point

Comparison Between Laboratory and Field Performance

Kim et al. (2012) investigated the fracture resistance of various asphalt mixes using the SCB and IDT test methods [38]. The study included five laboratory asphalt mixes and more than 20 field projects. The researchers measured J_c values, IDT-strength, and IDT-toughness index for Laboratory Mixed-Laboratory Compacted (LMLC) and Plant Mixed-Laboratory Compacted (PMLC) mixes. The researchers found a good correlation between J_c values and field cracking rate for LMLC mixes as shown in Figure 10. In addition, the J_c values had a good correlation with the toughness index.

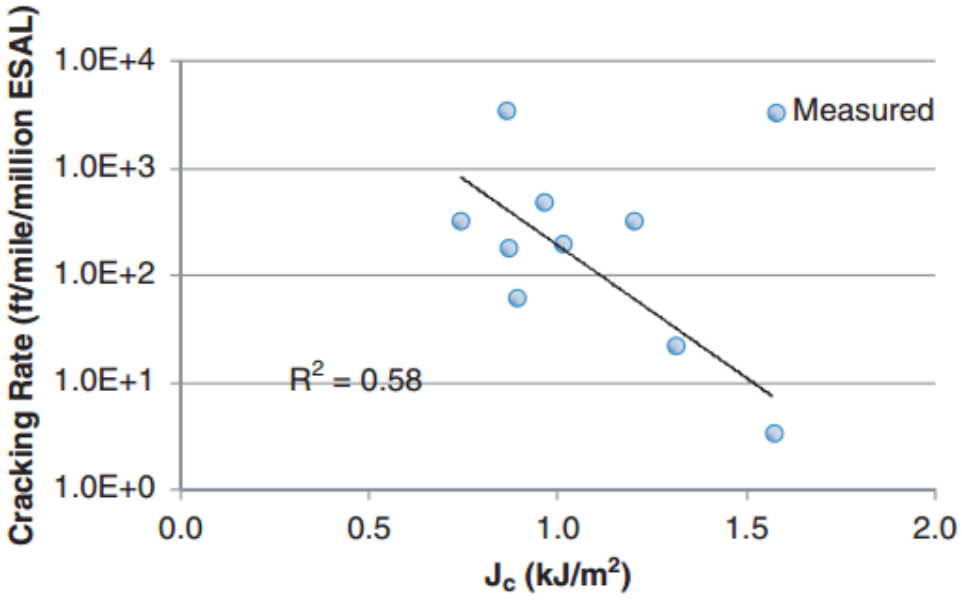

Figure 10 Relationship between Field Cracking Resistance and SCB Jc Values [38]

Mohammad et al. (2012) evaluated the correlation between J_c and field fatigue performance for asphalt mixes [39]. The study included nine field projects distributed across Louisiana. The J_c values were computed for PMLC and LMLC mixes at the time of construction. The J_c values were between 0.74 k/m^2 and 1.57 kJ/m^2. Field cracking resistance were monitored using an Automated Road Analyzer (ARAN) system. The study reported a good correlation between J_c values and field cracking performance. The researchers developed a regression model between J_c and field cracking rate. The authors concluded that the J_c showed a good correlation with the field cracking performance.

Nsengiyumva (2015) examined the effect of several test conditions on SCB test results, including

specimen thickness, notch length, loading rate, and test temperature [40]. Four different thicknesses (30 mm, 40 mm, 50 mm, and 60 mm), five different notch lengths (0 mm, 5 mm, 15 mm, 25 mm, and 40 mm), five different loading rates (0.1 mm/min, 0.5 mm/min, 1.0 mm/min, 5 mm/min and 10 mm/min), and three test temperatures (15 °C, 21 °C, and 40 °C) were evaluated in this study. The researchers measured the fracture energy (G_f) of the test samples at these various test conditions and recommended a thickness range of 40 mm to 60 mm and a notch length of 15 mm for good test repeatability. The loading rate was not found to affect the variation of test results. In addition, a test temperature of 21 °C was recommended.

Al-Qadi et al. (2015) proposed a new cracking testing protocol (SCB-Illinois) and cracking assessment indicator (Flexibility Index [FI]) [35]. In the SCB-Illinois test, a test specimen with one notch depth (15 mm) is loaded at a constant displacement rate of 50 mm/min at 20 °C. Al-Qadi et al. (2015) demonstrated that using G_f as standalone performance indicator is not sufficient, thus they introduced FI to overcome the limitations of G_f. The FI parameter is a normalization of fracture energy (G_f) with respect to the post-peak slope (Figure 9). Higher FI indicates better cracking resistance. The new testing protocol and performance indicator were validated using 11 LMLC, 15 PMLC, and numerous field projects. The authors proposed performance thresholds based on FI indicator. The performance of asphalt mixes in terms of crack resistance was categorized into three categories 1) poor performance, 2) intermediate performance, and 3) best performance. Asphalt mixes with poor cracking resistance had an FI of less than 2, while mixes with intermediate resistance to cracking had FI between 2 and 6.5. Asphalt mixes with good resistance to cracking had FI higher than 6.5.

Ozer et al. (2016) evaluated 11 LMLC mixes with different RAP and RAS contents [41]. The researchers examined the cracking resistance in the field and correlated the results to FI measured in the laboratory. Based on the results of this study, the researchers proposed threshold values for FI for different mixture classifications as presented in Table 4. The authors recommended to adjust the proposed thresholds to account for PMLC mixes and local conditions [41].

Table 4 Proposed Flexibility Index (FI) Performance Threshold [41]

Mixture Classification	Acceptance	Flexibility Index (FI)	Rut depth
Stiff and Flexible	Acceptable and High Performance (I)	FI > 10	<7.5 mm
Stiff and Flexible	Acceptable (II)	FI > 6	<12.5 mm
Soft and Flexible	Crack Retardant Interlayer Type of Mixes	FI > 10	NA
Stiff and Brittle	Reject	FI < 6	<12.5 mm
Soft and Unstable	Reject	FI > 6	>12.5 mm

Cooper III et al. (2016) evaluated a simplified SCB test as an end result parameter for testing asphalt

concrete mixes [42]. The researchers evaluated 40 mixes from the Louisiana Transportation Research Center (LTRC) database and various mixes from six field projects were evaluated. They examined various notch depths (i.e., 25.4 mm, 31.8 mm, and 38 mm) and tested four samples at each notch depth. The air void was 7.0 ± 0.50 percent for all the test specimens. The test temperature was fixed at 25 °C and a loading rate of 0.5 mm/min was used in the test. The researchers found that, the computed J_c values for gyratory compacted specimens (PL) and field cores (PF) did not indicate any indicative trend as shown in Figure 11. In addition, the researchers found that the average J_c increased with an increase of PG as shown in Figure 12. They recommended a minimum J_c of 0.5 kJ/m^2 for mixes made with binder PG less than 76 and J_c of 0.6 kJ/m^2 for mixes made with binder PG of 76 or greater.

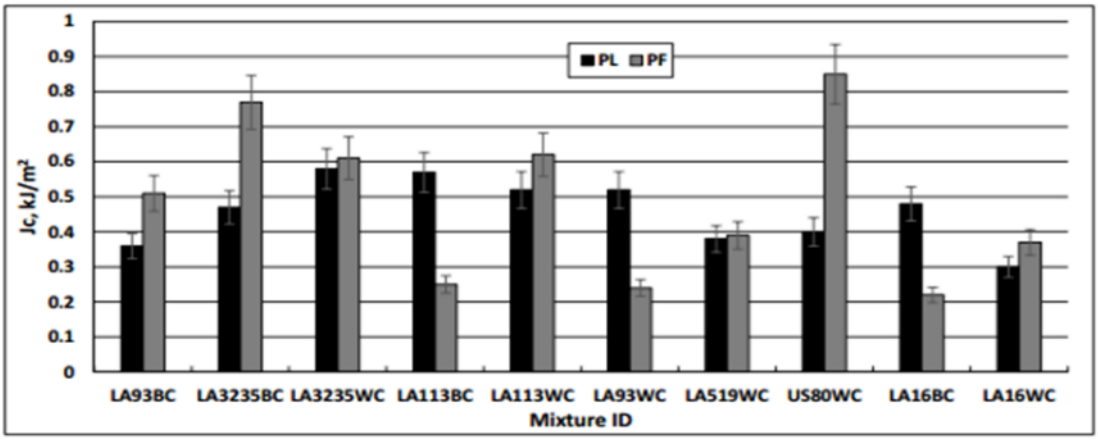

Figure 11 Comparison of SCB Jc Values between Laboratory and Field Cores [42]

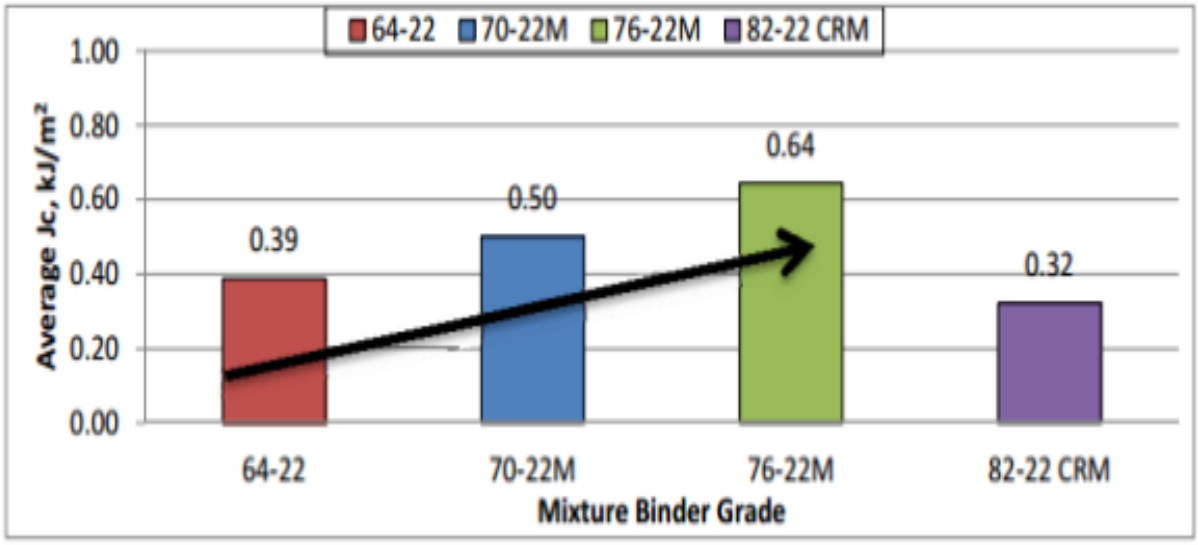

Figure 12 Fracture Performance for Different PG [42]

West et al. (2018) evaluated top-down cracking using Energy Ratio (ER), Overlay test (OT), NCAT Modified Overlay Test (NCAT-OT), J_c, FI, and IDEAL-CT_{index} test [43]. The study included seven asphalt mixes used at the NCAT test track. The results demonstrated that J_c was not able to distinguish between mixes with good and poor resistance to cracking. While, FI, OT, NCAT-OT, and ER had good agreement in ranking the mixes in terms of their resistance to cracking. The FI results showed a better statistical grouping compared to J_c and IDEAL-CT_{Index}. The FI classified mixes into six statistical groups, J_c classified mixes into two statistical groups, while IDEAL-CT_{index} classified mixes into four different statistical groups. In addition, the study evaluated Pearson correlation between performance indicators as summarized in Table 5. The IDEAL-CT_{Index} had strong correlation ($|r| > 0.8$) with Texas OT, NCAT-OT, and FI, and fair correlation with J_c (r= 0.3). The FI had a direct correlation with Texas OT and NCAT-OT tests and weak correlation with J_c (r = 0.117). Conversely, J_c had weak correlations with all parameters. The study evaluated the proposed performance threshold in the literature for various parameters (e.g., FI, J_c). Only two mixes (N2 and S16) had J_c higher than 0.5 kJ/m^2 while, only one mixture had FI higher than 8.

Kaseer et al. (2018) proposed a new cracking resistance indicator called Cracking Resistance Index (CRI)[44]. CRI is a normalization of fracture energy by the peak load (Figure 13). higher CRI values indicate better cracking resistance. The CRI was proposed to overcome the limitations of the Illinois Flexibility Index (FI) including moderate/higher variability of test results, difficult index calculations, and inability to study brittle mixture behavior especially for mixes with higher quantities of RAP and/or RAS [44]. The study examined the sensitivity of CRI and FI to mixture properties (i.e., binder content, binder grade, specimen thickness, air void content, and aging). LMLC, PMLC mixes, and field projects were evaluated.

Table 5 Pearson Correlation between Mixture Ranking [43]

	Resilient Modulus	**Creep Rate**	**$DCSE_{HMA}$**	**Energy Ratio**	**TX-OT**	**NCAT-OT**	**SCB (Louisiana)**	**I-FIT**
Creep Rate	-0.742	1.000						
$DCSE_{HMA}$	-0.519	0.212	1.000					
Energy Ratio	0.563	-0.956	-0.071	1.000				
TX-OT	-0.347	0.59	-0.349	-0.585	1.000			
NCAT-OT	-0.39	0.635	-0.166	-0.627	0.973	1.000		
SCB (Louisiana)	0.415	-0.062	-0.333	-0.158	0.426	0.48	1.000	
IFIT	-0.732	0.76	0.207	-0.641	0.83	0.891	0.117	1
IDEAL-CT	-0.461	0.656	-0.248	-0.624	0.991	0.973	0.343	0.887

The findings showed that CRI and FI were sensitive to change in binder grade, binder content, aging, and RAP/RAS materials. Softer binder (PG 58-28) had better cracking resistance than stiffer binder (PG 64-22). The study results showed that CRI was able to differentiate between more performance groups compared to FI. The variability in test results was dependent on aging condition. CRI had less variability than FI for Short Term Aging Conditions (STOA), while opposite trend was observed for Long Term Aging Conditions (LTOA) (i.e., brittle mixes). CRI and FI had good correlation ($R^2 > 0.90$), but both indicators showed dependency on specimen thickness and air void content. FI and CRI had an indirect relation with specimen thickness and direct relation with air void content.

$$CRI = \frac{G_{Fracture}^{Total}}{\mathrm{P}_{Peak}}$$

Figure 13 CRI Calculation Equation

where:

CRI = Cracking resistance index (J/m^2.KN)

$G_{Fracture}^{Total}$ = Total fracture energy (J/m^2)

P_{Peak} = Peak load (KN)

t = Specimen thickness (mm)

Indirect Tension (IDT) Test

The indirect tension (IDT) test involves applying a compressive load with a constant rate on cylindrical asphalt specimens (Figure 14). The load is applied until the specimen is split along the direction of the applied load. The axial and horizontal deformations are measured using Linear Variable Displacement Transducers (LVDTS) [45]. The test conditions such as loading mode, temperature, and test setup can be adjusted to measure different material properties. The IDT test has many advantages. The test procedure and sample preparation are simple. The failure of the test specimen occurs due to tensile stress, and it is not affected by the surface conditions of the test specimen [46].

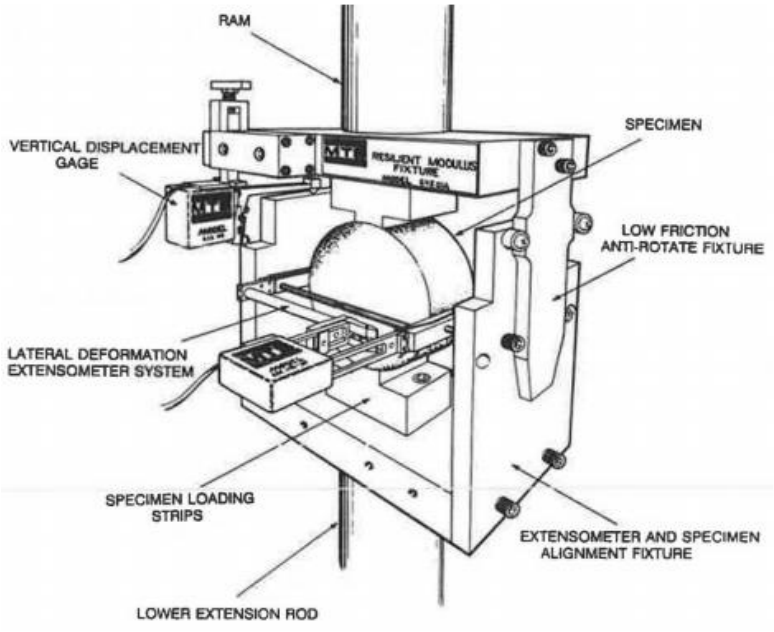

Figure 14 IDT Test Setup [47]

Indirect Tension Test- Strength Test

The IDT test is used to measure the strength asphalt mixture samples according to ASTM D-6931 [48] and AASHTO T 322 [49]. The test specimen is loaded at a constant deformation rate until failure. The strength is obtained by dividing peak load by its geometry (Figure 15). A loading rate of 50 mm/min is recommended in ASTM D-6931 while it is 12.5 mm/min in AASHTO T 322.

$$\sigma_{tesnile}{}^{IDT} = \frac{2000\text{x}P_{Peak}}{\pi \times t \times D}$$

Figure 15 Indirect Tensile Strength Calculation Equation

where:

$\sigma_{tesnile}{}^{IDT}$ = Tensile strength (kPa) determined from IDT test

P_{Peak} = Peak load (N)

t = Specimen thickness (mm)

D = Specimen diameter (mm)

Indirect Tension Test- Creep Compliance

IDT is also used to conduct creep compliance test on asphalt mixes. This test is used to assess the resistance to thermal cracking. It is one of the primary inputs in AASHTO pavement ME design. The creep compliance is the ratio between time-dependent (creep) strain to applied stress. In this test, a constant compression load is applied to the test specimen. The maximum horizontal deformation should be maintained between 0.00125 mm to 0.0190 mm for 150 mm diameter specimens. The test is conducted at three different temperatures depending on the binder PG. The creep compliance is calculated as a function of time (Figure 16). The creep compliance test is conducted in accordance with AASHTO T 322.

$$D(t)_{avg} = \frac{\Delta X_{tm} \times D_{avg} \times b_{avg}}{P_{avg} \times GL} \times C_{Cmpl}$$

$$C_{Cmpl} = 0.6354 \times \left(\frac{X}{Y}\right)^{-1} - 0.332$$

Figure 16 Creep Compliance Calculation Formulas

where:

D(t) = Creep compliance at time t (kPa)

GL = Gauge length in meters (0.038 m for 150 mm diameter specimens)

D_{avg} = Average diameter of test specimens (nearest 0.001 meter)

b_{avg} = Average thickness of test specimens (nearest 0.001 meter)

P_{avg} = Average creep load (kN)

$\Delta X_{tm,t}$ = Trimmed mean of the normalized horizontal deformations (nearest 0.001 meter)

$\left(\frac{X}{Y}\right)$ = Absolute value normalized trimmed mean of the horizontal deformation ratios

Indirect Tension Test – Fatigue Characterization

The IDT is also used to conduct fatigue tests. The test specimens are subjected to repeated loading, and the number of cycles until failure (N_f) is often used to describe the fatigue life. However, other failure criteria were proposed including 50 percent reduction in initial value of the resilient modulus [5] and 0.1 in of deformation [47]. Cocurullo et al. (2008) selected a total vertical deformation of 9 mm as failure criteria [50]. Khalid (2000) introduced theoretical criteria based on energy ratio for both control stress and strain mode of loading [51]. Kim and Wen (2002) introduced logit model that uses the fracture energy as indicator for fatigue cracking [46]. Kim et al. (2012) selected a reduction in normalized pseudo stiffness of 50 percent as failure criteria [52]. Nguyen et al. (2016) introduced a new approach that replies on using digital camera to measure the crack propagation during the test [53]. The failure criteria is selected as the number of cycles when the rate of crack propagation increases rapidly.

Comparison Between Laboratory and Field Performance

Christensen et al. (2000) correlated the IDT strength test to the rutting resistance of asphalt mixes [54]. They examined 10 asphalt mixes prepared with both modified and unmodified binders. The researchers developed recommendations for the IDT strength with expected rutting performance as presented in Table 6.

Table 6 Recommended Guidelines for Rut Resistance using IDT Strength [54]

IDT Strength (kPa)	Rut Resistance
> 440	Excellent
> 320 to 440	Good
> 200 to 320	Fair
200≥	Poor

Marasteanu et al. (2012) studied the performance of laboratory-prepared samples and field cores from the same mixes [55]. They examined nine different mixes. The researchers conducted several laboratory tests that included IDT creep and IDT strength tests, SCB test, and disk-shaped compact tension (DCT)

tests. The DCT fracture energy values for the laboratory samples and field cores were close as shown in Figure 17. Marasteanu et al. (2012) did not find a strong correlation between SCB fracture energy, SCB fracture toughness, and IDT tensile strength when they compared the results of laboratory samples to field cores.

Wen and Kim (2002) performed IDT creep tests and IDT strength tests on eight fine and coarse mixes in the laboratory as well as on field cores from the same mixes collected from the WesTrack [56]. The researchers used Digital Image Correlation (DIC) instead of the conventional LVDT to measure the strain and calculate the fracture energy. The Poisson's ratio was computed based on the measured strains and it was used to calculate the fracture energy from the IDT strength test. They found that the fracture energy calculated at 20 °C correlated well with the field performance of the same mixes at WesTrack. Figure 18 shows the correlation between the fracture energy and fatigue cracking at different traffic levels.

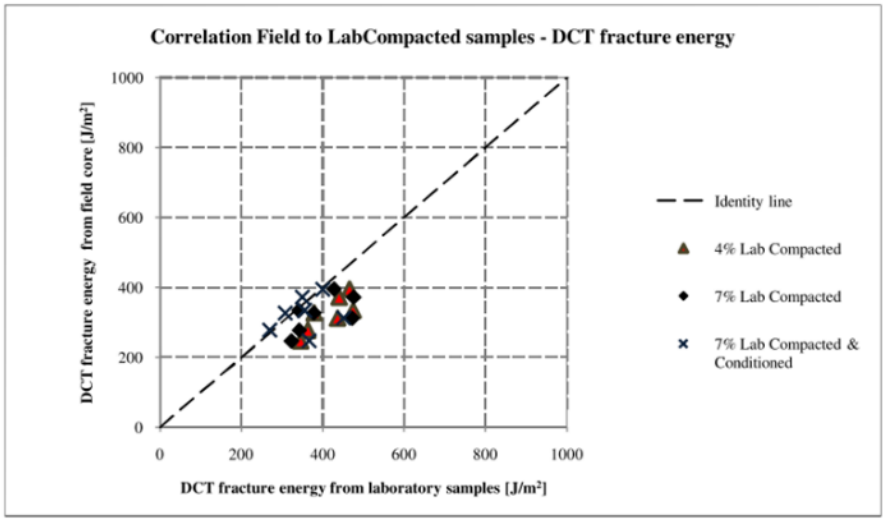

Figure 17 Results Comparison Field to Laboratory Compacted, DCT Fracture Energy [55]

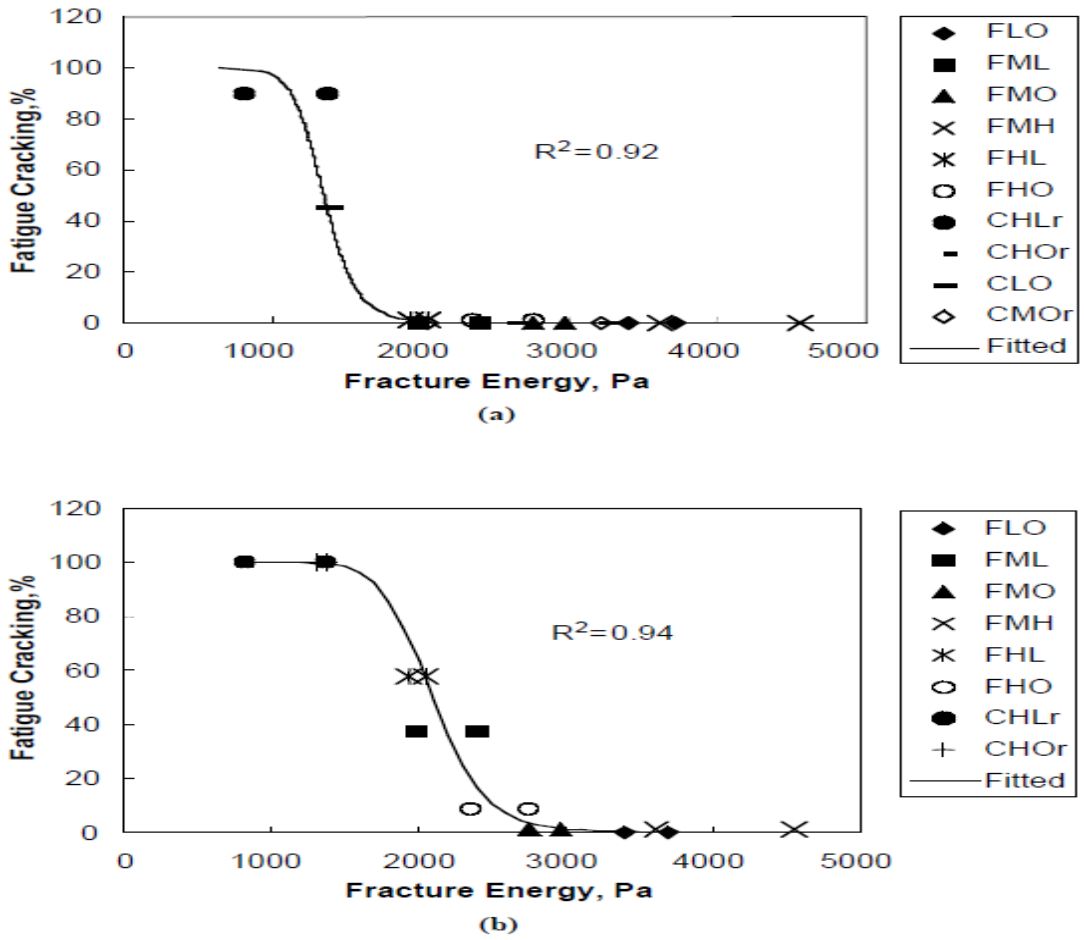

Figure 18 Relationship between Field Fatigue Performance and Fracture Energy (a) at 2.2 Million ESALs and (b) at 5 Million ESALs [56]

Zofka and Braham (2009) collected field cores from 10 pavement sections in Minnesota and Illinois. Performance laboratory tests (SCB, IDT and DCT) were performed on the field cores [57]. They compared the results to the field performance against low temperature cracking. The researchers found that the DCT and SCB test are the most suitable methods for evaluating the performance of asphalt mixes to low temperature cracking. In addition, SCB fracture toughness and IDT strength test results had good correlations with the field performance (Figure 19). The researchers recommended validating the findings of the study with more laboratory testing and field evaluation.

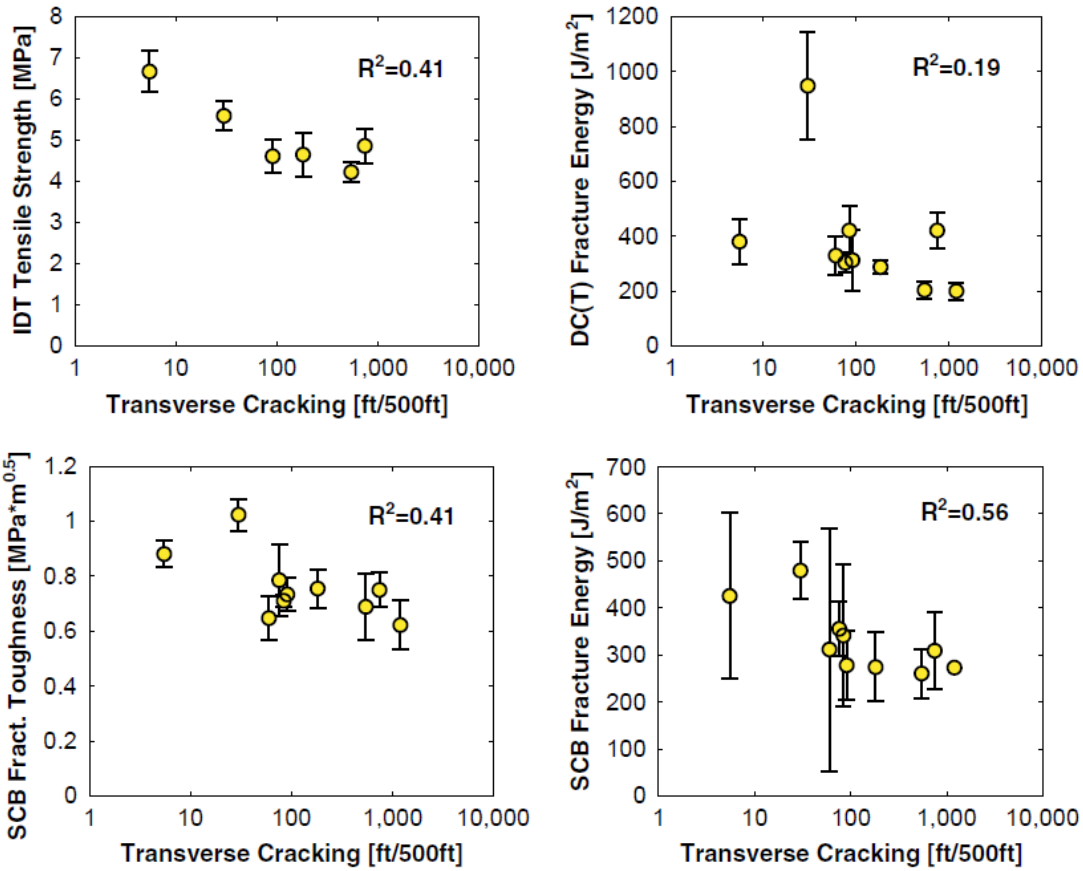

Figure 19 Comparison of Laboratory Parameters and Field Performance Data [57]

Wen and Bhusal (2013) studied the correlations between IDT test results and the AMPT flow number [58]. The AMPT flow number test was conducted according to the AASHTO T 378. The researchers found a good correlation between the AMPT flow number and IDT flow time (Figure 20 and Figure 21). In addition, the AMPT flow number correlated well with the IDT strength at high temperature. The researchers recommended validation of the findings with field performance.

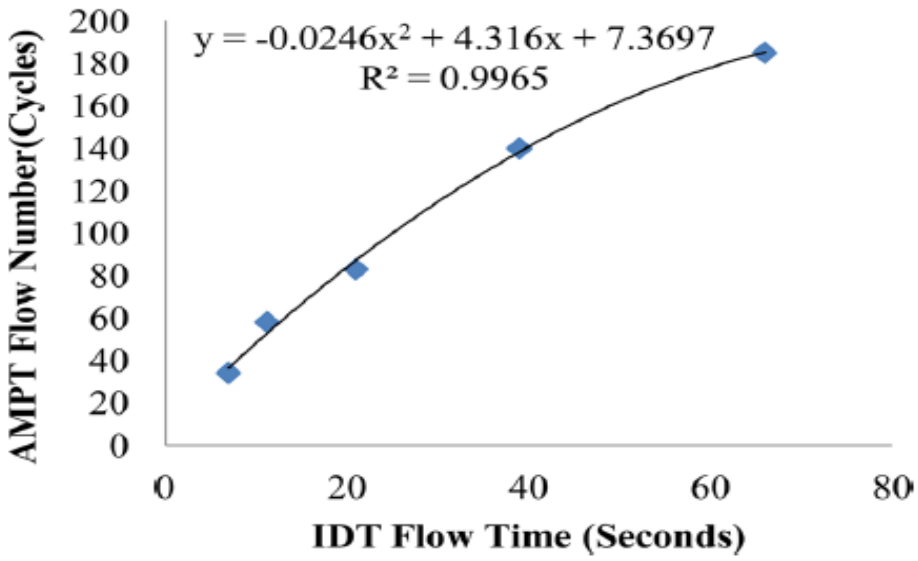

Figure 20 Correlation between IDT Flow time and AMPT Flow Number

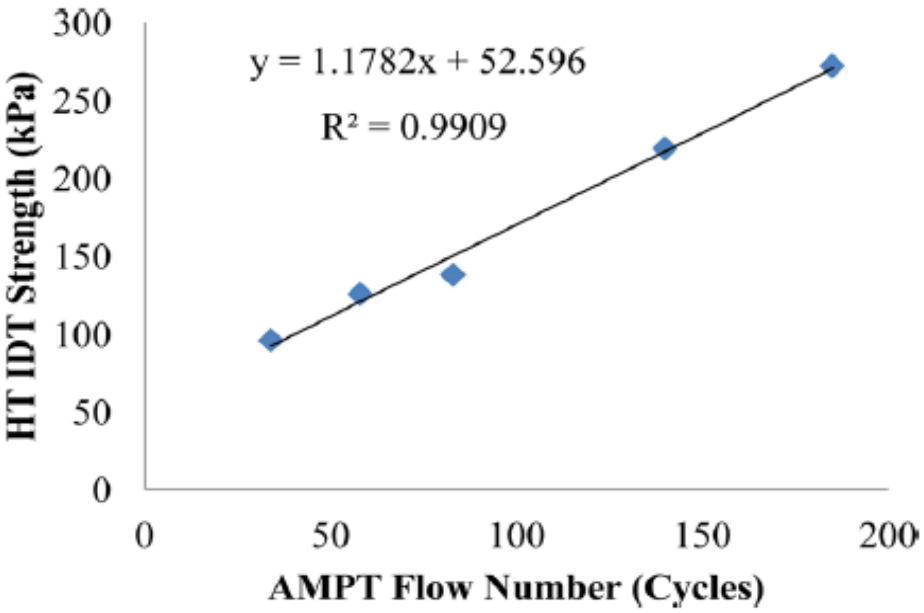

Figure 21 Linear Correlation between HT IDT Strength and AMPT Flow [58]

West et al. (2018) evaluated four cracking assessment tests including IDT (AASHTO T 283), SCB-Louisiana, Cantabro test (AASHTO TP108-14), and modified OT (TEX-248-F) [59]. The study correlated the laboratory results and field performance of eight Accelerated Loading Facility (ALF) test sections (Figure 22). Laboratory specimens were prepared from loose materials collected from construction sites. They

selected several performance indicators including $IDT_{strength}$, $IDT_{Modulus}$, and Nflex factor (IDT test), J_c (SCB test), average percent loss (Cantabro test), and modified OT cycles to failure (OT test). Results showed that Jc had no correlation with field performance ($R^2 = 0.05$). Weak correlations were also found with modified OT cycles ($R^2 = 0.41$) and $IDT_{strength}$ ($R^2 = 0.34$). Moderate correlations between field performance and percent loss ($R^2 = 0.54$), $IDT_{Modulus}$ ($R^2 = 0.47$), and Nflex ($R^2 = 0.55$) were documented. The correlation between field performance and Nflex was improved ($R^2 = 0.67$) after the researchers adjusted the fatigue field performance (Figure 23).

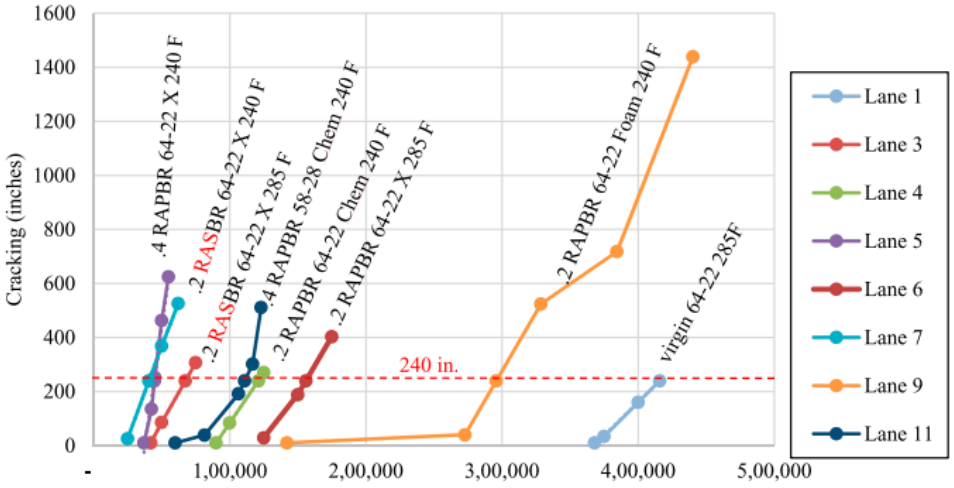

Figure 22 ALF Sections Fatigue Performance [59]

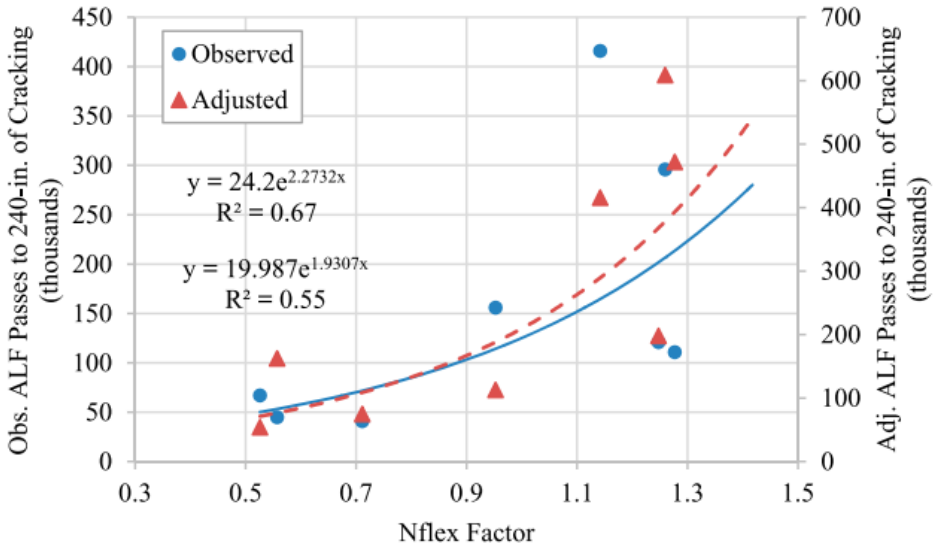

Figure 23 Correlation between Nflex Factor (IDT test) Parameter and Field Fatigue Performance [59]

Chapter 3
Materials Description and Specimen Preparation

Introduction

Chapter 3 provides information about asphalt mixes and field projects evaluated in this study. It also discusses the current ITD specifications for HMA mixes. In addition, this chapter documents the methods used by the researchers to evaluate the performance of field projects in terms of resistance to rutting and cracking.

ITD Hot Asphalt Mixes

Currently, there are three common asphalt mixes used in Idaho. These mixes include Superpave SP2, SP3, and SP5 as presented in Table 7 [60,61]. Mix type depends on the project design ESALs. ITD specifies several requirements for asphalt mixes including density (Table 7), aggregate properties and gradation (Table 8, Table 9, and Table 10), and binder PG adjustments (Table 3.5). Binder PG is selected based on the project temperature zone using LTPPBind. Moisture damage additives (e.g., antistripping agent or lime) are added to the mixture as a percent of binder content (minimum of 0.5 percent by weight). ITD allows using RAP materials but the Recycle Binder Replacement (RBR) should be less than 30 percent, and the virgin binder PG may need to be adjusted (Table 11) [61]. No binder PG adjustment is required for asphalt mixes with RBR less than 17 percent (Level 1). Mixes with RBR between 17 percent and 30 percent require binder adjustment (Level 2). The binder adjustment is performed using one grade lower than virgin binder PG at either the high-temperature or low-temperature or both (Table 11) or using AASHTO M323 blending charts. The adjustment is used to account for the effects of aged RAP binders.

Table 7 ITD Superpave Mixes Requirements [61]

Mixture Type	SP2	SP3	SP5
Design ESALs (millions)	< 1	1 ≤ 10	≥10
Gyratory Compaction (Gyrations for Nini)	6	7	8
Gyratory Compaction (Gyrations for Ndes)	50	75	100
Gyratory Compaction (Gyrations for Nmax)	75	115	160
Relative Density, percent Gmm@ Nini	≤ 90.5	≤89.0	≤89.0
Relative Density, percent Gmm@ Ndes	96.0	96.0	96.0
Relative Density, percent Gmm@ Nmax	≤98.0	≤98.0	≤98.0
Air Voids, percent Va	4.0	4.0	4.0
Dust to Binder Ratio Range	0.6-1.2	0.6-1.2	0.6-1.2
Voids Filled with Asphalt (VFA)Range, percent	65-78	65-75	65-75

Table 8 ITD Aggregate Requirements for HMA Mixes [60,61]

Mixture Type	SP2	SP3	SP5
Design ESALs (millions)	< 1	1 < 10	≥ 10
Idaho Degradation, maximum loss, percent	5.0	5.0	5.0
Ethylene Glycol, minimum retained, percent	90	90	90
R-Value	80 or more minimum	80 or more minimum	80 or more minimum
LA Wear, Maximum percent loss	35	30	30
Sodium Sulfate Soundness Maximum loss after 5 cycles, percent	12	12	12
Fractured Face, Coarse Aggregate percent Minimum	65/-	75/60	98/98
Uncompacted Void Content of Fine Aggregate, percent Minimum	40	40	45
Sand Equivalent, Minimum	35	40	45
Flat and Elongated, percent Maximum	10	10	10

Table 9 ITD Aggregate Gradation Requirements for Nominal Maximum Aggregate Size (NMAS) between 38 mm and 9.50 mm [60,61]

Sieve size	38 mm	38 mm	25.4 mm	25.4 mm	9.5 mm	9.5 mm
	Restricted Zone	Control Points	Restricted Zone	Control Points	Restricted Zone	Control Points
2 in	—	—	—	—	—	—
11/2 in	—	90 to 100	—	100	—	—
1 in	—	90 max	—	90 to 100	—	100
3/4 in	—	—	—	90 max	—	90 to 100
1/2 in	—	40 to 70	—	—	—	90 max
3/8 in	—	—	—	42 to 70	—	52 to 80
No. 4	34.7	—	39.5	—	—	—
No. 8	23.3	15 to 41	26.8	19 to 45	34.6	23 to 49
No. 16	15.5	—	18.1	—	23.1	—
No. 30	11.7	—	13.6	—	16.7	—
No. 50	10	—	11.4	—	13.7	—
No. 100	—	—	—	—	—	—
No. 200	—	0.0 to 6.0	—	1.0 to 7.0	—	2.0 to 8.0
VMA	11.0	11.0	12.0	12.0	13.0	13.0
Primary Control Sieve	3/8 in	3/8 in	No. 4	No. 4	No. 4	No. 4
PCS Control Point (percent passing)	47	47	40	40	47	47

Table 10 ITD Aggregate Gradation Requirements for NMAS between 12.5 mm and 4.76 mm [60,61]

Sieve size	12.5 mm	12.5 mm	9.5 mm	9.5 mm	4.76 mm	4.76 mm
	Restricted Zone	Control Points	Restricted Zone	Control Points	Restricted Zone	Control Points
2 in	—	—	—	—	—	—
11/2 in	—	—	—	—	—	—
1 in	—	—	—	—	—	—
3/4 in	—	100	—	—	—	—
1/2 in	—	90 to 100	—	100	—	100
3/8 in	—	90 max	—	90 to 100	—	95 to 100(a
No. 4	—	—	—	90 max	—	90 to 100
No. 8	39.1	28 to 58	47.2	32 to 67	—	—
No. 16	25.6	—	31.6	—	—	30 to 55
No. 30	19.1	—	23.5	—	—	—
No. 50	15.5	—	18.7	—	—	—
No. 100	—	—	—	—	—	—
No. 200	—	2.0 to 10.0	—	2.0 to 10.0	—	6.0 to 13.0(a
VMA	14	14	15	15	16	16
Primary Control Sieve	No. 8	No. 8	No. 8	No. 8	No. 16	No. 16
PCS Control Point (percent passing)	39	39	40	40	42	42

Table 11 PG Adjustment Levels for Different RBR Percent [60,61]

Virgin Binder Grade	Adjusted Binder Grade	
Virgin Binder Grade	Level 1	Level 2
58-28	No adjustment needed	58-34
58-34	No adjustment needed	No Adjustment Needed
64-28	No adjustment needed	58-34
64-34	No adjustment needed	58-34
70-28	No adjustment needed	64-34
76-28	No adjustment needed	70-34

Testing Materials Properties

Laboratory Mixed-Laboratory Compacted (LMLC) Mixes

The researchers prepared and tested Laboratory Mixed-Laboratory Compacted (LMLC) asphalt mixes. These mixes were produced and tested to examine the effect of binder PG and content on rutting and cracking resistance. The testing matrix included six mixes as presented in Table 12. Mixes were designed

using two binders (i.e., PG 58-34 and PG 70-28) and three binder contents (Optimum Binder Content [OBC], OBC-0.75 percent, and OBC+0.75 percent). Other mixture properties (e.g., aggregate gradation and mix type) were kept constant for all test mixes. Basalt rock was used in preparing the test specimens and Figure 24 shows the aggregate gradation. All LMLC mixes had a Nominal Maximum Aggregate Size (NMAS) of 12.5 mm, no RBR, and one mix type (i.e., SP3).

Table 12 LMLC Asphalt Mixture Designed Properties

Mixture ID	Mix Type	NMAS	Binder Type	Binder Content (percent)
PG 70-4.25%	SP3	12.5 mm	PG 70-28	4.25
PG 70-5.00%	SP3	12.5 mm	PG 70-28	5.00
PG 70-5.75%	SP3	12.5 mm	PG 70-28	5.75
PG 58-4.25%	SP3	12.5 mm	PG 58-34	4.25
PG 58-5.00%	SP3	12.5 mm	PG 58-34	5.00
PG 58-5.75%	SP3	12.5 mm	PG 58-34	5.75

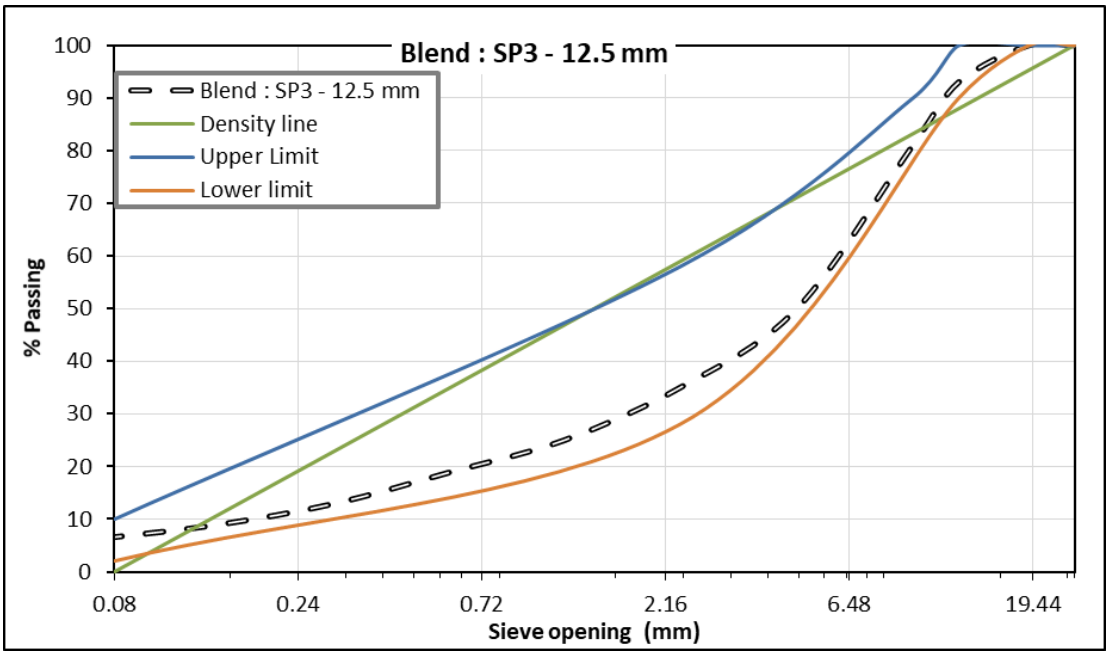

Figure 24 LMLC Aggregate Gradation (SP3-12.5mm)

Plant Mixed-Laboratory Compacted (PMLC)

Our research also evaluated Plant Mixed-Laboratory Compacted (PMLC) mixes obtained from new paving projects. The resistance of these mixes to cracking, rutting, and moisture damage were examined in the laboratory. In addition, we examined the variability of various test methods used to assess the performance of the PMLC and evaluated 10 PMLC mixes distributed across the state as presented in Table 13. About 200 lb of loose mixes were sampled and delivered in boxes to the laboratory. Each box

was clearly labeled with information about the project including key number, MP, Gmm, RAP, and binder content. The Job Mixes Formulas (JMFs) for all mixes are provided in Appendix A. Table 13 summarizes the main properties of PMLC mixes. The PMLC included two mix designs (SP3 and SP5), two NMAS (12.5 mm and 19.0 mm), five binder grades (PG 58-28, PG 64-28, PG 64-34, PG 70-28, and PG 76-28), five binder contents (4.8, 5.2, 5.3, 5.4, and 5.7 percent), and four RBR replacement (0, 29, 30, and 50 percent).

Table 13 PMLC Project Information and Mix Properties

#	District	Project ID	Construction year	Project Key No. (KN)	Location
1	1	D1L1	2017	19002	I-90, Northwest Blvd to Sherman Ave. CDA & US-95, Cocolalla CR Br,Bonner CO
2	2	D2L1	2017	19187	US-12, Arrow Br to Big Canyon Creek Br
3	2	D2L2	2018	19640	TOP of Bear CR. to Pine CR, Latah CO
4	3	D3L1	2017	13463	SH-44/JCT I84 to Star
5	3	D3L2	2017	19412	US20. Borchers Ln to locust grove
6	3	D3L3	2017	13924	SH-67, MP0 to JCT 51, Eklmore CO
7	3	D3L4	2017	13935	FY16 Capital maintenance ACHD
8	3	D3L5	2017	18723	I-84, Cleft to MP90, Elmore CO
9	5	D5L1	2017	13103	I-15, Sands Rd. upass to IC #89, Bingham CO
10	6	D6L1	2017	19543	Spalding Br. to US-12/SH-3

#	District	Project ID	Mix Type	Specified Binder PG	Virgin Binder PG	Binder Content Pb percent	RAP percent	NMAS	Max Specific Gravity G_{se}	Bulk Specific Gravity G_{sb}
1	1	D1L1	SP5	64-28	58-34	5.30	30	12.5	2.696	2.646
2	2	D2L1	SP3	70-28	64-34	5.70	50	12.5	2.771	2.672
3	2	D2L2	SP3	64-28	58-34	5.70	30	12.5	2.762	2.799
4	3	D3L1	SP3	70-28	52-34	5.20	50	12.5	2.600	2.575
5	3	D3L2	SP3	70-28	64-34	5.20	30	12.5	2.605	2.563
6	3	D3L3	SP3	64-28	58-34	5.30	30	12.5	2.640	2.582
7	3	D3L4	SP3	70-28	64-34	5.30	30	12.5	2.620	2.555
8	3	D3L5	SP5	76-28	70-34	5.30	30	12.5	2.612	2.578
9	5	D5L1	SP5	70-28	70-28	4.80	30	19.0	2.658	2.656
10	6	D6L1	SP5	64-34	64-34	5.40	0	12.5	2.649	2.614

Field Projects

The team also obtained field cores from various projects across the state. ITD Material Engineers extracted the cores and shipped them to the laboratory for testing. The cores were delivered in boxes. Each box had the proper information (e.g., project locations, route name, beginning Mile Post [MP] and end MP, construction year, and JMF if available). The cores were exacted from sites identified by ITD

Material Engineers based on a survey that was sent to them (see Table 14). In their responses, they identified field project with different performance (e.g., good, fair, and poor) to cracking, rutting, and moisture damage (as available). In addition, they provided information about the mixture design, binder PG, and age of the identified sections. Table 15 summarizes various mixture properties for the identified test sections. Table 16 provides information about the location and year of construction of the selected field projects. A total number of 35 test sections were identified and field cores were obtained and tested from 17 test sections. Cores from additional test sections were received but later discarded due to their geometry (very thin), age (> 35 years old), or incomplete information. The number of field cores extracted from each test section varied but in general about 20 field cores were obtained from each project. In addition, ITD engineers provided relevant information. Table 17 summarizes the properties of asphalt mixes for each section. JMFs for some of these field projects are provided in Appendix B.

Table 14 Survey to Identify Test Sections

Section information	**Section number**
Route e	
Milepost from	
Milepost to	
Age (Years) (<5, 5-10, >10)	
Mix type and aggregate type	
PG Grading	
Percent RAP (if any)? Percent binder replacement? Adjusted binder grade? Extracted RAP PG (if tested)?	
Cracking Rating (Good, Fair, Poor)	
Cracking Description (e.g., fatigue, thermal, etc.)	
Rutting Rating (Good, Fair, Poor)	
Rutting Description (Comments.)	
Moisture Damage, if any (e.g., stripping)	

Table 15 Characteristics of Identified Test Sections

Criteria	levels identified
Distress type	Fatigue cracking, Rutting, and moisture damage
Distress severity	Good, fair, and poor
Mixes type	SP2, SP3, SP4, SP5, SP6, CLASS I, CLASS II, and CLASS III
PG grading	58-28, 64-28, 64-34, 70-28, and 76-28
RAP (percent)	0-17, 17-30, and >30
Aging (years)	Unaged (Virgin materials), <5, 5-10, and >10

Table 16 Location of Selected Field Projects

#	District	Project ID	Route	Beginning MP	End MP	Construction Year
1	D2	D2C4	US95	366.6	373.2	2007
2	D2	D2C5	US95	242	251.1	2010
3	D2	D2C6	US95	222.4	223.3	2007
4	D2	D2C7	SH6	100	104	2007
5	D2	D2C8	US-95	233.5	239	2006
6	D2	D2C9	SH162	8	13	2007
7	D2	D2C10	SH13	11.2	25.4	2007
8	D2	D2C11	US12	90.7	111.4	2009
9	D2	D2C12	US95	267.6	271.5	2007
10	D2	D2C13	SH6	7.3	13.52	2010
11	D3	D3C2	US20/26	42.6	44	2016
12	D3	D3C3	SH55	44.7	51.7	2009
13	D3	D3C4	SH44	19.4	21.8	2009
14	D3	D3C5	SH44	14.3	16.2	2013
15	D5	D5C1	US26	272	282.8	1985
16	D6	D6C1	US-26	338.5	342	2010
17	D6	D6C2	US-20/26/93	225	227	2006

Table 17 Selected Field Projects Properties based on Designed JMF

#	*Project ID	Mix type	NMAS	OBC percent	RBR percent	Design Binder PG
1	D2C4	Hveem	19	**	**	58-28
2	D2C5	SP4	19	5.29	17.00	64-28
3	D2C6	SP3	**	**	**	70-22
4	D2C7	SP2	**	**	**	58-28
5	D2C8	SP3	19	5.00	0.00	70-28
6	D2C9	SP3	12.5	**	**	58-28
7	D2C10	SP3	12.5	5.27	0.00	64-28
8	D2C11	SP3	12.5	**	**	58-28
9	D2C12	SP3	12.5	5.53	0.00	64-28
10	D2C13	SP3	12.5	6.35	17.00	58-28
11	D3C2	SP3	12.5	5.20	50.00	76-28
12	D3C3	SP4	12.5	5.49	11.50	64-28
13	D3C4	SP4	12.5	5.56	9.00	64-28
14	D3C5	SP4	19	4.72	28.40	64-28
15	D5C1	Hveem	**	**	**	**
16	D6C1	SP4	19	5.29	17.00	64-34
17	D6C2	Hveem	**	**	**	64-34

** Missing information

Field Project Performance Evaluation

Based on the results of the survey filled by ITD Material Engineers, two main pavement distresses were observed; fatigue cracking and rutting. Moisture damage was not found to be a major distress based on the results of the survey. Also, none of these sections were reported to have any structural deficiency. Asphalt pavements in the state are designed using Idaho R-value, AASHTO T93, WinFlex 2006, or Pavement ME. Therefore, the researchers related the field performance to mix properties. In this section, methods used to evaluate the field performance of the test sections were discussed.

For the field cracking resistance, ITD performs an annual field pavement surface evaluation [62]. Two evaluation methods are used; windshield survey and profiler vehicle survey. Windshield survey involves visual inspection of pavement surface while driving on the road. The Asset Management Engineer is often the one who performs this evaluation. The Cracking Index (CI) is used to describe the cracking distresses. The CI ranges between 0 and 5, where 5 indicates excellent performance (no cracks) and 0 indicates severally cracked surface. Roads are divided into different performance groups (e.g., good, fair, poor, and very poor) based on the CI and road function class (i.e., collectors and interstate and arterials roads) as presented in Table 18 [62]. Pavement engineers use such classification to determine the need for maintenance and rehabilitation treatments.

Recently, ITD started using the profiler vehicle to conduct pavement distress survey that can replace the windshield survey. Figure 25 shows the PathRunner profiler used by ITD. This profiler is equipped with advanced equipment (e.g., high definition cameras, road profiler, GPS, and laser-based crack measurement) [63]. The profiler scans the pavement surface and collects information related to several

performance measures including rut depth, crack detection, roughness index, and longitudinal and transverse profile and it stores video logs of the pavement surface. This system determines the crack types (e.g., transverse, longitudinal, fatigue) and severity. Figure 26 and Figure 27 show examples of the data collected by the profiler vehicle. The automated crack detection and classification system are used to determine the overall condition index (OCI) for the tested pavements [62,64]. The OCI is the weighted average of Individual Pavement Distress Index (IDI). The IDI is determined based on the severity and extent of six different types of flexible pavement cracking including fatigue, edge, transverse, block, patch, and raveling. More details are provided by Poorbaugh (2017) and Kercher engineering (2015) [62,64]. The OCI ranges between 0 and 100, where higher OCI indicates pavement in good conditions. Pavement performance is classified into three groups: 1) good conditions (OCI ≥ 80), 2) fair conditions (80 < OCI ≥ 60), and 3) poor conditions (OCI < 60) [62,64].

Figure 25 PathRunner Profiler used by ITD

Table 18 Pavement Cracking Resistance Categorization based on the Greek Method [62]

Pavement condition category	Cracking Index (CI)	Cracking Index (CI)
Pavement condition category	Road functional class	Road functional class
Pavement condition category	Interstate and arterials	Collectors
Good	CI > 3	CI > 3
Fair	2.5≤ CI ≥3	2 ≤ CI ≥ 3
Poor	2≤ CI ≥2.5	1.5 ≤ CI ≥ 2
Very Poor	CI < 2	CI < 1.5

Figure 26 PathRunner Outputs for D1C1 between MP 53 and MP 54; (a) GPS Route Map (b) Road Perspective, (c) Rut Depth Profile (d) IRI Profile

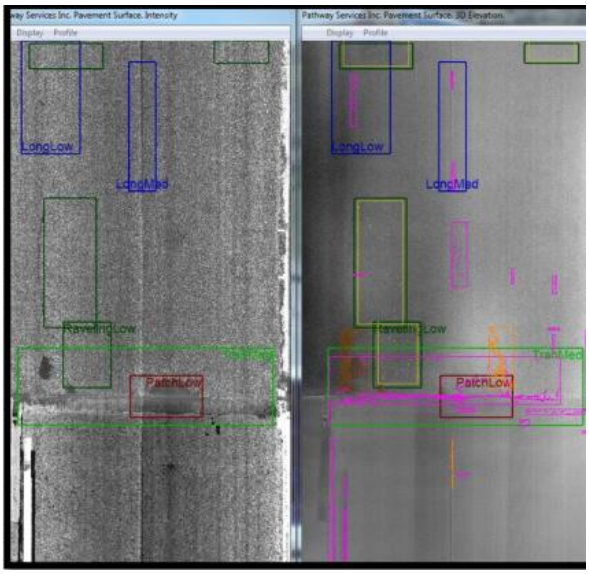

Figure 27 Example Crack Detection and Classification Software

In this study, CI, OCI, and ITD Material Engineer's subjective evaluation were collected. The CI data were obtained from the Agile Assets Transportation Asset Management System (TAMS database) managed by ITD. ITD Material Engineers' subjective evaluations were provided in the survey completed by the Material Engineers. In addition, the OCI values were calculated from the video logs. The OCI data were limited to the last four years. The current practice at ITD is to store the video logs for only four years, therefore, it was not possible to obtain the OCI prior to the last four years. The history of cracking resistance is needed to understand the performance decay (decrease in OCI) of test sections over time. The OCI is highly influenced by surface treatment (mostly seal coat). Such treatments improve the OCI since they seal the cracks at the surface thus there is a need for cracking resistance records over time to determine if higher OCI and CI are related to better mix resistance to cracking or it is caused by the applied preservation treatments.

The current practice at ITD is to apply a surface treatment as soon as needed, especially for commerce routes (routes with more than 300 CAADT). In 2017, only 12 percent of statewide pavements had very poor to poor performance [62]. Figure 28 shows an example of CI over time for one of the test sections (D2C8) evaluated in this study. This section is located at US 95 between MP 233.5 and 239. The section had poor performance (CI of 3) before a new construction that was conducted in 2006 which was examined in this study. Due to the new construction, the CI was increased to 5. A seal coat treatment was applied in 2009. After that, a small reduction in CI was documented. In 2016, the section had a CI of 4.7. Considering these observations, the section performance was described as good in terms of cracking performance. The research team examined the CI history for all test sections and considered the lowest CI in their analysis.

The researchers combined the CI and the subjective evaluation provided by ITD Material Engineers and developed Table 19 that presents the CI and subjective rating by the researchers. They classified the test sections into three groups; 1) test sections with good cracking resistance ($4.5 \leq CI \geq 5$), test sections with fair cracking resistance ($3.5 \leq CI > 4.5$), and test sections with poor cracking resistance ($CI < 3.5$). Figure 29 shows a graphical representation of the cracking resistance for all test sections. Sections with good cracking resistance are presented in green bars, sections with fair cracking resistance are presented in yellow bars, and sections with poor cracking resistance are presented in red bars. Only two projects were found to have poor cracking resistance (i.e., D2C13 and D5C2), while seven and eight projects showed fair and good cracking performance, respectively. In this study, the identified test sections with cracking deficiency are not likely to be related to any structure design issues. None of these sections were reported to have any structural deficiency based on the collected survey from ITD Materials Engineers.

Table 19 Pavement Cracking Resistance Categorization based on the Greek Method

Pavement condition category	Combined Cracking Index (CI) and ITD Material Engineers Survey	Combined Cracking Index (CI) and ITD Material Engineers Survey
Good	CI > 3	CI > 3
Fair	2.5≤ CI ≥3	2 ≤ CI ≥ 3
Poor	2≤ CI ≥2.5	1.5 ≤ CI ≥ 2
Very Poor	CI < 2	CI < 1.5

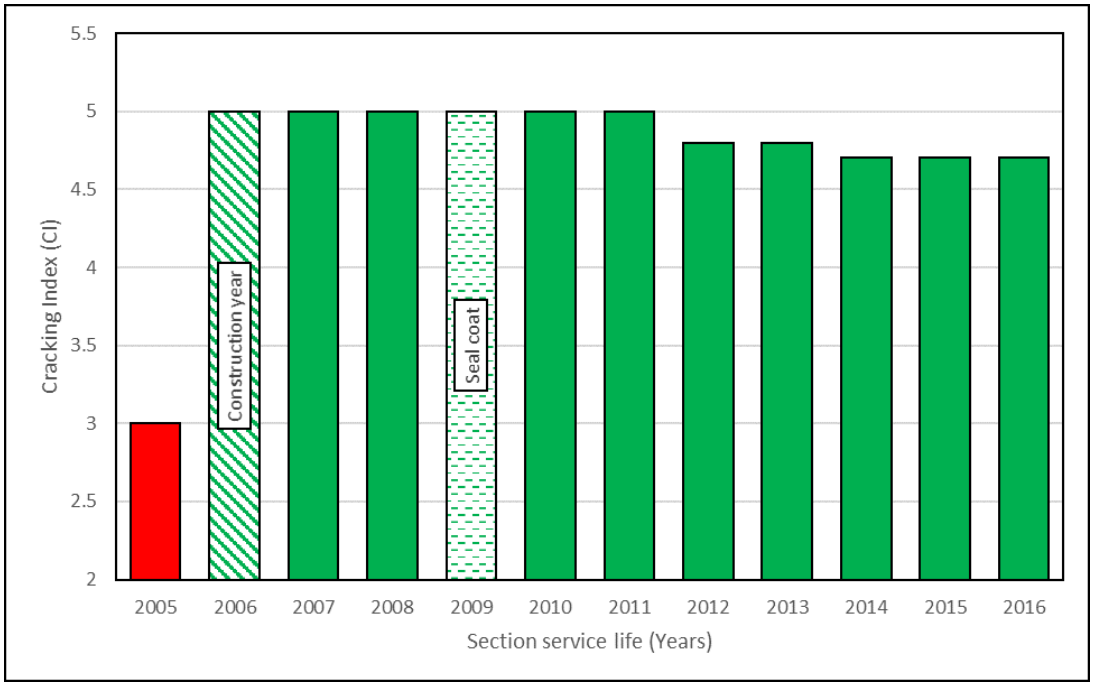

Figure 28 Example for CI Evaluation for D2C8 Test Section

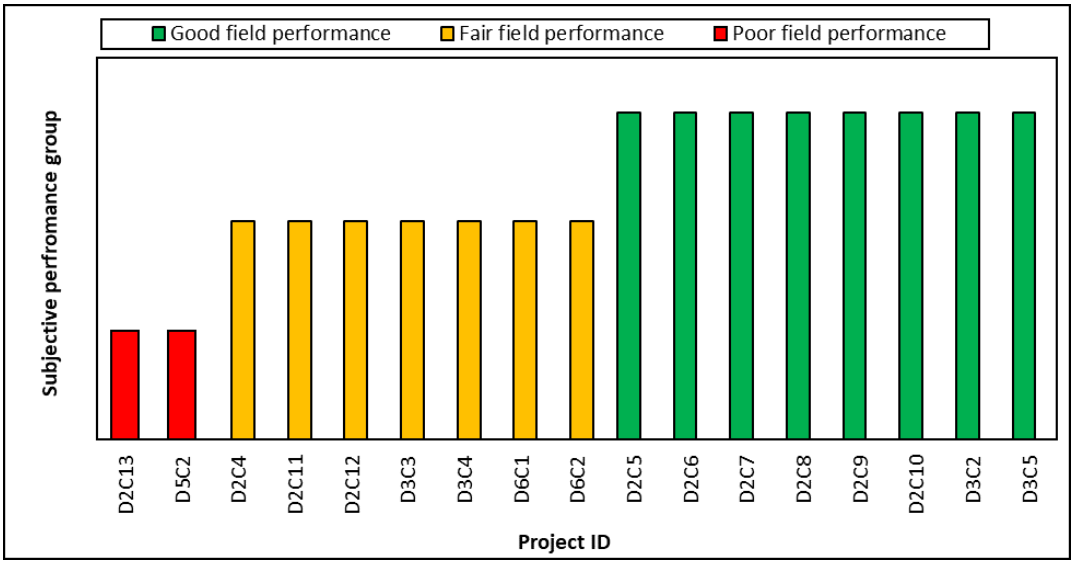

Figure 29 Cracking Resistance Evaluation for all Field Test Projects

We collected information about the rutting performance from different sources including the video logs collected by the profiler vehicle, TAMS database, and the PathWeb [62]. Similar to the OCI, the rutting measurements were available for the last four years from the video logs. Since the application of surface treatments improves the surface conditions, the rutting measurements over time are needed to accurately evaluate the performance of the test sections. Therefore, the rutting measurements calculated from the video logs (limited to only four years) were not sufficient. Instead, we used the TAMS and PathWeb to obtain rutting measurements over time. The maximum rut depth was considered and used in evaluating the field performance of the test sections. Figure 30 shows the measured rut depth for all test sections. The rut depth was between 2.80 mm and 8.64 mm. The test sections were classified into two groups based on the ITD's rutting criteria presented in Table 20. The ITD classification is a function of the measured rut depth and route functional class (e.g., interstate and arterials or collectors). Eleven projects had good rutting performance, while six projects showed fair rutting performance. None of the projects expedited poor rutting performance. The green bars in Figure 30 indicate projects with good performance while yellow bars indicate projects with fair performance.

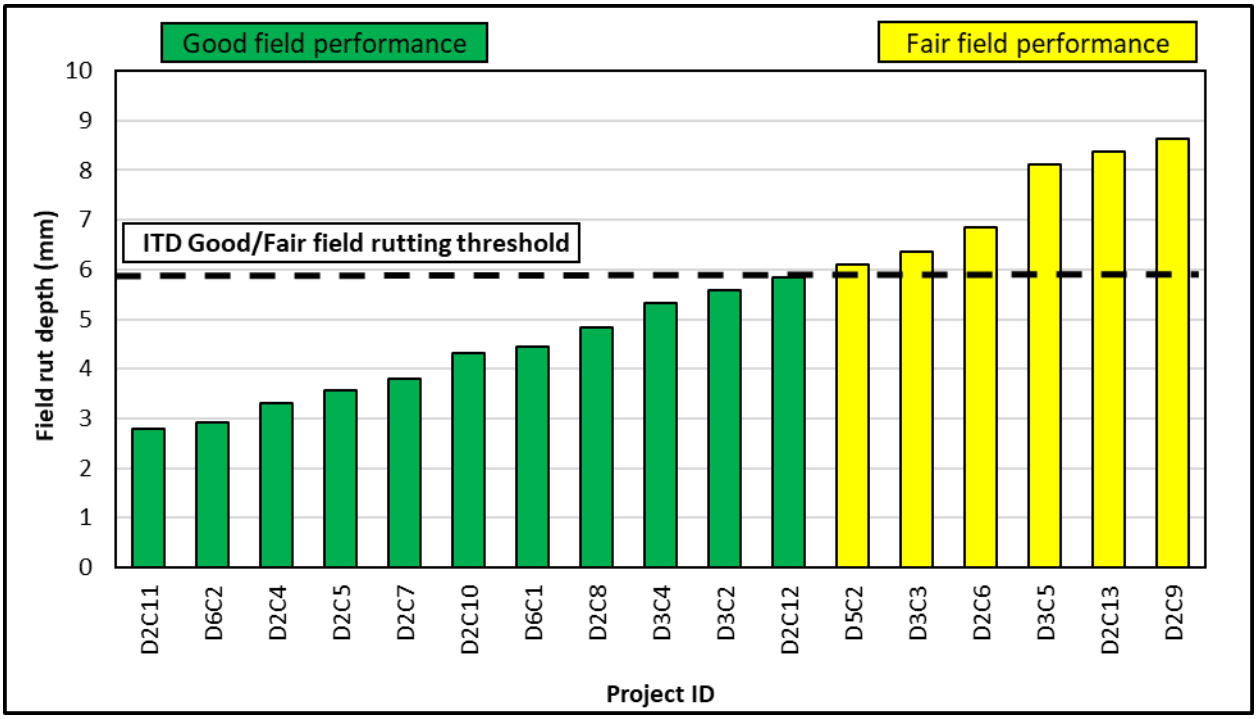

Figure 30 Field Rut Depth Measurements for Selected Locations

Table 20 ITD Field Rutting Performance Groups

Pavement Condition	Functional class	Functional class
Pavement Condition	Interstate and arterials (mm)	Collectors (mm)
Good	0.0 - 6.09	0.00 - 12.44
Fair	6.09 - 12.44	12.44 - 25.14
Poor	12.44 - 18.79	25.14 - 37.8
Very Poor	≥ 19.05	≥ 38.1

Specimens Preparation

Laboratory Mixed-Laboratory Compacted (LMLC) were prepared at the designated mixing temperature as specified in the JMFs. The LMLC mixes were short-term aged in accordance with AASHTO R30. The mixes were conditioned at 135 °C four hours before compaction [65]. A Superpave gyratory compactor was used to compact the test specimens to a target air void content of 7 ±0.5 percent in accordance with AASHTO T 312 [66]. The height of the test specimens varied depending on the testing protocols. Information about the geometry of test specimens for different tests is provided in Chapter 4.

The researchers also obtained loose mixes from the new paving projects and compacted in the laboratory. Plant Mixed-Laboratory Compacted (PMLC) mixes were produced by heating the loose materials to the compaction temperature specified in the JMFs. Similar to the LMLC, the PMLC were compacted to achieve a target air void content of 7 ±0.5 percent in accordance with AASHTO T 312 [66].

In addition to LMLC and PMLC, field cores were extracted from the test sections using a 150-mm coring bit. The cores were extracted from the shoulder of test sections or between the wheel path if the road had no shoulder. Upon extraction the field cores by ITD crew, the cores were labeled and shipped to the laboratory. The cores had different thickness as shown in Figure 31. Upon receiving the cores, the top layer was cut to the target thickness required for various tests as discussed in Chapter 4. Figure 32 illustrates the process of preparing the field cores for testing. It should be noted that any surface treatment (e.g., seal coat) was trimmed and excluded.

We also measured the bulk specific gravity (G_{mb}) in accordance with ASTM 2726 [67] for the test specimens after cutting to the required thickness. The theoretical maximum specific gravity (G_{mm}) was obtained from the provided JMF for different projects. In case that the JMF was not available, the researchers measured the G_{mm} according to ASTM D 6857 [8]. The test specimens for rutting evaluation (APA rut test and Hamburg) required additional sample preparation as illustrated in Figure 33. Some specimens were plastered as recommended in AASHTO T340 and T324 to meet the required thickness for those thin specimens (less than 60 mm and 75 mm for AASHTO T340 and T324, respectively).

Figure 31 Field Cores with Different thicknesses

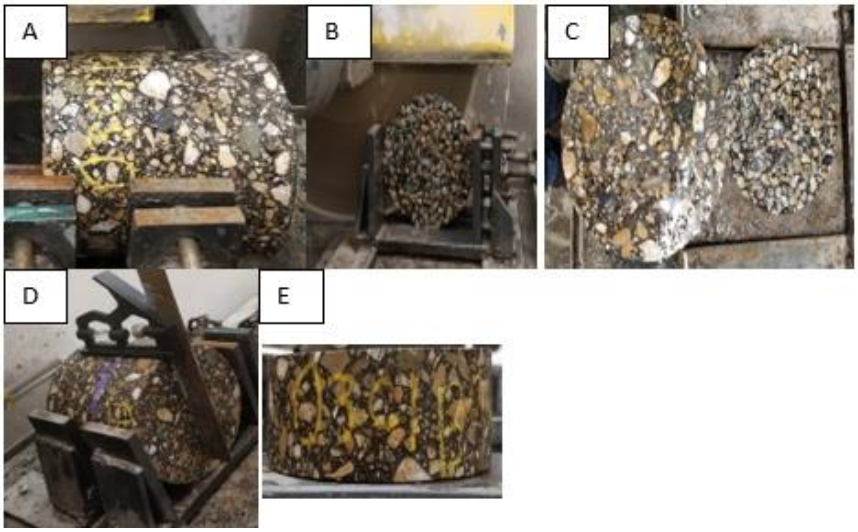

Figure 32 Example of field cores preparation for indirect tensile test; a) securing the specimen in a sample holder, b) trimming seal coat layer, c) excluded seal coat layer, d) cutting the surface layer, e) IDT test specimen

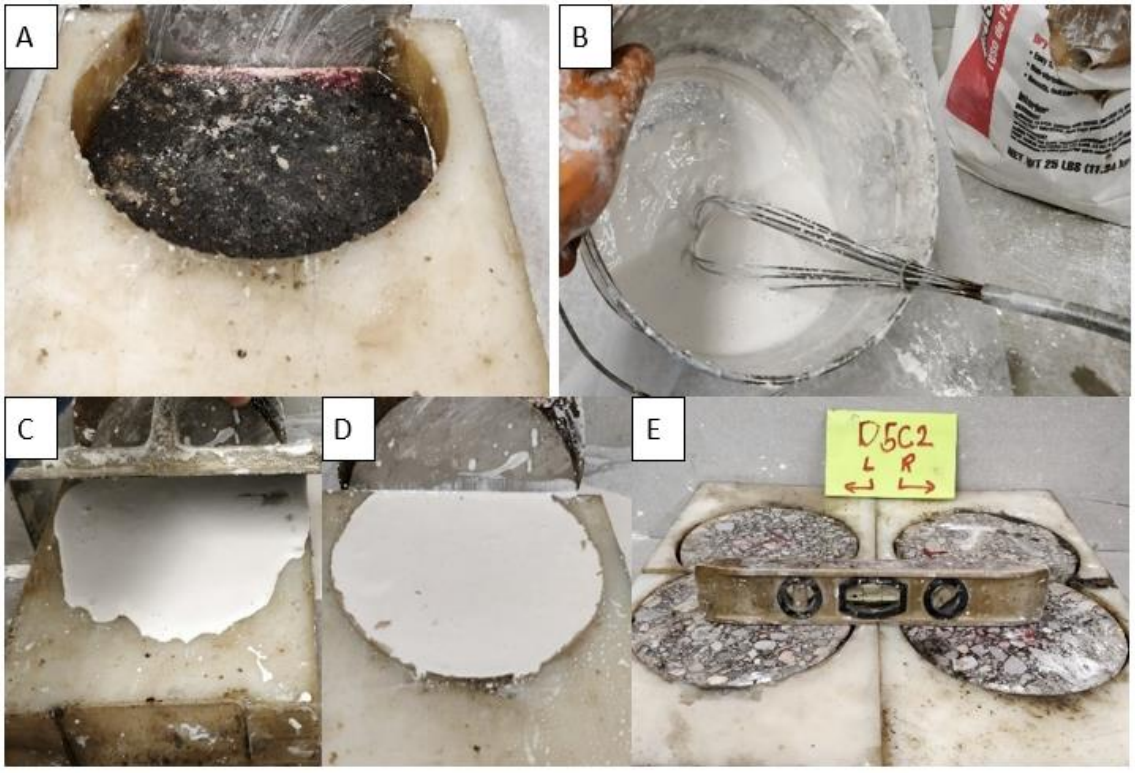

Figure 33 Hamburg Test Specimen Preparation; a) Placing the specimen in the casting mold, b) Mixing the plastering materials, c) Filling the gap with plastering materials and smoothing the surface, d) The bottom surface after plastering, e) Leveling the Hamburg test specimens

Chapter 4
Testing Protocols and Experimental Design

Introduction

Chapter 4 provides details about the selected testing protocols and mathematical calculations of various performance indicators used to assess the resistance of asphalt mixes to cracking and rutting. In addition, it discusses the development of a new dynamic cracking assessment test and an innovative performance indicator to assess the cracking perfomance of asphalt mixes.

Monotonic Cracking Testing Protocols

Selected Protocols

In the field, fatigue cracking results from repeated and heavy traffic loading [69]. This phenomenon is simulated in the laboratory using dynamic cracking resistance tests, where a repeated load is applied to a test specimen. Dynamic tests require complex and costly testing systems, long testing time, and complicated specimen preparation procedures [70]. These requirements make the dynamic tests less preferable to be used by the asphalt industry or transportation agencies. Conversely, monotonic tests are simple and require less expensive testing systems and have a short testing time and simple specimen preparation [70]. Although monotonic tests are not true fatigue cracking test, previous research studies reported that monotonic tests had a good correlation with field cracking resistance [38,39,43]. Currently, monotonic tests are used to assess asphalt mixture cracking resistance (e.g., LADOT uses SCB-Jc test) [15,35,39].

In this study, we evaluated three monotonic cracking testing protocols including SCB-J_c (TR330 or ASTM D8044), SCB-FI (AASHTO TP 124), and IDT tests (ASTM D6931). These tests have similar loading concept (constant displacement rate) and outputs (load-displacement curve), but they have different loading rate, specimen geometry, and use different performance indicators. Table 21 summarizes the testing conditions for each testing protocols. The IDT testing protocol (ASTM D6931) uses a circular specimen, while SCB testing protocols (AASHTO TP124, TR330, and ASTM D8044) use a notched Semi-Circular (SC) specimen. The standard AASHTO TP 124 testing protocol requires using one notch depth (15 mm), while ASTM D8044 and TR 330 standards require using three notch depths (i.e., 25.4 mm, 31.8 mm, and 38.4 mm). Laboratory prepared specimens and field cores can be tested using the three testing protocols (i.e., SCB-J_c, SCB-FI, and IDT). The geometry of the test specimens used in each test is provided in Table 21. The test specimens had a diameter of 150 mm for SCB tests and 101.6 mm or 150 mm for IDT test. No requirements on the thickness of field cores except for TR330, where the core should have a minimum thickness of 57 mm. The test temperature was 25˚C, except for ASTM D8044, where it is selected according to the intermediate binder PG temperature. ASTM D6931 and AASHTO TP 124 are performed at fast loading rate of 50 mm/min as compared to TR 330 or ASTM D8044 which are conducted at 0.5 mm/min. In this study, AASHTO TP 124, ASTM D6931, and TR330 were followed.

Table 21 Testing Protocols for Intermediate Cracking Evaluation [33,36,48,71,72]

Test	Test	SCB	SCB	SCB	IDT
Testing Standards	Testing Standards	TR330	ASTM D8044	AASHTO TP 124	ASTM D6931
Specimen geometry	Notch (mm) depth	25.4±1, 31.8±, and 38±1	25±1, 32±1, and 38±1	15±1	----------
Specimen geometry	Diameter (mm)	150	150	150	150 or 101.6
Specimen geometry	Specimen thickness (mm) for Lab prepared specimens	57	57	50 ±1	Minimum of 50.8 for a specimen with 101.6 mm diameter, or a minimum of 75 mm for specimens with 150 mm diameter.
Specimen geometry	Specimen thickness (mm) for field cores	57 (minimum)	38-60	25-50	Minimum of 38 mm for a specimen with 101.6 mm diameter.
Test temperature (°C)	Test temperature (°C)	25	Intermediate PG temperature	25	25
Loading rate (mm/min)	Loading rate (mm/min)	0.5	0.5	50	50 ±5
Test output	Test output	Load-displacement curve	Load-displacement curve	Load-displacement curve	Load-displacement curve

Monotonic Cracking Tests Output

The applied load and the actuator vertical displacement are recorded in the monotonic tests (i.e., IDT, SCB-Jc, and SCB-FI). Figure 34 shows a typical output of the selected monotonic tests. The load-displacement curve changes with changes in testing conditions and/or test materials. Figure 35 shows the load-displacement curves for mixes with different binder PG (i.e., PG 70-28 and PG 58-34) at the same binder content of 5.75 percent by weight. A similar trend can be observed for all monotonic tests. The applied load increases with displacement until the peak, then load decreases with the increase of the displacement until fracture. The Pre-Peak part of the curve describes the crack initiation in the specimen with no visible cracking observed [73]. The Post-Peak part of the curve describes crack

development and propagation where visible cracks appear and propagate until fracture.

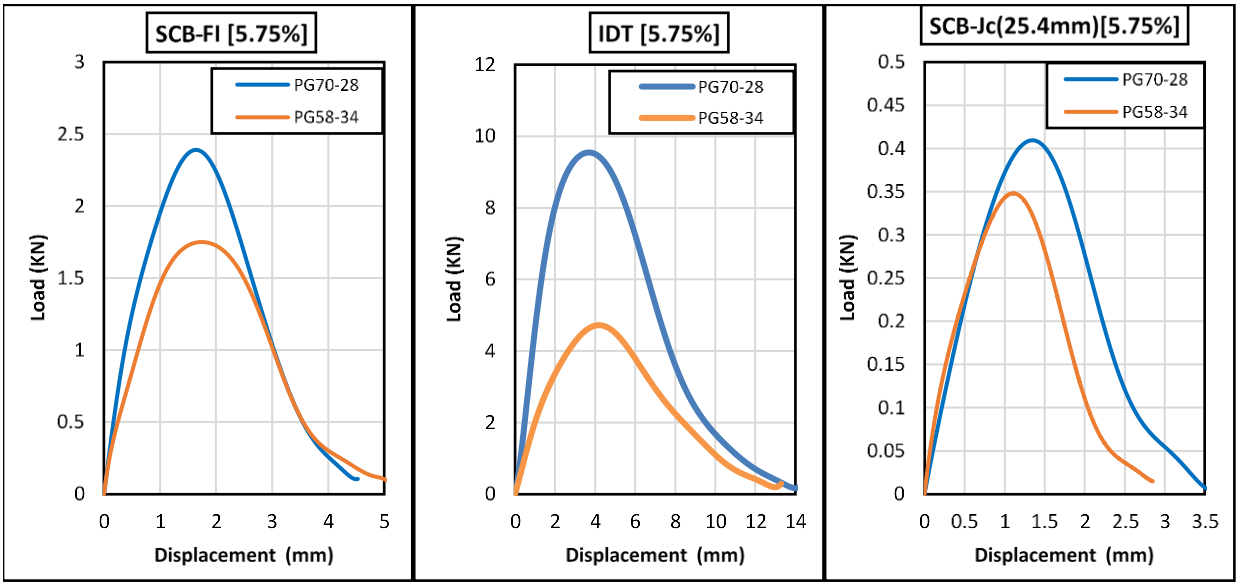

Figure 34 Typical Load-displacement Curve from IDT, SCB-J_c, and SCB-FI tests for LMLC Mixture PG 70, 5.75 Percent

Monotonic Cracking Resistance Indicators

Several performance parameters or indicators were used to analyze the load-displacement curve to assess the resistance of asphalt mixes to cracking. These indicators use one or more elements of the load-displacement curve to describe mixture performance. In this study, we assessed various performance indicators that were proposed in the literature, and developed a new and innovative performance indicator to assess the cracking resistance of asphalt mixes.

Review of Current Performance Indicators

The peak load (P_{Peak}) is the maximum load applied to the specimen until failure in the monotonic tests (Figure 35) and a measurement of a material's strength. Stiffer mixes often exhibit higher peak load compared to softer mixes. The peak load is determined as the maximum recorded load during the test.

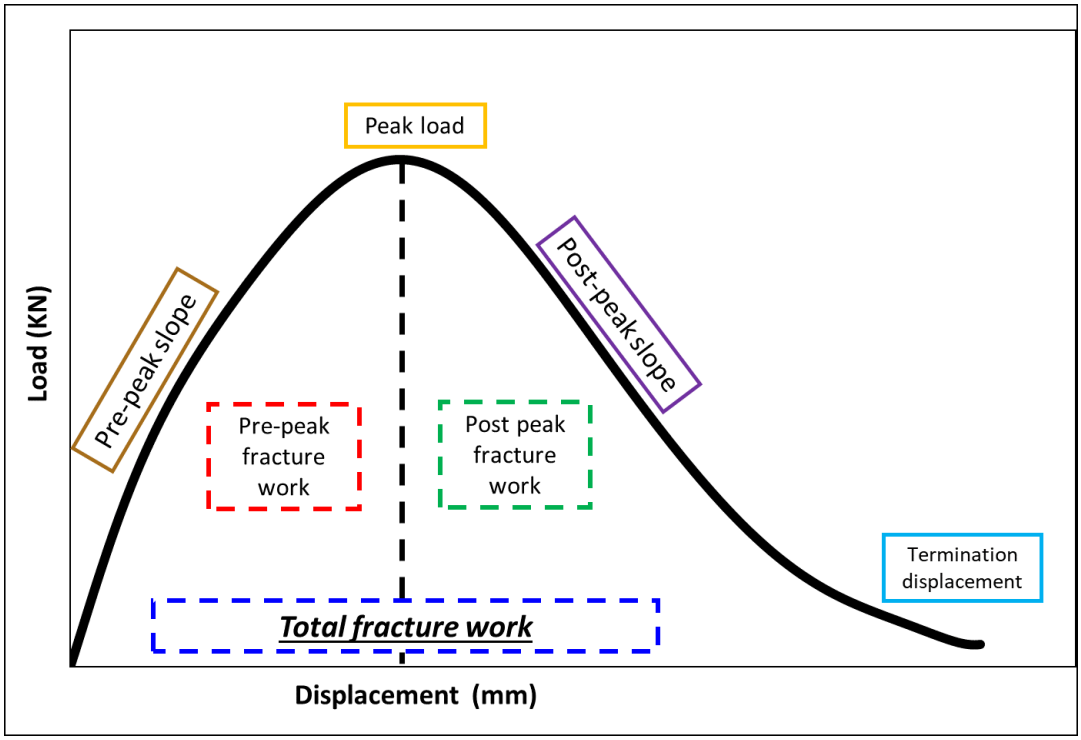

Figure 35 Load-displacement Basic Curve Elements

The fracture work is the area under the load-displacement curve (Figure 35). Three work-based performance indicators are identified; pre-peak work of fracture ($W_{Fracture}^{Pre-peak}$), post-peak work of fracture ($W_{Fracture}^{Post-peak}$) and total work of fracture ($W_{Fracture}^{Total}$) (Figure 36). The pre-peak work refers to the work required to initiate the cracks and it is computed as the area under the load-displacement curve until the peak load. The post-peak work refers to the work required for crack propagation and it is determined as the area under the load-displacement curve from the peak load until the failure point (test termination point). The total work of fracture refers to the total work needed to initiate and propagate the cracks and it is the summation of pre- and post-peak work.

$$W_{Fracture}^{Pre-peak} = \int_{0}^{Dis.\ at\ Peak\ load} (P.dx)$$

$$W_{Fracture}^{Post-peak} = \int_{Dis.\ at\ peak\ load}^{Dis.\ at\ test\ termination} (P.dx)$$

$$W_{Fracture}^{Total} = W_{Fracture}^{Pre-peak} + W_{Fracture}^{Post-peak}$$

Figure 36 Fracture Work Equations

where:

$W_{Fracture}^{Pre-peak}$ = Pre-peak work of fracture (J)

$W_{Fracture}^{Post-peak}$ = Post-peak work of fracture (J)

$W_{Fracture}^{Total}$ = Total work of fracture (J)

P = The applied load (KN)

X = Vertical actuator displacement (mm)

The fracture energy is defined as the energy needed to create a new unit fracture surface in the body [74]. It is a normalization of the fracture work by the cracking face area. The crack face area for Semi-Circular (SC) specimen is the ligament length (L_{lig}) (radius [r]- notch depth [a]) multiplied by specimen thickness (t) as presented in Figure 37 [35]. For circular specimen or IDT, the cracking face area is the specimen thickness (t) multiplied by specimen diameter (D) as presented in Figure 37 [73]. Similar to the fracture work, three fracture energy indicators are identified; pre-peak fracture energy ($Gf_{Pre\text{-}peak}$), post-peak fracture energy ($Gf_{Post\text{-}peak}$) and total fracture energy (G_f) (Figure 37). The pre-peak fracture energy is the consumed energy in crack initiation phase. The post-peak fracture energy is the consumed energy in the crack propagation phase. The total fracture energy is the energy consumed in crack initiation and propagation phases. Previous studies demonstrated that the total fracture energy is sensitive to the change in air void content, binder PG, and binder content [75]. The fracture energy decreases with the decrease in air void content and increase in binder content. Also, it increases with the increase in binder PG (i.e., stiffness) until a limit before it decreases [75].

$$SC_{crack\ face\ area} = (r - a)\ \times t$$

$$IDT_{crack\ face\ area} = D \times t$$

$$G_{Fracture}^{Pre-peak} = \frac{W_f^{Pre-peak}}{Crack\ face\ area}$$

$$G_{Fracture}^{Post-peak} = \frac{W_f^{Post-peak}}{Crack\ face\ area}$$

$$G_{Fracture}^{Total} = \frac{W_{Fracture}^{Total}}{crack\ face\ area}$$

Figure 37 Fracture Energy Equations

where:

$SC_{crack\ face\ area}$ = Crack face area for semi-circular specimen

r = Specimen radius (mm)

a = Specimen notch depth (mm)

t = Specimen thickness (mm)

$IDT_{crack\ face\ area}$ = The crack face area for circular specimen (mm^2)

$G_{Fracture}^{Total}$ = The total fracture energy (J/m^2)

$G_{Fracture}^{Pre-peak}$ = The pre-peak fracture energy (J/m^2)

$G_{Fracture}^{Post-peak}$ = The post-peak fracture energy (J/m^2)

$W_{Fracture}^{Pre-peak}$ = The pre-peak work of fracture (J)

$W_{Fracture}^{Post-peak}$ = The post-peak work of fracture (J)

$W_{Fracture}^{Total}$ = The total work of fracture (J)

The tensile strength is a normalization of the peak load (P_{peak}) with respect to specimen geometry. Several research studies investigated the calculations of the tensile stress of asphalt mixes using IDT and SCB tests [49,76–79]. Figure 38 is used to calculate the tensile strength using the IDT test [76]. Molenaar et al. (2002) proposed SCB tensile strength as an indicator for specimens without a notch (Figure 39) [77]. It is valid when the support span is 0.8 of specimen diameter. Huang et al. (2009) presented a generalized model that computes the tensile stress at various support span distances for specimen without a notch (Figure 40) [78]. Hofman et al. (2003) proposed a simple model for notched SCB specimen (Figure 41) [79]. The literature suggested that the tensile strength from SCB test is preferable than the IDT test. Walubita et al. (2010) demonstrated that IDT tensile strength overestimated the HMA mixes true tensile strength [80]. Also, Molenaar et al. (2002) reported that tensile strength from SCB is more accurate than IDT since the specimen is failed in tension cracking mode [77].

$$\sigma_{tesnile}^{\ IDT} = \frac{2000 \text{x} P_{Peak}}{\pi \times t \times D}$$

Figure 38 IDT Test Tensile Strength

$$\sigma_{tensile}^{\ SCB_{unnotched}} = \frac{4.8F}{D}$$

Figure 39 SCB Test Tensile Strength Proposed by Molenaar et al. (2002) [77]

$$\sigma_{tensile}^{\ SCB_{unnotched}} = \frac{6 \times P_{Peak} \times L_{support}}{t \times D^2}$$

Figure 40 SCB Test Tensile Strength Proposed by Huang et al. (2009)[78]

$$\boldsymbol{\sigma_{tensile}}^{\boldsymbol{SCB_{notched}}} = \frac{\mathbf{4.263} \times \boldsymbol{P_{Peak}}}{\mathrm{t}\times\mathbf{D}}$$

Figure 41 SCB Test Tensile Strength Proposed by Hofman et al. (2003) [79]

where:

$\sigma_{tesnile}^{IDT}$ = Tensile strength (kPa) determined from IDT test

$\sigma_{tensile}^{SCB_{unnotched}}$ = Tensile strength determined from the SCB (un-notched)

$\sigma_{tensile}^{SCB_{notched}}$ = Tensile strength determined from the SCB (notched)

P_{Peak} = Peak load (N)

t = Specimen thickness (mm)

D = Specimen diameter (mm)

F = Load per unit specimen width at failure (N/mm)

$L_{support}$ = Distance between the support span (mm)

The $IDT_{Modulus}$ (IDT Japan coefficient) is a normalization of IDT tensile strength with respect to the displacement at peak load as presented in Figure 42. This index is developed in Japan to assess the cracking resistance of RAP materials [81]. It serves as a measurement of a material strength and ductility. Asphalt mixture test specimens are prepared using 100 percent RAP and tested at a constant displacement rate of 50 mm/min at 20˚C. The test specimens should have a maximum $IDT_{Modulus}$ of 1.7 MPa/mm for acceptance [81]. A recent study by West et al. (2017) found that $IDT_{Modulus}$ has a moderate correlation (R^2 = 0.47) with field performance of eight Accelerated Loading Facility (ALF) test sections [59].

$$\mathrm{IDT_{modulus}} = \frac{\sigma_{\mathrm{Tensile}}{}^{\mathrm{IDT}}}{\mathrm{L_{Peak\ load}}}$$

Figure 42 $IDT_{Modulus}$ Equation

where:

$IDT_{Modulus}$ = Ratio of tensile strength to displacement at peak load (MPa)

$\sigma_{Tensile}^{IDT}$ = IDT tensile strength (MPa)

$L_{Peak\ load}$ = Displacement at the peak load (mm)

Al-Qadi et al. (2015) introduced and proposed the flexibility index (FI) as a normalization of the fracture energy with respect to the post-peak slope using an SCB test as presented in Figure 43 [35]. The post-peak slope is the slope of the post-peak part of the load-displacement curve which describes mixture's

flexibility or brittleness (Figure 35) [35,74,75,82]. Higher flexibility index indicates better flexibility and slower crack propagation and thus better cracking resistance. Al-Qadi et al. (2015) defined the post-peak slope as the tangent slope at the inflection point ($m_{Inflection}$) in the post-peak part of the load-displacement curve as presented in Figure 43.

Several research studies investigated the flexibility index as a cracking resistance indicator. Al-Qadi et al (2015) found the FI to have a good correlation with field performance of accelerated pavement test sections [35]. They proposed three cracking resistance performance categories: 1) poor cracking resistance (FI<2), intermediate cracking resistance (6.5 ≥ FI ≥ 2), and good cracking resistance (FI> 6.5). Hans et al. (2017) found that the FI is sensitive to the change in binder PG, RAP content, and aging conditions [83]. West et al. (2018) showed that FI has a strong direct Pearson correlation coefficient ($r > +0.8$) with Texas-Overlay Test (OT) and modified NCAT-Overlay tests (NCAT-OT)[43]. Also, it has a fair direct correlation (r of 0.3) with J_c parameter but FI showed better statistical mixture grouping compared to J_c. Kaseer et al. (2018) found FI is sensitive to change in binder PG, standard aging conditions, and RAP/RAS content, specimen thickness, and air void content [44]. Chen and Solaimanian (2018) demonstrated that FI is sensitive to binder content, binder PG, and air void content [75]. Kim et al. (2018) found that FI to increase with binder content and decrease with NMAS and the notch depth [84]. In the meantime, several studies documented some limitations of flexibility index at specific testing conditions [44,75,84]. For example, the FI showed an unexpected trend with the change in air void content and specimen thickness. The FI increased with the increase in air void content and decreased with the increase in specimen thickness. In addition, the FI was found to be highly affected by the post-peak slope [44,75,85]. An adjustment approach was proposed to normalize the FI with respect to air void content and sample thickness as presented in Figure 43 [35,44,86,87].

$$\mathrm{FI} = 0.01 * \frac{G_{Fracture}^{Total}}{\left|m_{\mathrm{Inflection}}^{Post-peak}\right|}$$

$$m_{\mathrm{Inflection}}^{Post-peak} = \frac{dy}{dx}[P = f(x)], \text{when } \frac{dy^2}{dx^2}[P = f(x)] = 0\,,$$

$$\mathrm{FI}_{50} = \mathrm{FI}_{\mathrm{t}} \times \frac{\mathrm{t}}{50} = 0.01 * \frac{G_{Fracture}^{Total}}{\left|m_{\mathrm{Inflection}}^{Post-peak}\right|} \times \frac{\mathrm{t}}{50}$$

$$FI_{7\%} = FI_{AV} \times \frac{7\%}{\mathrm{AV\%}}$$

$$FI_{\mathrm{AV\%}} = FI_{AV} \times \frac{0.0651}{\mathrm{AV}\text{-}AV^2}$$

Figure 43 Flexibility Index Equations

where:

FI	= Flexibility index
$G_{Fracture}^{Total}$	= Total fracture energy (J/m^2)
$m_{\mathrm{Inflection}}^{Post-peak}$	= Post-peak inflection point
t	= Specimen thickness (mm)
FI_{50}	= Adjusted flexibility index at specimen thickness of 50 mm
FI_{t}	= Flexibility index at specimen thickness t
$FI_{7\%}$	= Adjusted flexibility index at specimen's air void content of 7 percent
FI_{AV}	= Flexibility index at air void content AV. AV percent is the specimen air void

Zhou et al. (2017) proposed a new cracking resistance index called IDEAL-CT$_{\mathrm{Index}}$, which is a normalization of the fracture energy with respect to the post-peak slope and strain tolerance using the IDT test (Figure 44)[73]. The post-peak slope is determined as the tangent slope at 75 percent of the peak load ($m_{75\%}^{Postpeak}$) as presented in Figure 44. The strain tolerance ($\varepsilon_{\mathrm{v}}{}^{tolerance}$) is defined as the vertical strain until 75 percent of peak load (Figure 44). Higher IDEAL-CT$_{\mathrm{Index}}$ demonstrates better resistance to cracking. A number of studies evaluated the IDEAL-CT$_{\mathrm{Index}}$ as a cracking resistance indicator. Zhou et al. (2017) found that IDEAL-CT$_{\mathrm{Index}}$ to capture the change in RAP content, binder type, binder content, aging, and air void content [73]. However, the results had unexpected trends with air void content similar to flexibility index, where IDEAL-CT$_{\mathrm{Index}}$ increased with the increase in air voids. The IDEAL-CT$_{\mathrm{Index}}$ showed a strong correlation with field cracking resistance (R^2 = 0.87). Dong and Charmot (2019) found that the IDEAL-

CT_{Index} to increase with emulsion content and decrease with the decrease in binder content [88]. Bennert et al. (2018) evaluated the IDEAL-CT_{Index} as a quality control parameter in New Jersey [89]. They found a good correlation between IDEAL-CT_{Index} and overlay tester (OT); however, the IDEAL-CT_{Index} had lower variability in test results compared to OT. Currently, ASTM subcommittee D04.26 published a standardized method to calculate IDEAL-CT_{Index} using IDT test (ASTM D8225 – 19)[90].

$$CT_{Index} = \frac{G_{Fracture}^{Total}}{\left| m_{75\%}^{Postpeak}) \right|} \times \frac{t}{62} \times \varepsilon_v{}^{tolerance}$$

$$m_{75\%}^{Post-peak} = \left| \frac{P_{85\%} - P_{65\%}}{L_{85}\% - L_{65\%}} \right|,$$

$$\varepsilon_v{}^{tolerance} = \frac{L_{75\%}^{Postpeak}}{D}$$

Figure 44 IDEAL-CT_{Index} Equation

where:

CT_{Index} = Cracking test index

$G_{Fracture}^{Total}$ = Total fracture energy (J/m^2)

$m_{75\%}^{Postpeak}$ = Post-peak slope at 75 percent of the peak load

$\varepsilon_v{}^{tolerance}$ = Strain tolerance

T = Specimen thickness (mm)

$L_{75\%}^{Postpeak}$ = Displacement at 75 percent of peak-load.

P_{65}%, and P_{85}%, = Post peak load at 65% and 85% of the peak load (KN) respectively

The Cracking Resistance Index (CRI) is a normalization of the fracture energy with respect to the peak load (Figure 45). Kaseer et al. (2018) proposed the CRI to overcome the limitations of the FI (e.g., high variability, difficult computation process, and brittle mixes assessments (i.e., no post-peak data) [44]. Higher CRI values demonstrate better cracking resistance. Kaseer et al (2018) reported that CRI is sensitive to the change in binder grade, aging conditions, RAP/RAS content, specimen thickness, and air void content [44]. They found a strong correlation between CRI and FI (R^2 > 0.90); however, the CRI had lower variability, simple calculation procedures, and can differentiate between more mixes with different performance (Tukeys groups) compared to FI. Kaseer et al (2018) proposed equations to normalize CRI with respect to air void contents and specimen thickness as shown in Figure 45 [44].

$$CRI = \frac{G_{Fracture}^{Total}}{P_{Peak}}$$

$$CRI_{50} = CRI_t \times \frac{t}{50}$$

$$CRI_{7\%} = CRI_{AV} \times \frac{7\%}{AV\%}$$

Figure 45 Cracking Resistance Index (CRI) Equations

where:

CRI = Cracking resistance index (J/m^2.KN)

CRI_{50} = CRI value at 50 mm thickness

$G_{Fracture}^{Total}$ = Total fracture energy (J/m^2)

t = Specimen thickness (mm)

AV% = Specimen air voids

CRI_{50} = Adjusted CRI at specimen thickness of 50 mm (J/m^2.KN)

$CRI_{7\%}$ = Adjusted CRI at specimens' air void contents of 7%

West et al. (2017) proposed the Nflex parameter as a normalization of the mixture toughness with respect to the post-peak slope using the IDT test (Figure 46) [59]. The post-peak slope was determined as the tangent slope at the post-peak inflection point ($M_{\text{inflection}}^{Postpeak}$) under the stress-strain curve (Figure 46). Toughness was calculated as the area until the post-peak inflection point (Figure 46). The stress and strain were calculated using Figure 46. They studied the correlation between Nflex and field cracking resistance of eight ALF test sections. The results showed a reasonable correlation between Nflex and cracking resistance (R^2 = 0.55). Yin et al. (2018) found that Nflex had insignificant statistical sensitivity to binder PG and binder content and a significant sensitivity to RAP content and test temperature [91]. They reported that considering a constant Poisson's ratio may provide an inaccurate determination of Nflex [91]. Yin et al. (2018) found that the measured Poisson's ratio had a significant dependency on specimen air void content and test temperature. They recommended to estimate the Poisson's ratio using the secant approach as shown in Figure 46. This approach requires measuring the horizontal and vertical deformation during the IDT test which adds more complexity to the test setup and data analysis.

$$N_{flex} = \frac{\text{Toughness}}{m}$$

$$m_{inflection}^{Postpeak} = \frac{dy}{dx}[\sigma = f(\varepsilon_i)], \text{ when } \frac{dy^2}{dx^2}[P = f(\varepsilon_i)] = 0$$

$$\text{Toughness} = \int_0^{\text{Strain at } m_{inflection}^{Postpeak}} (\sigma . d\varepsilon)$$

$$\varepsilon_i = \frac{L_i \times \mu}{D}$$

$$\mu = 0.15 + \frac{0.35}{1 + e^{(a+bS_c)}}$$

Figure 46 Nflex Factor (Nflex) Equations

where:

N_{flex} = Nflex factor

$m_{\text{inflection}}^{Postpeak}$ = Tangent slope at post peak inflection point (kPa/ %)

σ_i = Estimated tensile stress at load i (kPa)

ε_i = Estimated tensile strain at load i (%)

toughness = Area under stress-strain curve until post peak inflection point

L_i = Vertical deformation at load i (m)

D = Specimen diameter (m)

μ is = Poisson's ratio

a and b = Regression fitting coefficients

S_c = Secant modulus defined as the ratio of peak load to displacement at peak load

Critical Strain Energy Release Rate (J_c) is defined as "a path independent integration of strain energy density, traction, and displacement along an arbitrary contour path around the crack" [92]. It describes the change in strain energy per unit depth with specimen notch depth (dU/da) (Figure 47) [92]. The strain energy to failure (U) is determined as the pre-peak work of fracture ($W_{Fracture}^{Pre-peak}$) as presented in Figure 47. The variation of strain energy with notch depth (dU/da) is normalized by the thickness (t). The J_c can be determined using two or three notch depths. Elseifi et al (2005) suggested using three notch depths for better determination of J_c [93]. Several researchers evaluated the use of J_c as performance indicator.

Bayomy et al. (2006) found that J_c to increase with binder content and the percentage of rough and angular aggregates and to decrease with the increase in percentage of flat and elongated aggregates in the mix. In addition, the J_c decreases for finer aggregate gradation [92]. Cao et al. (2018) found that J_c to decrease with RAP content [94]. Mohammad et al. (2012) found good correlation between J_c and field cracking resistance [39]. Louisiana Department of Transportation and Development (LADOTD) requires that mixes should have minimum J_c of 0.5 kJ/m^2 and 0.6 kJ/m^2 for Level 1 and Level 2 mix design, respectively [15].

$$J_c = -\left(\frac{1}{t}\right)\frac{dU}{da}$$

$$W_{Fracture}^{Pre-peak} = \int_0^{Dis.\ at\ Peak\ load}(P.dx)$$

Figure 47 Critical Strain Energy Release Rate (J_c) Equations

where:

J_c = Strain energy release rate (kJ/m^2)

U = Strain energy to failure (kJ)

t = Specimen thickness (mm)

a = Specimen notch depth (mm)

dU/da = Variation of strain energy with notch depth (kJ/mm)

$W_{Fracture}^{Pre-peak}$ = Pre-peak work of fracture (J)

P = Applied load (KN)

x = Vertical actuator displacement (mm)

Development of Weibull Cracking Resistance Index ($WEIBULL_{CRI}$)

As discussed in this chapter, various parameters were proposed to analyze the load-displacement curve of different monotonic tests to assess the performance of asphalt mixes to resist cracking. These parameters use one or more elements of the load-displacement. For instance, $IDT_{strength}$ uses the curve peak, fracture energy uses the area under the curve, CRI uses the area under the curve and peak load, while FI uses the area under the curve and post-peak slope. One or two elements cannot describe the entire load-displacement curve, and none of the current indicators can describe the overall variation in the load-displacement curve. Therefore, there is a need to develop alternative parameters to describe

the entire load-displacement curve and propose a performance indicator that can be used to evaluate the resistance of asphalt mixture to cracking. In this study, we used the Weibull distribution function to describe the entire load-displacement curve and used the fitting parameters to propose a performance indicator for cracking resistance [95]. This section discusses the development and analysis procedures for the proposed method.

For the load-Displacement Curve Fitting, the Weibull probability density function can be used to describe the load-displacement curve. Figure 48 presents a modified version of Weibull function where a scaling factor was added (i.e., parameter A). Figure 49 shows an example of using the proposed equation to fit the load-displacement curve from the IDT test. This function fits the entire curve data with excellent accuracy (coefficient of determination [R^2] = 0.997). In addition, Figure 49 demonstrates that the 95 percent confidence interval bands provide an accurate estimate of the measured values. The curve fitting is performed using Iterative Nonlinear Least Squares Fitting (INLSF) regression method. Brown (2001) presented simple fitting procedures using Excel SOLVER tool [96]. The fitting is optimized by providing a minimum Sum of Squared Errors (SSR) between the measured and the predicted load/stress values (Figure 50). Excel Solver requires an initial estimation of the fitting parameters. Table 22 provides recommended initial values for fitting parameters (i.e., A, β, η) for various testing protocols (e.g., IDT, SCB, and disk-shaped tests). The Standard Error (SE), coefficient of determination (R^2), and 95 percent confidence intervals (CI) can be computed using Equations presented in Figure 50.

$$P = A \times \left(\frac{\beta}{\eta}\right)\left(\frac{u}{\eta}\right)^{\beta-1} \times e^{-(\frac{u}{\eta})^{\beta}}$$

Figure 48 Modified version of Weibull Function

where:

P = The applied load (KN) or stress (kPa)

u = The measured displacement (vertical displacement or Crack Mouth Opening Displacement CMOD) or strain (percent)

β = Shape parameter (Weibull slope)

η = Scale parameter

A = Scaling factor equals to the area under the load-displacement curve

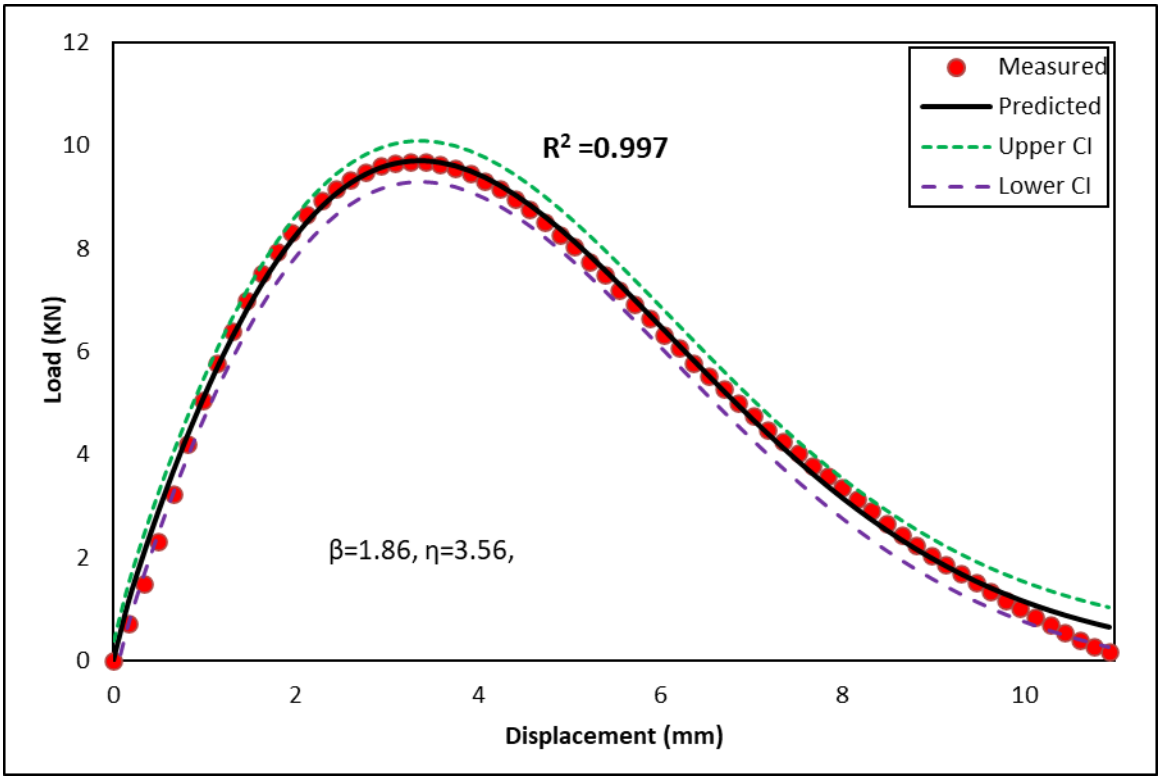

Figure 49 Fitting Results of the Load-displacement Curve using Modified Weibull Function

$$SSR = \sum_{i=1}^{n} [P_{measured} - P_{predicted}]^2$$

$$SE = \frac{SSR}{df}$$

$$R^2 = 1 - \frac{SSR}{\sum_{i=1}^{n} [P_{measured} - P_{mean}]^2}$$

$$CI = t_{critial} \times SE$$

Figure 50 Fitting Accuracy Check Tools

where:

SSR = The sum of squared error

$P_{measured}$ = The measured load/stress at displacement/strain i

$P_{predicted}$ = The predicted load/stress at displacement/strain i

i = Counter

n = Number of measured data points

df = Degrees of freedom ($df = n - 3$)

P_{mean} = The average value of measured load

$t_{critial}$ = The critical t value at 95 percent confidence interval

Table 22 Initial Values for Fitting Parameters based on Different Test Data Sources

Test data source	Initial proposed values	Initial proposed values	Initial proposed values
Test data source	Fitting Parameters	Fitting Parameters	Fitting Parameters
Test data source	A	β^{**}	η
IDT (stress-strain)	2000	1.80	2.30
IDT (load-displacement)	50.0	1.80	2.30
SCB intermediate temperature (load-displacement)	3.0	1.80	1.60
SCB Low temperature (load-displacement)	0.5	1.30	0.10
Disk shaped (Load -CMOD)	0.8	2.00	0.30

*Load is in KN, displacement in mm, stress in kPa, strain in percent, CMOD in mm
** β shall be larger than 1

For the interpretation of the Variation in the Load-displacement Curve Shape using Weibull Fitting Parameters, we used the fitting parameters (i.e., A, β, η) and proposed a performance indicator to evaluate the resistance of asphalt mixture to cracking. We first studied the effect of individual fitting parameters on the overall curve to fully understand its effect and how this may affect the resistance to cracking. Figures 51 through 53 demonstrate the effect of model parameters "*A*", "β", and "η" of the shape of the stress-strain curve of IDT test, respectively. The increase in the scale factor "A" pulls the peak of the curve upwards causing increased area under the curve, increased peak load, and increased pre- and post-peak slopes (Figure 51), which indicates improved mixture cracking resistance. The increase in the shape parameter "β", pulls the curve peak upwards and to the right causing an increase in pre- and post- peak and decrease in terminal strain (strain at 20 kPa), which demonstrates decreased cracking resistance (Figure 52). The increase in the scale parameter "η" pulls the curve downward resulting in a decrease in pre- and post-peak slopes and an increase in the terminal strain, which demonstrates increased cracking resistance as shown in Figure 53.

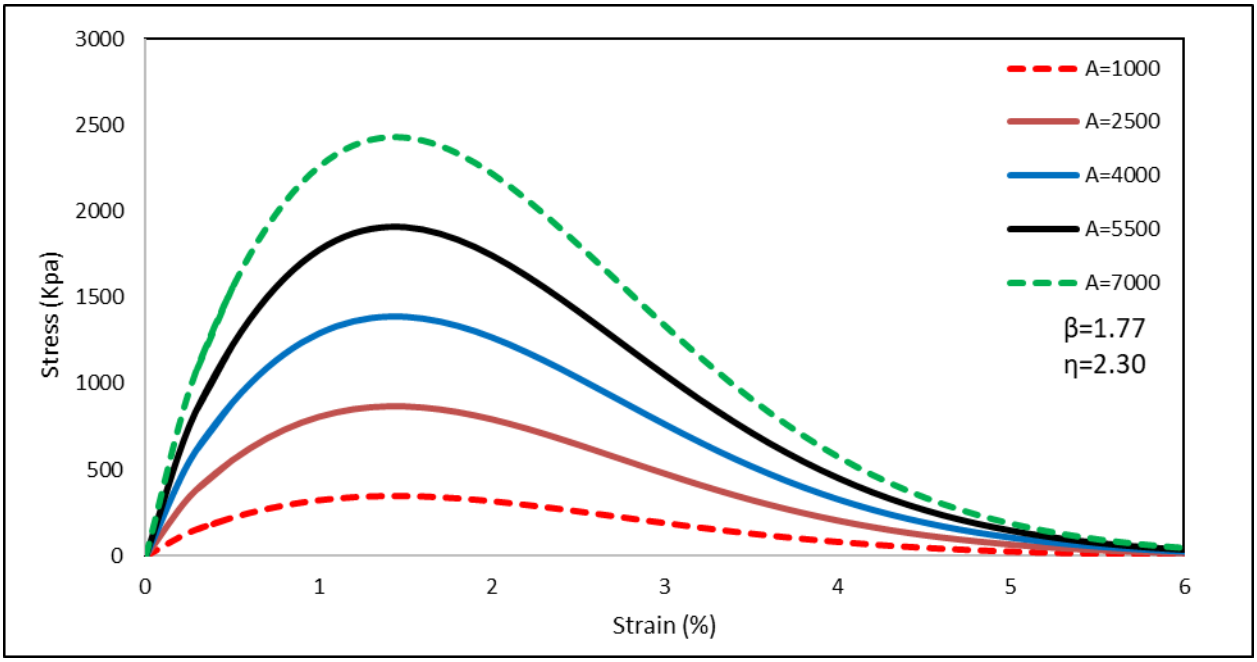

Figure 51 Effects of A parameter on the Stress-Strain Curve Shape

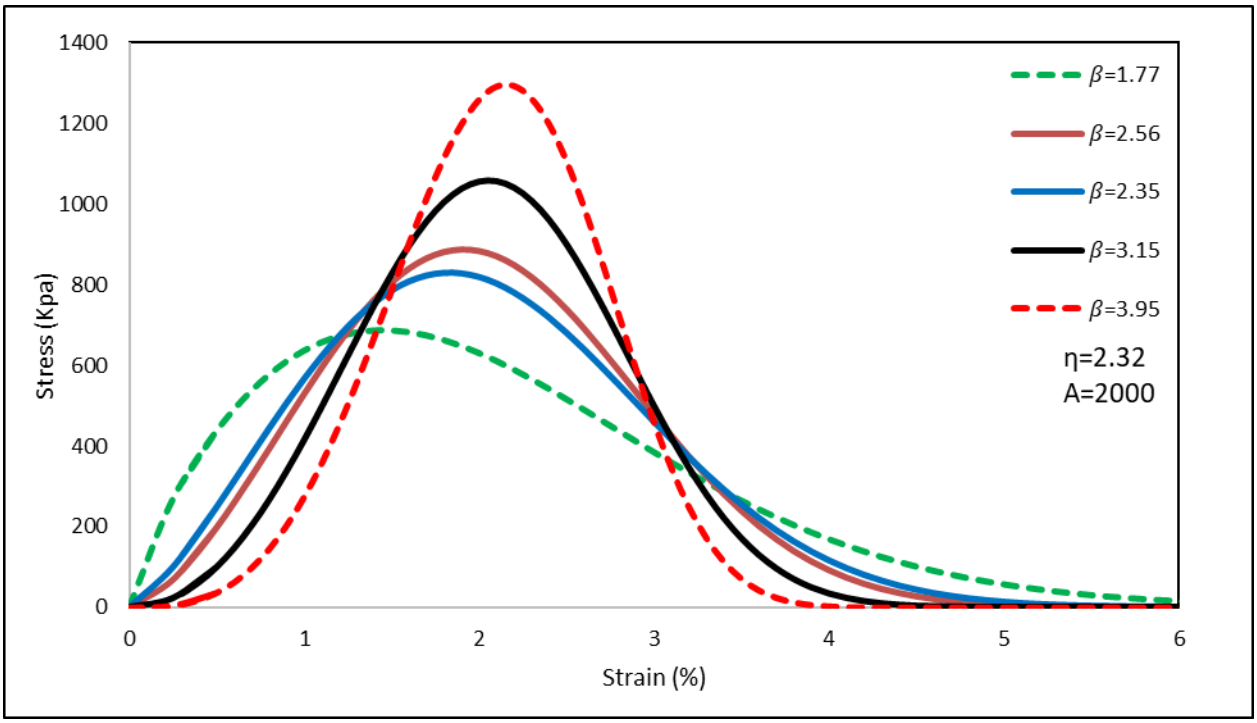

Figure 52 Effects of β Parameter on the Stress-Strain Curve Shape

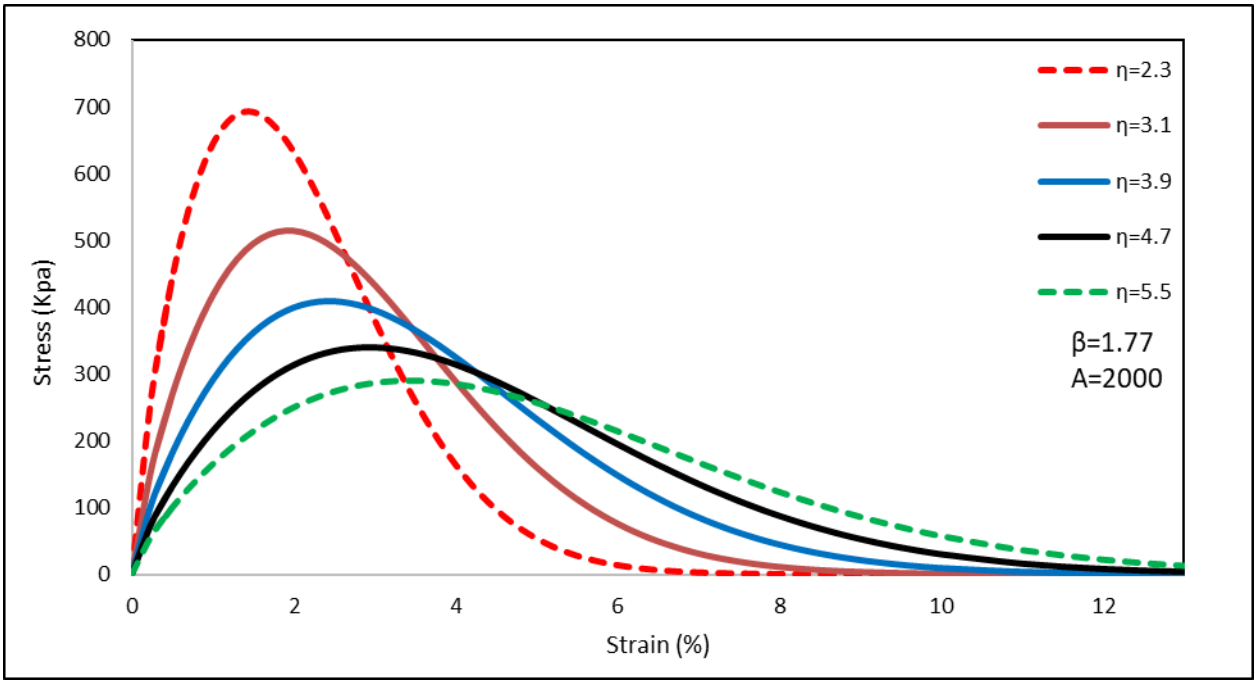

Figure 53 Effects of η Parameter on the Stress-Strain Curve Shape

The development of Weibull Cracking Resistance Index (WeibullCRI) was based on the findings of the previous section on the effect of fitting parameters of the modified Weibull function. The research team proposed an index called Weibull Cracking Resistance Index ($Weibull_{CRI}$). The $Weibull_{CRI}$ can be used as a performance indicator to evaluate the resistance of asphalt mixture to cracking. Figure 54 presents the proposed $Weibull_{CRI}$. This performance indicator is proposed based on the effect of fitting parameters on the shape of load-displacement or stress-strain curve. This $Weibull_{CRI}$ increases with the scale parameter "η" and scaling factor "A", while it decreases with the increase in the shape parameter "β". Higher $Weibull_{CRI}$ indicates better cracking resistance. Figure 54 includes an equation to normalize the $Weibull_{CRI}$ with respect to air void content and specimen thickness. The $Weibull_{CRI}$ is checked against other performance indicators derived from the monotonic tests as well as dynamic testing as discussed in detail in Chapter 5.

$$Weibull_{CRI} = \left(\frac{\eta}{\beta}\right) \times log[A]$$

$$Weibull_{CRI} = \left(\frac{\eta}{\beta}\right) \times log\left[A \times \left(\frac{7\%}{AV}\right) \times \left(\frac{50}{t}\right)\right]$$

Figure 54 Weibull Cracking Resistance Index Equations

where:

β = Shape parameter (Weibull slope)

η = Scale parameter

A = Fitting constant equals to the area under the load-displacement curve

t = thickness

AV = air void content

Development of Multi-Stage Semi Circle Bending Dynamic (MSSD) Test

Motivation

As discussed in the previous sections, the monotonic tests (e.g., IDT, SCB, etc.) are often used to evaluate the performance of asphalt mixes to cracking. The monotonic tests require less testing time, inexpensive testing setup, and they are simple to perform and analyze the data compared the dynamic tests. Meanwhile, fatigue cracking in asphalt mixes is initiated and propagated due to repeated traffic loading at intermediate temperature. Thus, dynamic tests are more appropriate to evaluate the resistance of asphalt mixtures to this type of cracking. However, there are several challenges associated with conducting dynamic testing of asphalt mixes including 1) longer testing time, 2) complex testing setup, 3) complicated sample preparation and instrumentation, 4) determination the proper testing conditions and protocols (e.g., proper stress level if stress-controlled test or strain level if strain-controlled test), and 5) higher variability of the test results.

The research team developed and proposed an alternative dynamic test called Multi-Stage Semi-circle bending Dynamic or (MSSD) test. The MSSD aims to address the limitations associated with the current dynamic tests. The MSSD test simulates the repeated loading (dynamic) in reasonable testing time, has a fixed loading sequence that works for mixes with different characteristics (e.g., mixture composition, percent air voids, thickness, etc.) and still utilizes similar testing equipment and specimen geometry used in monotonic tests. Table 23 summarizes the advantages of the proposed MSSD test compared to monotonic tests and other dynamic tests (e.g, Bending Beam Fatigue [BBF] test).

The MSSD and BBF apply a repeated load, while monotonic tests apply loading and a constant displacement rate. The dynamic tests simulate the true pavement fatigue cracking development behavior while monotonic tests use performance indicators to describe mixture cracking performance. Monotonic tests require short testing time (<30 minutes), while BBF testing time varies (from a few hours to several days) [70]. The MSSD requires shorter testing time (maximum of 9 hours) regardless of mixture characteristics. In addition, MSSD uses a SCB test specimen which is easy to prepare in the laboratory compared to the beams used in the BBF test. The MSSD can be used during the mix design to ensure adequate resistance to cracking while monotonic tests can used during the mix production and pavement construction to check the quality of the asphalt mix and its placement.

Table 23 Comparison between Monotonic, Fatigue, and MSSD Tests

Criteria	Monotonic (e.g., SCB, IDT)	MSSD	Bending Beam Fatigue
Loading	Constant displacement rate	Repeated load	Repeated load
Testing time	1-2 hour	<9 hours	30 minutes-several days
Specimen preparation	Easy	Easy	Difficult
Specimen geometry	Semi-circular and circular	Semi-circular	Beam
Evaluation of field cores	Yes	Yes	No
Testing system complexity	Simple	Simple	Complex
Equipment cost	Low (< $20,000)	Intermediate (< $80,000)	High (> $200,000)

Test Conditions

The MSSD test uses a semi-circular testing specimen with a radius of 75 mm and a notch depth of 15 ±1 mm. The thickness of the laboratory compacted test specimens is 50 mm, while the thickness of field cores can vary between 25 mm to 50 mm depending on the lift thickness. Figure 55 shows the schematic of the test setup. The support span of the test fixture is 120 mm. The test is performed at 25 °C and can be conducted using the Asphalt Mixture Performance Test (AMPT) machine or other servo hydraulic testing system (e.g., Universal Testing Machines [UTM], or Material Testing System [MTS]). In this study, the AMPT was used (Figure 58). The AMPT is available in typical materials and pavement laboratories and simple to operate and use compared to other systems.

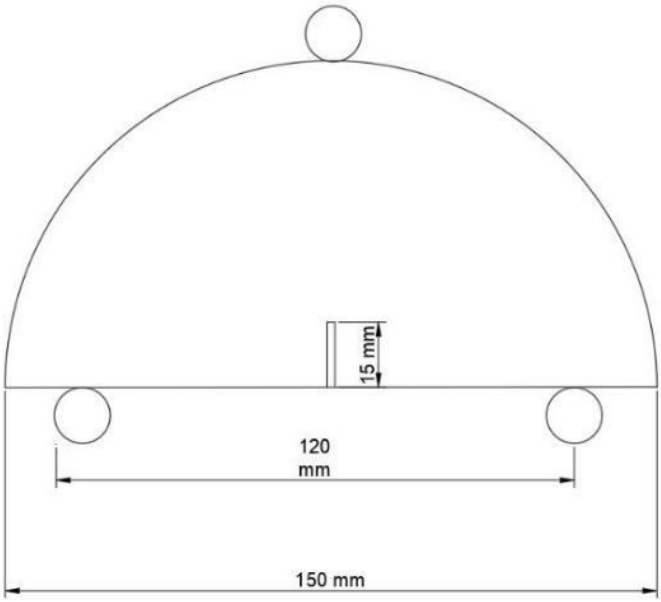

Figure 55 Schematic MSSD Test Specimen and Fixture

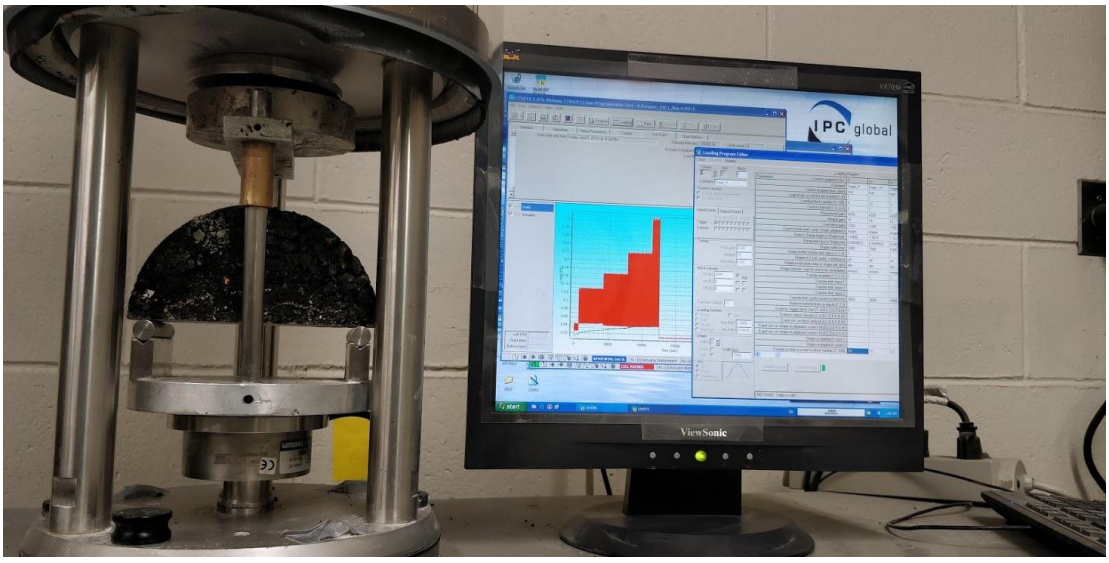

Figure 56 MSSD Test Fixture Inside the AMPT Chamber

Theory and Concept

For a notched test specimen (e.g., semi-circular), the magnitude of the stresses at the notch tip is a function of the specimen geometry and applied loading [97]. In Linear Elastic Fracture Mechanics (LEFM), the Stress Intensity Factor (SIF or K) describes the stress state at the notch tip after accounting for the effect of loading and geometry [97]. The SIF increases with an increase of in the applied load until reaching a critical value (fracture toughness [K_{IC}]), which is associated with crack initiation [72]. The fracture

toughness is computed at the critical load which is assumed to be the peak load [72]. The MSSD applies a series of compressive loads to a SCB test specimen with one notch (15 mm) that produce predetermined stress intensity factors. Figure 58 shows a flow chart that was used to select the applied loads at various stages. We used the monotonic test data that was conducted in accordance with AASHTO TP124 to select the dynamic loading levels. A total of 106 samples were tested. The test specimens included 17 field projects, 10 PMLC mixes, and six LMLC mixes. The fracture toughness for each specimen was computed using a model developed by Lim et al. (1993) as presented in Figure 57 [98]. This model is used in AASHTO TP105 and several research studies to estimate fracture toughness of asphalt mixes [72,99–103].

$$\frac{K_I}{\left(\sigma\sqrt{\pi a}\right)} = Y_{1_{\left(\frac{S0}{r}\right)}} + \frac{\Delta S_0}{r} B \qquad \text{for } 0.5 \leq \frac{S_a}{r} \geq 0.8$$

Figure 57 Stress Intensity Factor Equation Proposed by Lim et al. (1993) [98]

where:

K_I = Stress Intensity Factor for mode I loading ($N/mm^{3/2}$)

$\frac{S_a}{r}$ = Ratio of support span (S_a) to specimen radius (r)

$\frac{S_0}{r}$ = Ratio of support span (S_0) to specimen radius (r) used by lim et al (1993)

$\frac{\Delta S_0}{r}$ = $\frac{S_a - S_0}{r}$

σ = Tensile stress; $\sigma = \frac{P}{D \times t}$

P = Load (KN)

t = Specimen thickness (mm)

D = Specimen diameter (mm)

$Y_{1_{\left(\frac{S0}{r}\right)}}$ = Normalized SIF at predetermined (S_0/r) ratio

$Y_{1_{\left(\frac{S0}{r}\right)}} = C_1\text{-}C_2\left(\frac{a}{r}\right) + C_3 exp\left(C_4\left(\frac{a}{r}\right)\right)$,

C_1, C_2, C_3, C_4 = Regression constants

a = Specimen notch depth (mm)

$B = 6.55676 + 16.64035\left(\frac{a}{r}\right)^{2.5} + 27.97042\left(\frac{a}{r}\right)^{6.5} + 215.0839\left(\frac{a}{r}\right)^{16}$ for $0.03 \leq \frac{a}{r} \geq 0.8$

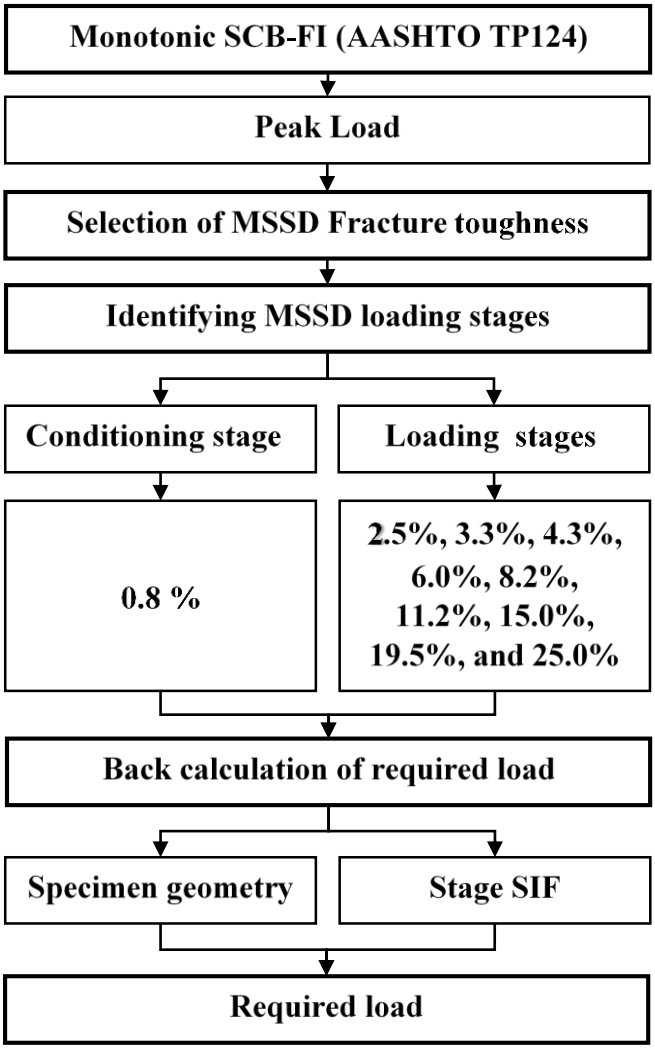

Figure 58 Flow Chart for MSSD Testing Stage Identification Procedures

Figure 59 shows the computed fracture toughness for the test specimens from the monotonic loading. Field projects had an average fracture toughness of 21.49 N/mm$^{3/2}$ and ranged between 8.72 N/mm$^{3/2}$ and 37.91 N/mm$^{3/2}$. PMLC mixes had an average fracture toughness of 19.62 N/mm$^{3/2}$ and ranged between 9.75 N/mm$^{3/2}$ and 34.68 N/mm$^{3/2}$. LMLC mixes had an average fracture toughness of 10.61 N/mm$^{3/2}$ and ranged between 5.01 N/mm$^{3/2}$ and 23.80 N/mm$^{3/2}$. The field projects had the highest fracture toughness compared to PMLC or LMLC mixes. The researchers believe that this is attributed to the aging effect. Field cores are aged (stiffer) compared to PMLC or LMLC mixes. As shown in Figure 59, all mixes had fracture toughness between 5.01 and 37.91 N/mm$^{3/2}$. Selection of appropriate fracture toughness for the dynamic test is needed to avoid premature failure or extended testing time. Therefore, we selected a fracture toughness of 24 N/mm$^{3/2}$ for this purpose.

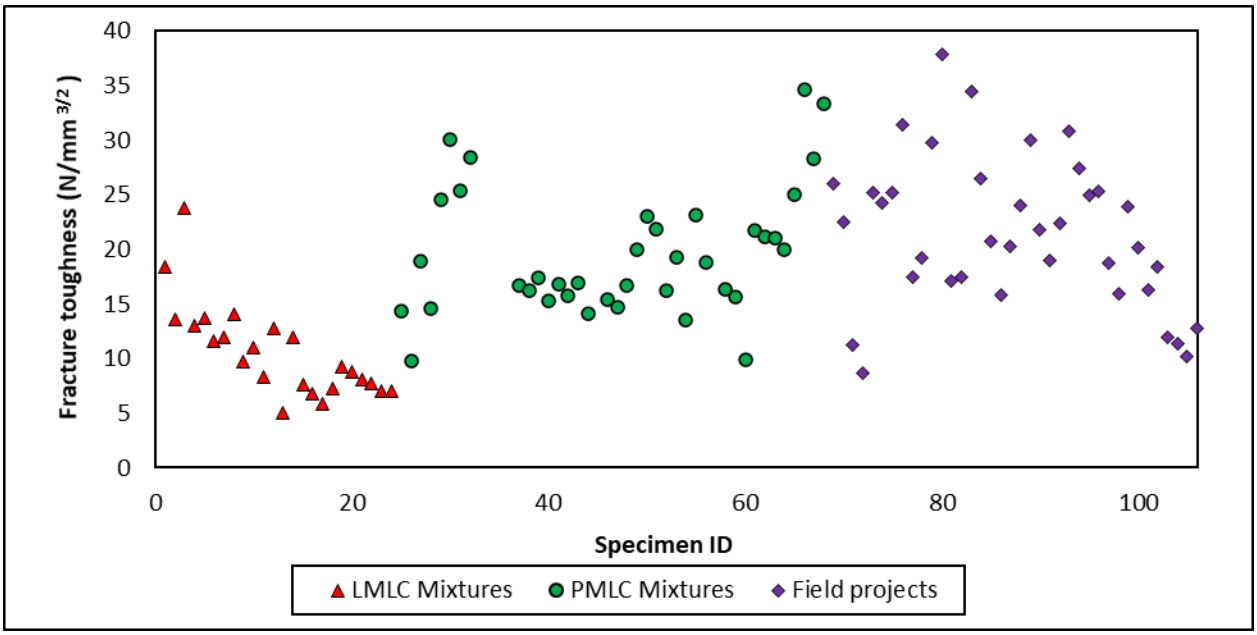

Figure 59 Computed Fracture Toughness for Monotonic SCB Specimens

As mentioned earlier, the MSSD applies a series of compressive loads that produce a predetermined series of SIF factors on the SCB test specimen. We selected a ten predetermined SIF that associated with ten loading stages, including one conditioning stage (stage-0) and nine loading stages (Stage-1 to Stage-9). Each loading stage applied a continuous haversine loading wave with a frequency of 1Hz (Figure 60). Each wave resulted in change in stress intensity factor of (ΔK) of K_{max}-K_{min}. The K_{max} is the stress intensity factor associated with maximum applied load, while K_{min} is the stress intensity factor associated with the setting load (Figure 60). In the MSSD test, the K_{min} and K_{max} were predetermined for each loading stage. K_{min} was selected as 0.12 N/mm$^{3/2}$ for the conditioning stage and 0.2 N/mm$^{3/2}$ for all loading stages. K_{max} was determined as a percent of the MSSD fracture toughness value (24 N/mm$^{3/2}$). Figure 61 shows the selected percent for each loading stage. Figure 62 shows K_{min}, K_{max}, and ΔK for each loading stage of the nine stages of the test. These stress intensity values were used to estimate the required compressive applied load using the equation presented in Figure 63.

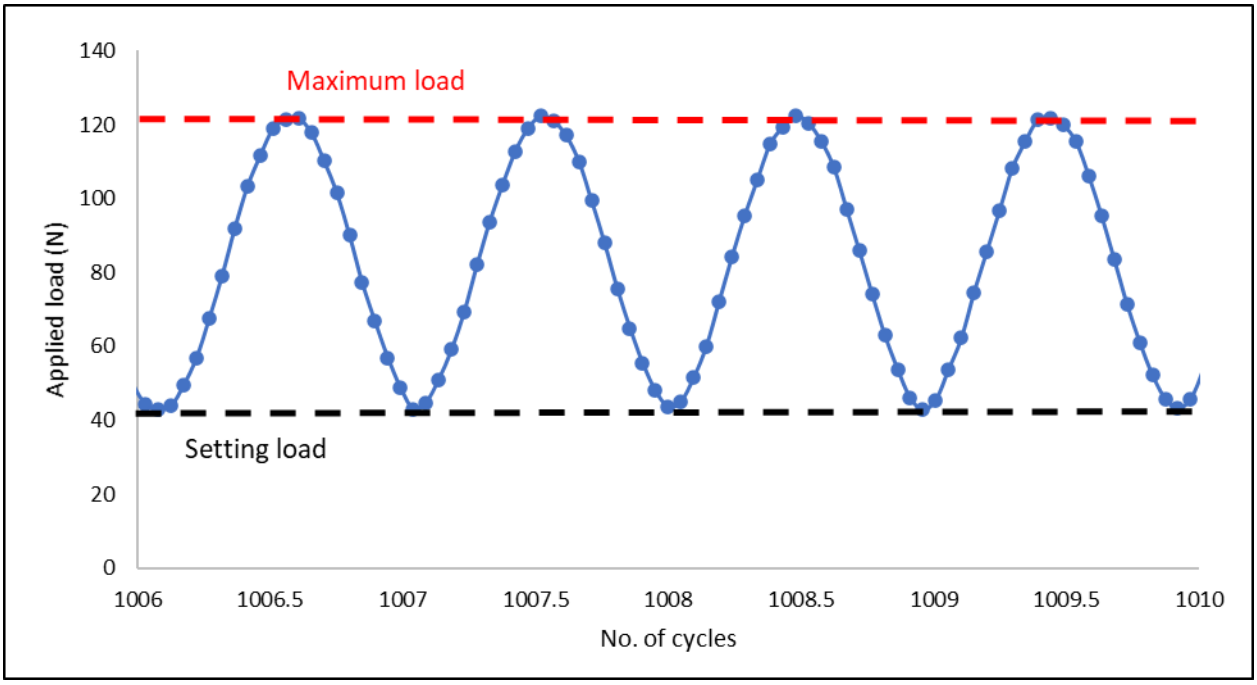

Figure 60 MSSD Continuous Haversine Loading Wave

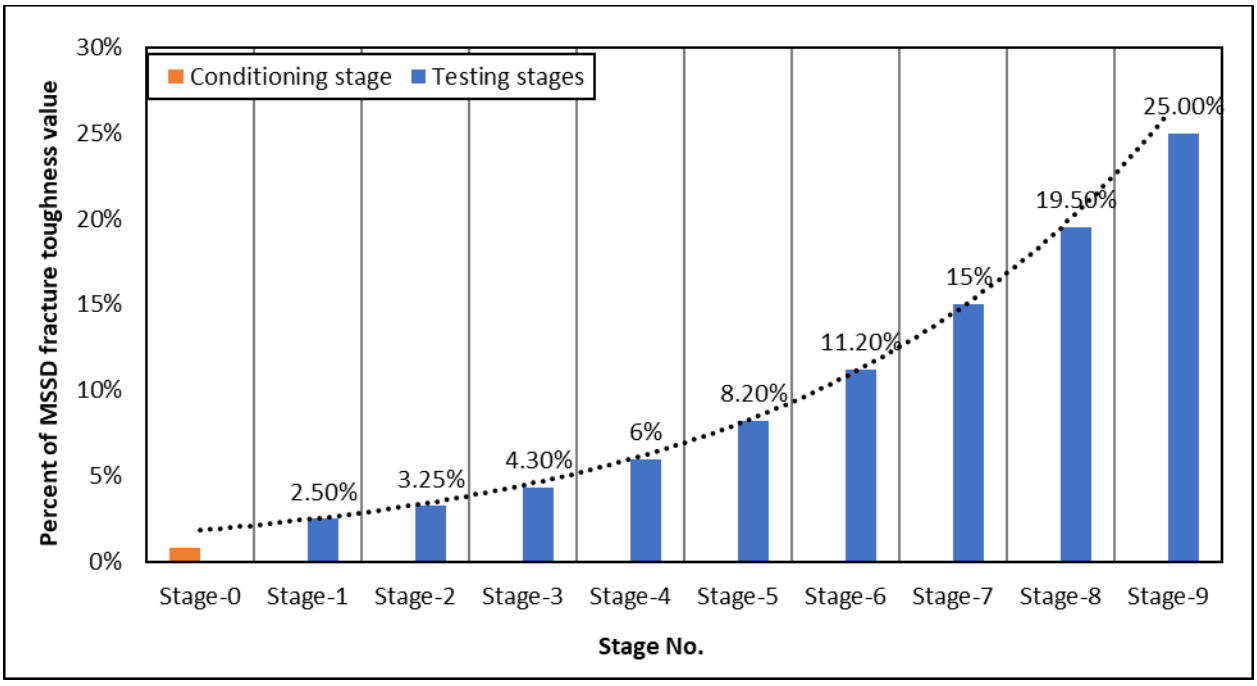

Figure 61 Selected K_{max} Value for each Loading Stage

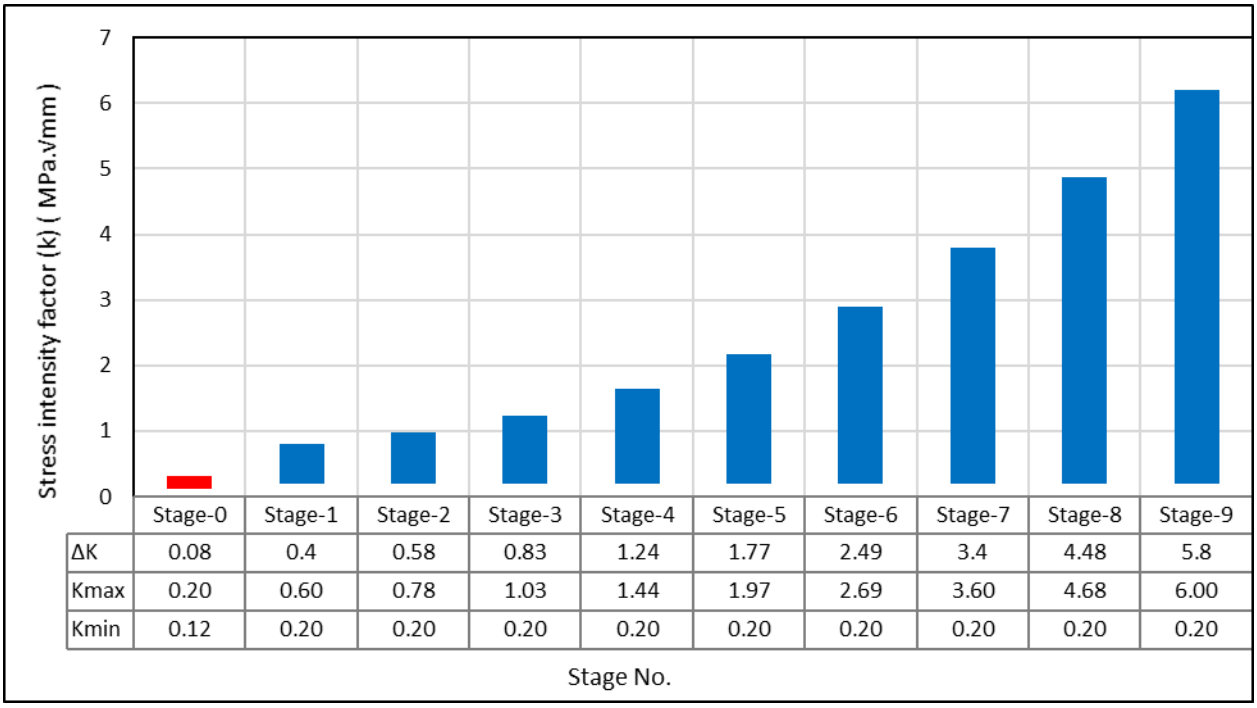

	Stage-0	Stage-1	Stage-2	Stage-3	Stage-4	Stage-5	Stage-6	Stage-7	Stage-8	Stage-9
ΔK	0.08	0.4	0.58	0.83	1.24	1.77	2.49	3.4	4.48	5.8
Kmax	0.20	0.60	0.78	1.03	1.44	1.97	2.69	3.60	4.68	6.00
Kmin	0.12	0.20	0.20	0.20	0.20	0.20	0.20	0.20	0.20	0.20

Figure 62 ΔK, K_{max}, and K_{min} for each Loading Stage

$$K_{IC} = \left(Y_{1_{(0.8)}}\right) \times \left(\sigma_{max}\sqrt{\pi a}\right)$$

$$P_{stage-i} = \left[\frac{24 \times (\%K_{IC\,stage-i})}{\left(Y_{1_{(0.8)}}\right) \times (\sqrt{\pi a})}\right] \times (D \times t)$$

Figure 63 Estimation of Applied Load for Different Loading Stages

where:

K_{IC} = Fracture toughness (N/mm$^{3/2}$)

$Y_{1_{(0.8)}}$ = $4.782\text{-}1.219\left(\frac{a}{r}\right) + 0.063exp\left(7.045\left(\frac{a}{r}\right)\right)$

$P_{stage-i}$ = Required load for stage-i

K_{ICU} = Universal fracture toughness (24 N/mm$^{3/2}$)

$\%K_{ICU}$ = Percentage of fracture toughness for stage-i (N/mm$^{3/2}$)

σ_{max} = Maximum tensile stress (N/mm^2); $\frac{P_{max}}{D \times t}$

P_{max} = Maximum load (N)

t = Specimen thickness (mm)

D = Specimen diameter (mm)

MSSD Test Outputs and Parameters

Figure 64 shows the collected data in the MSSD test including the applied load, the actuator vertical displacement, and the number of load cycles. The data are recorded at a rate of 20 Hz during the test. Six hundred cycles are used for test specimen conditioning (stage 0). The maximum stress intensity factor (K_{max}) increases after the completion of each stage (Figure 62), while the same minimum stress intensity factor (K_{min}) is maintained (0.2 N/mm$^{3/2}$) for all the stages as shown in Figure 62. The rate of change in the vertical displacement with the loading cycles followed S-shape curve as shown in Figure 65. The S-shape curve is divided into three phases I, II, and III.

The MSSD test parameters are inspired by the well-known Paris' law parameters. Paris' law studies the relation between crack growth rate and the change in SIF (ΔK) [104]. Measuring the crack length is not a simple task to perform. In order to simplify the MSSD test, the vertical actuator displacement was used as an alternative of the true crack length. Analogous formula to Paris' law was used to describe the relation between the rate of change in the vertical actuator displacement and the change in SIF (ΔK) as presented in Figure 67. It should be noted that Figure 67 does not represent Paris' law. Figure 67 has two MSSD parameters (H and z) that can be determined by performing the following steps:

1. Plot the vertical actuator displacement (v) versus the number of loading cycles (N) (Figure 69).
2. Fit the curve from step no. 1 with a 6th-degree polynomial function (Figure 69).
3. Determine the rate of change in vertical actuator displacement with the number of cycles ($\frac{dv}{dN}$) at the end of each testing stage and the failure cycle.
4. Determine the change in the change in SIF (ΔK) for each testing stage (Figure 62).
5. Plot ΔK versus the associated $\boldsymbol{\frac{dv}{dN}}$ in log-log scale (Figure 70).
6. Determine the MSSD parameters (H and z) by fitting the data using a power function.

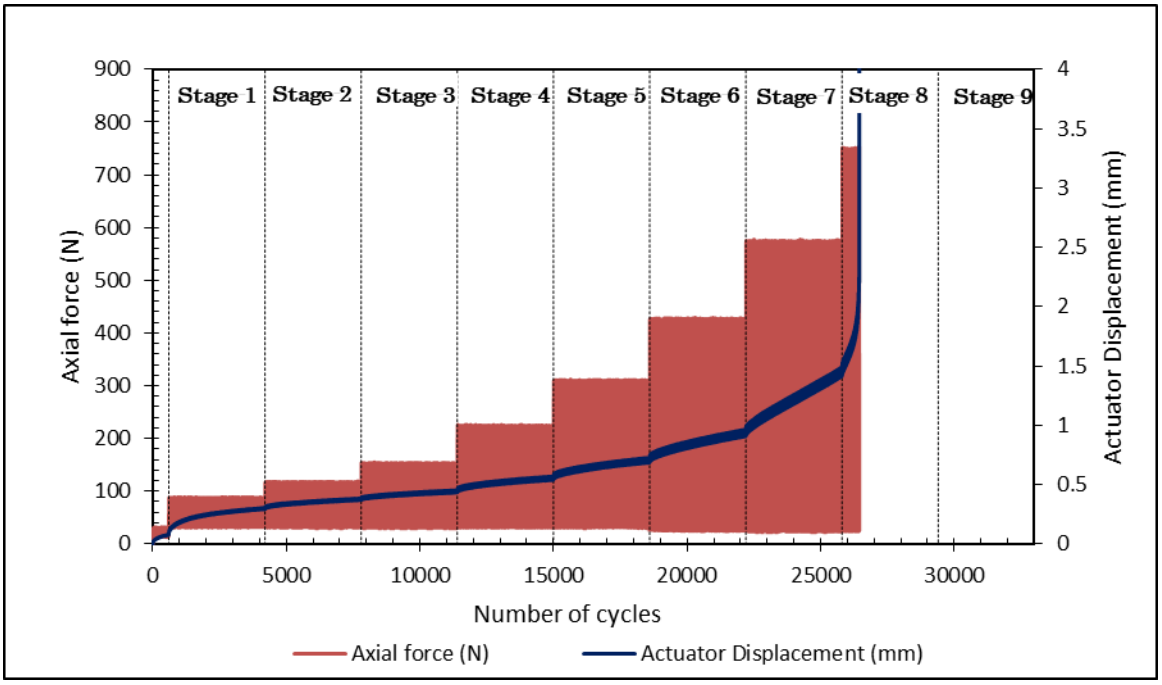

Figure 64 MSSD test typical output

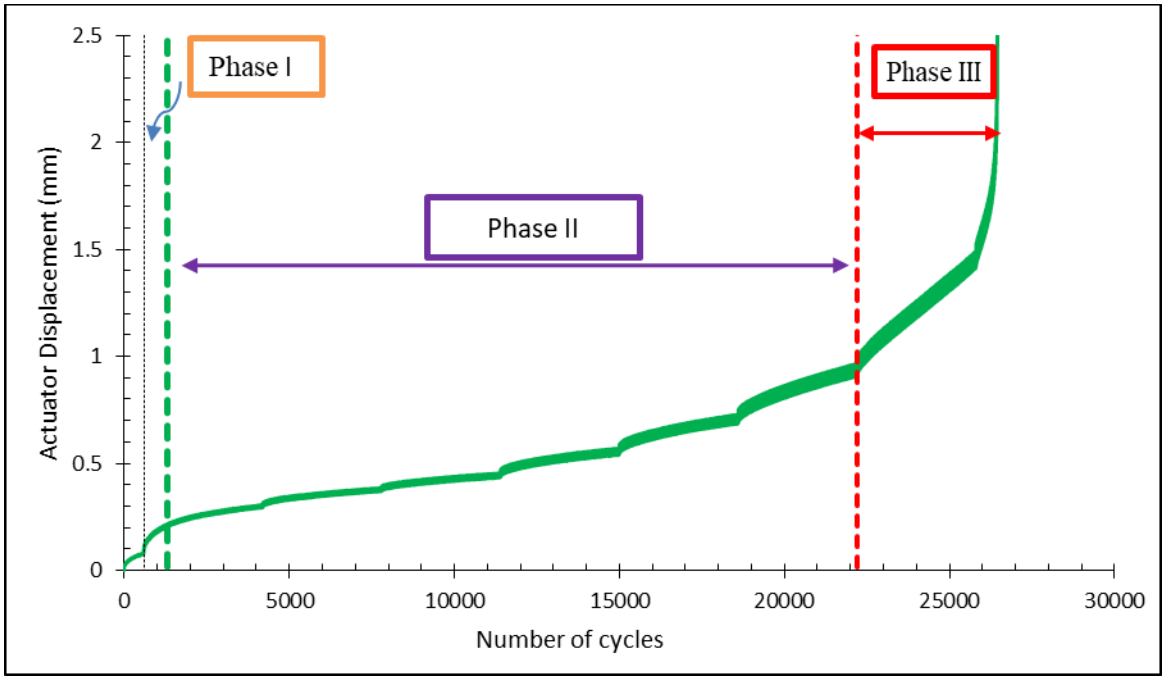

Figure 65 Typical Vertical Displacement S Shape Curve and Inflection Points

$$\frac{da}{dN} = A\,(\Delta K)^n$$

Figure 66 Paris' law Parameters

$$\frac{dv}{dN} = H\,(\Delta K)^Z$$

Figure 67 Modified Paris' Law Parameters

where:

a = Crack length (mm)

v = Vertical actuator displacement (mm)

N = Number of loading cycles

da/*dN* = Crack growth rate (mm/cycle)

dv/*dN* = Rate of vertical actuator displacement to number of cycles

ΔK = Mode I the change in SIF (K_{max} - K_{min})

A and *n* = Fitting constants for Paris law

H and *z* = Fitting constants for MSSD model

Figure 67 can be rearranged and presented in Figure 68. The value ofP<represents the intercept, while z value represents the slope. The intercept (log H) reflects the initial rate of displacement per cycle, while the slope (*z*) reflects the increment in the displacement rate with the change in stress intensity factor. Higher slope indicates faster rate of damage. Higher slope is associated with a lower absolute intercept (Abs [log *H*]). Therefore, mixes with low slope (*z*) and high Abs (log *H*) would exhibit higher resistance to cracking. Previous research reported good correlation between Paris' law parameters (A, n) as shown in Figure 68 [105,106]. Similar relationship between MSSD parameters (H and z) presented in Figure 68 is validated in Chapter 5.

$$log(\frac{dv}{dN}) = log\,H + z\,log\,\Delta K$$

$$n = C_1\,Log\,A + C_2$$
$$z = C_3\,Log\,H + C_4$$

Figure 68 Rearranged Modified Paris' law Parameters

where:

C_1, C_2, C_3, and C_4 = Linear regression fitting constants

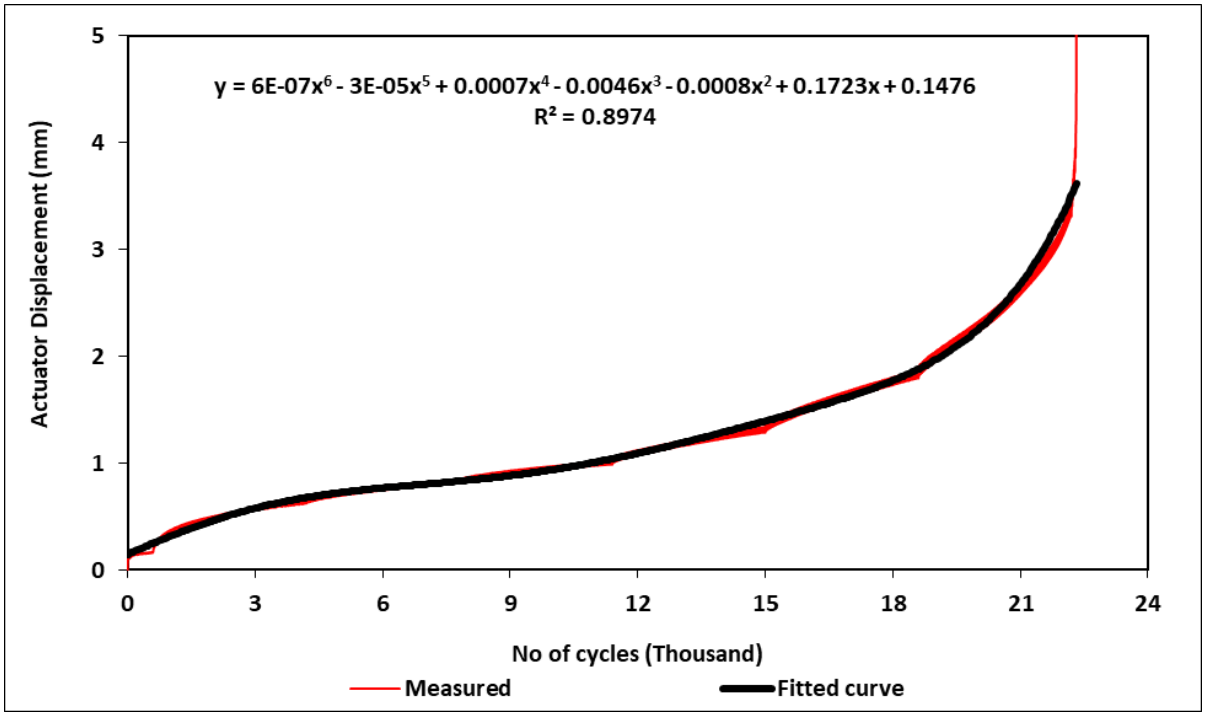

Figure 69 Fitting the S-curve with 6th degree polynomial function

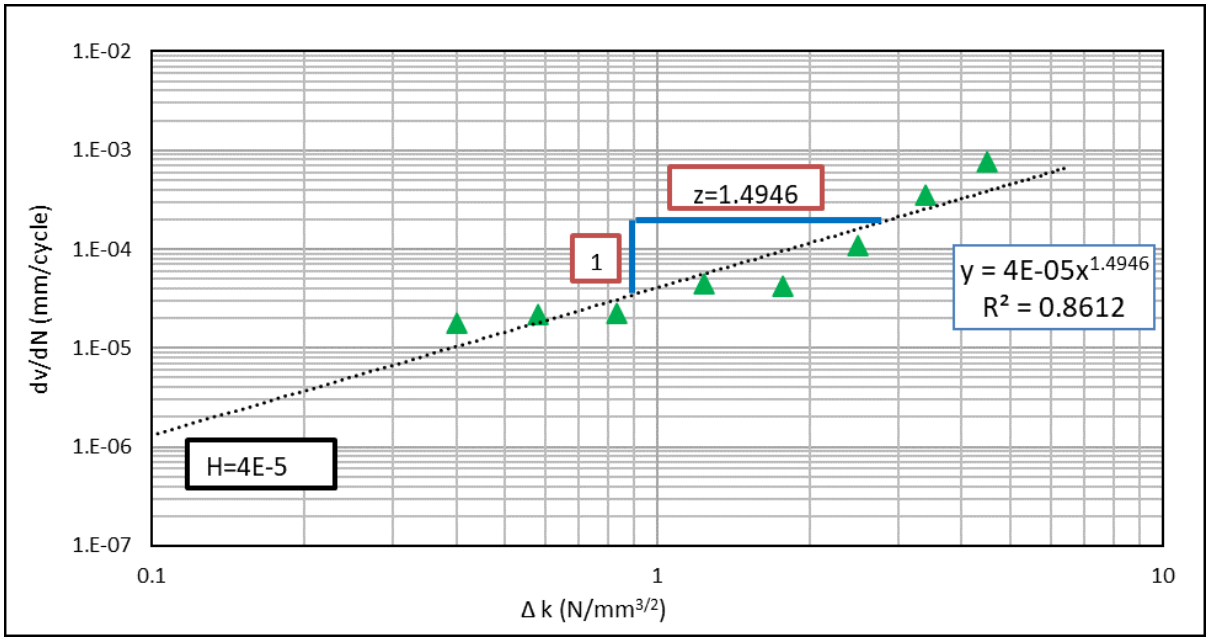

Figure 70 Determination of MSSD Parameters

Asphalt Mixture Rutting Tests

Selected Testing Protocols

Based on the findings of the literature review, two rutting assessment tests were selected and used in this study; Hamburg Wheel Tracking Test (HWTT) and Asphalt Pavement Analyzer (APA) rut test. The HWTT is conducted in accordance with AASHTO T324, while the APA rut test is conducted in accordance with AASHTO T340. In these tests, the test specimen is subjected to accelerated reciprocating wheel loading. Table 24 summarizes the test conditions and sample geometry for both HWTT and APA rut test. Both the tests can be performed a cylindrical specimen that is 150 mm in diameter and 60 mm or 75 mm thickness for HWTT and APA rut test, respectively. In addition, HWTT can be run using slab specimens or cylindrical ones. However, the cylindrical specimens are more preferable since they require less preparation time and can be performed on extracted field cores. Both tests can be evaluating a four or six cylindrical specimens per test; however, the number of tested specimens depends on number of wheel in the testing device (two or three wheels). Field cores can be evaluated using both tests. The tests allow using plastering materials for field cores with thickness less the testing mold height. HWTT requires conditioning the specimens in water bath for one hour at a specified temperature selected by the agency, while the specimens of the APA rut test are conditioned in air for six hours at a temperature equal to the higher binder PG. Since the HWTT samples are conditioned in water, this test can be used to assess the moisture susceptibility in addition to rutting. The HWTT loading wheels apply 705 N load directly on specimen surface at a constant moving rate of 52 pass/minute. The APA rut test loading wheels apply 578 N load on a pressurized rubber hose that has a constant pressure of 690 kPa at a constant moving rate of 60 cycle/minute. Both tests collect the rutting measurements with number of cycles or passes.

Table 24 Selected Testing Protocols for Rutting Assessments [107,108]

Test	HWTT	HWTT	APA rut test
Testing Standards	AASHTO T 324	AASHTO T 324	AASHTO T 340
Specimen shape	Cylindrical or	slabs	Cylindrical
Specimen replicates	4 or 6	2	4 or 6
Specimen diameter (mm)	150	150	150
Specimen thickness (mm) for lab prepared	60	38-100	75
Specimen thickness (mm) for field Projects	38 - 60	NA	38 -75
Test temperature (°C)	Specified by the agency	Specified by the agency	High binder PG
Specimen conditioning	Water bath	Water bath	Air bath
Conditioning time (hour)	1	1	6 – 24
Testing time (hour)	≈10	≈10	≈ 2
Wheel type	Solid steel	Solid steel	Concave wheel
Wheel speed (Pass/minute)	52	52	50 ± 5
Load (N)	705 ± 4.5	705 ± 4.5	578
Number of data collection locations	11 locations	11 locations	5 locations
Test output	passes-deformation curve	passes-deformation curve	Cycle-deformation curve
Distress assessed	Rutting and moisture susceptibility	Rutting and moisture susceptibility	Rutting

Rutting Depth Measurements

Figure 71 and Figure 72 show typical rut depth measurements for HWTT and APA, respectively. The HWTT data follow an S-curve shape, where three phases can be identified; primary (pre-consolidation), secondary, and tertiary [109]. The primary phase shows a high deformation rate per pass due to initial specimen consolidation. This stage is usually completed within the first 1,000 cycles [109]. In the secondary phase, the deformation continues to increase but at a smaller constant rate (creep slope). The deformation in the secondary phase is due to plastic flow. The tertiary phase exhibits a rapid increase in the rate of deformation (stripping slope). The deformation in the tertiary phase could be due to both rutting plastic flow and moisture damage. In the APA rut test, there are only two phases; primary (pre-consolidation) and secondary phase.

In the HWTT, the rut depth (deformation) is collected at 11 locations along each wheel path, while it is collected at five locations in the APA rut test. In this study, the average rut depth of all locations is reported for both tests as recommended by AASHTO T324 and AASHTO T340 [107]. The HWTT test is terminated after 20,000 passes or after a certain rut depth is recorded (e.g., 20 mm). Similarly, the APA test is terminated after 8,000 cycles.

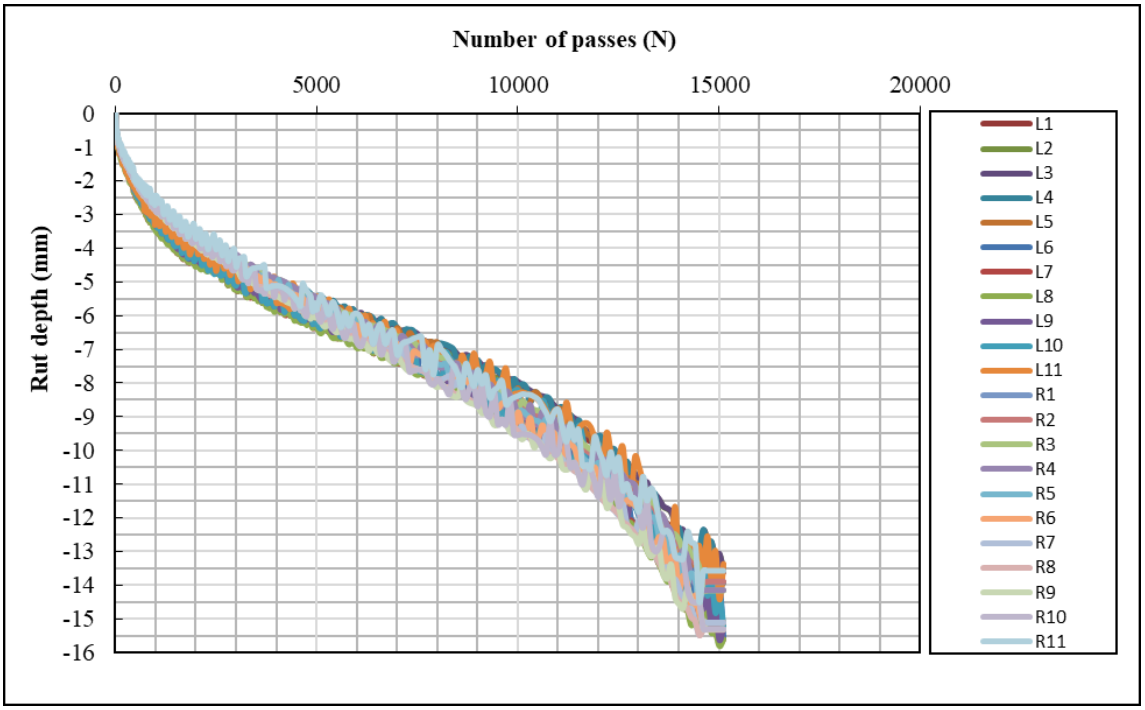

Figure 71 HWTT Left Wheel (L1- L11) and Right Wheel (R1-R11) Data Points

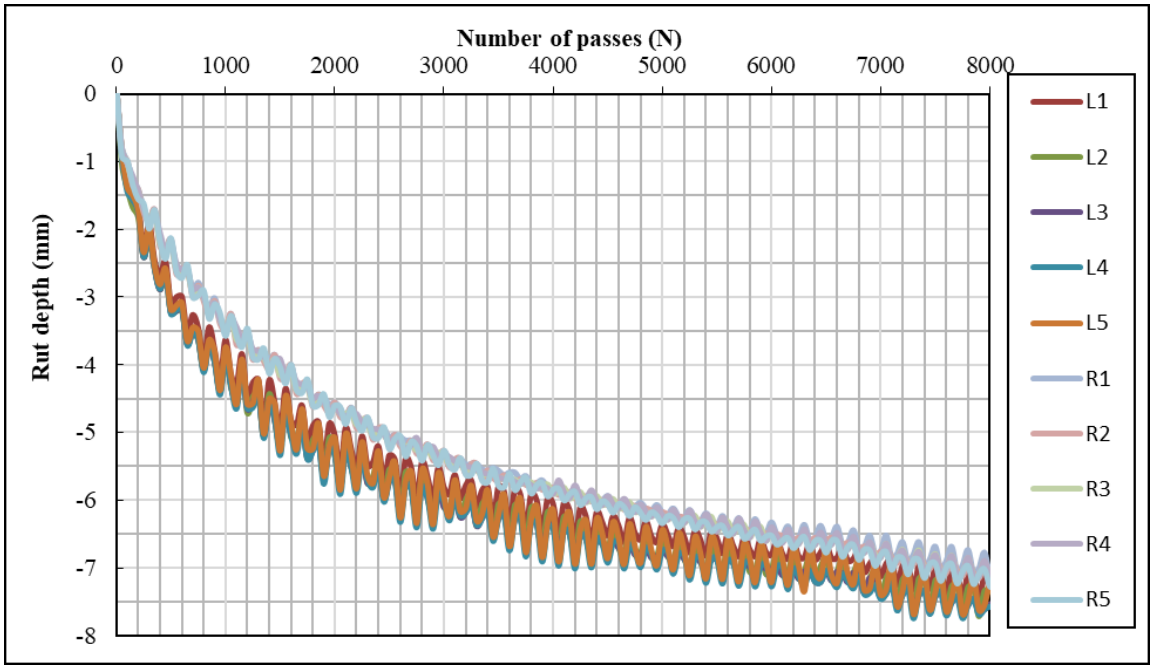

Figure 72 APA Rut Test Left Wheel (L1- L5) and Right Wheel (R1-R5) Deformation Measurement

Chapter 5
Comprehensive Evaluation of Cracking Resistance Tests

Cracking Resistance Evaluation of Field Cores Using MSSD Test

Figure 73 shows the rate of change in vertical actuator displacement with the number of cycles ($\frac{dv}{dN}$) versus the change in stress intensity factor (ΔK) for 16 field cores. D3C2 field project was not included in the dynamic testing due to the limited number of cores that were received. The change in $\frac{dv}{dN}$ increases with the increase ΔK. Mixes with higher $\frac{dv}{dN}$ failed faster as compared to mixes with lower $\frac{dv}{dN}$. Figure 74 shows an example of asphalt mixes with good resistance to cracking (D2C8) and poor resistance to cracking (D5C2). D2C8 had lower initial $\frac{dv}{dN}$ of 1.45 E-5 mm/cycle, while D5C2 had higher initial $\frac{dv}{dN}$ of 1.15 E-4 mm/cycle. D2C8 failed at the eighth loading stage (4.48 N/mm$^{3/2}$), while D5C2 failed at the third loading stage (0.832 N/mm$^{3/2}$). The MSSD parameters (i.e., *H* and *z*) were obtained by fitting the data with a power function (Figure 74). The power function fitted the test data with a coefficient of determination (R^2) of 0.94 for D5C2 and 0.90 for D2C8. The D2C8 mixture had a smaller slope (*z*) of 1.66 compared to mixture D5C2 (4.87). Smaller slope indicates a slower rate of damage, therefore D2C8 had better cracking resistance as compared to D5C2. These findings are consistent with the observed field cracking resistance where D2C8 showed good cracking resistance while D5C2 showed poor cracking resistance as discussed in Chapter 3 (Figure 29). This example demonstrates that the MSSD parameters were able to differentiate between mixes with good and poor cracking resistance.

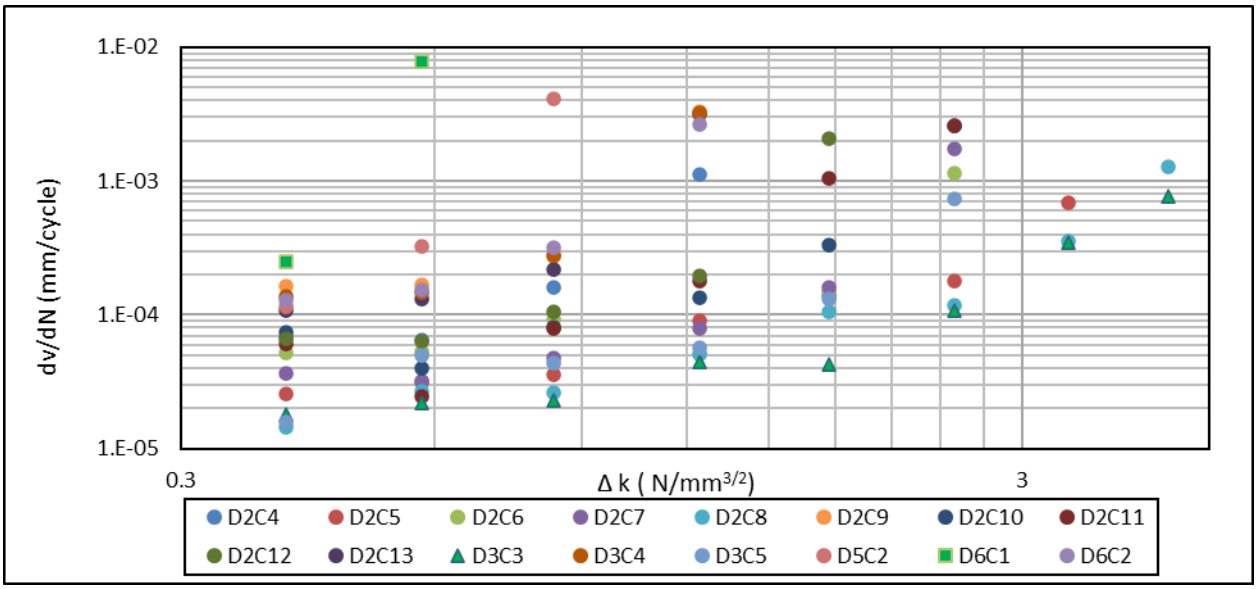

Figure 73 The Variation in the Rate of Change of Vertical Actuator Displacement and Number of Cycles versus the Change in Stress Intensity Factor (ΔK) for all Field Projects

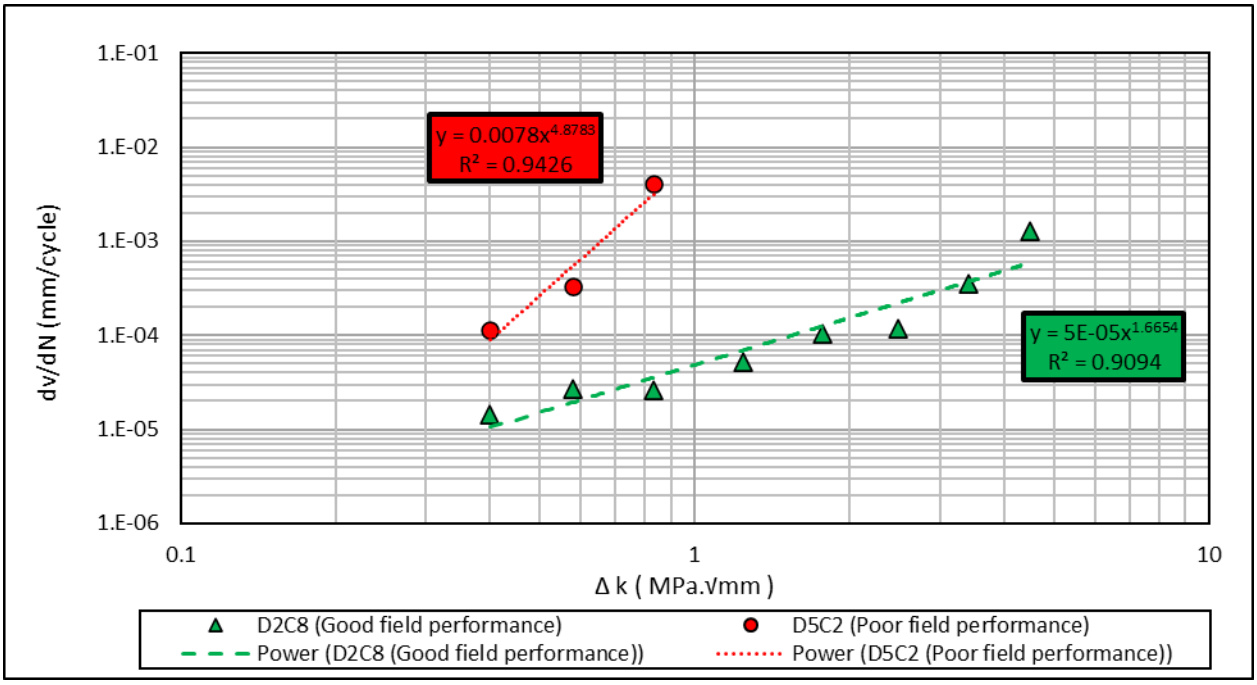

Figure 74 Example of MSSD Parameters (H and z) for Mixes with Good and Poor Field Cracking Performance

The same analysis process was followed and applied to all field projects. Two SCB specimens were tested for each project due to the limited number of field cores. Figure 75 shows the slope (*z*) parameter for all field projects tested using the MSSD test (total of 16 projects). The field projects had an average slope between 1.21 and 3.90 with a standard deviation (SD) between 0.02 and 0.97. The coefficient of variation (COV) of the calculated slope was relatively low (15.1%). Analysis of Variance (ANOVA) results showed a statistically significant (*p*-value < 0.05) difference between cracking resistance of various field projects. Tukey's Honestly Significant Difference (Tukey's HSD) categorized the mixes into two groups (i.e., A and B). Mixture D2C8 had the lowest slope of 1.21, while mixture D5C2 had the highest slope value of 3.90. In Figure 75, field projects with good cracking resistance are presented in green bars, field projects with fair cracking resistance are presented in yellow bars, while field projects with poor cracking resistance are presented in red bars. The results presented in Figure 75 demonstrate that field projects with good cracking resistance had a slope less than 1.9, projects with poor cracking resistance had a slope higher than 2.9, while projects with fair cracking resistance had a slope between 1.9 and 2.9. Smaller slope indicates slower rate of damage and thus better cracking resistance. ANOVA indicated a significant difference between cracking resistance groups (*p*-value < 0.05). Tukey HSD results showed a statistically significant difference between good and fair/poor cracking resistance groups and a statistical insignificant difference between fair and poor cracking resistance groups.

Figure 76 shows the absolute intercept (abs [log H]) parameter calculated from the MSSD test. The field projects had average values between 1.92 and 4.26 with SD between 0.0 and 0.472. This parameter also had a low COV (4.4 percent). ANOVA analysis results showed a significant difference between the results (*p*-value < 0.05). Tukey's HSD test categorized mixes into five groups; A, B, C, D, and E. The Abs (log *H*)

was able to differentiate between mixes with different cracking resistance (Figure 76). In general, mixes with higher Abs (log *H*) showed better cracking resistance compared to mixes with lower Abs (log *H*).

Overall, projects with good cracking resistance had an absolute intercept (Abs [log *H*]) higher than 3.6, projects with fair cracking resistance had an absolute intercept (Abs [log *H*]) between 3.0 and 3.6, while projects with poor cracking resistance had an absolute intercept (Abs [log *H*]) less than 3.0. In the meantime, identifying performance thresholds based on the Abs (log *H*) parameter was not simple and direct compared to the slope (*z*) parameter due to higher overlap between good/fair and fair/poor performance groups. Therefore, the proposed thresholds based on the slope (*z*) parameter are considered more reliable compared to the ones based on the Abs (log *H*) parameter. Similar to the slope parameter, the ANOVA results indicated a significant statistical difference between cracking resistance groups (*p*-value < 0.05) based on the Abs (log *H*) parameter. Tukey HSD results showed a significant statistical difference between the good cracking resistance group and fair/poor groups, while there was insignificant statistical difference between the fair and poor cracking resistance groups.

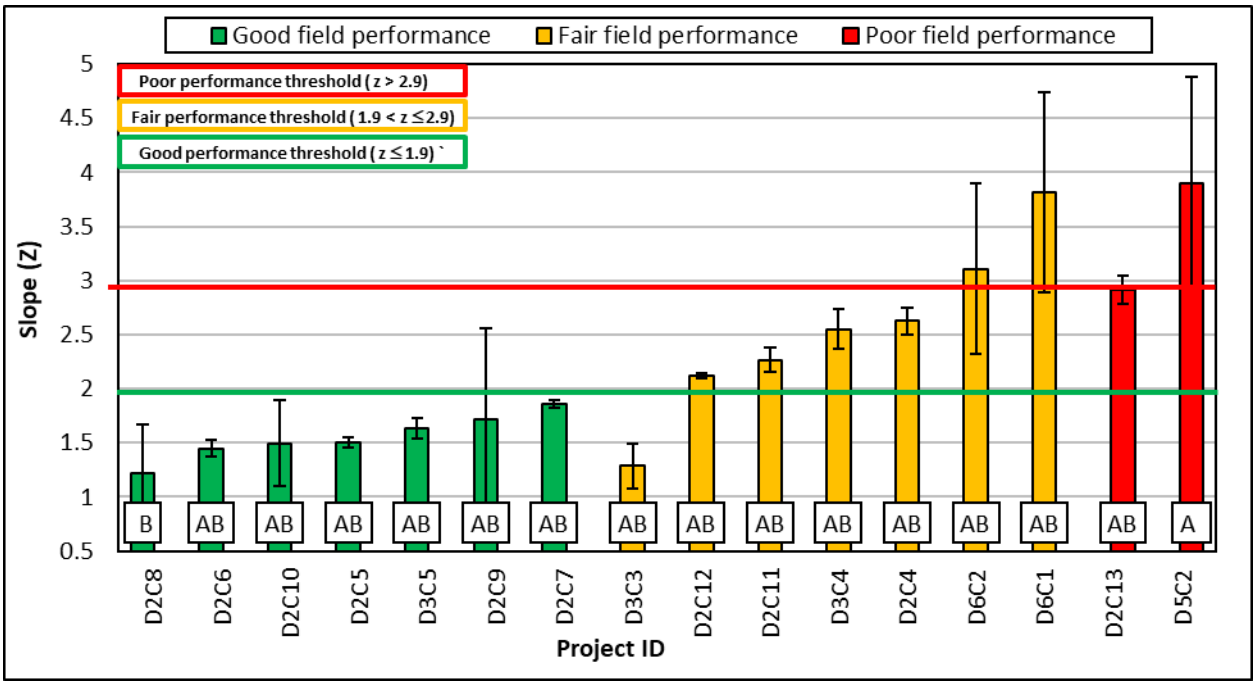

Figure 75 MSSD Slope (*z*) Parameter Results and Proposed Performance Thresholds for Field Projects

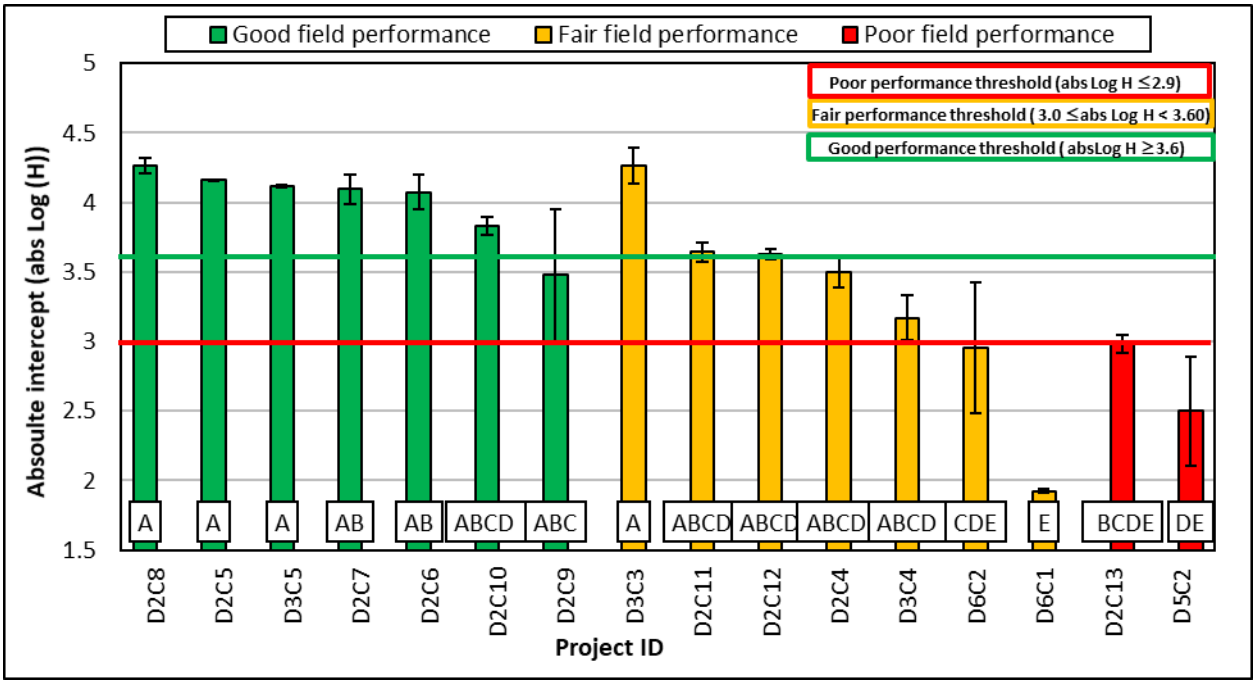

Figure 76 MSSD Absolute Intercept (Abs [Log H]) Parameter and Proposed Performance Thresholds for Field Projects

Performance Evaluation of PMLC Mixes Using MSSD Test

Figure 77 shows the change in vertical actuator displacement with the number of cycles ($\frac{dv}{dN}$) versus the change in stress intensity factor (ΔK) for all PMLC mixes. Similar to the field projects, the computed MSSD parameters (z and Abs [log *H*]) were obtained by fitting the data with a power function. The R^2 for the fitting ranged between 0.661 and 0.926. Figure 78 shows the slope (z) parameter for PMLC mixes. Four SCB specimens were tested for each mixture. The slope ranged between 1.20 and 4.25 with SD between 0.1 and 1.40. The slope results had a COV of 25 percent. ANOVA results showed significant difference between mixes results (*p*-value < 0.05). Tukey's HSD categorized mixes into two groups; A and B. Based on the performance thresholds developed based on the field projects, mixes D2L2, D3L2, D6L1, and D2L1 are expected to have good field cracking resistance in the field. Mixes D5L1, D1L1, D3L5, and D3L4 are expected to have fair field cracking resistance, while mixes D3L3 and D3L1 are expected to have poor field cracking resistance.

Similarly, Figure 79 shows the Abs (log *H*) parameter for PMLC mixes. This parameter ranged between 1.94 and 4.43 with SD between 0.03 and 0.98. Also, the Abs (log *H*) results had COV of 11 percent. ANOVA results showed significant different between results (*p*-value <0.05). Tukey's HSD categorized the PMLC mixes into two groups; A and B. Based on the performance thresholds developed based on with field projects, almost all PMLC mixes are expected to have good cracking resistance except two mixes (i.e., D3L3 and D3L1). Mixture D3L3 is expected to have fair cracking resistance, while mixture D3L1 is expected to have poor cracking resistance. The cracking resistance of asphalt mixes is affected by its composition. Previous research reported that cracking resistance is improved with higher binder content,

lower binder PG, using polymer modifier binder, higher aggregate angularity, smaller NMAS, lower air voids, lower RAP content, unaged binder, replacing sand with crush fine aggregates [31,110–112]. PMLC mixes have different characteristics (e.g., mix design, binder content, binder grade, etc.) as presented in Table 13. In this study, the performance of PMLC mixes was explained and related to its compositions compared to other mixes.

Mixture D2L2 had the lowest MSSD slope (1.20) which indicates better cracking resistance, while mixture D3L1 had the highest slope (4.25) (i.e., higher rate of damage) which demonstrates poor cracking resistance. Mixture (D2L2) had the highest binder content (5.70 percent), softer virgin binder content (PG 58-34), and small NMAS (12.5 mm). Mixture D3L1 had the highest RBR content (50 percent) and stiffer specified binder (PG 70-28). The use of higher RBR content with relatively stiffer binder may have reduced the resistance of mixture D3L1 to cracking. Also, based on the MSSD slope results, mixture D1L1 is expected to provide better cracking resistance compared to mixture D3L3. Both mixes have the same RBR content (30 percent), binder content (5.30 percent), NMAS (12.5 mm), PG (PG 64-28), and softer virgin PG (PG 58-34), but D1L1 is SP5 while D3L3 is SP3. SP5 mixes is expected to provide better cracking resistance since it is designed for higher traffic levels.

The results demonstrated that mixture D1L1 have better cracking resistance compared to D3L5. Both mixes (i.e., D1L1 and D3L5) have the same RBR content (30 percent), binder content (5.3 percent), NMAS (12.5 mm) and mix type (SP5), but D1L1 has softer specified binder (PG 64-28) and softer virgin binder (PG 58-34) compared to D3L5 which has stiffer specified binder (PG 76-28) and virgin binder (PG 70-34) than D3L5. It is believed that softer binder used in D1L1 improved its cracking resistance compared to D3L5. Mixture D2L1 was found also to provide better cracking resistance compared to D3L1. Both mixes have the same RBR content (50 percent), PG (PG 70-28), NMAS (12.5), and mix type (SP3), but D2L1 has higher binder content (5.7 percent) compared to D3L1 (5.20 percent), therefore the higher binder content could improve the cracking resistance of D2L1 compared to D3L1. Furthermore, the results demonstrated that mixture D2L2 exhibited better cracking resistance compared to D2L1. Both mixes have the same NMAS (12.5), mix type (SP3), and binder content (5.7 percent), but D2L2 has lower RBR content (30 percent), softer specified binder (PG 64-28) and virgin PG (PG 58-34) as compared to D2L1 that has RBR of 50 percent, specified PG of 70-28, and virgin PG of 64-34. It is believed that the softer binder and low RBR content improved the cracking resistance of D2L2 compared to D2L1. Similar to the slope (z) parameter, the absolute intercept parameter (Abs [log H]) had good agreement with mixture's composition as discussed above.

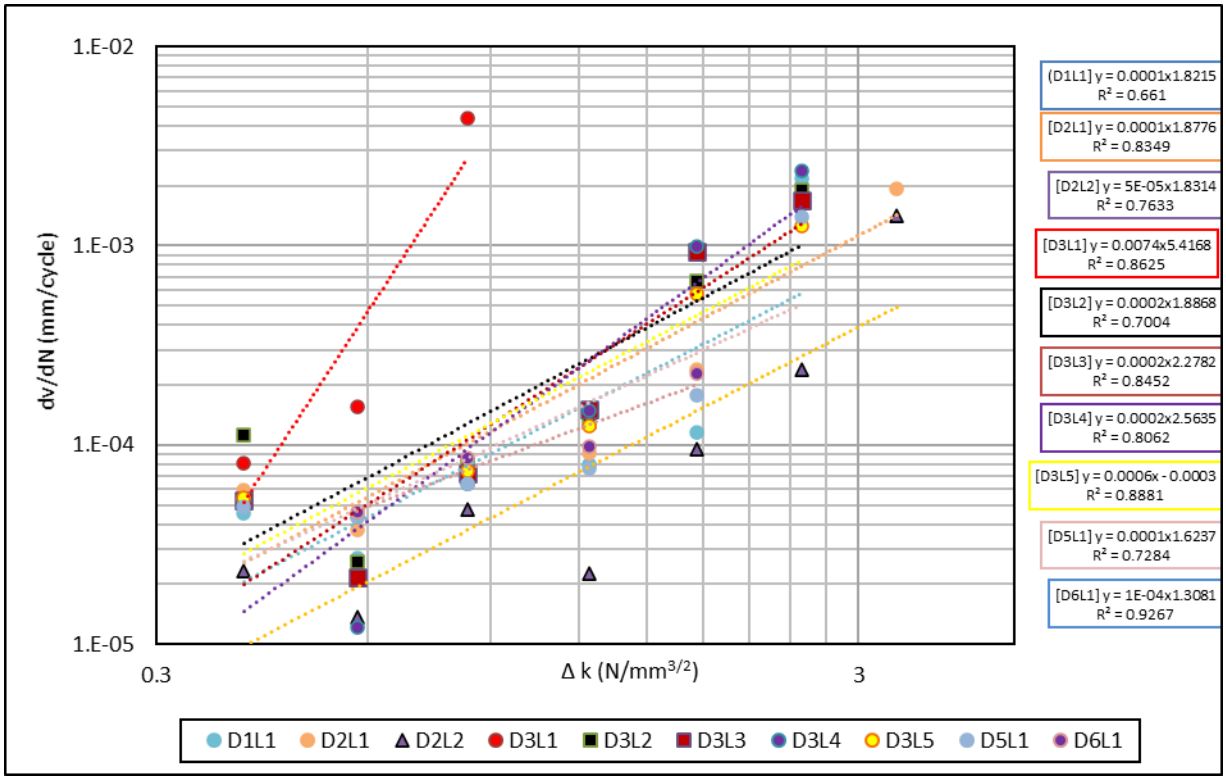

Figure 77 Determination of MSSD Parameters (z and Abs [log *H*]) PMLC Mixes

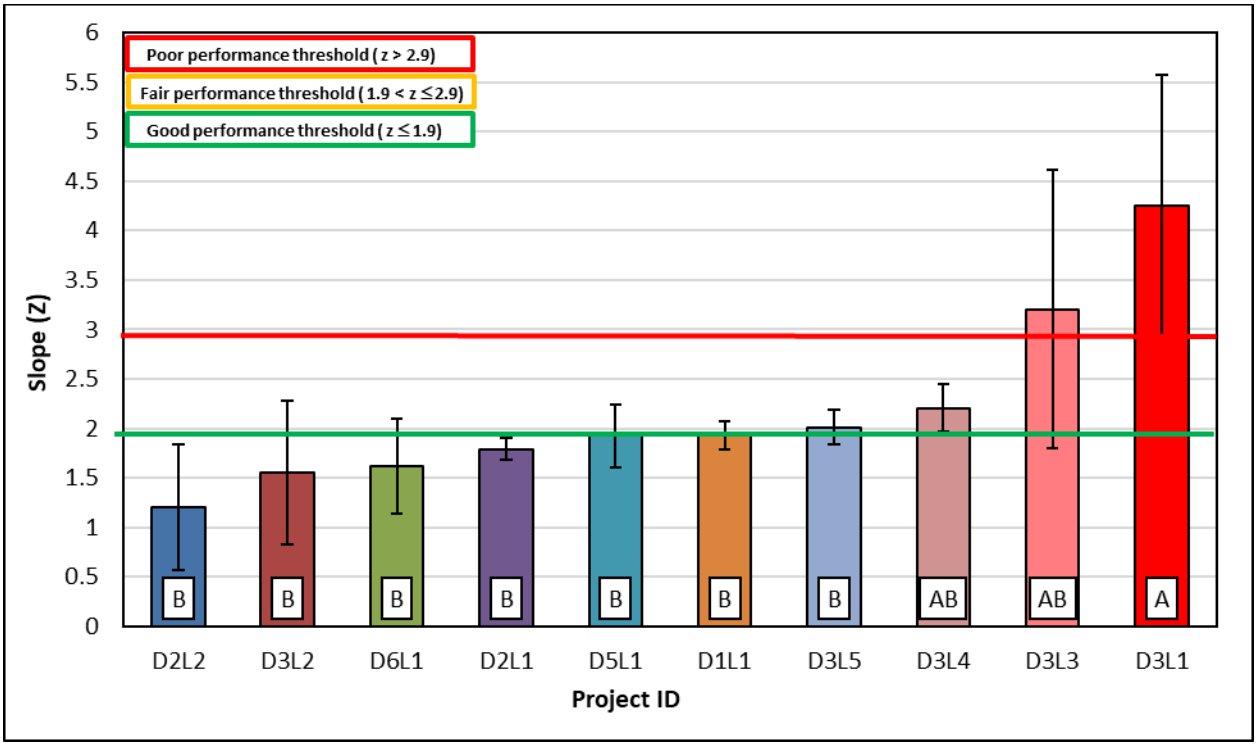

Figure 78 MSSD Slope (*z*) Parameter for PMLC Mixes

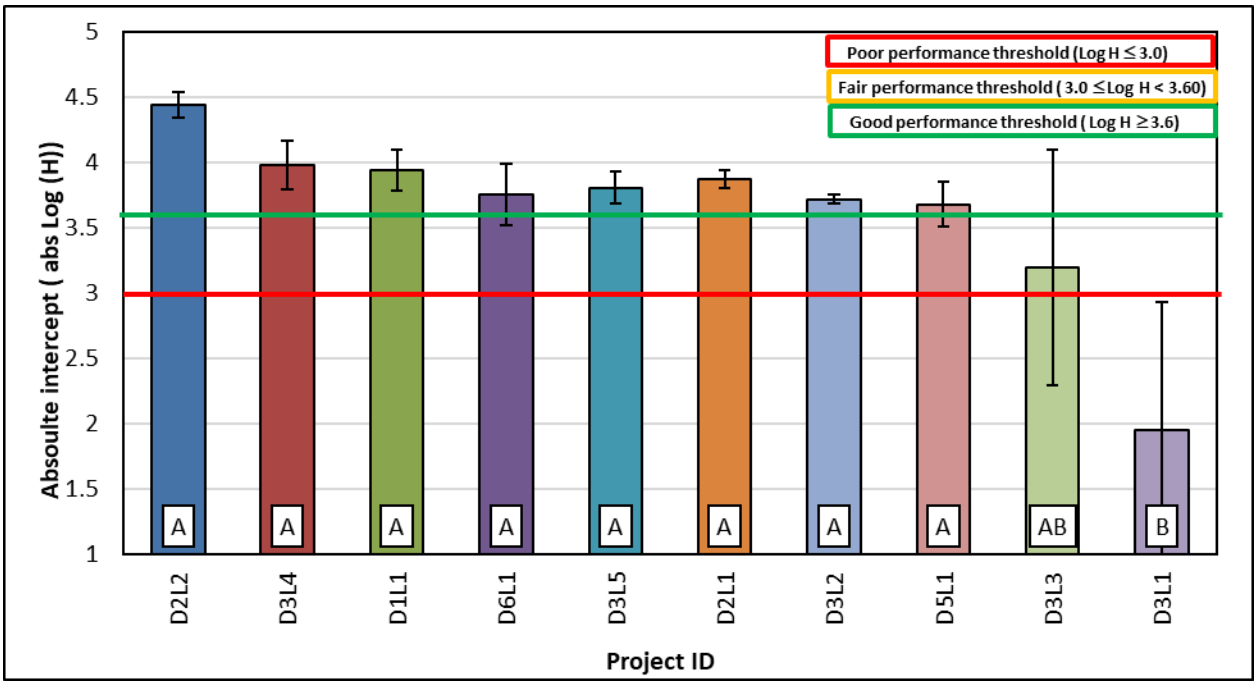

Figure 79 MSSD Abs (log *H*) Parameter for PMLC Mixes

Correlation between MSSD Parameters

Previous research reported that Paris' Law parameters are correlated [105,106]. A direct linear correlation was reported between n and Log A (Figure 67). Similarly, the research team evaluated the correlation between MSSD parameters (z and Abs [log *H*]). Figure 81 shows the correlation between these two parameters for the PMLC mixes and field projects. The results demonstrate that there is a direct relationship between both parameters. Field projects had a coefficient of determination (R^2) of 0.80, while R^2 = 0.75 for PMLC mixes. Such relationship indicates that higher slopes are associated with lower values of Abs (log *H*). A similar relationship was reported by Rooijen and Bondt (2008) for Paris' Law parameters computed using dynamic SCB (Figure 80) [113]. Rooijen and Bondt (2008) model provided R^2 of 1.0 [113].

$$Log\ A = -1.4397 \times n - 2.5273$$

Figure 80 Correlation between n and Log A Rooijen and Bondt (2008) [113]

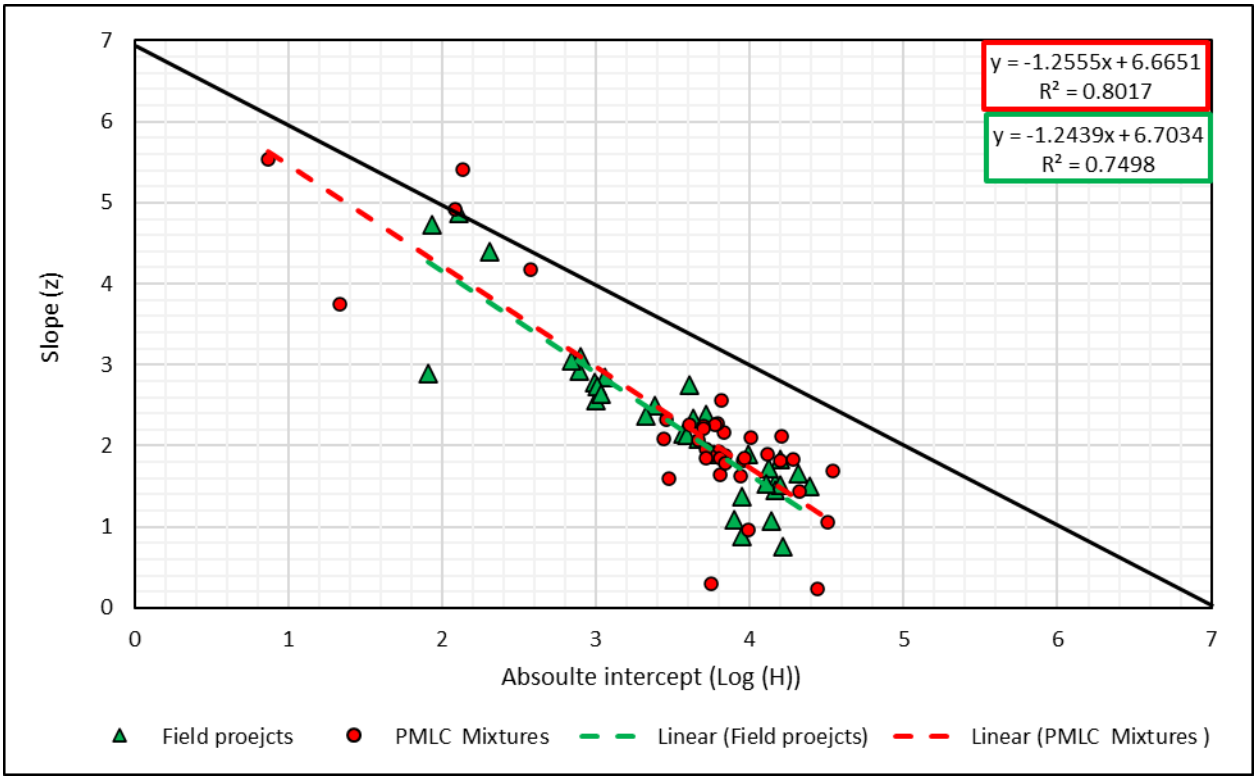

Figure 81 Correlation between MSSD Test Parameters (z and Abs [log *H*]) for both Field and PMLC Mixes

Monotonic Cracking Assessment Tests

In this study, three monotonic tests were conducted (i.e., SCB-FI, SCB-Jc, and IDT) and several performance indicators were calculated using the test data. Table 25 presents the evaluated performance indicators and the data source for each indicator. A total of 12 different performance indicators were considered. These performance indicators have been used in the literature to evaluate the resistance of asphalt mixes to cracking. Chapter 4 discussed these performance indicators. In this section, the research team assessed the sensitivity of each performance indicator to the composition of asphalt mixes. The LMLC mixes were used for the sensitivity analysis.

Table 25 Selected Performance Indicator and Test Data Source

#	Symbol	Test Data Source	Performance Indicator Concept (Chapter 3)
1	$G_{fracture}$ (IDT)	IDT test	Total Fracture Energy
2	$G_{fracture}$ (SCB-FI)	SCB-FI	Total Fracture Energy
3	CRI (IDT)	CRI	Cracking Resistance Index
4	CRI (SCB-FI)	SCB-FI	Cracking Resistance Index
5	FI (IDT)	IDT test	Flexibility Index
6	FI (SCB-FI)	SCB-FI	Flexibility Index
7	IDEAL-CT_{Index}	IDT test	IDEAL-CT_{Index}
8	Nflex factor	IDT test	Nflex factor
9	$IDT_{Strength}$	IDT test	$IDT_{Strength}$
10	$IDT_{Modulus}$	IDT test	$IDT_{Modulus}$
11	J_c	SCB-Jc	Strain energy release rate
12	$Weibull_{CRI}$	IDT test	$Weibull_{CRI}$

Sensitivity of Monotonic Cracking Tests to Mixture Properties

The laboratory-mixed laboratory-compacted mixes (LMLC) were used to examine the sensitivity of the monotonic cracking tests including indirect tensile (IDT) test, semi-circular bending-flexibility index (SCB-FI) test, and semi-circular bending-Jc (SCB- Jc) test to binder content and binder grade. The LMLC specimens were prepared using three binder contents (i.e., OBC, OBC-0.75 percent, and OBC+0.75 percent) and using two binders (i.e., PG 70-28 and PG 58-34). Figure 82 shows the load-displacement curves from each monotonic test at different binder content for each binder grade. It should be noted that the SCB- Jc is conducted using specimens with three notch depths (38.4 mm, 31.8 mm, and 25.4 mm). In this example, the load-displacement curve at 25.4 mm notch depth for the SCB- Jc was used; however, the test was conducted at the three notch depths.

The load-displacement curve changes with the change in binder content. Figure 83 demonstrates such change in the load-displacement curve for different monotonic tests at different binder contents. As the percent binder decreases, the pre-peak slope, curve peak, and post-peak slope of the load-displacement curve increase (Figure 83). The increase in these curve elements indicates overall reduction in cracking resistance. The performance indicators calculated from the monotonic tests use one or more of the load-displacement curve elements to assess cracking performance. The results in Figure 82 demonstrate that the test data source (i.e., SCB-FI, SCB-J_c, or IDT) did not affect the overall shape variation in the load-displacement curve. The SCB-J_C (at 25.4 mm notch depth) showed a higher increase in the peak with the decrease in binder content when compared to the IDT and SCB-FI tests for the same binder grade.

However, all tests were able to capture the same expected trend.

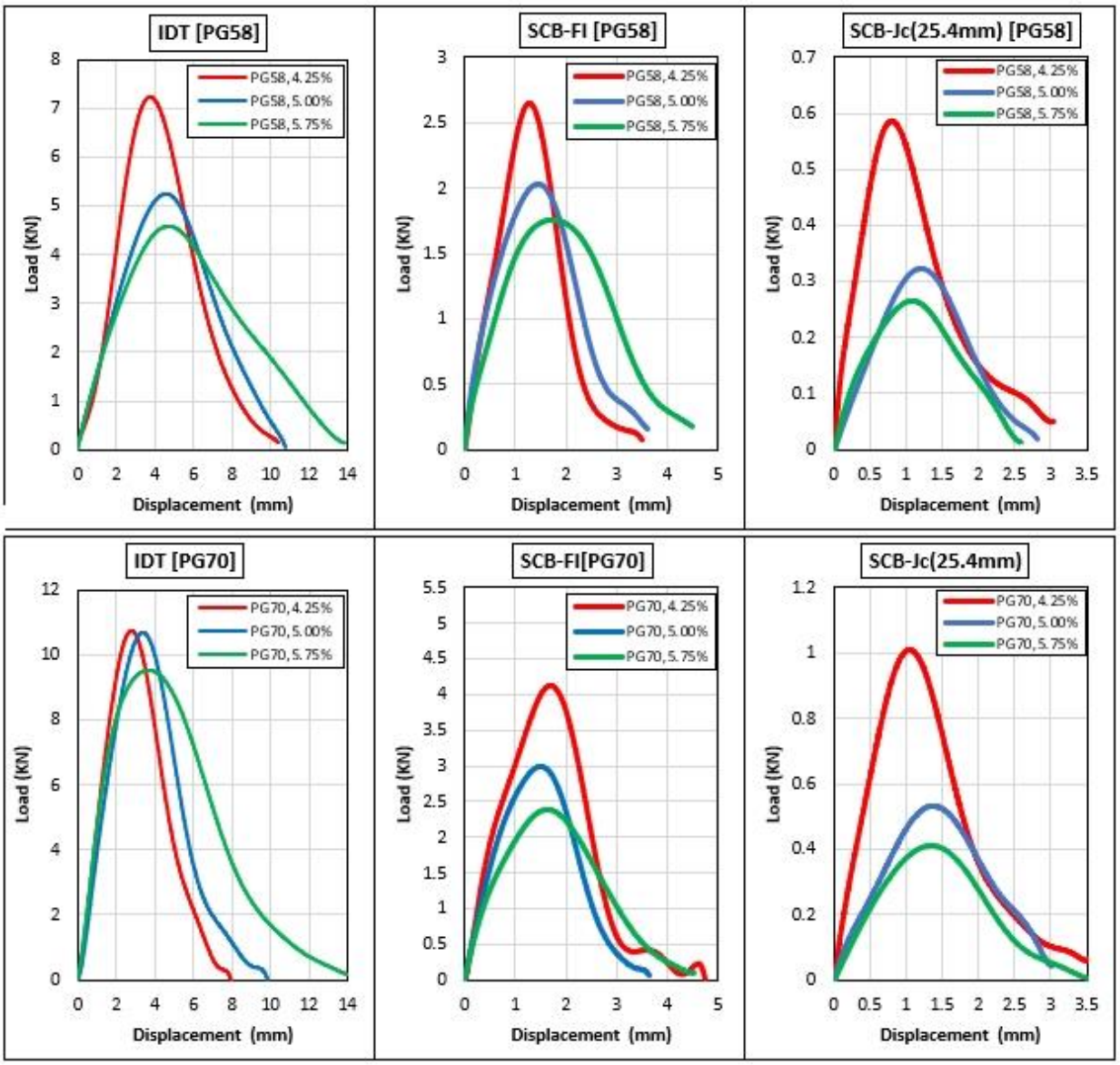

Figure 82 Monotonic Tests Load-displacement Curve at Different Binder Contents

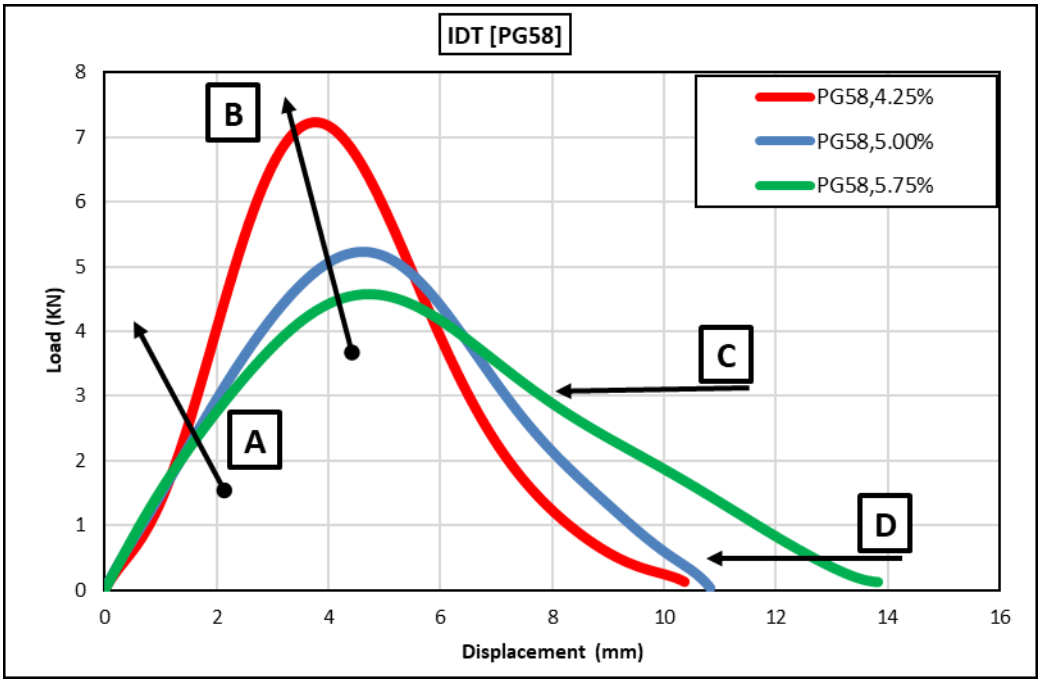

Figure 83 Example of Variation in Load-displacement Curve with the Decrease in Binder Content; (A) Increasing Pre-Peak Slope, (B) Increasing Peak, (C) Increasing Post-Peak Slope, and (D) Decreasing Failure Displacement

Figure 84 illustrates the load-displacement curves for binder with different PG (i.e., PG 70-28 and PG 58-34) and binder contents (i.e., 4.25 percent, 5.0 percent, and 5.75 percent). The change in binder PG affected the shape of the load-displacement curve. The pre-peak slope, curve peak, and post-peak slope of the load-displacement curve increased for the stiffer binder (PG 70-28) compared to the softer binder (PG 58-34). In general, all monotonic tests (e.g., IDT, SCB-FI, SCB-Jc) exhibited the same trend.

Sensitivity of Monotonic Cracking Resistance Indicators to Mixture Properties

The LMLC specimens were used to study the sensitivity of selected performance indicators to the variation in binder content and binder PG. The sensitivity to binder PG was evaluated using a statistical t-test at each binder content (two binder PG groups at each binder content). Sensitivity to binder content was evaluated using ANOVA and Tukey's Honestly Significant Difference (Tukey HSD) at each binder content (three binder content groups at each binder grade). Both tests were performed at 95 percent confidence interval (i.e., $\alpha = 0.05$). Figure 85 shows the average fracture energy calculated from the IDT test ($G_{fracture}$ [IDT]). The error bars represent ± one standard deviation from the average value. The statistical analysis results (Tukey HSD groups) are included in the form of letters or numbers at the bottom of each bar. Mixes that do not share the same letter/number are significantly different in terms of their fracture energy. Sensitivity for PG was evaluated using t-test at each binder content (two PG groups at each binder content).

The $G_{fracture}$ (IDT) results showed a low variability (COV = 11 percent). In addition, the $G_{fracture}$ (IDT) was sensitive to the variation in binder PG and binder content. The mixes prepared with PG70-28 binder had

higher fracture energy when compared to mixes prepared with PG 58-34 binder for a given binder content. Higher fracture energy is associate with better cracking resistance [35]. Meanwhile, it is expected that a softer binder (e.g., PG 58-34) would provide better cracking resistance to cracking when compared to a stiffer binder (e.g., PG 70-28). A significant difference in fracture energy was found at all binder content; *p-value* = 0.016, 0.029, 0.005 at 4.25 percent, 5.00 percent, and 5.75 percent binder content, respectively. Figure 85 shows that the fracture energy increases with binder content. Mixes prepared with the PG 70-28 binder were more sensitive to the change in binder content as compared to mixes prepared with the PG 58-34. The PG 70-28 mixes showed a statistically significant difference (*p*-value < 0.05) between mixes prepared at 4.25 percent and 5.75 percent binder content. Meanwhile, there was no statistically significant difference between mixes with different binder contents for PG 58-34 binder (*p*-value = 0.113).

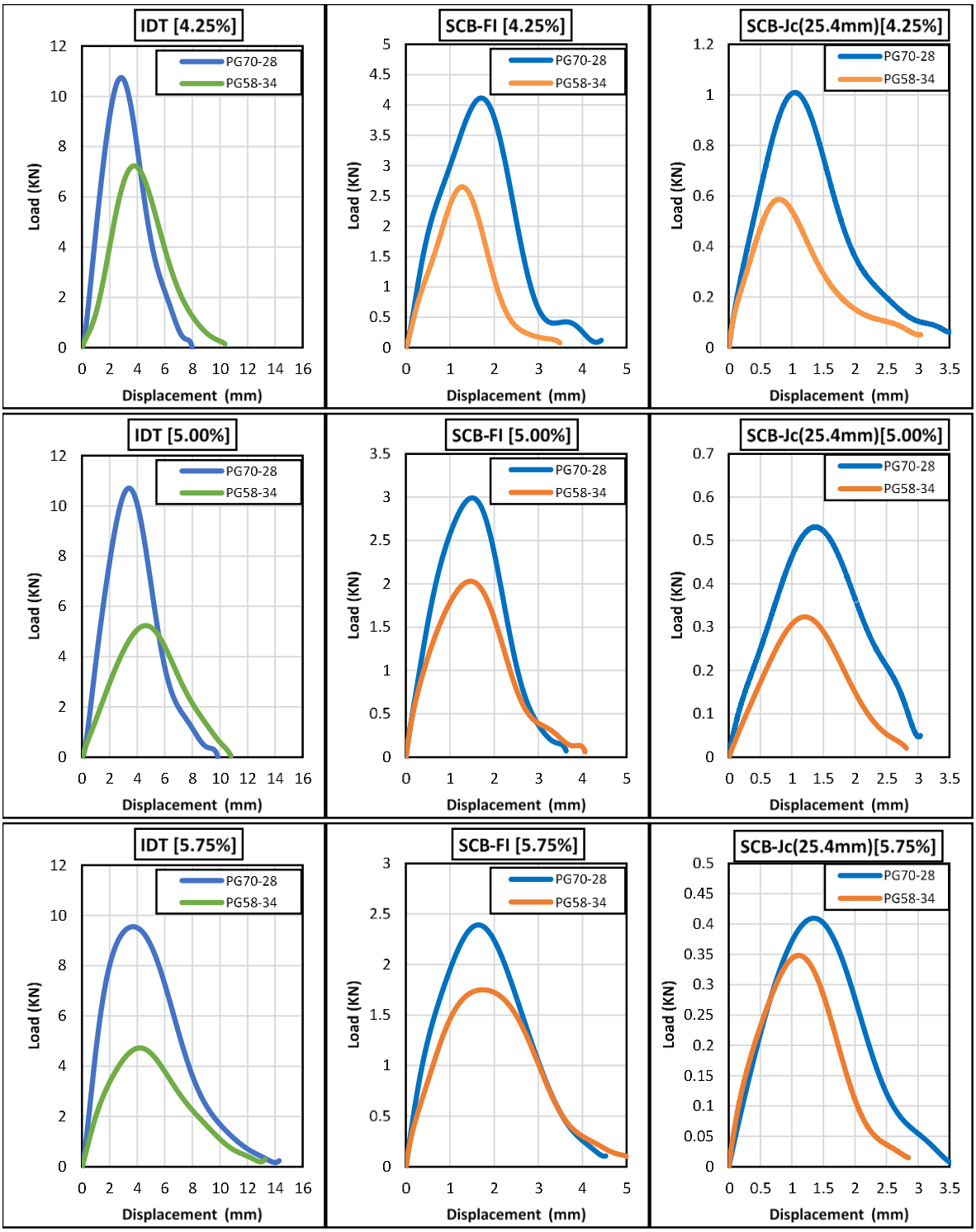

Figure 84 Monotonic Tests Load-displacement Curve at Different Binder Content and PG

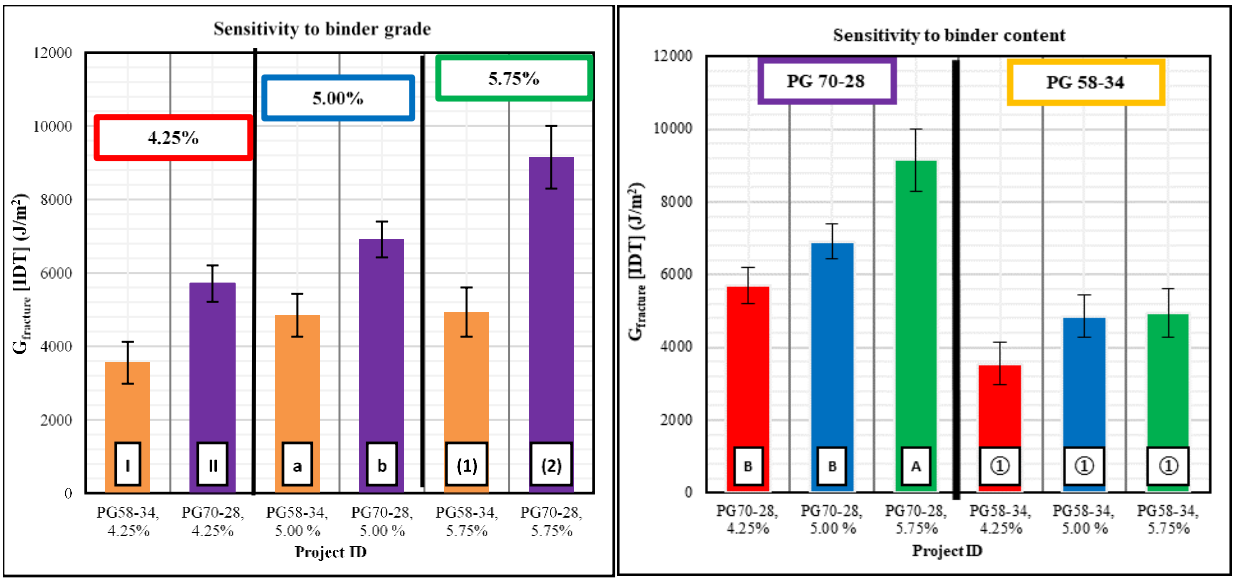

Figure 85 Sensitivity of Total Fracture Energy Calculated from the IDT Test to the PG and Binder Content

The analysis for other monotonic indicators was repeated. Table 26 summarizes the results of the analysis for all twelve selected performance indicators. The results of $G_{fracture}$ (IDT), $G_{fracture}$ (SCB-FI), $IDT_{strength}$, $IDT_{Modulus}$, and J_c indicate that mixes prepared with the PG 70-28 binder are expected to provide better cracking resistance compared to mixes prepared with the PG 58-34 binder. Other parameters including CRI (IDT), CRI (SCB-FI), FI (IDT), FI (SCB-FI), IDEAL-CT_{Index}, and Nflex factor showed that PG 58-34 mixes are expected to provide better cracking resistance compared to PG 70-28. The results of $Weibull_{CRI}$ showed that the mixes prepared with the PG 58-34 binder at 5.0 percent binder content to provide better cracking resistance compared to mixes prepared with the PG 70-24 binder at the same binder content. However, the mixes prepared with the PG 70-24 binder at 4.25 percent and 5.75 percent had higher $Weibull_{CRI}$ compared to mixes prepared with the PG 58-34 binder at the corresponding binder content.

Several performance indicators including CRI (IDT), CRI (SCB-FI), FI (IDT), FI (SCB-FI), IDEAL-CT_{Index}, Nflex factor, and $Weibull_{CRI}$ showed that cracking resistance is improved with the increase in binder content for the same binder PG (e.g., PG 70-28 and PG 58-34) as expected. Other performance indicators including $G_{fracture}$ (IDT), $G_{fracture}$ (SCB-FI), $IDT_{strength}$, $IDT_{Modulus}$, and J_c showed mixed trends with increasing binder content. The $G_{fracture}$ (SCB-FI) and $IDT_{strength}$ results showed statistical insignificant difference at various binder contents. It should be noted that the sensitivity analysis was conducted on LMLC specimens that were prepared using only two binders at three different binder contents. Investigation of additional mixes with various properties including mix design is recommended. Sensitivity plots for all performance indicators to binder content and binder type are included in Appendix C.

Table 26 PG Sensitivity of Monotonic Performance Indicators to Binder Content and Binder

Performance indicator	Parameter	Parameter	Parameter	Parameter
Performance indicator	Binder PG (using softer binder)	Binder PG (using softer binder)	Binder content (increasing binder content)	Binder content (increasing binder content)
Performance indicator	Trend	Statistically Significant?	Trend	Statistically Significant?
$G_{fracture}$ (IDT)	↙ (not as expected)	✓	⇳ (mixed trend)	⇔
$G_{fracture}$ (SCB-FI)	↙ (not as expected)	×	⇳ (mixed trend)	×
CRI (IDT)	↗ (As expected)	×	↗ (As expected)	⇔
CRI (SCB-FI)	↗ (As expected)	⇔	↗ (As expected)	⇔
FI (IDT)	↗ (As expected)	×	↗ (As expected)	⇔
FI (SCB-FI)	↗ (As expected)	✓	↗ (As expected)	⇔
IDEAL-CT_{Index}	↗ (As expected)	×	↗ (As expected)	⇔
Nflex factor	↗ (As expected)	×	↗ (As expected)	⇔
$IDT_{strength}$	↙ (not as expected)	✓	↙ (not as expected)	×
$IDT_{Modulus}$	↙ (not as expected)	⇔	⇳ (mixed trend)	⇔
J_c	↙ (not as expected)	N/A	⇳ (mixed trend)	N/A
$Weibull_{CRI}$	⇳[3] (mixed trend)	⇔	↗ (mixed trend)	⇔

1 ↙ indicates worse cracking resistance.
2 ↗ indicates better cracking resistance.
3 ⇳ shows both trends
4 ✓ test results are statistically different (e.g., binder content and binder PG)
5 × test results are not statistically different (e.g., binder content and binder PG)
6 ⇔ Results showed statistically significant/insignificant difference at comparison levels (e.g., binder content and grade)
Note: J_c indicator had only one value for each mixture, thus ANOVA and Tukey tests could not be performed

Correlation between Monotonic Performance Indicators and Field Performance

In this section, the correlation between monotonic performance indicators and field performance was assessed. The objective of this task was to propose performance thresholds for cracking resistance using monotonic performance indicators. There are factors that were found to affect the results of monotonic performance indicators. These factors include air void content and sample thickness [35,44,86,87]. Several other researchers have proposed methods to correct for the effect of both air void content and thickness [35,44,86,87].

Effect of Air Void Content and Sample Thickness on Monotonic Performance Indicators

Air void content plays an important role in the performance of asphalt mixes including the resistance to cracking. Linden et al. (1989) reported that 1 percent increment above the target air void content (i.e., 7 percent initial air voids) resulted in 10 percent reduction in pavement life [114]. Tran et al. (2016) reported that a reduction of 1 percent in air void content improved the cracking resistance between 8.2 percent and 43.8 percent [115]. In addition, Kassem et al. (2011) reported that air void content distribution affected fatigue cracking resistance [10].

Higher air void content results in improved cracking resistance using most of the performance indicators (except ITD tensile and modulus) which is misleading [35,44,86,87]. Figure 87 shows an example to illustrate the variation in the load-displacement curve due to the change in air void content [87]. The figure shows the load-displacement curve for five percentages of air void (i.e., 2 percent, 4 percent, 6 percent, 8 percent, and 10 percent). The curve peak, post-peak slope, pre-peak slope decreases, and failure displacement increase with the decreases in air voids. Such changes indicate less resistance to cracking using most of the performance indicators. In addition, Figure 87 shows that the area under the curve decreases with the increase in air voids. Based on the results of this example, it can be seen that some elements of the load-displacement (e.g., decreased peak and area under and curve) curve follow the expected trend with increased air void content. However, other curve elements including increasing the pre- and post-peak slopes provide misleading conclusions with the reduction in air void content since the higher post-peak slope indicates faster rate of damage or cracking propagation. Reduction in air void content is associated with better resistance to cracking and improved performance as discussed earlier [114,115,10]. Therefore, previous research proposed a correction to the monotonic performance indictors (e.g., flexibility index) to account for the effect of air void content as presented in Figure 86 [35,44,86,87].

$$FI_{7\%} = FI_{AV} \times \frac{7\%}{\text{AV}\%}$$

$$FI_{7\%} = FI_{AV} \times \frac{0.0651}{\text{AV-}AV^2}$$

Figure 86 Air Void Content Adjustment for Flexibility Index

where:

AV% = Specimen air void content

FI_{50} = Adjusted flexibility index at specimen thickness of 50 mm

$FI_{7\%}$ = Adjusted flexibility index at specimen air void content of 7%

FI_{AV} = Flexibility index at any given air void content AV

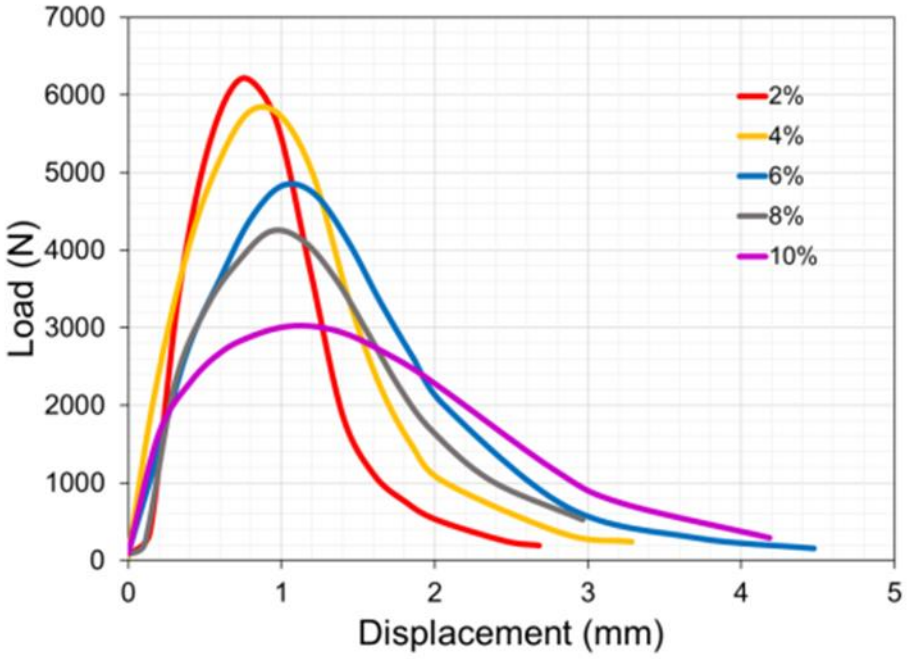

Figure 87 Effects of Air Void Content on the Shape of Load-displacement Curve of SCB Test [87]

Similar to the effect of air void content on the load-displacement curve, the specimen thickness was found to greatly affect the monotonic performance indicators [35,44,86,87]. For example, Figure 88 presents an example of the effect of thickness on the load-displacement curve. The curve peak, post-peak slope, pre-peak slope increases with thickness. An increased post-peak slope would indicate less resistance to

cracking which is opposite of what one can expect from a thicker specimen in terms of its resistance to cracking. Therefore, previous research proposed a correction to the monotonic performance indictors (e.g., FI) to account for the effect of thickness as presented in Figure 89 [35,44,86,87].

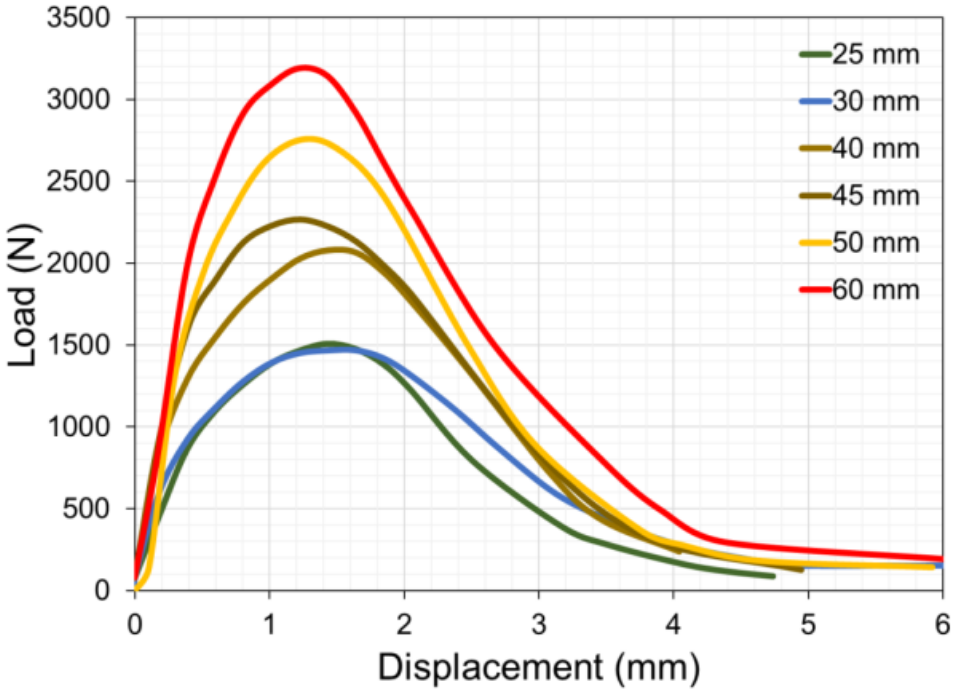

Figure 88 Effects of Specimen Thickness on the Shape of Load-displacement Curve of a SCB Test [87]

$$FI_{50} = FI_t \times \frac{t}{50}$$

Figure 89 Thickness Adjustment for Flexibility Index

where:

FI_{50} = Adjusted flexibility index at specimen thickness of 50 mm

FI_t = Flexibility index at specimen thickness t

t = Specimen thickness (mm)

In this study, the extracted field cores had different air void content and thicknesses as shown in Figure 90 and Figure 91. The thickness of field cores depends on the pavement structural design and historical maintenance treatments, while the air void content depends on the initial compaction and densification under traffic. The percent air void content was measured in accordance with ASTM D3203. The recovered cores had air void content ranging from 2.85 percent to 9.78 percent with a standard deviation between 0.16 percent and 4.25 percent. The thickness of the field cores was between 40.6 mm and 54.4 mm with a standard deviation between 0.2 mm and 1.23 mm. Various performance indicators

were calculated before and after corrections to account for different air void content and thickness using Figure 92.

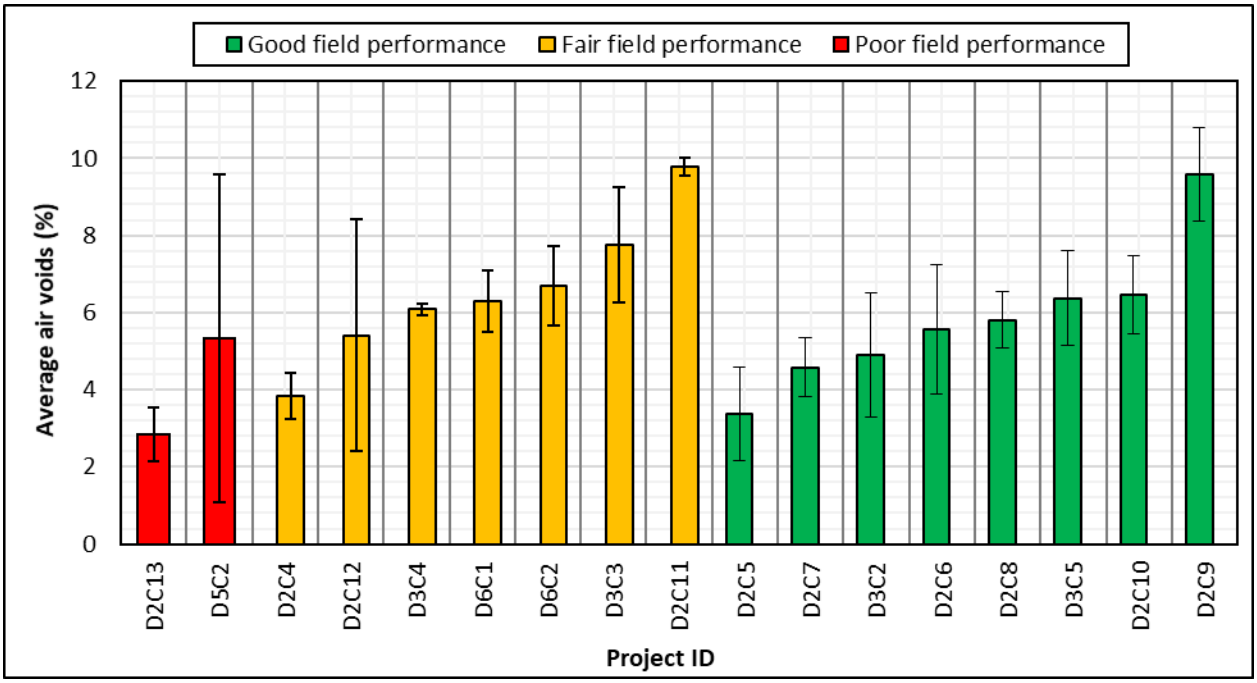

Figure 90 Average Air Void Content for the Extracted Field Cores

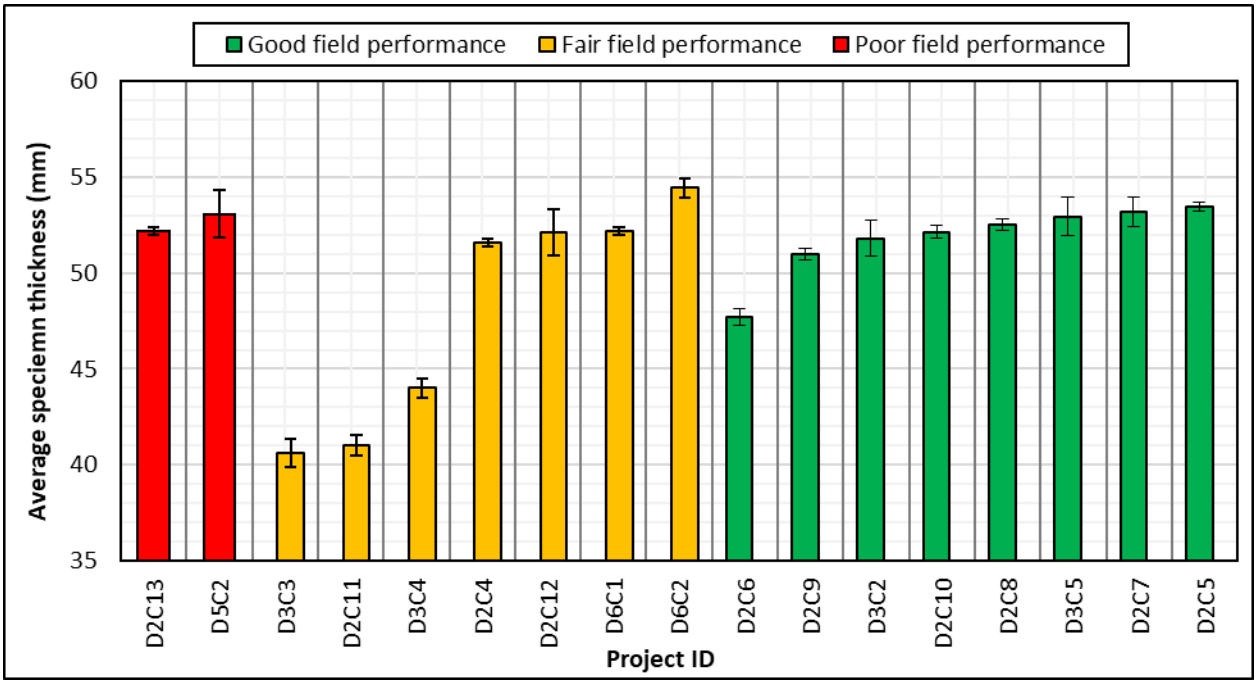

Figure 91 Average Thickness for the Extracted Field Cores

$$X_{Corrected} = \mathrm{X} \times \frac{7\%}{\mathrm{AV\%}} \times \frac{\mathrm{t}}{50}$$

Figure 92 Air Void Content and Thickness Adjustment for Performance Indicators

where:

AV% = Specimen air void content

X = Computed performance indicator

$X_{Corrected}$ = Corrected performance indicator

t = Specimen thickness

Monotonic Performance Indicators of the Field Cores

Similar to the efforts performed by the research team to develop performance thresholds using the MSSD test, they examined various performance indicators to group projects with good, fair, and poor field cracking performance. It should be noted that none of these sections were reported to have any structural deficiency. Asphalt pavements in the state are designed using Idaho R-value, AASHTO T93, WinFlex 2006, or Pavement ME. Therefore, the researchers related the field performance to mix properties. Figure 93 and Figure 94 show an example of the flexibility index (FI [SCB-FI]), before and after correction (to account for different thicknesses and air void contents). As it can be observed in the figures, this performance indicator (before or after correction) was not able to group or distinguish between mixes with different cracking resistance due to overlap of the test results. Similarly, Figure 95 and Figure 96 show the IDEAL-CT_{Index} before and after correction, respectively. These parameters failed to distinguish between projects with different cracking performance. All the remaining monotonic performance indicators were not able to differentiate between mixes with different cracking performance due to the overlap in test results. Appendix D includes the results of the remaining monotonic performance indicators. Table 27 provides the average values for various performance indicators for field projects with different field performance.

It should be noted that the proposed correction to the performance indicators to account for different air void contents and thicknesses was not always effective [44]. In fact, this is one of the limitations of the monotonic performance indicators. Kaseer et al (2018) found that the CRI and FI were still affected after correcting for air void contents. Perez. et al. (2018) indicated that the correction factor was to be applied when the air void content was less than 8 percent [85]. They observed that when specimen had air void contents higher than 8 percent, the SCB-FI test could not be considered as fracture test. The researchers concluded that developing a direct correlation between field performance and monotonic performance indicators was not feasible. Therefore, the research team used another approach to develop thresholds for selected performance indicators as discussed later in this chapter.

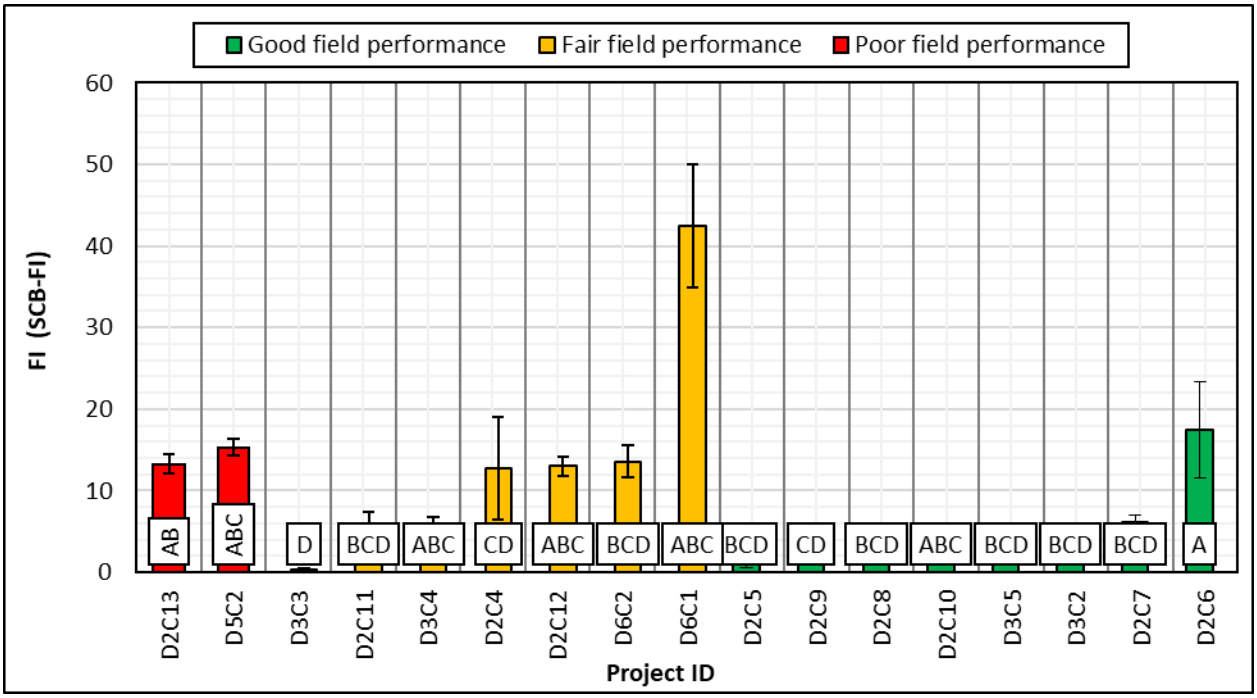

Figure 93 Correlation between FI from Computed from SCB Test with Field Project Performance

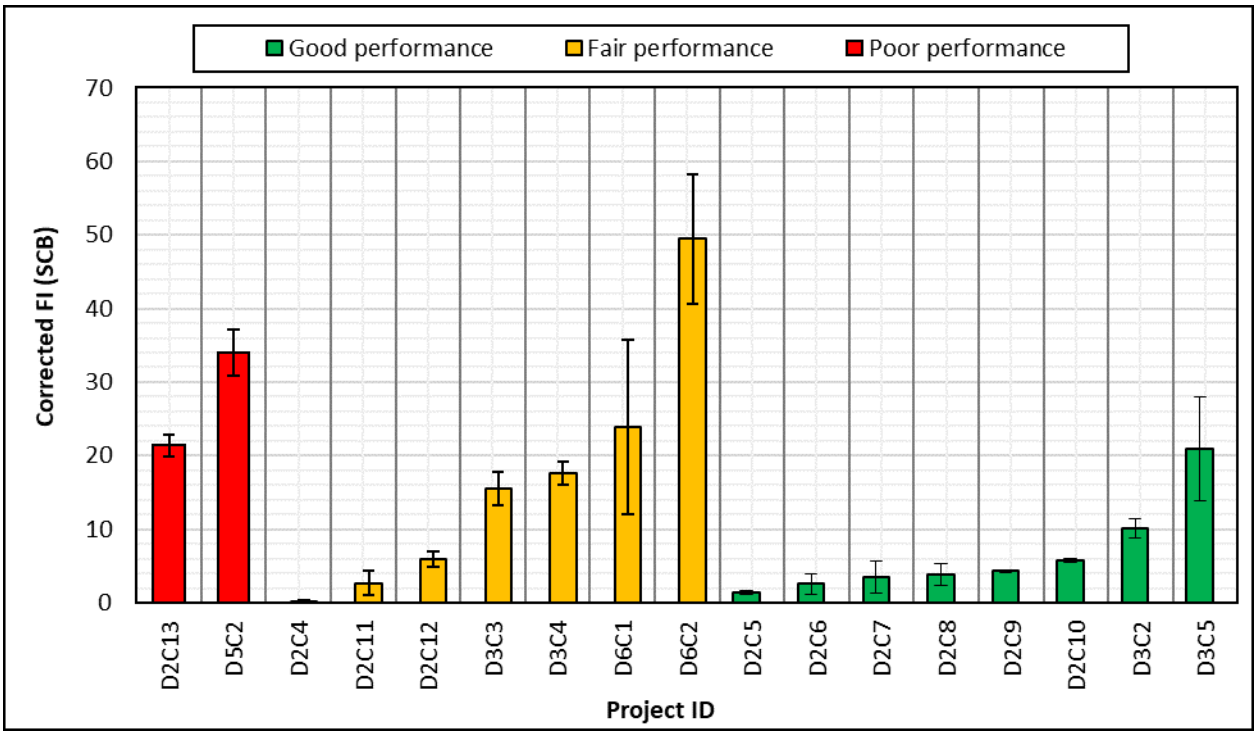

Figure 94 Correlation between Corrected FI from Computed with Field Project Performance

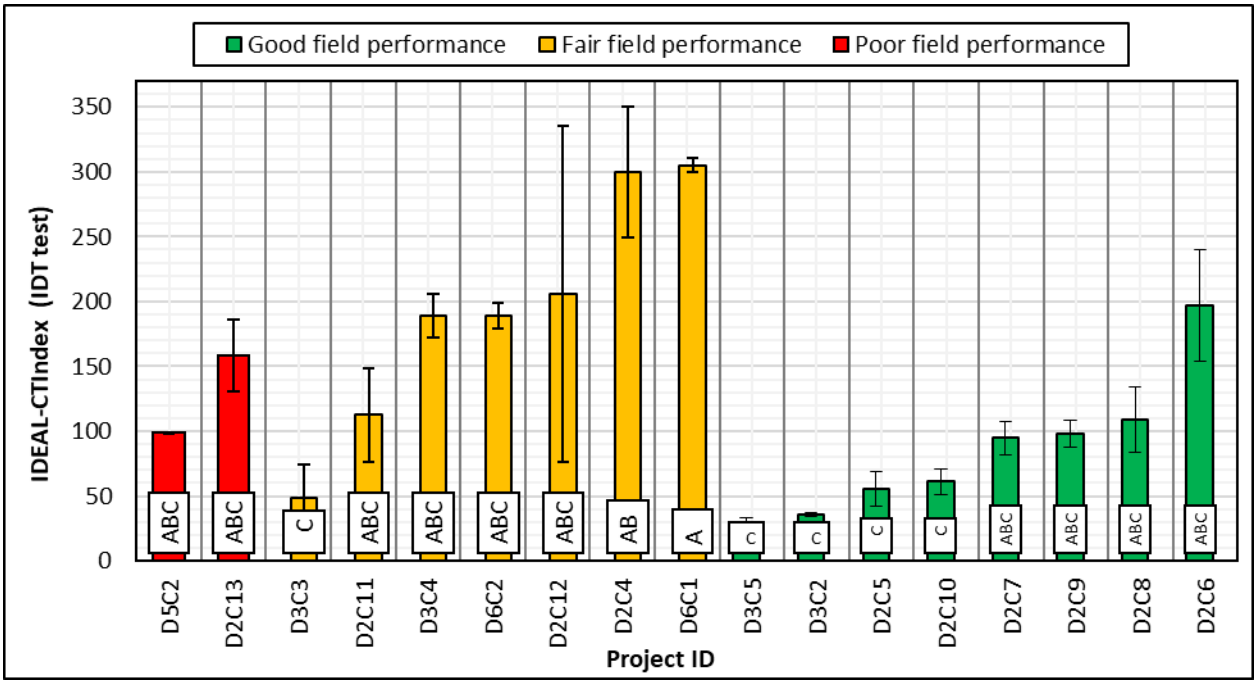

Figure 95 Correlation between IDEAL-CT$_{Index}$ from Computed with Field Project Performance

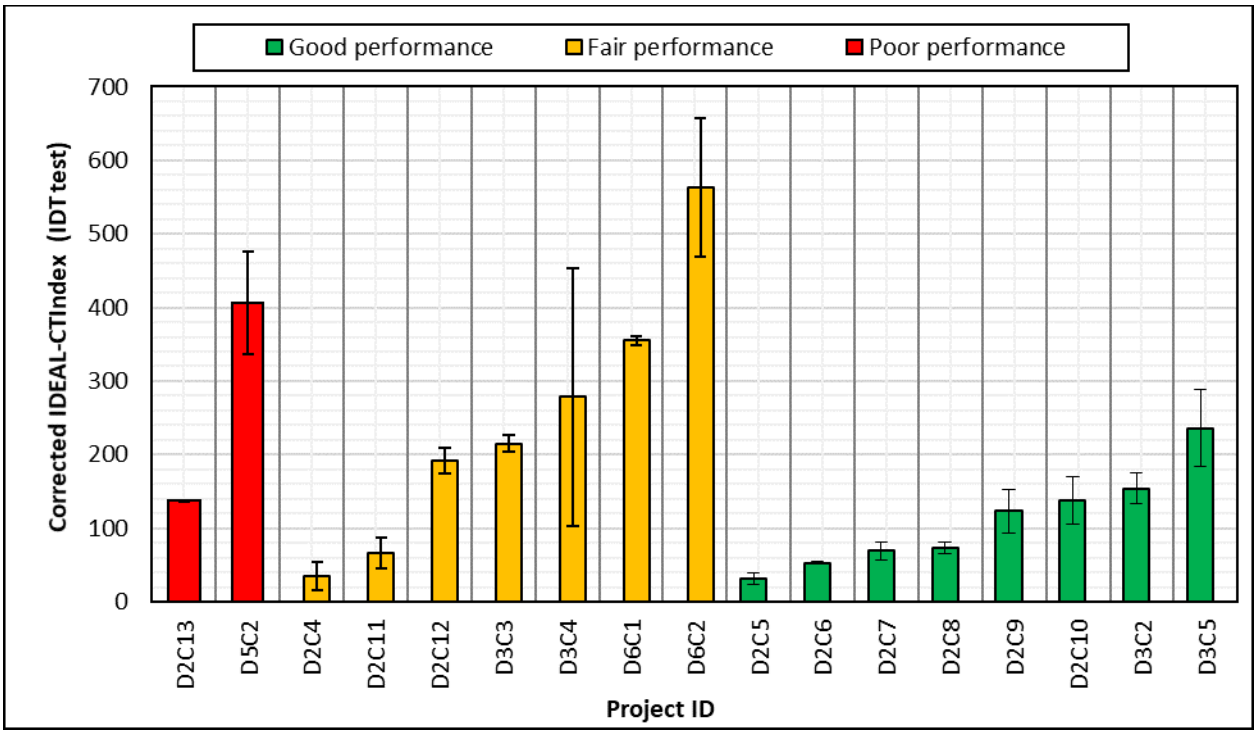

Figure 96 Correlation between Corrected IDEAL-CT$_{Index}$ with Field Project Performance

Table 27 Monotonic Indicators Sensitivity to Binder Content and PG

Performance indicator	**Estimated indicators values**	**Estimated indicators values**	**Estimated indicators values**	**Corrected indicators values**	**Corrected indicators values**	**Corrected indicators values**
Performance indicator	Field cracking resistance group	Field cracking resistance group	Field cracking resistance group	Field cracking resistance group	Field cracking resistance group	Field cracking resistance group
Performance indicator	Good	Fair	Poor	Good	Fair	Poor
$G_{fracture}$ (IDT) (J/m^2)	9963±418	8782±464	8708±666	13695±530	9472±499	18314±1146
$G_{fracture}$ (SCB-FI) (J/m^2)	2681±384	2600±259	3866±191	3582±562	2942±314	7811±280
CRI (IDT)	713±47	920±112	826±38	952±70	1069±131	1657±92
CRI (SCB-FI)	539±61	719±78	998±88	700±87	851±89	2045±183
FI (IDT)	29±3.4	48±8.5	40±4.1	38±4.8	58±10.4	83±10.5
FI (SCB-FI)	5±1.4	13±3.0	14±1.1	6.55±1.75	16.46±3.88	27.67±2.30
IDEAL-CT_{Index}	85±15.5	192±39	128±14	109±21	243±49	272±35
Nflex factor	0.83±0.11	1.4±0.26	1.21±0.12	1.1±0.16	1.67±0.32	2.49±0.28
$IDT_{strength}$ (kPa)	1263±67	929±106	946±112	1766±101	956±103	1950±215
$IDT_{Modulus}$ (kPa/mm)	370±47	246±68	248±31	514±64	249±67	510±58
J_c	0.95±0.4	.88±0.5	1.29±0.6	0.95±0.49	0.89±0.4	2.20±0.45
$Weibull_{CRI}$	4.8±0.3	6.8±1.4	5.5±0.3	6.45±2.3	8.1±3.8	11.3±4.6

Cracking Resistance Evaluation of PMLC Mixes using Monotonic Tests

In this section, the monotonic performance tests and indicators were used to assess the cracking resistance of PMLC mixes. The results of various performance indicators for the PMLC mixes were compared to the recommended thresholds from the literature to evaluate the cracking resistance of asphalt mixes currently produced in Idaho compared to other states. The variability of each performance indicator was studied. In addition, the results of various performance indicators were compared to the MSSD test to assess the correlation between both monotonic and dynamic test parameters and propose performance thresholds for selected monotonic performance indicators. The performance of asphalt mixes depends on their composition. The variation in one or more of the design parameters affects the overall mixture cracking resistance. Several research studies examined the effect of specific design parameters on the overall mixture cracking resistance. The results demonstrated that the cracking resistance improved with higher binder content, softer binder grade, using polymer modifier binder, higher aggregate angularity, smaller NMAS, lower air void content, lower RAP content, unaged binder, and replacing sand with crushed aggregate [31,110–112]. In this study, the effect of PMLC mixture composition on the cracking resistance was discussed.

Monotonic Performance Indicators

Fracture Energy

Figure 97 shows the fracture energy calculated from the IDT test ($G_{fracture}$ [IDT]). The $G_{fracture}$ (IDT) ranged from 5300 J/m^2 to 7540 J/m^2 with a standard deviation (SD) between 694 J/m^2 and 1214 J/m^2. Higher fracture energy is associated with better cracking resistance [116]. The $G_{fracture}$ (IDT) had low variability (COV = 10 percent). ANOVA test indicated a significant difference in the test results (p-value < 0.05). Tukey's HSD test classified the mixes into four performance groups; A (higher $G_{fracture}$ [IDT]), B, C, and D (lower $G_{fracture}$ (IDT)). The $G_{fracture}$ (IDT) results were consistent with expected performance. For example, it was expected that D2L2 to exhibit better cracking resistance compared to D3L1 and D3L5 mixes because mixture D2L2 has the highest binder content (5.70%), softer virgin binder (PG 58-34), small NMAS (12.5 mm), while mixture D3L1 has the highest RBR content (50 percent) and stiffer binder PG (PG 70-28). Similarly, $G_{fracture}$ (IDT) results showed that D1L1 would provide better cracking resistance than D3L5 because these mixes have the same RBR (30 percent), binder content (5.3 percent), NMAS (12.5 mm) and mix type (SP5), but D1L1 has a softer binder PG (PG 64-28) than D3L5 (PG 76-28). Thus, it was expected that D1L1 to provide better cracking resistance as compared to D3L5.

Also, $G_{fracture}$ (IDT) results showed that D2L1 provided better cracking resistance when compared to D3L1 because these mixes have the same RBR (50 percent), binder PG (PG 70-28), NMAS (12.5), and mix type (SP3), but D2L1 had higher binder content (5.7 percent) compared to D3L1 (5.20 percent). Thus, it was expected that D2L1 to provide better cracking resistance as compared to D3L1. Furthermore, $G_{fracture}$ (IDT) results showed that mixture D2L2 had better performance when compared to D2L1 because these mixes had the same NMAS (12.5), mix type (SP3), and binder content (5.7 percent), but D2L2 has a lower RBR (30 percent) and softer design binder PG (PG 64-28), and softer binder PG (PG 58-34) as compared to D2L1 with RBR of 50 percent, design binder PG of 70-28, and virgin PG of 64-34. Thus, it was expected

that D2L2 to exhibit better cracking resistance as compared to D2L1. Meanwhile, it was expected that D1L1 to provide better cracking resistance than D3L3, but $G_{fracture}$ (IDT) showed opposite results. D1L1 and D3L3 have the same RBR (30 percent), binder content (5.30 percent), NMAS (12.5 mm), binder PG (PG 64-28), and softer virgin binder PG (PG 58-34), but D1L1 has better mix type (SP5) than D3L3 (SP3). Thus, it was expected to have better cracking resistance. However, laboratory results showed that D3L3 had higher $G_{fracture}$ (IDT) than D3L3.

Figure 98 shows the fracture energy calculated from the semi-circular bending-flexibility index ($G_{fracture}$ [SCB-FI]) test. The $G_{fracture}$ (SCB-FI) ranged from 1404 J/m^2 to 2899 J/m^2 with a SD between 120 J/m^2 and 453 J/m^2. The $G_{fracture}$ (SCB-FI) results exhibited low variability (COV = 11 percent). The ANOVA indicated a statistically significant difference in the test results (p-value < 0.05). Tukey's HSD classified the mixes into four performance groups; A (higher $G_{fracture}$ [SCB-FI]), B, C, and D (lower (higher $G_{fracture}$ [SCB-FI]). Similar to the results of $G_{fracture}$ (IDT), D2L2, D6L1 and D2L1 had the highest $G_{fracture}$ (SCB-FI) while D3L1 and D3L5 had the lowest $G_{fracture}$ (SCB-FI). Tukey HSD demonstrated a statistically significant difference between these mixes where D1L1, D6L1 and D2L2 were classified in group A, while D3L1 and D3L5 were classified in group D. Also, similar to $G_{fracture}$ (IDT), $G_{fracture}$ (SCB-FI) provided a good agreement between expected cracking performance based on mix composition. $G_{fracture}$ (SCB-FI) results showed that D2L2 had better cracking resistance than D2L1 and D3L1; in addition, mixture D1L1 had better cracking resistance than D3L5 and D3L1. Also, D2L1 provided better cracking resistance than D3L1, which is in good agreement with the $G_{fracture}$ (SCB-FI) results.

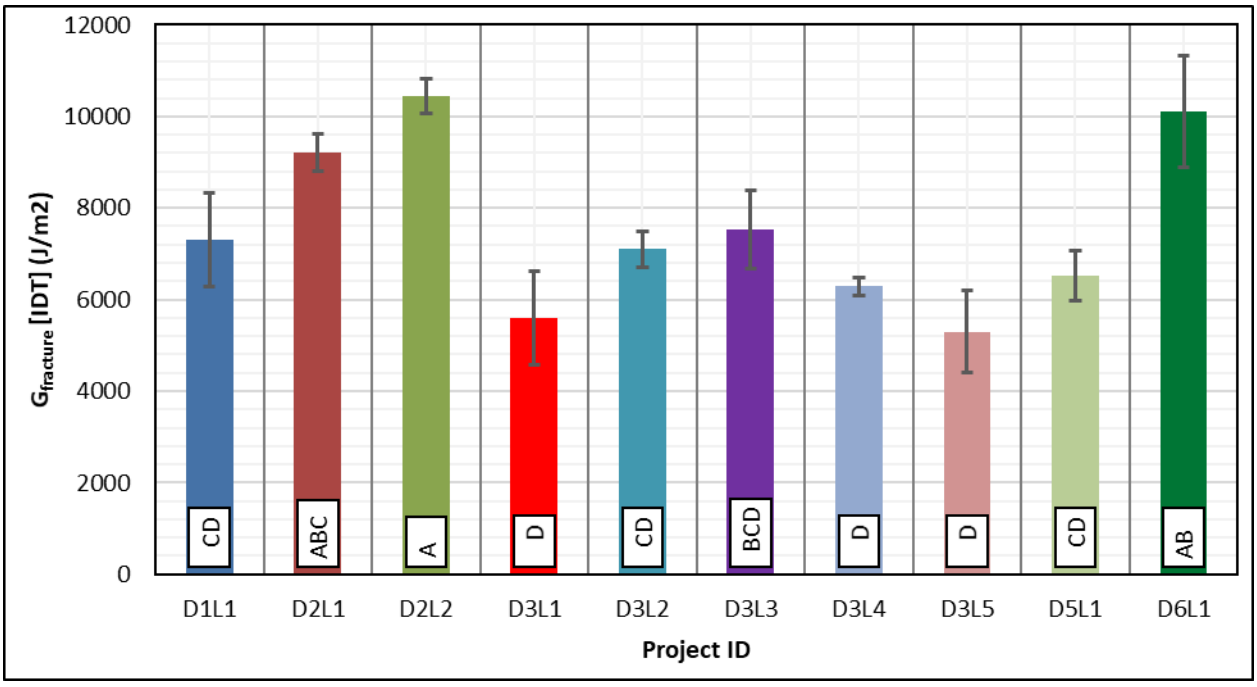

Figure 97 Total Fracture Energy Calculated from the IDT Test for the PMLC Mixes

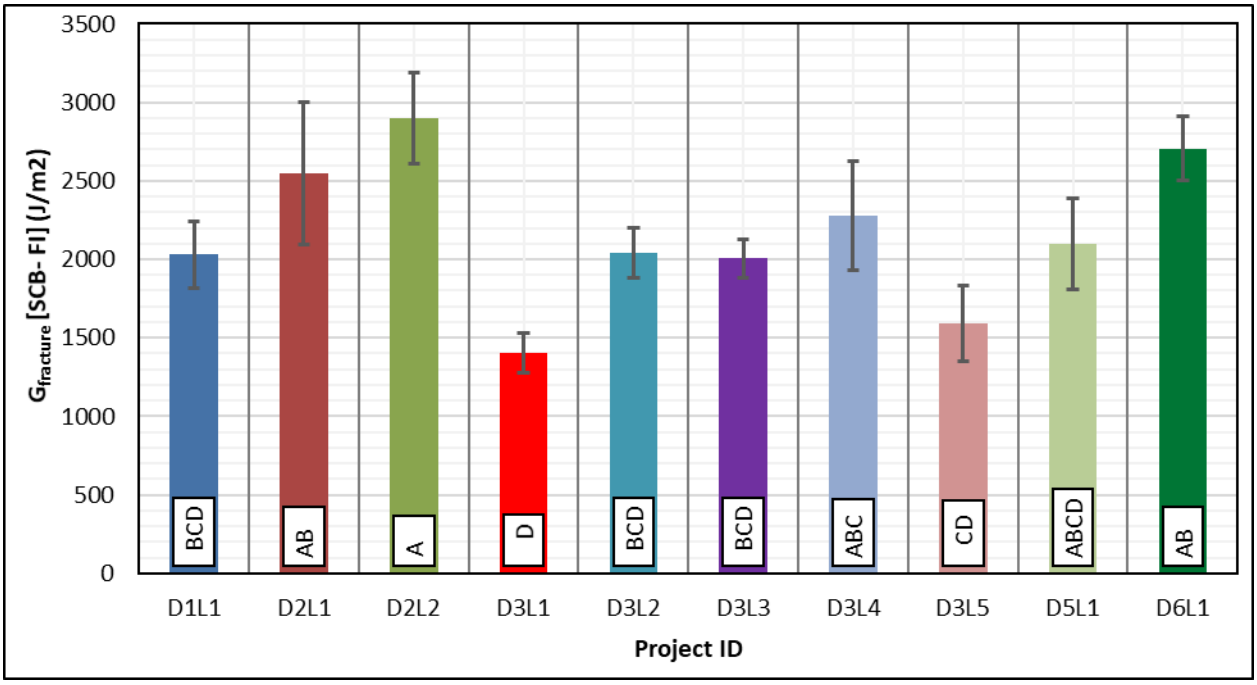

Figure 98 Total Fracture Energy Calculated from the SCB-FI Test for the PMLC Mixes

Cracking Resistance Index (CRI)

The Cracking Resistance Index (CRI) was calculated using the test data from the IDT test as well as the SCB-FI test. Figure 99 and Figure 100 show the CRI (IDT) and CRI (SCB-FI), respectively. The CRI (IDT) ranged from 431 and 707, with SD between 17 and 97. The CRI [SCB-FI) ranged from 384 and 618 with SD between 65 and 152. Both indicators had low variability (COV = 9 percent and 11 percent for CRI [IDT] and CRI [SCB-FI], respectively) in the test results. The CRI results showed less dependency on the specimen geometry as compared to the fracture energy. The ANOVA analysis indicated a statistically significant difference between mixes performance (p-value < 0.05) for both indicators. Tukey's HSD classified mixes into four performance groups; A (higher CRI), B, C, and D (lower CRI) for both indicators. Higher CRI indicates higher resistance to cracking [44]. Similar to $G_{fracture}$ (SCB-FI), CRI (IDT) and CRI (SCB-FI) showed good agreement with expected performance based on mix composition. The results showed that D2L2 had better cracking resistance than D2L1 and D3L1, D1L1 had better cracking resistance than D3L5 and D3L1, and D2L1 would have better cracking resistance than D3L1.

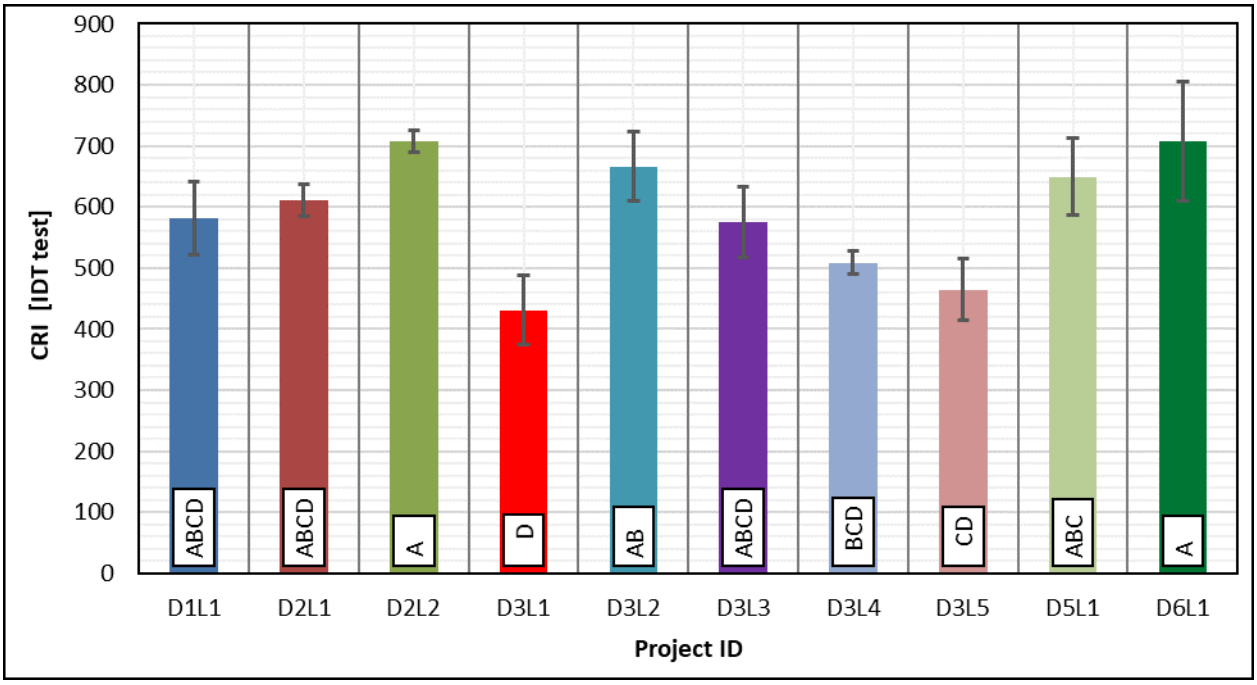

Figure 99 Cracking Resistance Index Calculated from the IDT Test for the PMLC Mixture

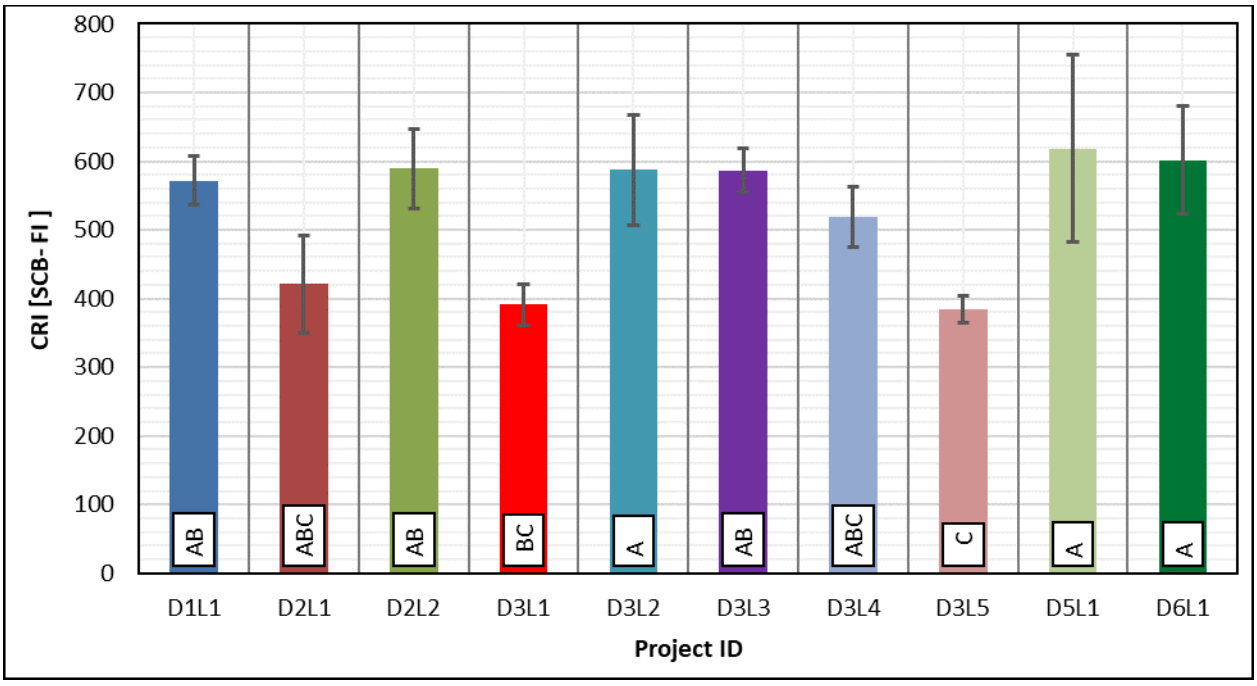

Figure 100 Cracking Resistance Index Calculated from the SCB-FI Test for the PMLC Mixes

Flexibility Index (FI)

The Flexibility Index was calculated using test data from the SCB-FI test and from IDT tests. Figure 101 and Figure 102 show FI (SCB-FI) and FI (IDT), respectively. Figure 101 shows that the PMLC have a flexibility index between 2 and 7. According to Ozer et al. (2016) [41] mixes with FI higher than 6 are expected to have acceptable performance and mixes with FI higher than 10 are expected to have higher cracking resistance. They recommended adjusting the proposed thresholds to account for PMLC mixes and local conditions. Based on such thresholds, it is expected that most of the PMLC mixes to have fair resistance to cracking.

Recently, the Illinois Department of Transportation (IDOT) [35] specified a minimum FI threshold of 8. The researchers believe that this is could be a conservative limit. The Tukey's HSD analysis classified all the PMLC into two groups A and B. Group A had higher FI than group B and these two groups were statistically different. The FI (IDT) (Figure 102) had lower average COV (about 19 percent) when compared to FI (SCB-FI) (COV = 27 percent). Similar to the FI (SCB-FI), the Tukey's HSD analysis classified the FI (IDT) results into two groups. The FI (IDT) results showed that D6L1 had the highest flexibility index, while D3L1 had the lowest FI. Similar to $G_{fracture}$ (SCB-FI), FI (IDT) and FI (SCB-FI) results provided good agreement with expected performance based the composition of the mix. Indicator results showed that D2L2 had better cracking resistance than D2L1, and D3L1 and D1L1 would have better cracking resistance than D3L5 and D3L1, and D2L1 would have better cracking resistance than D3L1.

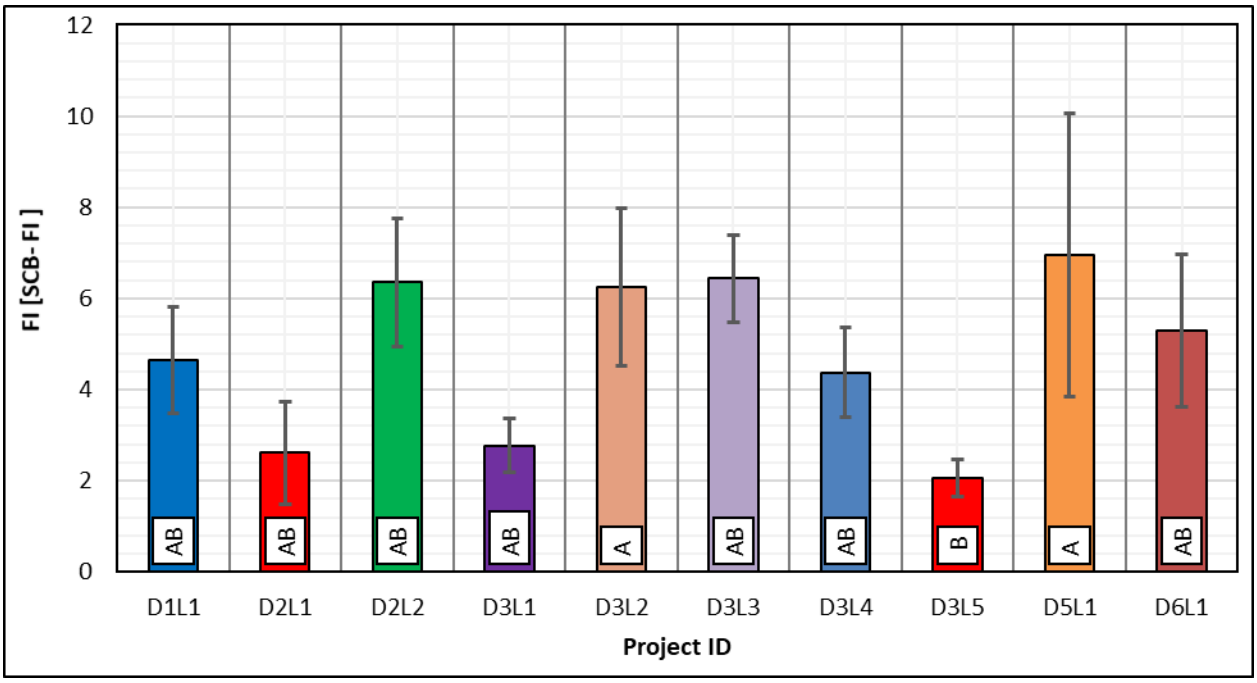

Figure 101 Flexibility Index Calculated from the SCB-FI Test for the PMLC Mixes

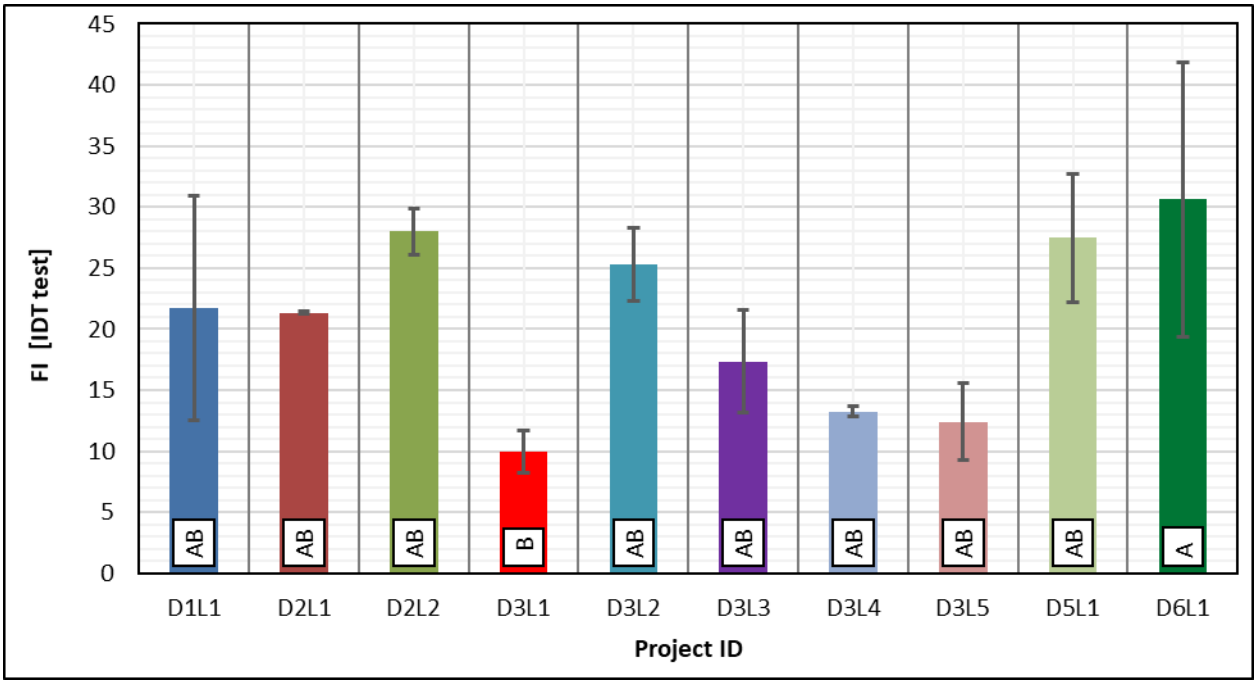

Figure 102 Flexibility Index Calculated from the IDT Test for the PMLC Mixes

IDEAL-CT_{Index}

This IDEAL-CT test is conducted in accordance with ASTM D8225 – 19. Figure 103 shows the results of the IDEAL-CT_{Index} for all PMLC mixes. The IDEAL-CT_{Index} ranged from 27 and 106 with a SD between 2.8 and 35. This index exhibited a moderate variability in the test results (average COV of 24 percent). Tukey HSD analysis classified the mixes into two groups (i.e., A and B). Group A had higher IDEAL-CT_{Index} when compared to group B. Higher IDEAL-CT_{Index} indicates better cracking resistance [73]. Based on the results, it was expected that mixes with higher IDEAL-CT_{Index} (e.g., D1L1 and D2L2) provided better cracking resistance compared to other mixes. Similar to $G_{fracture}$ (SCB-FI), IDEAL-CT_{Index} results provided good agreement with expected performance. Diefenderfer and Bowers (2019) [117] proposed a threshold of 80 for the Virginia Department of Transportation (VDOT). Most of the PMLC mixes had lower IDEAL-CT_{Index} than the proposed threshold of 80 except D1L1, D2L2, D3L2, and D6L1.

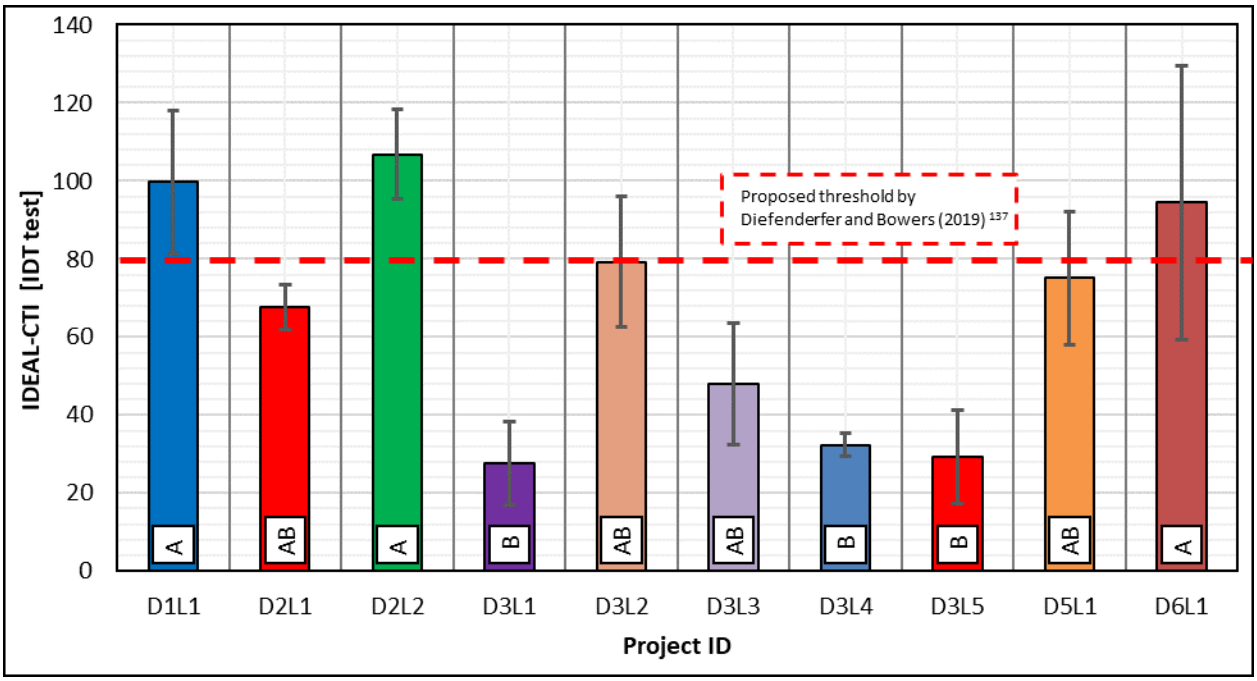

Figure 103 IDEAL-CT$_{Index}$ Calculated from the IDT Test for the PMLC Mixes

Nflex Factor

Figure 104 shows the Nflex factor calculated using the IDT test data. The mixes had average values between 0.34 and 0.98 with a SD between 0.005 and 0.245. The test had a COV of 17%. The Tukey's HSD analysis classified the mixes into two groups; A and B. Group A had higher Nflex factor when compared to Group B, with higher Nflex factor indicating better resistance to cracking. The Nflex factor results showed that D6L1 and D2L1 had good cracking resistance, while D3L1 and D3L5 had poor cracking resistance. West et al. (2017) [59] recommended a threshold of 0.8 for Nflex factor to ensure adequate resistance to cracking. Based on the proposed threshold, it is expected that mixes D2L2, D3L2, D5L1, D6L1 to exhibit good cracking resistance while the other mixes to have poor cracking resistance.

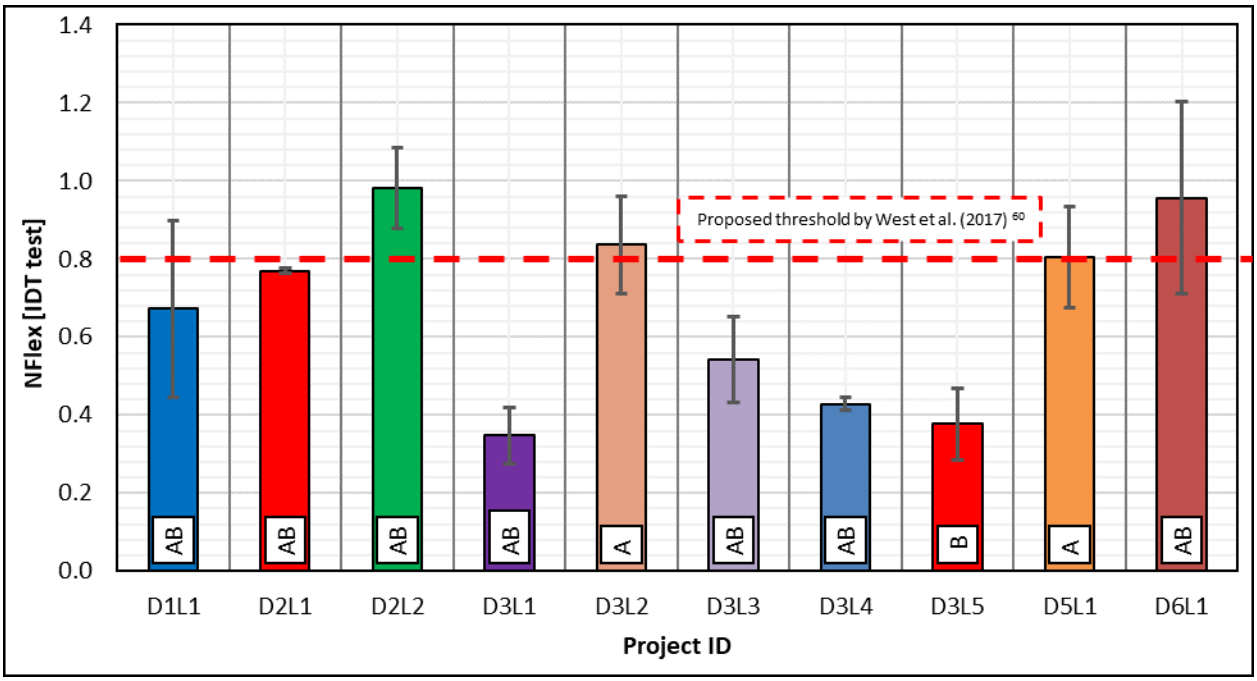

Figure 104 Nflex Factor Calculated from the IDT Test for the PMLC Mixes

$IDT_{strength}$

Figure 105 shows the $IDT_{strength}$ calculated from the IDT test data. The mixes had average strength values between 835 kPa and 1225 kPa with SD between 4.22 kPa and 173 kPa. Overall, the data showed a low variability (COV = 6 percent). Tukey HSD analysis classified the mixes into two group A and B. Group A had higher $IDT_{strength}$ when compared to group B. Higher $IDT_{strength}$ does not necessary indicate better cracking resistance thus this index could be misleading. Both strength and deformation should be considered when evaluating the resistance of asphalt mixes to cracking. $IDT_{strength}$ provided limited agreement with expected performance based on the composition of the mix. The results of this indicator showed that D2L2 had higher $IDT_{strength}$ than D3L1; D1L1 had a higher $IDT_{strength}$ than D3L5; and D2L1 had higher $IDT_{strength}$ than D3L1. However, D2L1 showed higher $IDT_{strength}$ than D2L2, and D3L3 had higher $IDT_{strength}$ than D1L1. Figure 104 shows that only D2L1, D2L2, D3L1 and D3L3 were expected to have good cracking resistnance based on the proposed thresholds using the field cores results.

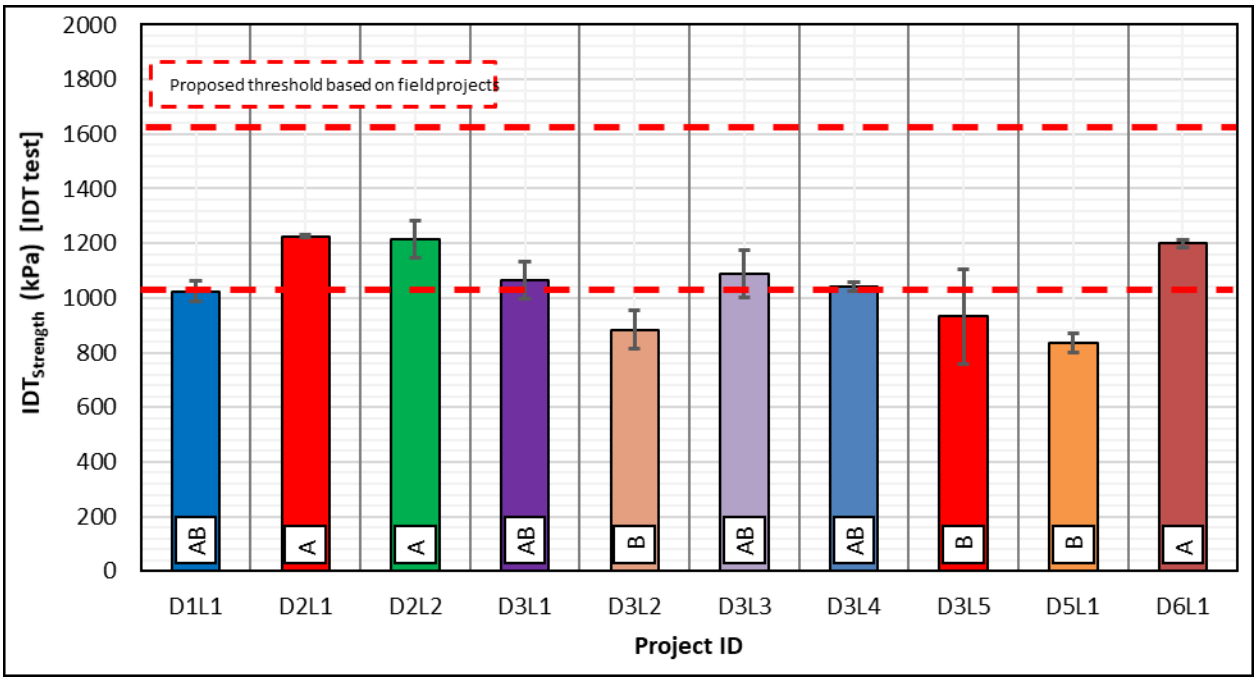

Figure 105 IDT-strength for the PMLC Mixes

$IDT_{Modulus}$

Figure 106 shows the $IDT_{Modulus}$ for all PMLC mixes calculated using the IDT test data. The $IDT_{Modulus}$ ranged from 249 kPa/mm to 363 kPa/mm with SD between 16 kPa/mm and 126 kPa/mm. The results of this test had COV of 18%. The ANOVA results indicated insignificant statistically difference between the test results for all the mixes (*p*-value = 0.713). In other words, there was no statistically significant difference in the $IDT_{Modulus}$ for all the mixes. A maximum threshold of 1700 kPa/mm is used in Japan for 100 percent RAP specimens [81]. Asphalt mixture test specimens were prepared using 100 percent RAP and tested at a constant displacement rate of 50 mm/min at 20℃. All the PMLC mixes had $IDT_{Modulus}$ less than the specified threshold thus these mixes are expected to have good resistance to cracking. $IDT_{Modulus}$ results showed that D2L1 had better cracking resistance than D3L1, which opposite to expected performance.

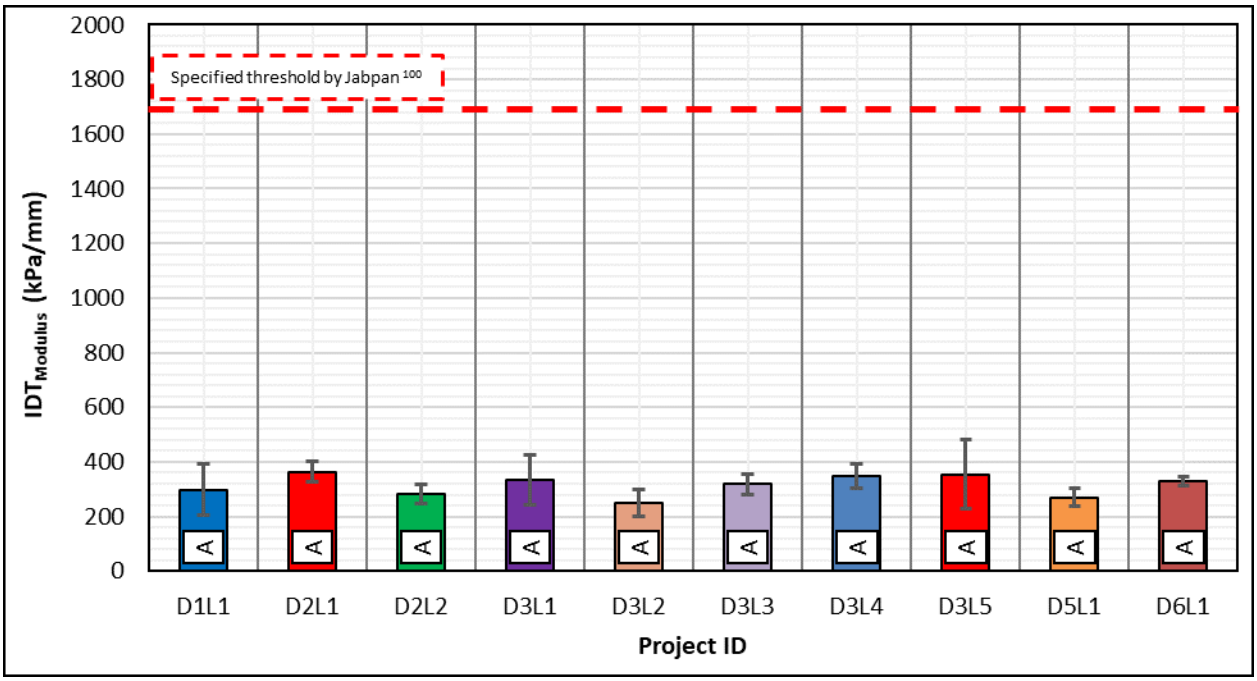

Figure 106 $IDT_{Modulus}$ Calculated from the IDT Test for the PMLC Mixes

Strain Energy Release Rate (J_c)

Figure 107 shows the J_c results calculated from the SCB- J_c test. The J_c for the PMLC mixes ranged from 0.1 kJ/m^2 to 0.97 kJ/m^2. Mixture D6L1 had the highest J_c (0.97 kJ/m^2), while D3L1 had the lowest J_c (0.10 kJ/m^2). Previous research has shown that higher J_c is associated with better resistance to cracking [15]. LADOT specifies a minimum threshold of 0.5 kJ/m^2 and 0.6 kJ/m^2 for Level-1 and Level-2 mix design, respectively [15]. Based on the Level-1 threshold (0.5 kJ/m^2), mixes D2L2, D3L2, D3L3, D3L4, D3L5 and D6L1 are expected to exhibit good cracking resistance, while the remaining mixes are expected to have poor cracking resistance.

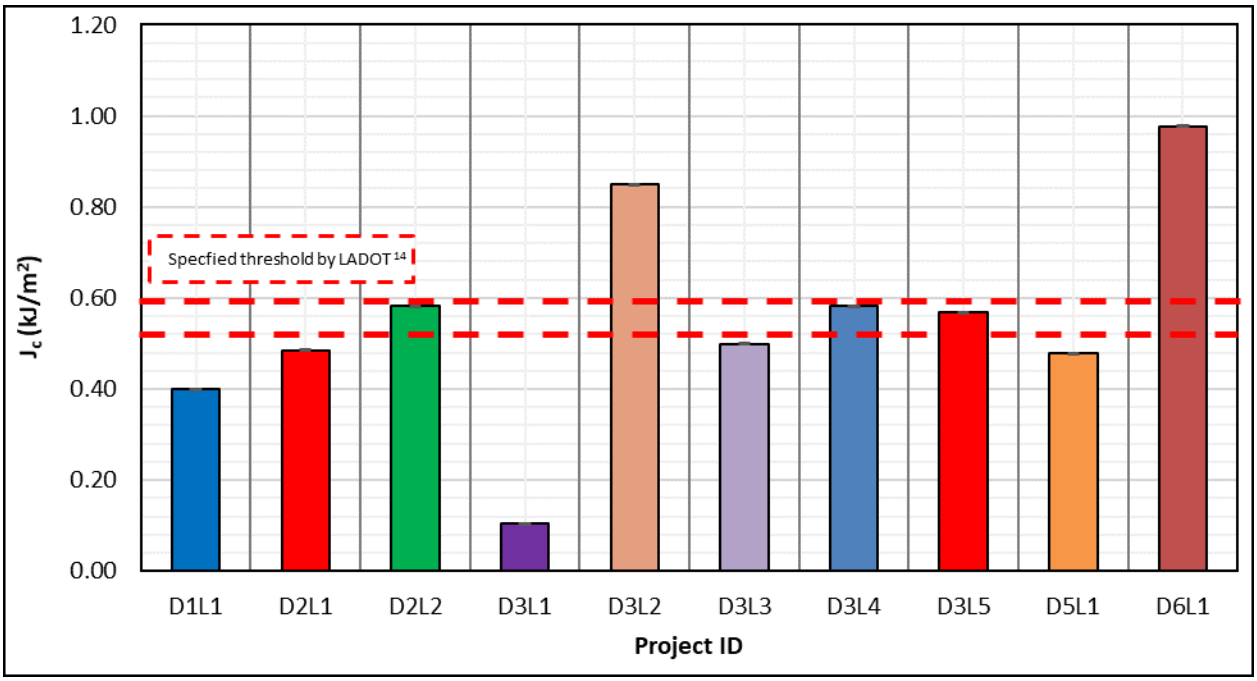

Figure 107 J_c Test Results Calculated from the SCB- J_c Test for the PMLC Mixes

$Weibull_{CRI}$

Figure 108 shows the $Weibull_{CRI}$ results for all PMLC mixes. The $Weibull_{CRI}$ ranged from 2.93 to 5.59 with a SD between 0.02 and 0.79. The results showed low variability (average COV = 6 percent). The ANOVA results indicated a significant difference between mixes (*p*-value < 0.05). Tukey HSD test classified mixes into four statistical group; A (highest $Weibull_{CRI}$), B, C, and D (lowest $Weibull_{CRI}$). As discussed in Chapter 4, mixes with higher $Weibull_{CRI}$ are expected to provide better resistance to cracking. Mixes D6L1 and D2L2 had the highest $Weibull_{CRI}$, while D3L1 had the lowest $Weibull_{CRI}$. Therefore, the former is expected to provide better racking as compared to the latter. $Weibull_{CRI}$ results provided good agreement with expected performance based on the composition of the mix. The results of this indicator showed that D2L2 had cracking resistance (higher $Weibull_{CRI}$) when compared to D2L1 and D3L1. Also, as expected D1L1 had better cracking resistance than D3L5 and D3L1 had cracking resistance than D3L1 which is in good agreement with the $Weibull_{CRI}$ results.

Monotonic Performance Indicators Variability

One important advantage of the monotonic tests over the dynamic tests is that the monotonic tests have lower variability in the results as compared to the dynamic tests. Lower variability yields more repeatable performance indicators thus improving the overall cracking resistance assessment. The COV was used to assess the variability of the various tests. The coefficient of variation (COV) is one of the statistical tools that can be used to study the variability of the test data around the mean value. The coefficient of variation (COV) is the ratio of standard deviation to the mean. COV is independent of the units of performance parameters thus it can be used to compare the variability of performance indicators [118]. The COV ranges from 0 to 100 percent where higher values indicate more variation with

respect to the mean.

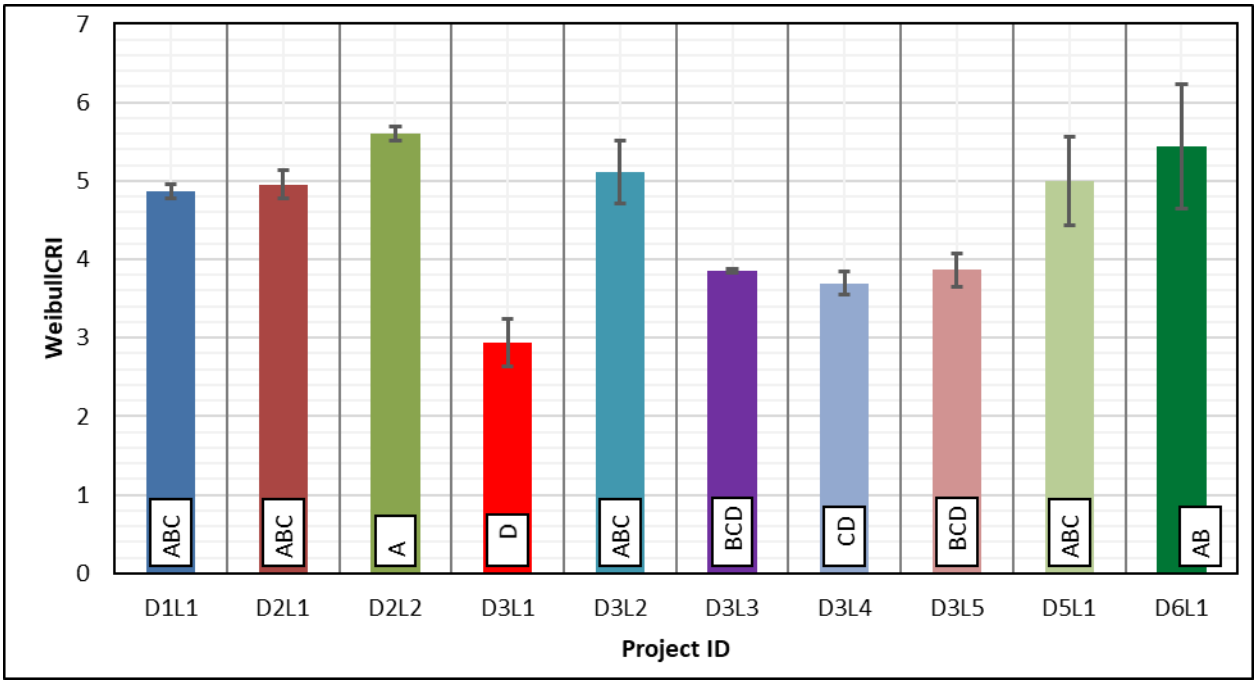

Figure 108 Weibull-CRI Calculated from IDT Test for PMLC Mixes

Figure 109 shows the average and the range of the COV for various performance indicators calculated from the respective monotonic tests for both LMLC and PMLC. The field projects were not included in this comparison since they have different air void content and thickness which may affect the variability of different performance indicators. The indicators were classified into three categories based on their COV; low variability (COV <10 percent), moderate variability (20 percent < COV < 35 percent), and high variability (COV > 35 percent). The results demonstrate that the $Weibull_{CRI}$ had the lowest average COV (7.4 percent). The flexibility index (FI) calculated from the SCB-FI test had the highest average COV (25.8 percent). Performance indicators with low variability included $Weibull_{CRI,}$ $IDT_{strength,}$ CRI (IDT), $G_{fracture}$ (IDT), $G_{fracture}$ (SCB-FI) and CRI (SCB-FI), while $IDT_{strength}$, Nflex, FI (IDT), FI (SCB-FI) and IDEAL-CT had moderate variability. In general, performance indicators calculated from the IDT test data exhibited low variability compared to indicators calculated from the SCB test data. $G_{fracture}$ (IDT) had an average COV of 10.3 percent while $G_{fracture}$ (SCB-FI) had an average COV of 14.2 percent. FI (IDT) had an average COV of 19 percent, while FI (SCB-FI) had an average COV of 25.8 percent. CRI (IDT) had an average COV of 8.7 percent, while CRI (SCB-FI) had an average COV of 11.3 percent.

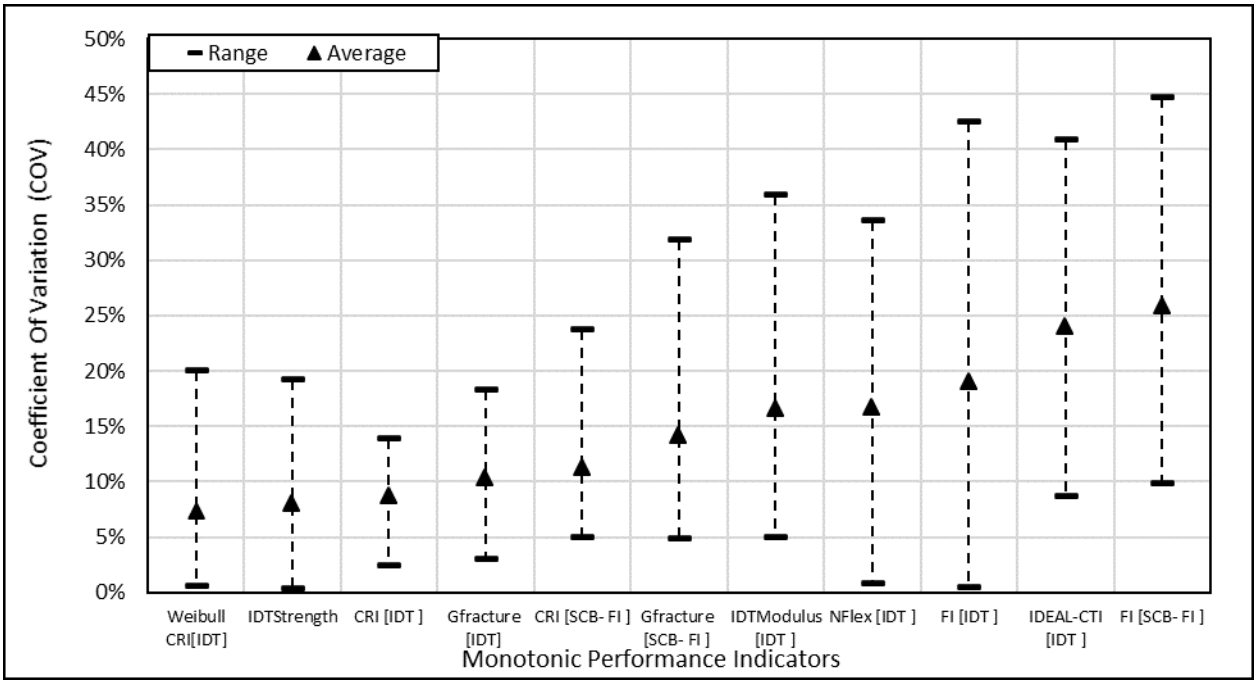

Figure 109 COV Percent Range for Different Performance Indicators using LMLC and PMLC Data

Correlation between Monotonic Performance Indicators

This study evaluated several cracking resistance performance indicators that were calculated from different testing protocols. This section studied the type and strength of the correlation between various performance indicators. The correlation is defined as "a measure of association between two variables that expresses the degree to which the two variables are rectilinearly related" [118]. Two statistical tools were used to examine the correlation between the monotonic performance indicator; the Pearson product moment correlation coefficient (r) and the Spearman rank correlation coefficient (r_s). The Pearson coefficient examines the linear relationship between two performance indicators [118]. The Spearman rank coefficient is a particular case of the Pearson coefficient where it examines the agreement on mixture performance ranking between two performance indicators [118]. The coefficients (r and r_s) range between -1 and +1. The coefficient magnitude indicates the relationship strength, the higher the value, the better the correlation. The coefficient sign indicates the relationship type, where a positive sign indicates a direct relationship, and a negative sign indicates an inverse relationship [118]. The coefficients were computed using Minitab statistical analysis software.

Table 28 presents the computed Pearson coefficients. All coefficients had a direct (positive sign) correlation with each other except with $IDT_{Modulus}$. Performance indicators from different tests (i.e., IDT or SCB) showed excellent or good correlation. There was a strong correlation between $G_{fracture}$ (IDT) and $G_{fracture}$ (SCB-FI) (r = 0.912). There was a good correlation between CRI (IDT) and CRI (SCB-FI), FI (IDT) and FI (SCB-FI) with r = 0.774, 0.742, and 0.713, respectively. J_c and $IDT_{strength}$ do not correlate well or no correlation at all with other indicators. On the other side, the $Weibull_{CRI}$ correlated with more indicators than any other performance indicators. The $Weibull_{CRI}$ had strong correlation with CRI (IDT) (r =0.941), FI

(IDT) (r =0.950), IDEAL-CT_{Index} (r =0.922), and Nflex factor (r =0.922). Also, the $Weibull_{CRI}$ had good correlation with $G_{fracture}$ (IDT) (r =0.767), $G_{fracture}$ (SCB-FI) (r =0.784) and fair correlation with and J_c (r =0.634), FI (SCB-FI) (r =0.516), and $IDT_{Modulus}$ (r = - 0.498). Such good correlation of $Weibull_{CRI}$ with most of the performance indicators was attributed to its calculation method. Each indicator uses one or more elements of the load-displacement curve, while $Weibull_{CRI}$ describes the entire load-displacement curve.

Understanding the correlation between indicators is needed; however, it is more important to examine how various performance indicators rank the same test mixes in terms of cracking resistance. Table 29 presents the computed Spearman correlation coefficients. The $Weibull_{CRI}$ had better ranking agreement with more indicators than any other performance indicators. The $Weibull_{CRI}$ had excellent agreement (r_s > 0.9) with CRI (IDT), FI (IDT), and Nflex factor. Also, it had good ranking agreement (0.7< r_s > 0.9) with $G_{fracture}$ (IDT), $G_{fracture}$ (SCB-FI), CRI (SCB-FI), and IDEAL-CT_{Index}. The CRI (IDT) had an excellent ranking agreement with FI (IDT) (r_s = 0.975) and perfect agreement (r_s of 1) with Nflex factor. J_c had fair to poor ranking agreement with all indicators. $IDT_{Modulus}$ ranking had an indirect ranking with other indicators. The Pearson and Spearman correlation results clearly demonstrated the advantages of using $Weibull_{CRI}$ over other parameters. It had better ranking agreement and correlation with more indicators than any other performance indicators.

Table 28 Pearson Coefficient (r) for Monotonic Performance Indicators

Pearson *coefficient	$Weibull_{CRI}$	$G_{fracture}$ (IDT)	$G_{fracture}$ (SCB-FI)	CRI (IDT)	CRI (SCB-FI)	FI (IDT)	FI (SCB-FI)	IDEAL-CT_{Index}	Nflex factor	$IDT_{strength}$	$IDT_{Modulus}$	Jc
$Weibull_{CRI}$	1											
$G_{fracture}$ (IDT)	0.767[2]	1										
$G_{fracture}$ (SCB-FI)	0.784	0.912	1									
CRI (IDT)	0.941[1]	0.805	0.810	1								
CRI (SCB-FI)	0.626	0.426	0.507	0.774	1							
FI (IDT)	0.950	0.742	0.738	0.975	0.760	1						
FI (SCB-FI)	0.516	0.342	0.409	0.713	0.952	0.673	1					
IDEAL-CT_{Index}	0.922	0.756	0.700	0.878	0.685	0.902	0.562	1				
Nflex factor	0.962	0.830	0.807	0.981	0.674	0.977	0.606	0.911	1			
$IDT_{strength}$	0.199	0.758	0.617	0.231	-0.110	0.147	-0.178	0.257	0.281	1		
$IDT_{Modulus}$	-0.4984[4]	-0.093	-0.101[4]	-0.572[3]	-0.731	-0.586	-0.801	-0.576	-0.538	0.471	1	
Jc	0.634	0.476	0.560	0.668	0.499	0.628	0.384	0.433	0.601	0.054	-0.228	1

[1] Green cells indicate excellent correlation ($r \geq 0.9$),[2] orange cells indicate good correlation ($0.7 < r < 0.9$),[3] yellow cells indicate fair correlation ($0.5 < r \leq 0.7$) white cells indicate poor correlation ($0.1 < r \leq .5$), and [4] red cells indicate not correlation

Table 29 Spearman Coefficient (r_s) for Monotonic Performance Indicators

Spearman Coefficient	$Weibull_{CRI}$	$G_{fracture}$ (IDT)	$G_{fracture}$ (SCB-FI)	CRI (IDT)	CRI (SCB-FI)	FI (IDT)	FI (SCB-FI)	$IDEAL\text{-}CT_{Index}$	Nflex factor	$IDT_{strength}$	$IDT_{Modulus}$	Jc
$Weibull_{CRI}$	1											
$G_{fracture}$ (IDT)	0.697[2]	1										
$G_{fracture}$ (SCB-FI)	0.733	0.745	1									
CRI (IDT)	0.964[1]	0.794	0.806	1								
CRI (SCB-FI)	0.721	0.564[3]	0.576	0.818	1							
FI (IDT)	0.927	0.745	0.758	0.964	0.891	1						
FI (SCB-FI)	0.442[4]	0.418	0.273	0.576	0.879	0.624	1					
$IDEAL\text{-}CT_{Index}$	0.842	0.770	0.661	0.879	0.709	0.891	0.515	1				
Nflex factor	0.964	0.794	0.806	1.000	0.818	0.964	0.576	0.879	1			
$IDT_{strength}$	0.139	0.685	0.479	0.212	-0.091[5]	0.115	-0.176	0.152	0.212	1		
$IDT_{Modulus}$	-0.515	-0.236	-0.115	-0.576	-0.758	-0.600	-0.830	-0.612	-0.576	0.442	1	
Jc	0.491	0.309	0.539	0.503	0.345	0.442	0.127	0.285	0.503	0.103	-0.103	1

[1] Green cells indicate excellent correlation ($r_s \geq 0.9$),[2] orange cells indicate good correlation ($0.7 < r_s < 0.9$),[3] yellow cells indicate fair correlation ($0.5 < r_s \leq 0.7$) white cells indicate poor correlation ($0.1 < r_s \leq .5$) and [4] red cells indicate not correlation

Correlation between Monotonic and Dynamic Performance Indicators

Earlier in this chapter, the researchers correlated the monotonic tests to field performance, but the comparison was not favorable. It is believed that the different air void contents and thicknesses of the field cores highly affected the monotonic test results. Conversely, the team proposed thresholds based on the MSSD test that were found to distinguish between mixes with different field cracking resistance. The MSSD test is easy to conduct using an AMPT or MTS and the specimen preparation is simpler. However, the longer testing time (3 to 9 hours) could be a disadvantage compared to the short testing time of the monotonic tests. Therefore, the researchers searched for possible ways to develop threshold performance criteria for selected performance indicators calculated from monotonic tests. The team compared the MSSD testing parameters (i.e., slope [*z*] and absolute intercept [Abs (log *H)*]) to various performance indicators of the monotonic tests for PMLC mixes. The PMLC mixes were prepared at the required thickness of the different monotonic tests as well as the MSSD test, in addition they had same average percent air void content (7±0.5 percent). Fixing the thickness and percent air void content for the test specimens eliminated the effect of these variables on the results of the monotonic tests, thus leading to better performance evaluation. Figure 111 illustrates an example of the correlation between MSSD parameters (i.e., slope [z] and absolute intercept [Abs (log *H*)]) and $Weibull_{CRI}$ performance indicator calculated using the IDT test. The correlation between $Weibull_{CRI}$ performance indicator and MSSD slope (*z*) parameters provided a coefficient of determination (R^2) of 0.81 and 0.51 for the MSSD

absolute intercept [Abs (log *H*)]) parameters. Such correlations can be described using an exponential function (Figure 110). The $Weibull_{CRI}$ decreases with the slope while it increases with the absolute intercept. Both trend lines agree with the definition of each parameter/indicator. Higher $Weibull_{CRI}$, lower slope, and higher absolute intercept indicate better resistance to cracking. Since the slope provided a better correlation with $Weibull_{CRI}$, the next step was to transfer the MSSD performance thresholds to the $Weibull_{CRI}$ as illustrated in (Figure 112). The slope (*z*) parameter proposed three cracking resistance thresholds; good cracking resistance ($z < 1.9$), fair cracking resistance ($1.9 \leq z \leq 2.9$), and poor cracking resistance ($z > 2.9$). These thresholds were transferred to $Weibull_{CRI}$ using the correlation function between $Weibull_{CRI}$ and z parameter (Figure 112). Three thresholds for $Weibull_{CRI}$ were proposed, good cracking resistance ($Weibull_{CRI} > 4.7$), fair cracking resistance ($3.57 \leq Weibull_{CRI} \leq 4.7$), and poor cracking resistance ($Weibull_{CRI} < 3.57$).

$$Y = C_4 \times e^{C_5 X}$$

Figure 110 Correlation between MSSD Parameters

where:

Y = MSSD indicators (slope, or absolute intercept)

X = Monotonic performance indicators

C_4 and C_5 = Exponential fitting constants

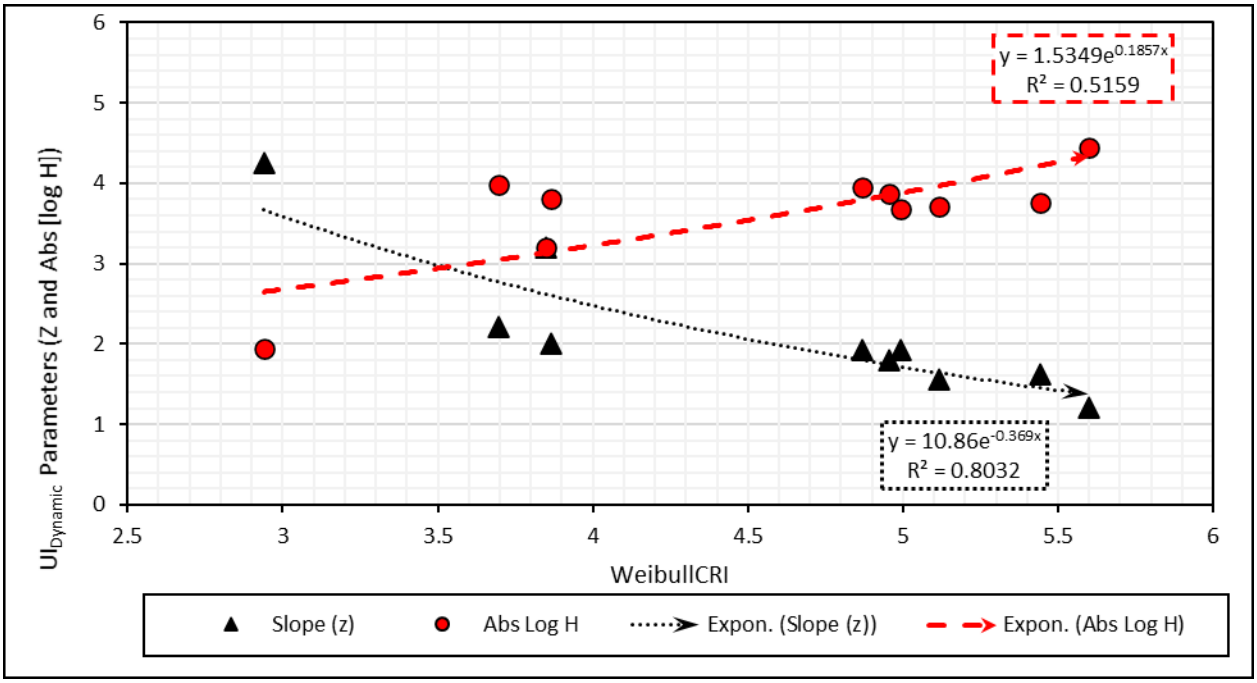

Figure 111 Correlation between MSSD Parameters (Slope, and Absolute intercept) and $Weibull_{CRI}$

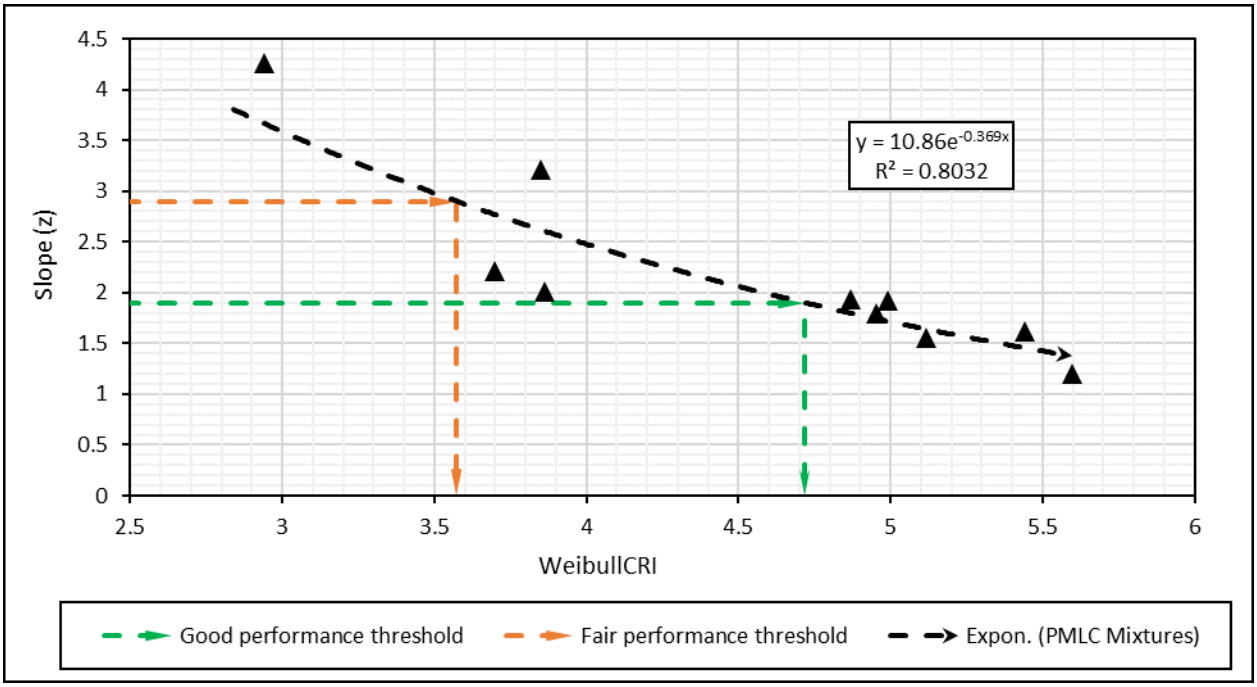

Figure 112 Proposed Weibull$_{CRI}$ Performance Thresholds based on the MSSD Slope (*z*) Parameter

The same above procedure was repeated and followed with all other monotonic parameters and presented in Appendix E. Table 30 summarizes the correlation coefficients (C_4 and C_5), coefficient of determination (R^2), and the proposed thresholds for other monotonic performance indicators. The results of Table 30 demonstrate that all monotonic indicators had better correlation (higher R^2) with the slope (*z*) as compared to the absolute intercept parameter. The best correlation was found between the slope (*z*) and Weibull$_{CRI}$ (R^2 of 0.8). Good correlations were found between the slope (*z*) and Nflex factor, CRI (IDT), FI (IDT), IDEAL-CT$_{Index}$, and $G_{fracture}$ (SCB-FI) with R^2 values of 0.62, 0.59, 0.57, 0.55, and 0.55, respectively. Fair correlations were found between the slope (*z*) and J_c and Gfracture (IDT), and with R^2 values of 0.46 and 0.38, respectively. Poor correlations were found between the slope (*z*) and CRI (SCB-FI), FI (SCB-FI), and IDT$_{Modulus}$ with R^2 values of 0.18, 0.13, and 0.10, respectively. No correlation was found between the slope (*z*) and IDT$_{strength}$ (R^2 of 0.01).

Monotonic performance thresholds were proposed for Weibull$_{CRI}$, Nflex factor, CRI (IDT), FI (IDT), IDEAL-CT$_{Index}$, Gfracture (SCB-FI), and J_c. The correlation plots are provided in Appendix E. The proposed thresholds for the selected performance indicators are provided in Table 30. The research team compared the proposed thresholds for the selected performance indicators with the thresholds proposed in other studies. West et al. (2017) recommended Nflex factor as a performance cracking indicator and specified a minimum threshold of 0.8 to have good cracking resistance [59]. This study proposed a threshold of 0.7 for good cracking resistance which is close to the threshold recommended by West et al. (2017) [59]. Sreedhar et al. (2018) data showed that FI (IDT) value of 27 was able to differentiate between cracked and uncracked mixes [119]. This study proposed a threshold of 22.6 for good cracking performance. Diefenderfer and Bowers (2019) proposed the IDEAL-CT$_{Index}$ to evaluate the cracking resistance of asphalt mixes and proposed a minimum threshold of 80 as initial performance

criteria for Virginia Department of Transportation (VDOT) [117]. This study proposed a threshold of 73.7 was established to ensure good cracking performance. Also, LADOT uses J_c as a cracking resistance indicator and requires a minimum J_c of 0.5 kJ/m^2 and 0.6 kJ/m^2 for Level-1 and Level-2 mix design, respectively [15]. In this study, a threshold of 0.6 was established to ensure good resistance to cracking.

In general, the proposed performance thresholds were comparable to the ones proposed by other researchers for the respective tests. These findings support the approach followed by the research team to determine the corresponding performance thresholds for selected monotonic tests to the ones developed using the MSSD test. Among all monotonic performance indicators, the $Weibull_{CRI}$ had the best correlation with MSSD slope parameter (R^2 of 0.8), which is expected to provide more reliable performance thresholds. The research team recommends the selection of $Weibull_{CRI}$ as a performance indicator for cracking resistance of asphalt mixes. This indicator had the best correlation with MSSD (R^2 of 0.8) as well as the lowest variability in the test results (average COV = 7.4 percent).

Table 30 Correlation Results between MSSD Parameters and Monotonic Cracking Resistance Indicators

MSSD paramaters and monotonic indicators	MSSD Slope (z) Parameter Exponential Fitting	MSSD Slope (z) Parameter Exponential Fitting	MSSD Slope (z) Parameter Exponential Fitting	MSSD Absolute Intercept Parameter Exp. Fitting	MSSD Absolute intercept Parameter Exp. Fitting	MSSD Absolute Intercept Parameter Exp. Fitting	Proposed Performance Threshold (minimim)	Proposed Performance Threshold (minimim)
Paramater/perf.	C_4	C_5	R^2	C_4	C_5	R^2	Fair	Good
Gfracture (IDT)	5.18	-1.24 E-4	0.383	2.22	5.85E-5	0.21	----	----
$G_{fracture}$ (SCB-FI)	7.08	-5.77E-4	0.55[2]	1.7	3.32E-4	0.46	1546	2280
CRI (IDT)	11.0	-2.86E-3	0.59	1.56	1.39E-3	0.35	466	614
CRI (SCB-FI)	4.94	-1.86E-3	0.18	2.02	1.07E-3	0.19	----	----
FI (IDT)	4.46	-3.79E-2	0.57	2.48	1.74E-2	0.33	11.4	22.6
FI (SCB-FI)	2.80	-6.68E-2	0.10	2.95	3.91E-2	0.09	----	----
$IDEAL\text{-}CT_{Index}$	3.67	-8.94E-3	0.55	2.70	4.16E-3	0.32	26.4	73.7
Nflex factor	4.60	-1.21	0.62	2.49	0.533	0.30	0.40	0.70
$IDT_{strength}$	2.85	-3.23E-4	0.01[4]	3.15	1.14E-4	0.00	----	----
$IDT_{Modulus}$	0.68	3.47E-3	0.13	4.19	-1.0E-3	0.03	----	----
Jc	3.60	-1.03	0.46	2.57	0.588	0.37	0.20	0.60
$Weibull_{CRI}$	10.8	-0.36	0.80[1]	1.53	0.18	0.51	3.6	4.7

[1] Green cells indicate good correlation ($R^2 \geq 0.80$,[2] yellow cells indicate fair correlation ($0.5 < r_s \leq 0.7$), [3] white cells indicate poor correlation ($0.1 < r_s \leq .5$), and [4] red cells indicate no correlation

Chapter 6
Comprehensive Evaluation of Rutting Performance

Introduction

Chapter 6 discusses the evaluation of rutting characteristics of the evaluated mixes. Two rutting testing protocols were conducted (i.e., HWTT and APA rut test). The sensitivity of these tests to the characteristics of the mixes was examined. Three different rutting performance indicators were considered including the HWTT rut depth after 15,000 passes ($HWTT_{15000}$), the HWTT rut depth at 20,000 passes ($HWTT_{20000}$), and the APA rut depth after 8,000 cycles (APA_{8000}).

Sensitivity to Mixture Properties

HWTT Test

Figures 113 and 114 show the rut depth for the LMLC mixes after 15,000 and 20,000 passes in the HWTT, respectively. Both indicators ($HWTT_{15000}$ and $HWTT_{20000}$) were sensitive to the variation in binder content and binder PG. Mixes prepared with PG 70-28 binder exhibited less rutting when compared to the ones prepared with PG 58-34 binder at the corresponding binder contents, and the difference was statistically significant (p-value < 0.05). The results also demonstrated that the rut depth increased with the increase in binder content for both PG 70-28 and PG 58-34 binders. However, for both binders, the difference in rut depth was only statistically significant between 4.25 percent and 5.75 percent and between 5.00 percent and 5.75 percent binder contents, while it was not statistically significant between 4.25 percent and 5.00 percent. The average coefficient of variation (COV) of the HWTT test results was 15 percent and 14 percent after 15,000 and 20,000 passes, respectively. None of the LMLC mixes exhibited any sign of moisture damage although antistrip additives were not used.

APA Rut Test

Figures 115 shows the APA rut depth for the LMLC mixes after 8,000 load cycles. The mixes prepared with PG 70-28 binder were tested at 70 °C, while the mixes prepared with PG 58-34 binder were tested at 58 °C as per AASHTO T340 test procedure. Mixes with PG 70-28 binder experienced higher rut depth compared to mixes with PG 58-34 binder at the corresponding binder content and the difference was statistically significant (p-value <0.05). Asphalt mixes with stiffer binders are expected to have higher resistance to rutting compared to mixes with softer binders if both are tested at the same temperature. The results also show that the APA rutting increased with the binder content for both binders (i.e., PG 70-28 and PG 58-34). The difference in rut depth for the mixes prepared with the PG 70-28 binder was significant between 4.25 percent and 5.75 percent and between 5.00 percent and 5.75 percent. For the mixes prepared with the PG 58-34 binder, the difference in performance between all binder contents was statistically significant. The APA rut depth increased with binder content. The average COV of the APA rut test results was 8 percent which was smaller than the coefficient of variation of the HWTT.

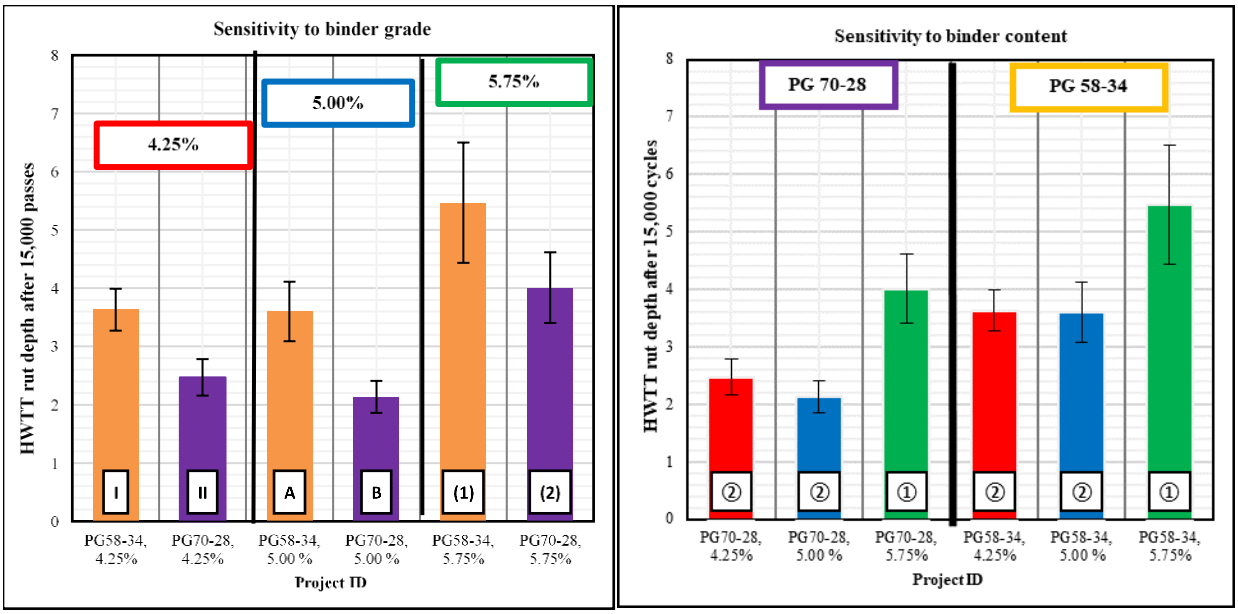

Figure 113 Sensitivity of HWTT Rut Depth after 15,000 Cycles to PG and Binder Content

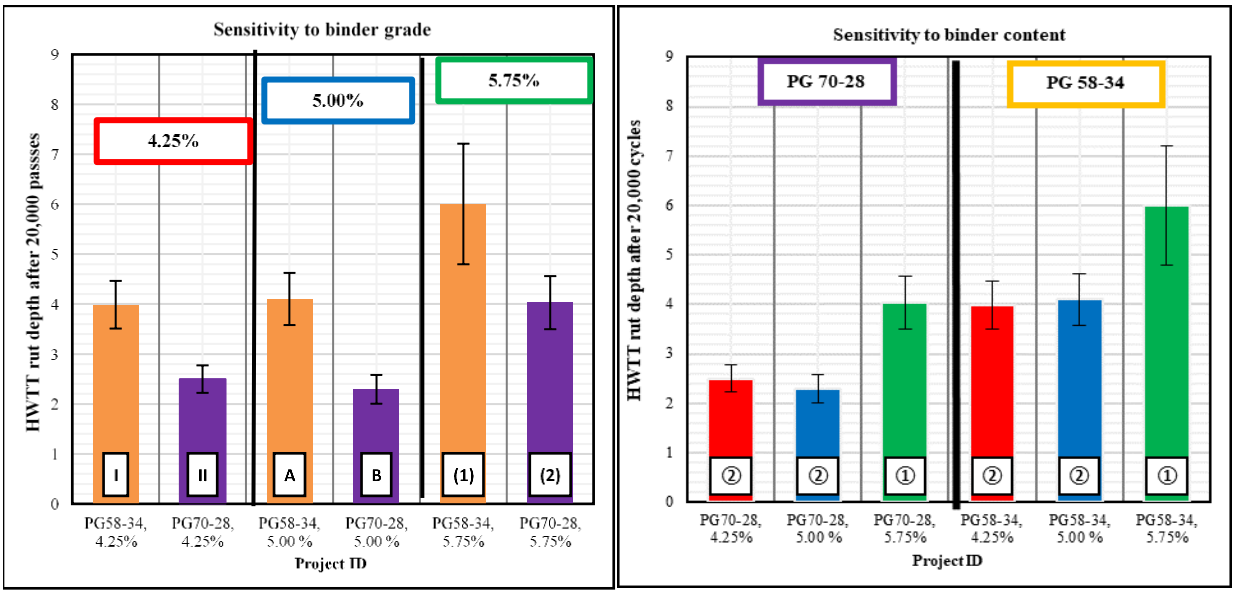

Figure 114 Sensitivity of HWTT Rut Depth after 20,000 Cycles to PG and Binder Content

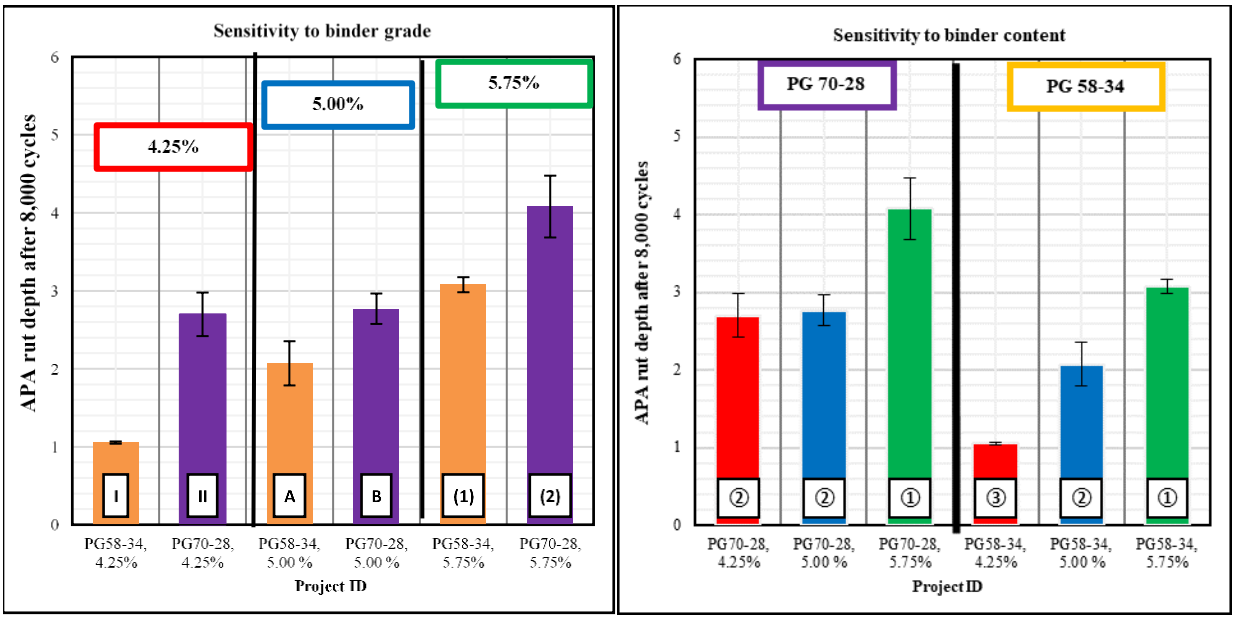

Figure 115 Sensitivity of APA Rut Depth at 8,000 Cycles to PG and Binder Content

Rutting Evaluation of Field Projects

The researchers evaluated the rutting resistance of extracted field cores. These cores were obtained from 17 different field projects across the state. Both HWTT and APA rut test were conducted on the recovered cores. This section discusses the test results of the rutting performance evaluation.

HWTT Test

Figures 116 and 117 show the HWTT rut depth after 15,000 and 20,000 passes, respectively. The field cores had an average rut depth between 2.63 mm and 14.39 mm with a standard deviation between 0.28 mm and 4.57 mm after 15,000 passes. Also, the field cores had an average rut depth between 2.82 mm and 14.39 mm after 20,000 passes with a standard deviation between 0.21 mm and 4.05 mm. The coefficient of variation of the HWTT rut depth was 4.1 percent and 5 percent after 15,000 and 20,000 passes, respectively. Tukey's HSD results classified the tested field cores into ten groups based on the results of both parameters (i.e., rut depth after 15,000 and 20,000 cycles). Only two mixes (D5C2 and D2C11) out of 17 mixes exhibited signs of moisture damage. Mixture D5C2 exceeded the HWTT test termination rut depth (14.39 mm after 15,000 cycles) (Figure 118). Mixture D2C11 showed inconsistent results, the left wheel specimens had good rutting resistance (average rut depth of 5.2 mm at 20,000 cycles) while the right wheel had poor rutting resistance and moisture damage (average rut depth of 12.42 at 14,800 cycles) (Figure 119). This could be contributed to different air void content between the left and right wheel specimens, but the researchers were not able to test additional cores due to the limited number of field cores received from this project.

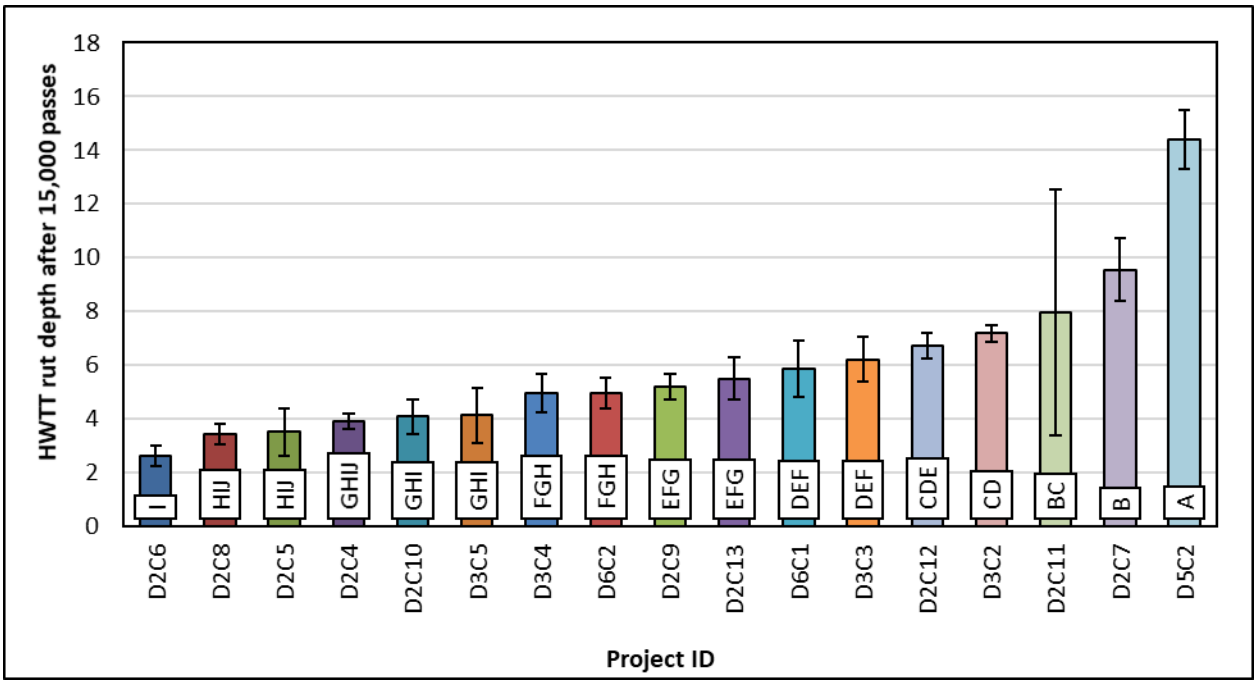

Figure 116 HWTT Rut Depth after 15,000 Cycles for Field Cores

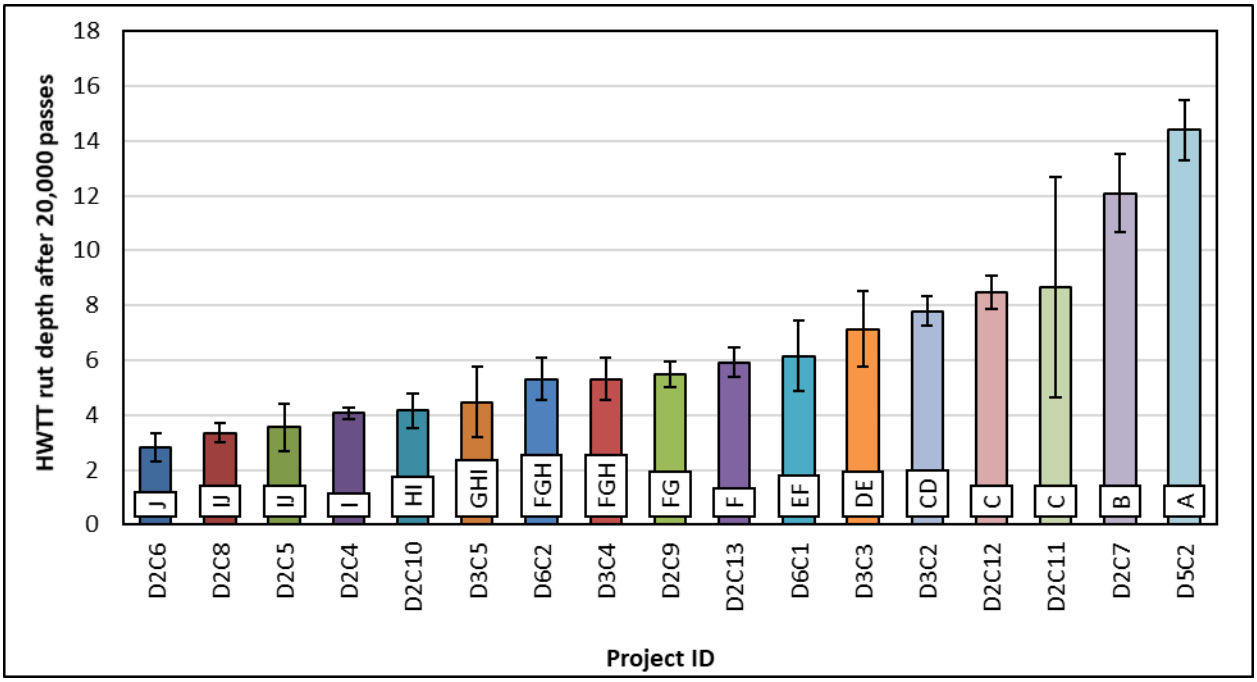

Figure 117 HWTT Rut Depth after 20,000 Cycles for Field Cores

Figure 118 Mixture D5C2 Specimens after Testing using HWTT Test

Figure 119 Mixture D2C11 Specimens after Testing using HWTT Test

APA Rut Test

Figure 120 shows the APA rut depth measurements after 8,000 load cycles. Due to the limited number of field cores obtained from some of the field projects, only 12 field projects were tested using the APA rut test. The field cores had an average rut depth between 1.86 mm and 7.15 mm with a standard deviation between 0.03 mm and 0.63 mm. The APA rut depth results showed low variability (COV of 2 percent). Tukey's HSD classified the mixes into four groups as shown in Figure 120. Cores extracted from project

D5C2 had the highest rut depth (7.15 mm), while cores from field project D2C6 had the lowest rut depth (1.86 mm) when compared to other projects (Figure 120).

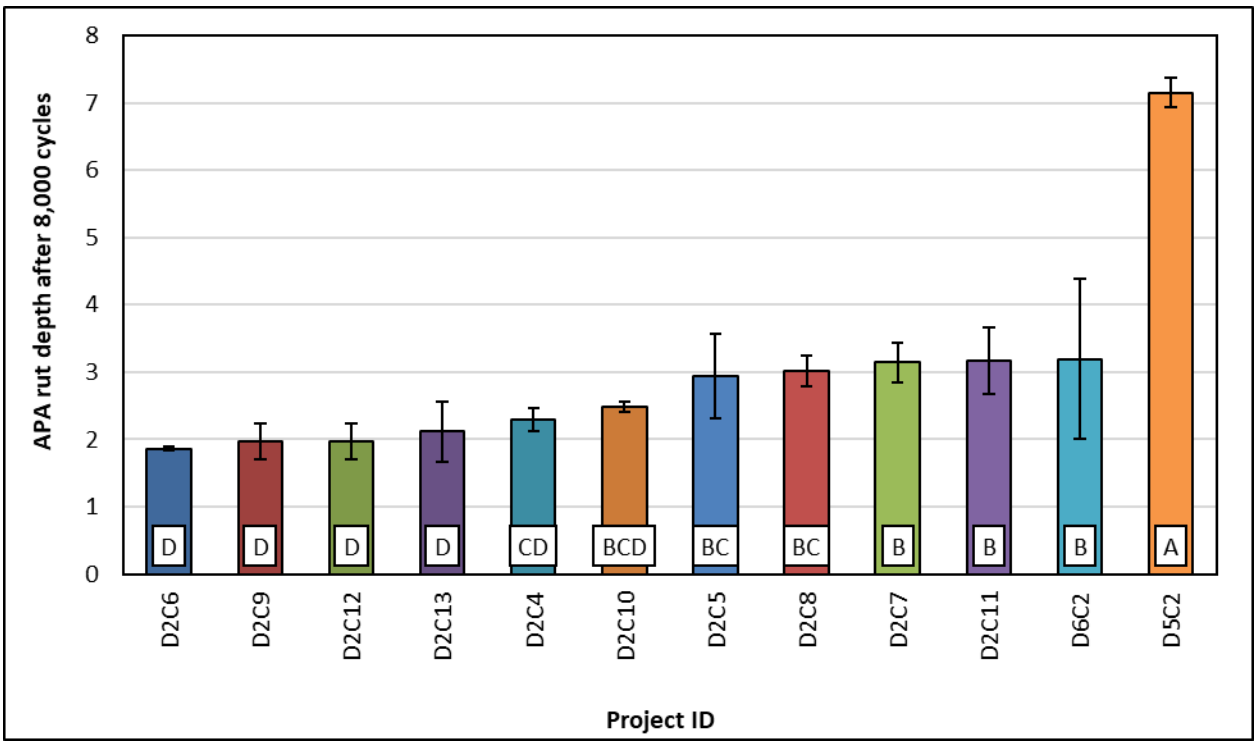

Figure 120 APA Rut Depth after 8,000 Cycles for Field Cores

Figure 121 Mixture D5C2 Specimens after Testing using APA Test

Correlation between Laboratory and Field Rutting Measurements

Figures 122 and 123 show the field rut depth versus the HWTT rut depth after 15,000 and 20,000 passes,

respectively. All field projects had either good (rut depth < 6.09 mm) or fair rutting performance (rut depth < 12.44 mm) according to ITD criteria (Table 12). The plots were divided into three shaded areas; green, yellow, and red. The green shaded area represents projects with good resistance to rutting, the yellow shaded area represents projects with fair resistance to rutting, while the red shaded area represents projects with poor to very poor resistance to rutting. The field rutting performance demonstrated that 11 mixes had good rutting resistance and six had fair field rutting resistance. None of the mixes had poor or very poor rutting resistance. Similarly, Figure 124 shows the field rut depth versus the APA rut depth after 8,000 cycles.

The laboratory and field results clearly demonstrate no rutting problems in asphalt mixes in Idaho and this is consistent with inputs received from the Material Engineers. Superpave mix design tends to produce dry mixes which provides good resistance to rutting. In addition, the current practice at ITD is to use the APA rut test to evaluate the rutting resistance of all 75- and 100-gyration asphalt mixes produced and used in the state. The results show that this is an effective practice that should be maintained. Based on the laboratory rutting evaluation and the findings of the literature review, the research team proposed performance thresholds to ensure that asphalt mixes have good/fair rutting performance. Different thresholds were proposed for the three performance indicators: 1) HWTT rut depth after 15,000 passes ($HWTT_{15000}$), 2) HWTT rut depth after 20,000 passes ($HWTT_{20000}$), and 3) APA rut depth after 8,000 cycles (APA_{8000}). A maximum rut depth of 10 mm for $HWTT_{15000}$ (Figure 122), 12.5 mm for $HWTT_{20000}$ (Figure 123), and 5 mm for APA_{8000} (Figure 124) were proposed. These thresholds can differentiate between good/fair and poor/very poor mixes.

Similar thresholds are used by several transportation agencies. For example, Washington Department of Transportation (WSDOT) specifies a maximum rut depth of 10 mm for $HWTT_{15000}$ (for mixes designed for more than 3 million ESAL's tested at 50 °C without any sign on moisture damage)[120]. Louisiana Department of Transportation (LADOT) specifies a maximum rut depth of 10 mm rut depth for $HWTT_{20000}$ for wearing course tested at 50 °C [15]. Table 2 presents different thresholds used by various transportation agencies. Similarly, other DOTs including ITD adopted the APA rut test and use different thresholds as presented in Table 3. For example, Alabama Department of Transportation (ALDOT) specifies a minimum value of 4.5 mm for "E" mixes ($1E10^7$ < ESALs < $3E10^7$) after 8000 cycles. Also, Virginia Department of Transportation (VDOT) specifies minimum values of 3.5 mm, 5.5 mm, and 7 mm for mixture designation A, D, and E, respectively after 8000 cycles. Currently, ITD specifies a maximum rut depth of 5 mm for APA_{8000} for SP3 and SP5 mixes.

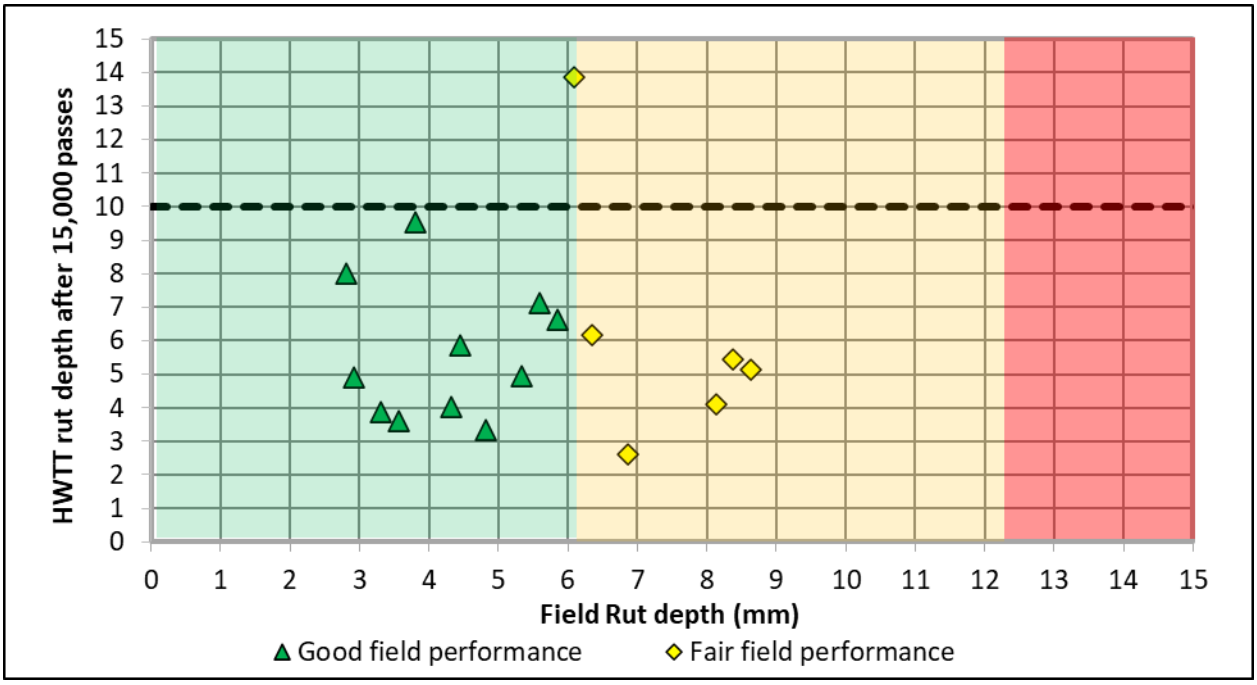

Figure 122 Laboratory HWTT Rut Depth after 15,000 Passes versus Field Performance

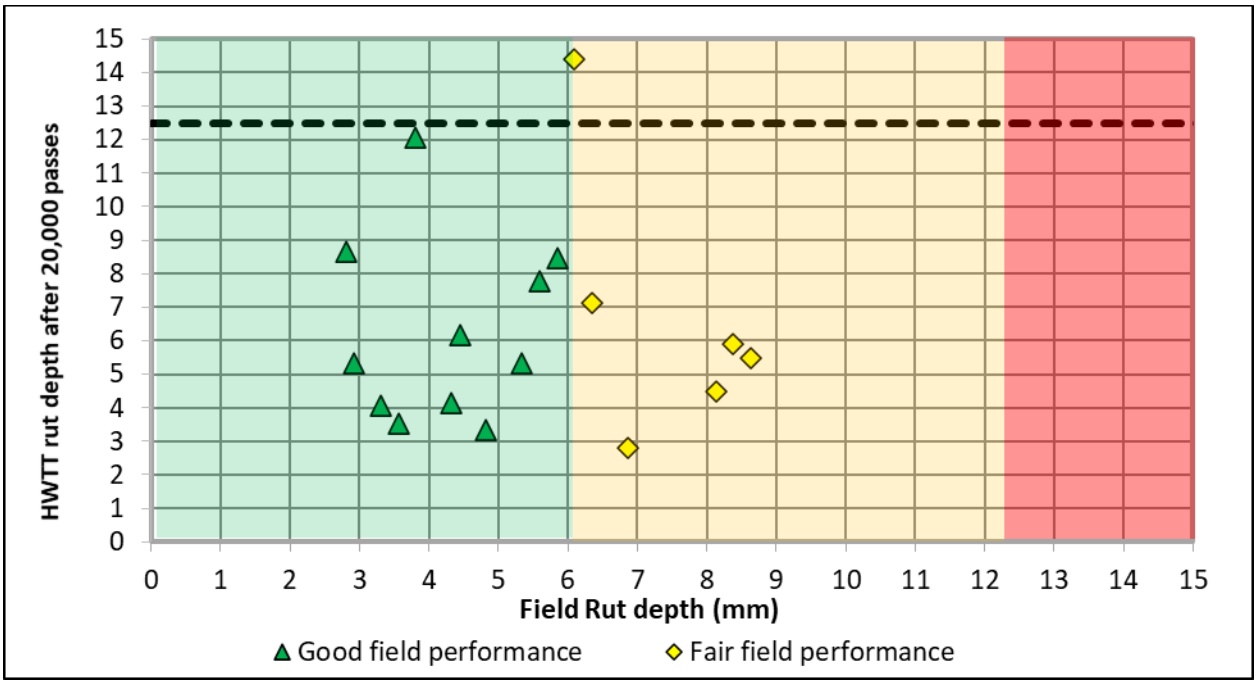

Figure 123 Laboratory HWTT Rut Depth after 20,000 Passes versus Field Performance

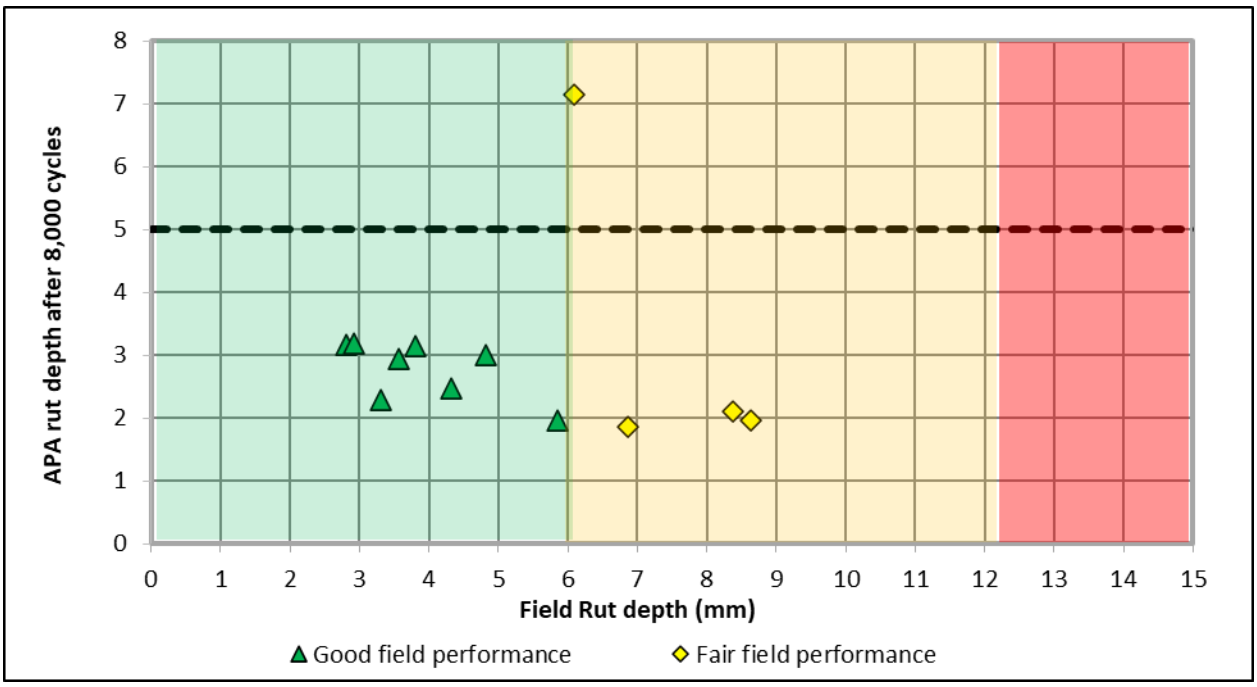

Figure 124 Laboratory APA Rut Depth after 8,000 Cycles versus Field Performance

Rutting Performance Evaluation of PMLC Mixes

This section discusses the results of rutting tests conducted on the Plant-Mixed Laboratory-Compacted (PMLC) mixes collected from the 10 new paving projects. Similar to the field cores, both the HWTT and APA rut test were used to test the PMLC mixes. The HWTT can be used to evaluate the moisture damage performance in addition to rutting as discussed earlier.

HWTT Rut Depth after 15,000 Passes ($HWTT_{15000}$)

Figure 125 shows the HWTT rut depth measurements after 15,000 passes. The PMLC mixes had an average rut depth between 1.62 mm and 4.84 mm, with a standard deviation between 0.05 mm and 0.81 mm. The results showed low variability of the test results (COV = 5 percent). Tukey's HSD classified the PMLC mixes into seven different groups. The results showed that D3L3 and D3L4 had higher rut depth compared to other mixes, while D2L1 had the lowest rut depth. None of the PMLC mixes showed signs of moisture damage. It should be noted that the current ITD specifications require the use of anti-strip agents or additives as percent of binder by weight (minimum of 0.5 percent) [77]. In addition, ITD uses the immersion compression test (ASTM D1075) to evaluate the resistance of asphalt mixes to moisture damage. In the immersion compression test, the index of retained strength is used to assess the moisture damage. The index of retained strength reflects the ratio of compressive strength of test specimens in dry and water-immerged conditions. A minimum retained strength of 85 percent is selected as pass criteria as per ITD standard specifications. Figure 126 shows the retained strength for the PMLC mixes. All mixes satisfied the threshold requirements per current ITD specifications.

Figure 127 shows the $HWTT_{15000}$ results for all mixes evaluated in this study including LMLC, PMLC, and field cores. The PMLC mixes exhibited better rutting resistance (lower rut depth) when compared to recovered field cores. All the PMLC mixes had HWTT rut depths lower than the proposed threshold (10 mm) after 15,000 passes. These results demonstrate that PMLC mixes would show good rutting performance if proper field construction and compaction are achieved and the required density is met.

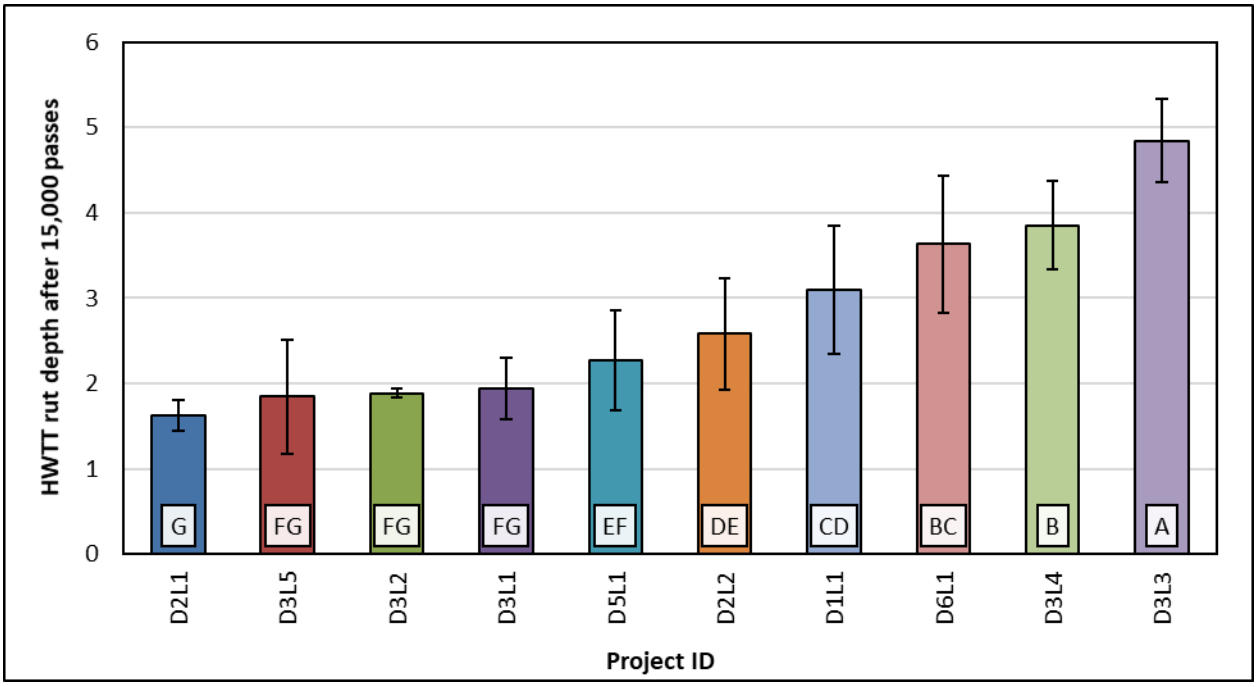

Figure 125 HWTT Rut Depth after 15,000 Passes for PMLC Mixes

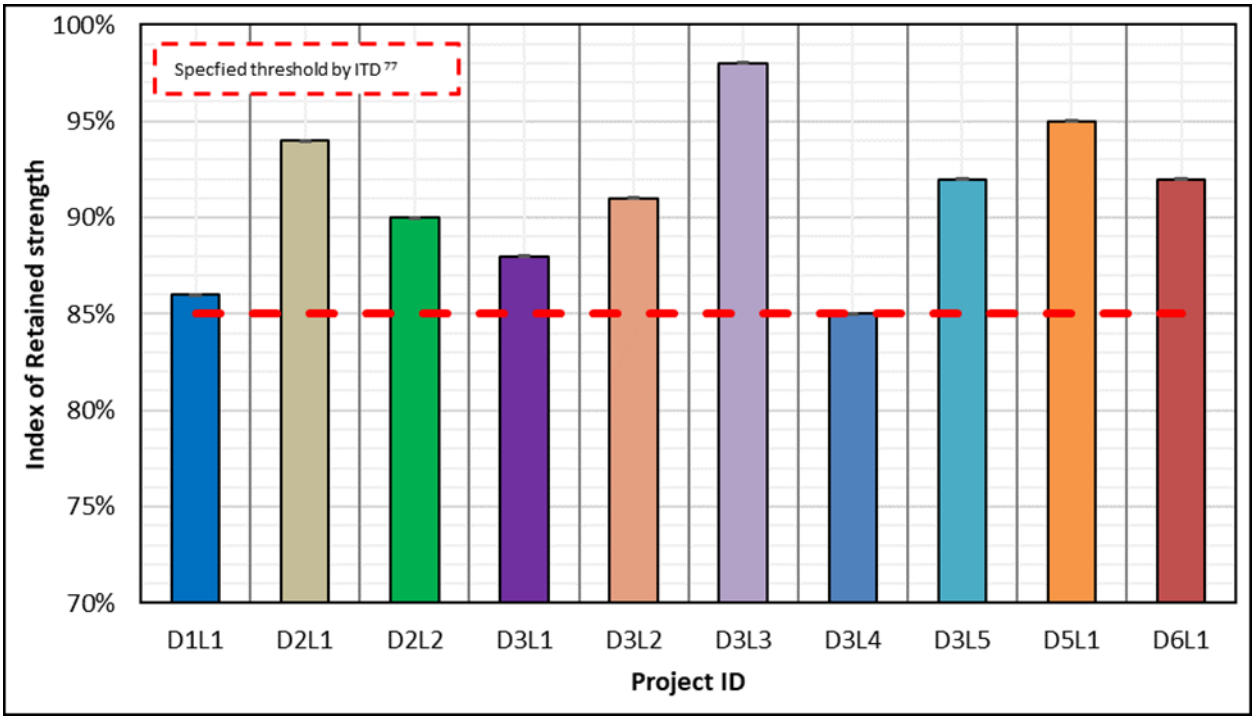

Figure 126 Index of Retained Strength for the PMLC Mixes

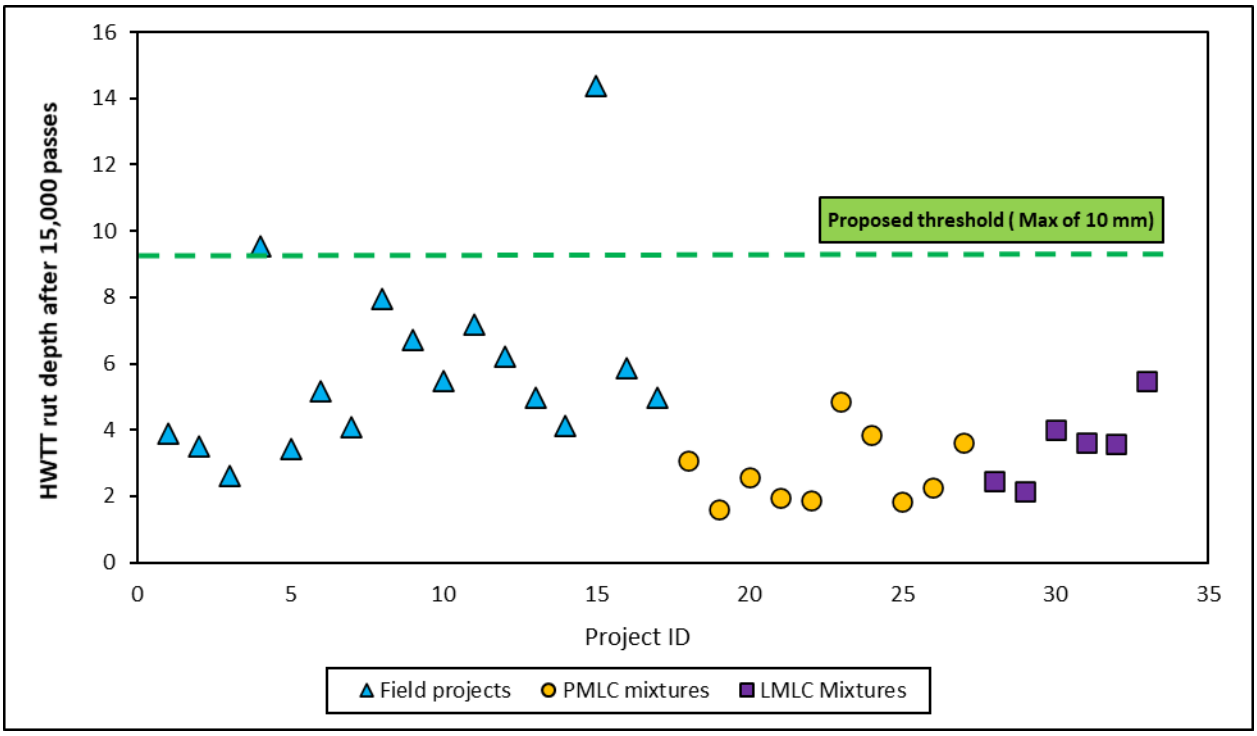

Figure 127 HWTT Rut Depth after 15,000 Passes for all Test Mixes (LMLC, PMLC, and Field Cores)

HWTT Rut Depth after 20,000 Passes ($HWTT_{20000}$)

Figure 128 shows the HWTT rut depth after 20,000 passes for the PMLC mixes. The mixes had an average rut depth between 1.74 mm and 5.09 mm and a standard deviation between 0.04 mm and 0.85 mm. The HWTT results showed low variability (COV = 5 percent). Tukey's HSD classified PMLC mixes into six different groups that are statistically significant different in terms of the rut depth. Figure 129 shows the $HWTT_{20000}$ results for all mixes evaluated in this study including LMLC, PMLC, and field projects. All the PMLC mixes had lower HWTT rut depth than the proposed threshold (12.5 mm) after 20,000 cycles. Again, these results demonstrate that PMLC mixes would show good rutting performance of proper construction and compaction practices are followed in the field.

Figure 130 shows the correlation between HWTT rut depth after 15,000 passes and 20,000 passes. There was excellent correlation between the two indicators. Field projects had a coefficient of determination (R^2) of 0.9, PMLC mixes had an R^2 of 0.98, while LMLC mixes had an R^2 of 0.99. In addition to the higher coefficient of determination (R^2), the Spearman rank correlation coefficient (r_s) was also evaluated. This coefficient was used to study the ranking correlation (from best to worst in terms of rutting resistance) between both rutting indicators (e.g., $HWTT_{15000}$ and $HWTT_{20000}$). Excellent ranking agreement between both indicators (r_s = 0.98) was found. These results demonstrate that the two rutting performance indicators ($HWTT_{15000}$ and $HWTT_{20000}$) are highly correlated and thus using one or the other would be sufficient. Since the $HWTT_{15000}$ requires less number of passes which reduces the HWTT testing time, it is recommended over $HWTT_{20000}$.

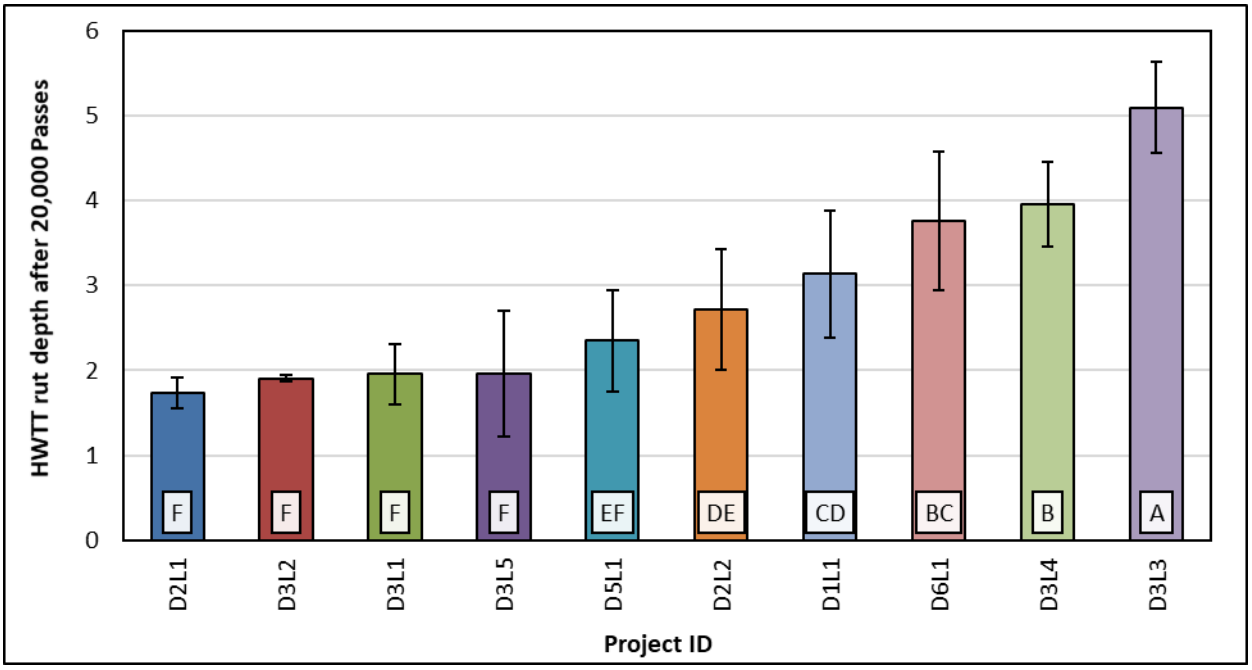

Figure 128 HWTT Rut Depth after 20,000 Passes for PMLC Mixes

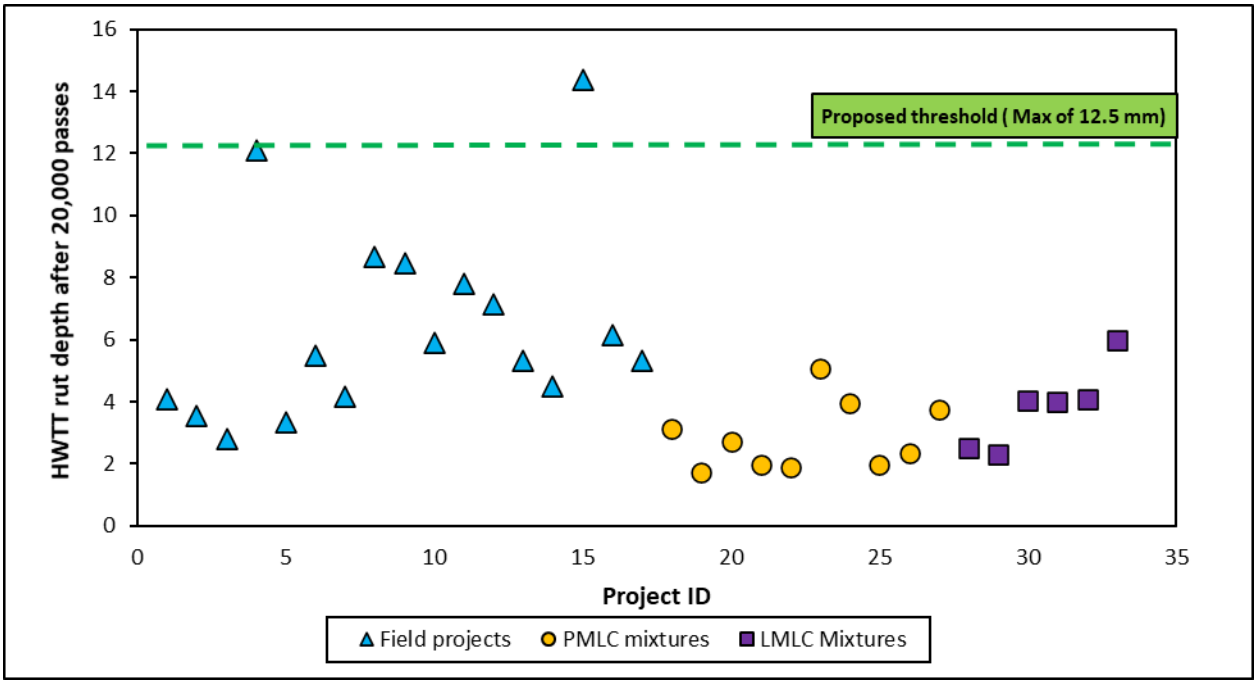

Figure 129 HWTT Rut Depth after 20,000 Passes for all Test Mixes (LMLC, PMLC, and Field Cores)

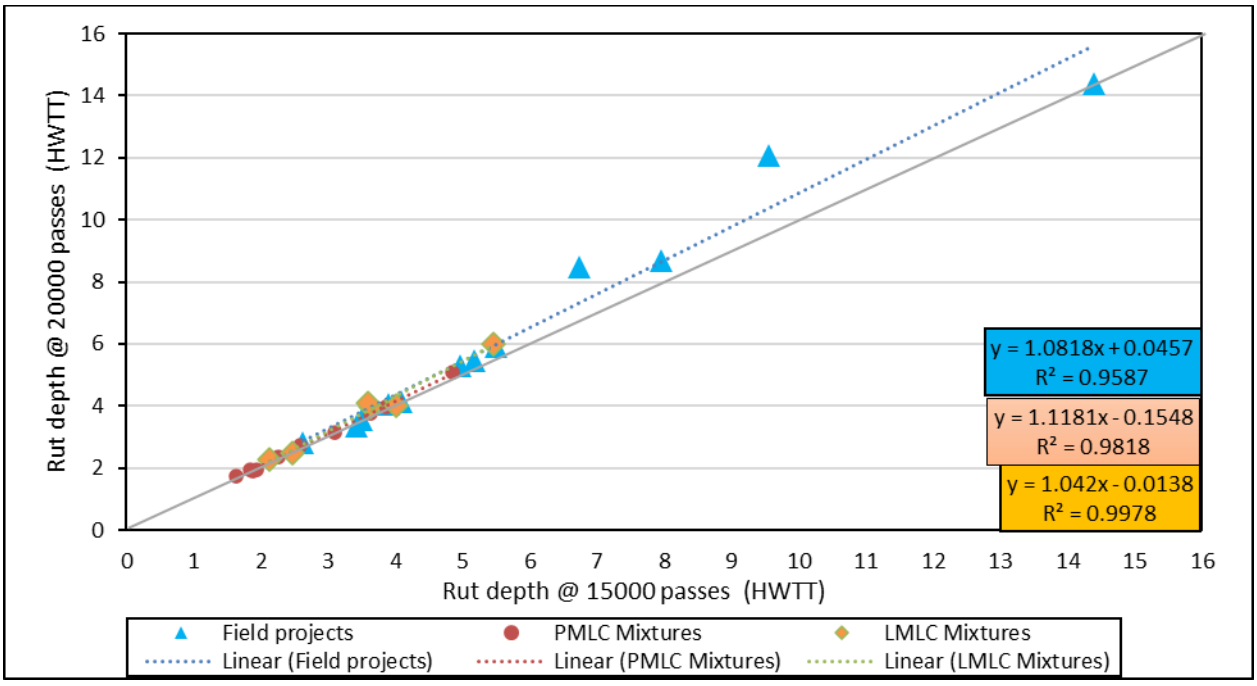

Figure 130 Correlation between $HWTT_{15000}$ and $HWTT_{20000}$ Indicators

APA Rut Depth after 8,000 Cycles (APA_{8000})

Figure 131 shows the APA rut depth after 8000 cycles for the PMLC mixes. The mixes had an average rut depth between 1.67 mm and 4.36 mm and a standard deviation between 0.01 mm and 0.69 mm. The

results show that the APA rut test had low test variability (COV = 11 percent). Tukey's HSD classified the PMLC mixes into seven different groups. The results showed that both mixes D3L3 and D5L1 had the highest rut depth, while mixture D2L1 had the lowest rut depth.

Figure 132 shows the APA rut depth after 8000 cycles for all evaluated mixes including field projects, PMLC mixes, and LMLC mixes. Based on current ITD specification of maximum APA rut depth of 5 mm, all PMLC mixes are expected to have good rutting resistance. Figure 133 and Figure 134 show the correlation between APA_{8000} and both $HWTT_{15000}$ and $HWTT_{20000}$, respectively. The results showed no correlation between HWTT and APA performance indicators. The HWTT and APA rut test evaluate asphalt mixes under different testing temperatures and conditions. For instance, the HWTT test was performed at 50 °C, while APA rut test was performed at the high binder performance grade. Since the viscosity of asphalt binder changes with the testing temperature, it is expected that asphalt mixes provide different performance. In addition, the HWTT test is conducted in wet conditions, while the APA rut test is conducted in dry conditions. The APA rut test was also found to have poor ranking agreement with both $HWTT_{15000}$ and $HWTT_{20000}$ rutting indicators (R_s = 0.14 and 0.10 with $HWTT_{15000}$ and $HWTT_{20000}$, respectively).

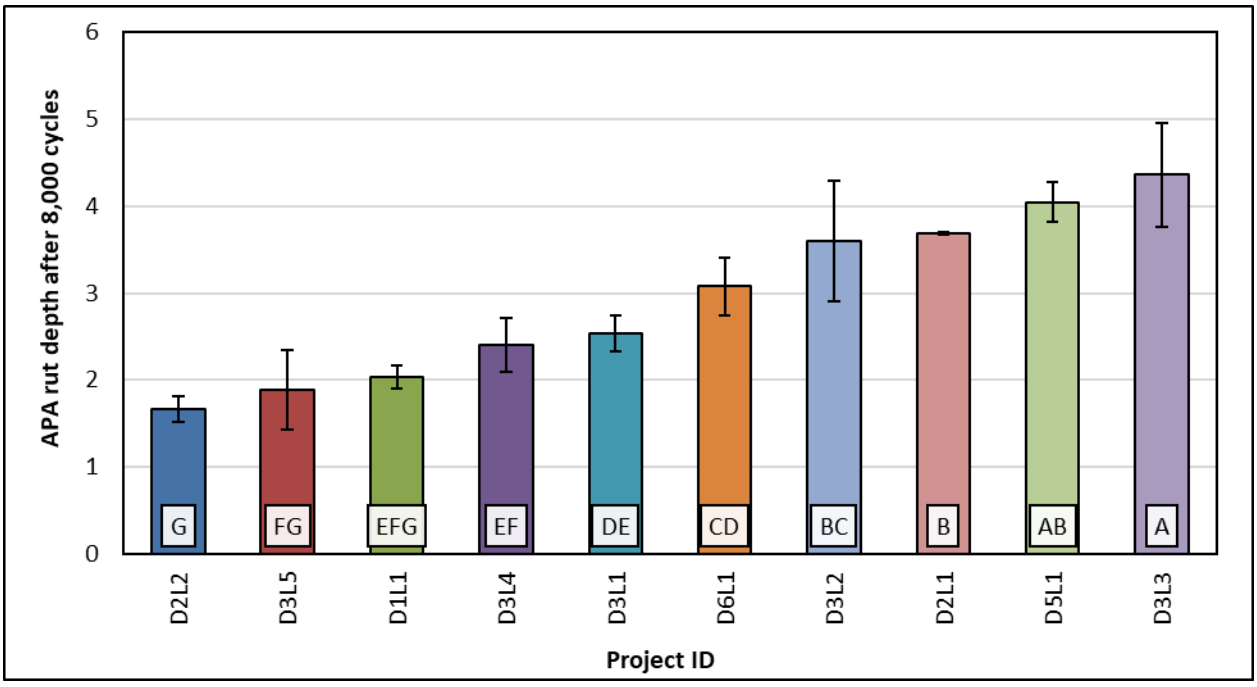

Figure 131APA Rut Depth after 8,000 Cycles for PMLC Mixes

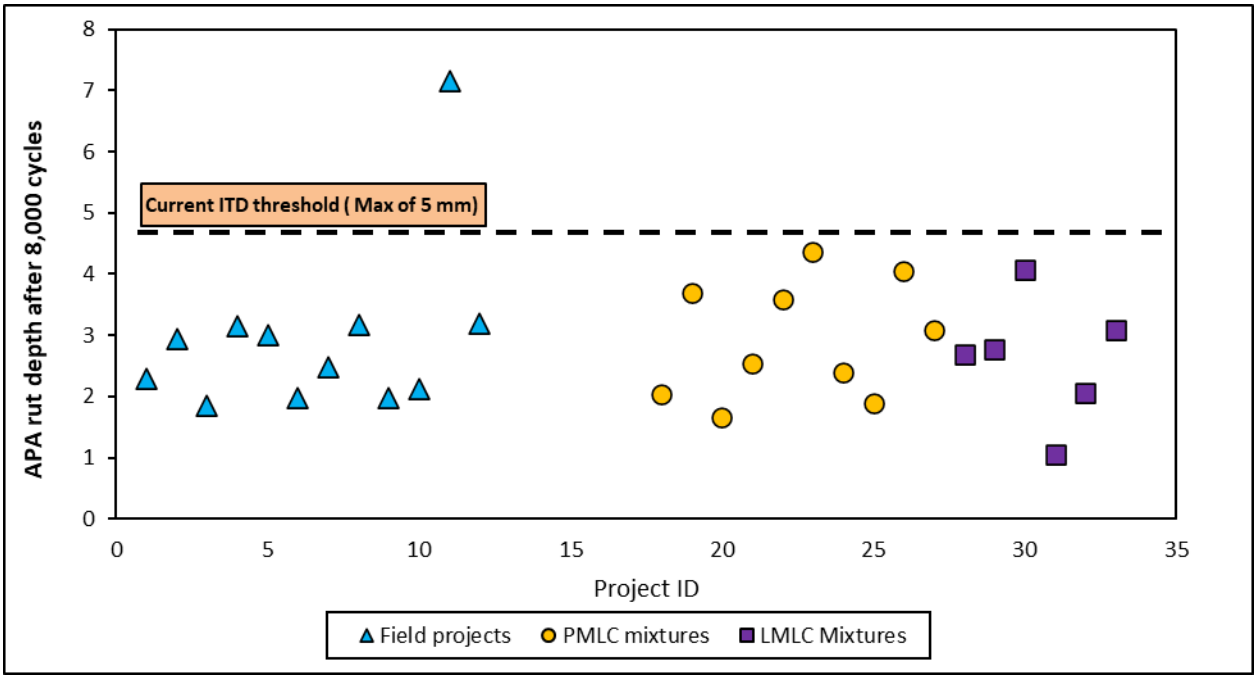

Figure 132 APA Rut Depth after 8,000 Cycles for all Test Mixes (LMLC, PMLC, and Field Cores)

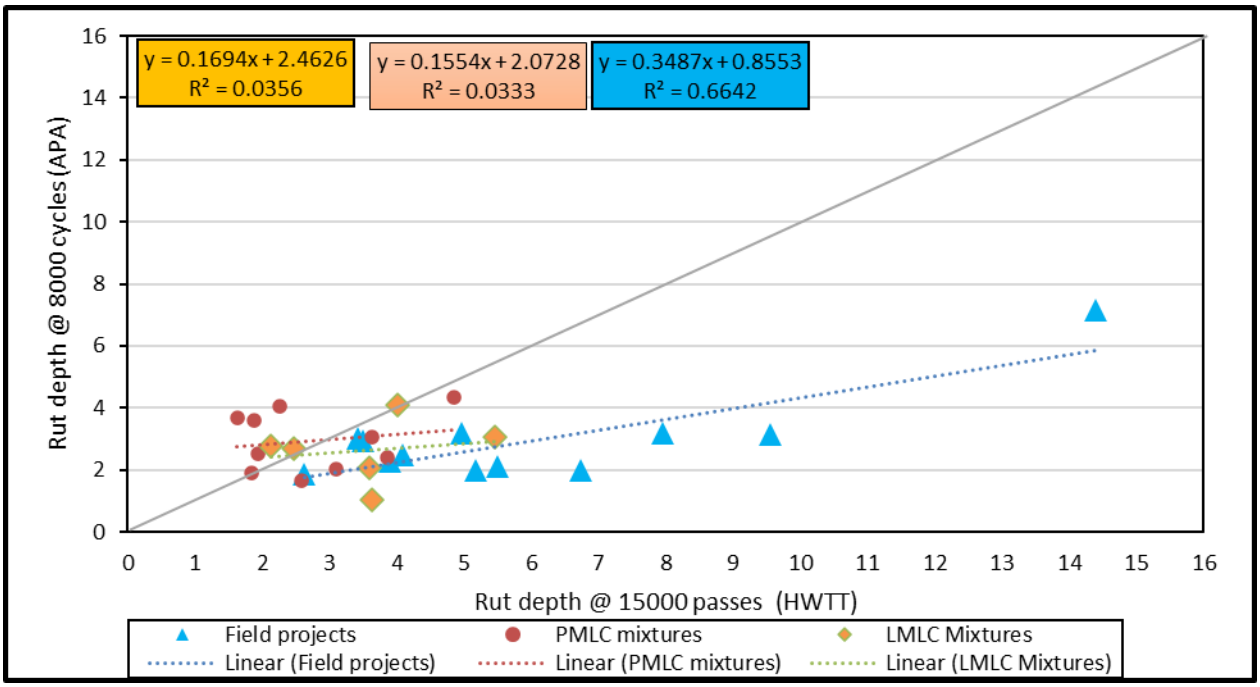

Figure 133 Correlation between $HWTT_{15000}$ and APA_{8000} indicators

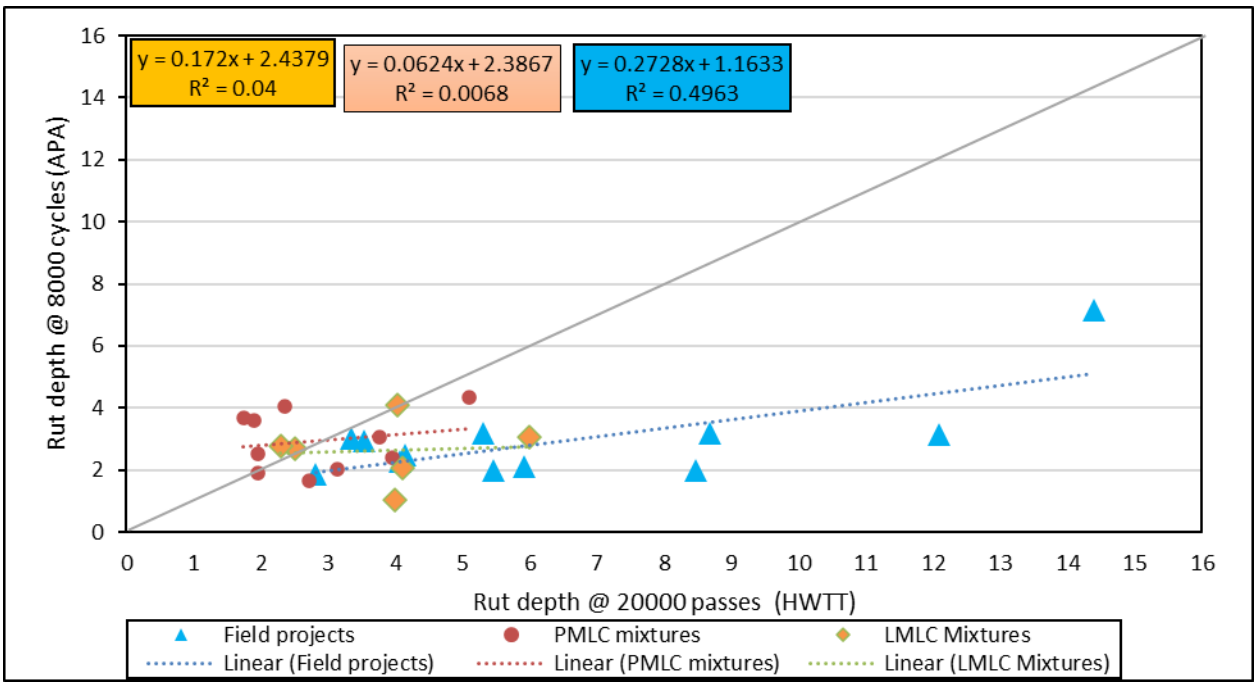

Figure 134 Correlation between $HWTT_{20000}$ and APA_{8000} Indicators

Chapter 7
Conclusions, Implementation and Recommendations

Conclusions

This study examined the cracking and rutting performance of various asphalt mixes in Idaho including field projects, PMLC mixes, and LMLC mixes. The LMLC mixes were tested to examine the sensitivity of various performance indicators and tests to binder content and binder PG. The PMLC were tested to evaluate the performance of current mixes produced in the state to cracking and rutting based on performance specifications provided in the literature. In addition, field cores were tested in the laboratory and the results were compared to the observed field performance to develop cracking and rutting performance thresholds.

Based on the findings of the literature review, two rutting tests were selected and used in this study; Hamburg Wheel Tracking Test (HWTT) and Asphalt Pavement Analyzer (APA). The HWTT is conducted in accordance with AASHTO T324, while the APA rut test is conducted in accordance with AASHTO T340. The HWTT can also be used to evaluate asphalt mix resistance to moisture damage. The cracking tests conducted in this study include monotonic tests (IDT [ASTM D6931], SCB-FI [AASHTO TP 124], and SCB-Jc [TR 330]), and a new dynamic test called Multi-Stage Semi circle bending Dynamic (MSSD) test that was developed by the research team in this study. A total number of 12 performance indicators calculated from the monotonic tests were evaluated in this study, including a new performance indicator developed also by the research team called $Weibull_{CRI}$. The main findings of this study can be summarized as follows:

- The monotonic tests are simple to conduct and have less variability in the test results compared to the dynamic tests; however, the results of these tests are highly influenced by the percent of air voids and specimen thickness. Monotonic tests can be used to compare mixtures with similar percent air voids and thickness and the dynamic testing is recommended when the test specimens have different air voids and thickness.

- Table 23 provides comparison between the monotonic and dynamic tests. Such comparison includes various criteria including testing time, specimen preparation, specimen geometry, complexity of testing systems and cost. The monotonic tests require less expensive testing systems and have shorter testing time compared to the dynamic tests.

- The IDT monotonic tests require simple specimen preparation compared to SCB monotonic tests and often have less variability in the test results. Performance indicators determined from IDT monotonic tests such as $Weibull_{CRI}$, IDEAL-CT_{Index}, and Nflex factor are recommended over performance indicators determined from SCB monotonic tests.

- The newly developed and proposed dynamic test (MSSD) was able to address several limitations associated with other current dynamic tests. This test simulates the repeated loading (dynamic) in a reasonable testing time, has well-defined and fixed loading sequences that work for various mixes irrespective of their characteristics (e.g., mixture composition, percent air void content, thickness, etc.), and use similar testing equipment and specimen geometry used in the monotonic tests.

- The MSSD parameters (*z* and Abs [log *H*]) were able to differentiate between field projects with different cracking resistance (e.g., good, fair, and poor). The research team proposed three thresholds to distinguish between mixes; good cracking resistance ($z < 1.9$) or (Abs [log *H*]>3.60), fair cracking resistance ($1.9 \leq z \leq 2.9$) or ($3.0 \leq$ Abs [log *H*] ≤ 3.60), and poor cracking resistance (z> 2.9) or (abs [log H] <3.0). The slope parameter (z) was found to correlate well with the intercept parameter (Abs [log H]), in addition there was less overlap in the slope results compared to the intercept parameter. Therefore, the researchers recommend the use of the slope thresholds. In this study, the dynamic testing was used to evaluate the cracking performance of cores extracted from the field and the results were compared to field cracking performance. Future studies could utilize the results of MSSD test in performance models to predict pavement performance which was not an objective of this project.

- Various monotonic cracking resistance indicators proposed in the literature were evaluated in this study. Unlike the dynamic test, none of the monotonic cracking resistance indicators was found to differentiate between field projects. Field cores have different air void content and thicknesses, and it is believed that the results of the various cracking resistance indicators were influenced by these conditions. Instead of developing performance thresholds using a direct correlation between the monotonic cracking resistance indicators and field performance (as was performed for the dynamic test), the results of the performance indicators were compared to the results of dynamic test for the PMLC mixes. Performance thresholds of the dynamic test were used to estimate the corresponding thresholds for the selected monotonic performance indicators. In the meantime, some monotonic cracking indicators were able to detect the change in mix composition and thus they can be used to examine the change from mix design to field production.

- Various monotonic cracking resistance indicators proposed in the literature were evaluated in this study. However, none of these indicators can describe the entire load-displacement curve. In this study, the authors proposed a new and innovative performance indicator called Weibull Cracking Resistance Index ($Weibull_{CRI}$), which is used to describe the entire load-displacement curve and evaluate resistance of asphalt mixture to cracking. This index was found to provide the best correlation ($R^2 = 0.8$) with the dynamic test results of the PMLC compared to other monotonic performance indicators. In addition, the $Weibull_{CRI}$ was found to have the lowest variability in the test results compared to other monotonic cracking resistance indicators.

Therefore, the research team recommended the use of $Weibull_{CRI}$ over other monotonic performance indicators evaluated in this study.

- We used the correlation between the MSSD test and $Weibull_{CRI}$ for the PMLC mixes to develop performance thresholds for the $Weibull_{CRI}$ corresponding to the thresholds of the MSSD slope parameter (z). Three performance thresholds for the $Weibull_{CRI}$ were proposed: good cracking resistance ($Weibull_{CRI} > 4.7$), fair cracking resistance ($3.57 \leq Weibull_{CRI} \leq 4.7$), and poor cracking resistance ($Weibull_{CRI} < 3.57$). Similarly, thresholds for other performance indicators including $G_{fracture}$ (SCB-FI), CRI (IDT), J_c, IDEAL-CT_{Index}, FI (IDT), and Nflex factor were proposed. For example, three performance thresholds for the IDEAL-CT_{Index} were proposed: good cracking resistance (IDEAL-$CT_{Index} > 73.7$), fair cracking resistance ($26.4 \leq$ IDEAL-$CT_{Index} \leq 73.7$), and poor cracking resistance (IDEAL-$CT_{Index} < 26.4$). The proposed thresholds for some performance indicators were comparable to the ones proposed by other researchers. These findings support the approach followed by the research team to develop thresholds for the selected monotonic tests corresponding to the ones developed using the MSSD test.

- Various performance indicators including $G_{fracture}$ (IDT), $G_{fracture}$ (SCB-FI), CRI (IDT), CRI (SCB-FI), FI (IDT), FI (SCB-FI), IDEAL-CT_{Index}, Nflex factor, $IDT_{Strength}$, $IDT_{Modulus}$, J_c, and $Weibull_{CRI}$ were sensitive to the variation in binder content and binder PG. However, some indicators showed unexpected trend with binder content including $G_{fracture}$ (IDT), $G_{fracture}$ (SCB-FI), $IDT_{Strength}$, and J_c and with PG type (e.g., $IDT_{Strength}$). In addition, some indicators didn't show clear trend including $G_{fracture}$ (IDT), $G_{fracture}$ (SCB-FI), $IDT_{Modulus}$, and J_c.

- $G_{fracture}$ (IDT), $G_{fracture}$ (SCB-FI), CRI (IDT), FI (IDT), Nflex factor, and $Weibull_{CRI}$(IDT) showed that mixes D2L2 and D6L1 are expected to exhibit good cracking resistance compared to mixture D3L1 which is expected to have poor cracking resistance. This is because mixture D6L1 had the lowest RBR content (0 percent), higher binder content (5.40 percent), softer design binder (PG 64-34), dense aggregate gradation (SP5), and small NMAS (12.5mm). Mixture D2L2 also had high binder content (5.70 percent), softer virgin binder (PG 58-34), and small NMAS (12.5 mm). Conversely, mixture D3L1 had the highest RBR content (50 percent) and stiffer binder PG (PG 70-28).

- Monotonic cracking resistance indicators had different Pearson correlation coefficients and Spearman ranking correlation coefficients among each other. The $Weibull_{CRI}$ correlated with more indicators than any other performance indicators. The $Weibull_{CRI}$ had strong correlation with CRI (IDT), FI (IDT), IDEAL-CT_{Index}, and Nflex factor. Also, the $Weibull_{CRI}$ had good correlation with $G_{fracture}$ (IDT), $G_{fracture}$ (SCB-FI) and fair correlation with and J_c, FI (SCB-FI), and $IDT_{Modulus}$. Such good correlation of $Weibull_{CRI}$ with most of the performance indicators was attributed to its calculation's method. Each indicator uses one or more elements of the load-displacement curve, while the $Weibull_{CRI}$ describes the entire load-displacement curve.

- The HWTT and APA rutting indicators (i.e., APA_{8000}, $HWTT_{15000}$ and $HWTT_{20000}$) were sensitive to binder content and binder PG. $HWTT_{15000}$ and $HWTT_{20000}$ indicators provided an expected trend with the variation in binder content and binder PG, while the APA_{8000} trend was expected for the binder content only. Both tests (e.g., Hamburg and APA) had similar variation in the test results. The average COV values for Hamburg and APA were 5 percent and 11 percent, respectively.

- HWTT and APA rut test rutting indicators (APA_{8000}, $HWTT_{15000}$ and $HWTT_{20000}$) indicators were used to differentiate between field projects with different cracking resistance (e.g., good, fair, and poor). Different thresholds were proposed for the three performance indicators: 1) HWTT rut depth after 15,000 cycles ($HWTT_{15000}$), 2) HWTT rut depth after 20,000 cycles ($HWTT_{20000}$), and 3) APA rut depth after 8,000 cycles (APA_{8000}). A maximum rut depth of 10 mm for $HWTT_{15000}$, 12.5 mm for $HWTT_{20000}$, and 5 mm for APA_{8000} are proposed. These thresholds are proposed to ensure adequate resistance to rutting. Also, the HWTT thresholds can be used to ensure adequate resistance to moisture damage. Similar thresholds are used and adopted by several transportation agencies.

- The current practice of ITD is to use the APA rut test to evaluate the rutting resistance of all 75- and 100-gyration asphalt mixes produced and used in the state. The results of this study demonstrated that such practice is very effective and should be maintained. The proposed APA rut test rutting threshold in this study is the same as the current ITD threshold.

- All of the PMLC mixes and most of the field projects (except D2C5 and D2C11) showed no signs of moisture damage. It should be noted that ITD specifies adding antistripping additives (e.g., liquid antistripping agent or lime) to asphalt mixtures as a percent of binder by weight (minimum of 0.5 percent) [77]. The results suggested that such practice is very effective and should be maintained. In addition, ITD could consider using the HWTT since it evaluates both rutting and moisture damage resistance. Several DOTs (e.g., TxDOT, WSDOT, CODOT, LaDOT, and MTDOT) use HWTT.

- Spearman ranking correlation showed excellent ranking agreement between both HWTT indicators (r_s = 0.98). These results demonstrate that the two HWTT rutting performance indicators (e.g., $HWTT_{15000}$ and $HWTT_{20000}$) are highly correlated and thus using only one or the other would be sufficient. Since the $HWTT_{15000}$ requires less number of passes which reduces the HWTT testing time, it is recommended over $HWTT_{20000}$. Also, APA rut test was also found to have poor ranking agreement with both $HWTT_{15000}$ and $HWTT_{20000}$ rutting indicators (R_s = 0.14 and 0.10 with $HWTT_{15000}$ and $HWTT_{20000}$, respectively).

Implementation

ITD can implement and adopt the proposed performance thresholds to ensure adequate resistance to cracking, rutting and moisture damage. Figure 135 and Figure 136 illustrate the concept of implementing

the proposed cracking and rutting thresholds during the mixture design process using the APA rut test and HWTT, respectively. Only one rutting test (either APA rut test or HWTT) is required. Meanwhile, HWTT is recommended over the APA since the HWTT can evaluate both rutting and moisture damage, while APA rut test can be used only for rutting. This example shows that the cracking resistance is improved (higher $Weibull_{CRI}$) with binder content while the rutting resistance decreases (rut depth increases). Initially, the binder content is determined using Superpave volumetric procedures then it would be optimized to achieve balanced (engineered) mix design with improved performance. The binder content parameter can be replaced with other mix characteristics such as RAP content. For instance, RAP content can be optimized to produce mixes with favorable performance. Also, combined parameters can be optimized (e.g., binder content, RAP, and rejuvenator) to allow the use of higher RAP in asphalt mixes yet meeting the performance specifications.

ITD can also use the proposed performance thresholds during the production and placement of asphalt mixes in the field as quality control tool. Mixture performance changes with the change in percent binder and RAP content. Loose mixes can be collected during the construction and test samples can be prepared and tested for rutting (APA or HWTT) and cracking ($Weibull_{CRI}$). Changes in these performance indicators during the production indicate deviation from the original mix design.

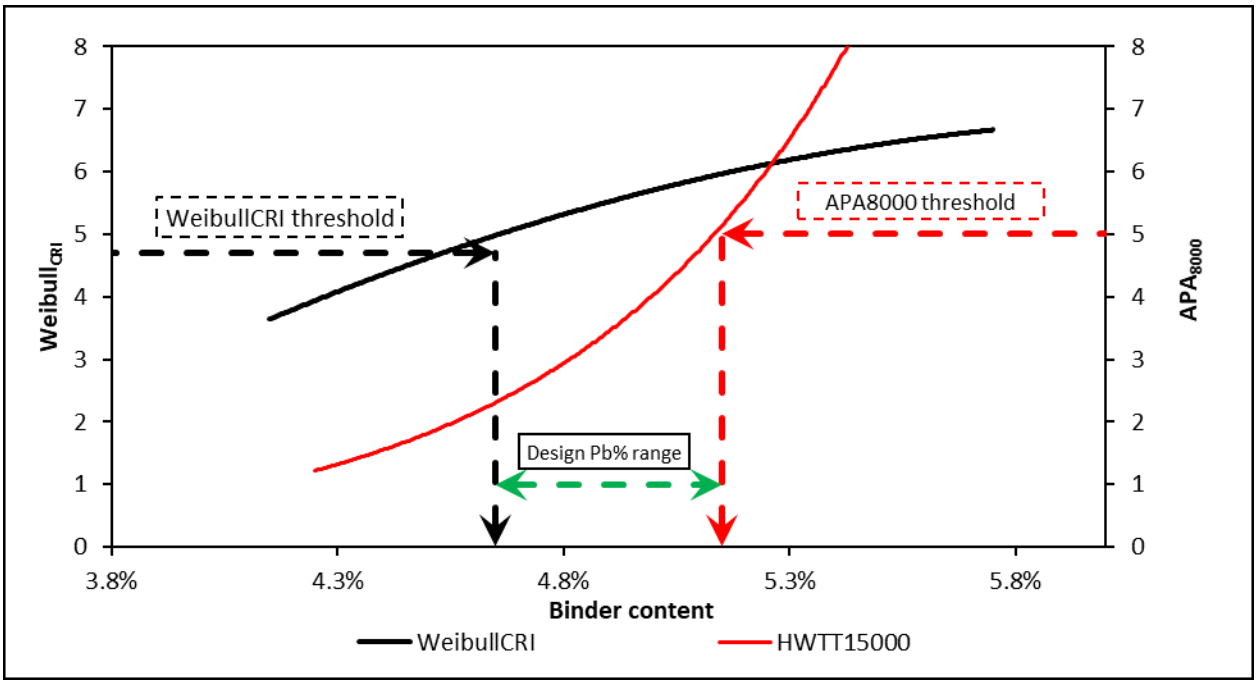

Figure 135 Schematic of Implementation of the Proposed APA Rutting and Cracking Thresholds

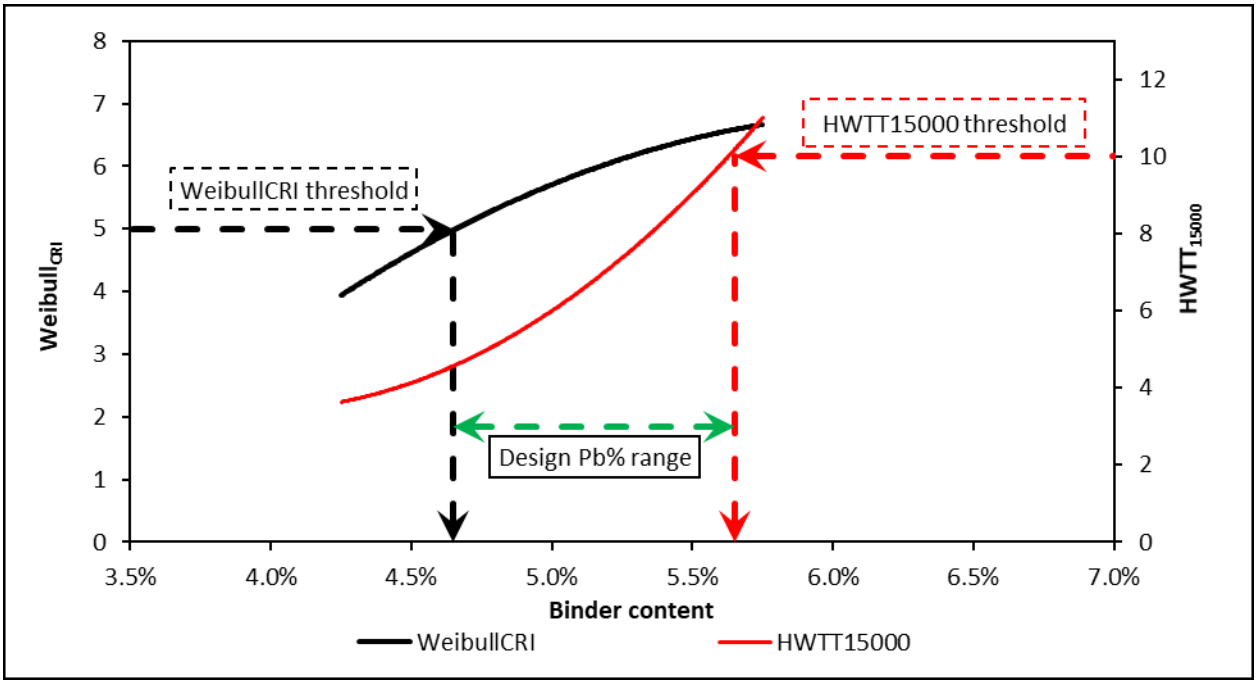

Figure 136 Schematic of Implementation of the Proposed HWTT Rutting and Cracking Thresholds

The proposed performance thresholds can also be used as additional requirements to the current Superpave volumetric design method similar to the current practice to assess asphalt mix resistance to rutting. The proposed performance tests can be conducted after the volumetric design to satisfy the minimum requirements of performance thresholds for both cracking and rutting. Figure 137 shows an example of mixtures with different binder contents and PG. Asphalt mixes fail to achieve the required cracking or rutting thresholds need to be redesigned to improve the mixture resistance to cracking and/or rutting. In Figure 137, mixes in green shaded area have good resistance to both cracking and rutting. Mixes in the orange shaded area have fair cracking resistance and good rutting resistance, while mixes in the red shaded areas had either poor cracking or rutting resistance.

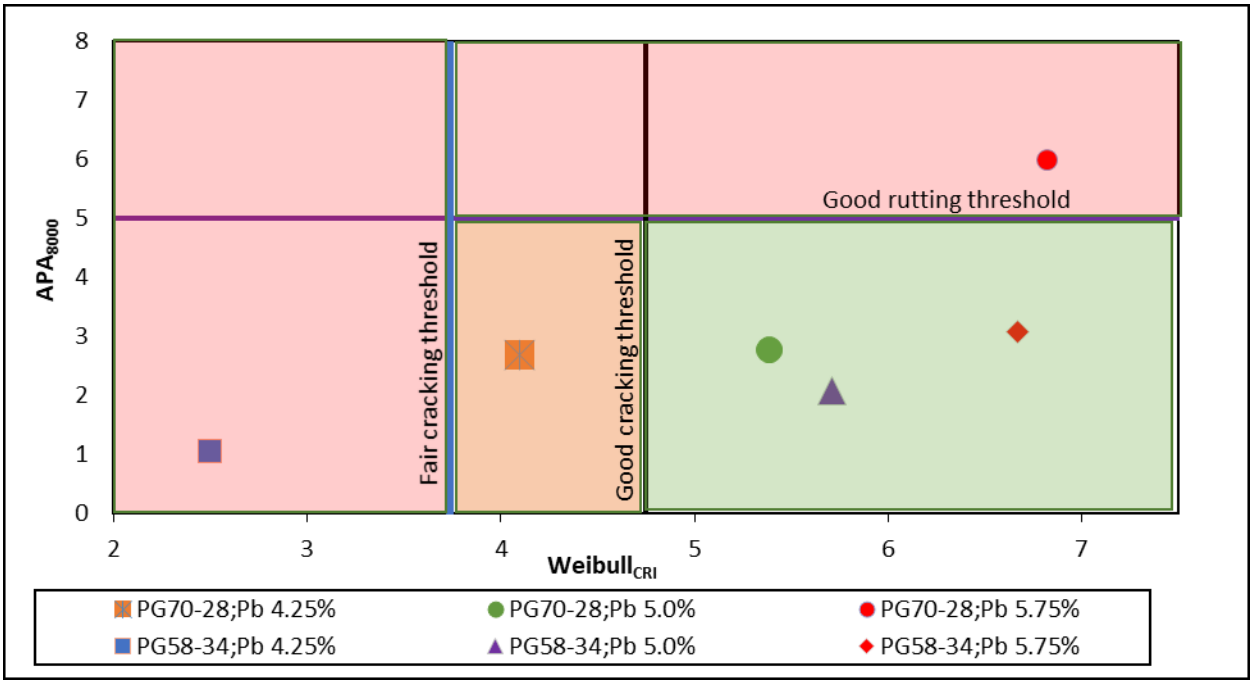

Figure 137 Implementation of Performance Tests as Part of Superpave Design Method

Recommendations

- It is recommended that more mixes produced in Idaho to be tested for cracking ($Weibull_{CRI}$) and rutting (APA or HWTT) and the proposed thresholds can be revised and adjusted based on the mix design (SP3 or SP5) and traffic level.

- It is recommended to evaluate the moisture susceptibility using both HWTT and Lottman test and assess the correlation between these two tests and the applicability of HWTT to evaluate the resistance of asphalt mixes to moisture damage.

- Further research investigation is recommended to reduce the testing time of the developed MSSD test. Currently, this test can take up to 9 hours.

References

1. Cominsky, R., Huber, G. a, Kennedy, T. W. & Anderson, M. The Superpave Mix Design Manual for New Construction and Overlays. *Publication NO SHRP-S-407 Strategic Highway Research program, U.S.* 184 (1994).

2. Miller, J. S. & Bellinger, W. Y. Distress Identification Manual for the Long-Term Pavement Performance Program. *Publication NO FHWA-RD-03-031. FHWA, U.S. Department of Transportation* 129 (2003). doi:FHWA-RD-03-031

3. Witczak, M. W. *Specification Criteria for Simple Performance Tests for Rutting Volume I: Dynamic Modulus (E*) Volume II: Flow Number and Flow Time NATIONAL COOPERATIVE HIGHWAY RESEARCH PROGRAM*. *Transportation Research* I, (2007).

4. National Cooperative Highway Research Program (NCHRP). *NCHRP Report 673: A Manual for Design of Hot-Mix Asphalt with Commentary*. (2011). doi:10.17226/14524

5. Witczak, M. W., Kaloush, K., Pellinen, T., El-Basyouny, M. & Quintus, H. Von. *Simple Performance Test for Superpave Mix Design*. *Design* (2002).

6. Masad, E., Kassem, E. & Little, D. Characterization of Asphalt Pavement Materials in the State of Qatar. *Road Materials and Pavement Design* 12, 739–765 (2011).

7. Witczak, M. W. *Simple Performance Tests: Summary of Recommended Methods and Database*. *NCHRP REPORT 547* (2005). doi:10.17226/13949

8. Izzo, R. & Tahmoressi, M. Use of the Hamburg Wheel-Tracking Device for Evaluating Moisture Susceptibility of Hot-Mix Asphalt. *Transportation Research Record* 1681, 76–85 (1999).

9. Lu, Q. & Harvey, J. Evaluation of Hamburg Wheel-Tracking Device Test with Laboratory and Field Performance Data. *Transportation Research Record* 1970, 25–44 (2006).

10. Kassem, E., Masad, E., Lytton, R. & Chowdhury, A. Influence of Air Voids on Mechanical Properties of Asphalt Mixtures Influence of Air Voids on Mechanical Properties of Asphalt Mixtures. *Road Materials and Pavement Design* 37–41 (2011). doi:10.3166/RMPD.12.493-524

11. Texas Department of Transportation (TxDOT). *Standard Specifications for Construction and Maintenance of Highways, Streets, and Bridges*. (2014).

12. Texas Department of Transportation (TxDOT). *Test procedure for Hamburg Wheel-Tracking Test (Tex-242-F)*. (2014).

13. Washington State Department of Transportation (WSDOT). *Standard Specifications for Road, Bridge, and Municipal Construction*. (2016).

14. Colorado Department of Transportation (CODOT). *Standard Method of Test for Hamburg Wheel-Track Testing of Compacted Bituminous Mixtures (CP-L 5112)*. (2015).

15. Louisiana Department of Transportation and Development (LaDOT). *Louisiana Standard Specification for Roads and Bridges*. (2016).

16. Montana Department of Transportation (MTDOT). *Standard Specifications for Road and Bridge Construction*. (2014).

17. Montana Department of Transportation (MTDOT). *Method of Sampling and Testing Hamburg Wheel-Track Testing of Compacted Bituminous Mixtures*. (2014).

18. American Association of State Highway and Transportation (AASHTO). *Standard Method of Test for Determining the Rutting Susceptibility of Asphalt Paving Mixtures Using the Asphalt Pavement Analyzer (APA)*. *AASHTO specifications and test Method* (2009).

19. Choubane, B., Page, G. & Musselman, J. Suitability of Asphalt Pavement Analyzer for Predicting Pavement Rutting. *Transportation Research Record* 1723, 107–115 (2000).

20. Skok, E., Johnson, E. & Turk, A. Asphalt Pavement Analyzer (APA) Evaluation. *Minnesota Department of Transportation Office of Research Services, Report MN/RC 2003-02 2.* (2003).

21. Georgia Department of Transportation (GDOT). *Hot Mix Asphalt Level II Quality Control Technician Certification Study Guide*. (2005).

22. Georgia Department of Transportation (GDOT). *ROAD Standards-Section 828 - Hot Mix Asphaltic Concrete Mixtures-Attachment G*. (2013).

23. ALDOT. *RUTTING SUSCEPTIBILITY DETERMINATION OF ASPHALT PAVING MIXTURES USING THE ASPHALT PAVEMENT ANALYZER 1(ALDOT-401)*.

24. Alabama Department of Transportation(ALDOT). *Standard Specifications-section 410 - Asphalt Pavements*. (2013).

25. Transportation Research Board. *Application of Asphalt Mix Specifications*. *Transportation RESEARCH Circular E-C189* (2014). doi:10.17226/22248

26. Virginia Department of Transportation (VDOT). *Method of Test For Determining Rutting Susceptibility Using The Asphalt Pavement Analyzer – (Asphalt Lab) (Virginia Test Method -110)*. (2008).

27. Virginia Department of Transportation (VDOT). *Road and Bridge Specifications*. (2016).

28. Chong, K. P. & Kuruppu, M. D. New specimen for fracture toughness determination for rock and other materials. *International Journal of Fracture* 26, 59–62 (1984).

29. Rice, J. R. A Path Independent Integral and the Approximate Analysis of Strain Concentration by Notches and Cracks. *Journal of Applied Mechanics* 35, 379–386 (1968).

30. Mull, M. A., Stuart, K. & Yehia, A. Fracture resistance characterization of chemically modified crumb rubber asphalt pavement. *Journal of Materials Science* 37, 557–566 (2002).

31. Bayomy, F. & Abdo, A. A. Performance Evaluation of Idaho HMA Mixes Using Gyratory Stability. *NIATT puplication No. KLK 482 ITD Project No. SPR-0004(022) RP 175, US, Idaho Transportation Department* (2007).

32. Mohammad, L. N., Wu, Z., Aglan, M. A. & Rouge, B. Characterization of Fracture and Fatigue Resistance on Recycled Polymer-Modified Asphalt Pavements. *Fifth International RILEM*

Conference on Reflective Cracking in Pavements (2004).

33. Louisiana Department of Transportation and Development (LaDOT). *Evaluation of Asphalt Mixture Crack Propagation using the Semi-Circular Bend Test (SCB) (TR 330-14)*. (2014).

34. Jung, S. J. *et al.* Development and Evaluation of Performance Tests to Enhance Superpave Mix Design and its Implementation in Idaho Phase B: Evaluation of Mix Resistance to Fracture and Fatigue Cracking. *Publication number KLK 483/KLK479* (2010).

35. Al-Qadi, I., Ozer, H., Lambros, J., El Khatib, A. & Singhvi, D. *Testing protocols to ensure performance of high asphalt binder replacement mixes using RAP and RAS*. (2015).

36. American Association of State Highway and Transportation (AASHTO). *Standard Method of Test for Determining the Fracture Potential of Asphalt Mixtures Using Semicircular Bend Geometry (SCB) at Intermediate Temperature (AASHTO TP 124)*. *AASHTO specifications and test Method* 3, (2016).

37. Illinois department of transportation (IDOT). *CIRCULAR LETTER 2016-25. Illinois Flexibility Index Test*. 30 (2016).

38. Kim, M., Mohammad, L. N. & Elseifi, M. a. Characterization of Fracture Properties of Asphalt Mixtures as Measured by Semicircular Bend Test and Indirect Tension Test. *Transportation Research Record: Journal of the Transportation Research Board* 2296, 115–124 (2012).

39. Mohammad, L., Kim, M. & Elseifi, M. Characterization of Asphalt Mixture's Fracture Resistance Using the Semi-Circular Bending (SCB) Test. *7th RILEM International Conference on Cracking in Pavements SE - 1* 4, 1–10 (2012).

40. Nsengiyumva, G. Development of Semi-Circular Bending (SCB) Fracture Test for Bituminous Mixtures. (2015).

41. Ozer, H. *et al.* Fracture Characterization of Asphalt Mixtures with High Recycled Content Using Illinois Semicircular Bending Test Method and Flexibility Index. *Transportation Research Record: Journal of the Transportation Research Board* (2016).

42. Cooper III, S., King, W. & Kabir, M. S. Properties of Asphalt Concrete Mixtures. 70808, (2016).

43. West, R. *et al. NCAT TEST TRACK FINDINGS (NCAT draft Report 18-04 PHASE V [2012-2015])*. (2018).

44. Kaseer, F. *et al.* Development of An Index to Evaluate the Cracking Potential of Asphalt Mixtures Using The Semi-Circular Bending Test. *Construction and Building Materials* 167, 286–298 (2018).

45. Kennedy, T. W. & Anagnos, J. N. Procedures for the Static and Repeated-Load Indirect Tensile Test. (1983).

46. Kim, Y. R. & Wen, H. Fracture energy from indirect tension testing. in *Asphalt Paving Technology* 71, 779–793 (2002).

47. Kim, Y. R., Khosla, N. P. & Kim, N. Effect of Temperature and Mixture Variables on Fatigue Life Predicted By Diametral Fatigue Testing. *Transportation Research Record* 128–138 (1991).

48. American Society for Testing and Materials (ASTM). Standard Test Method for Indirect Tensile (IDT) Strength of Bituminous Mixtures. *ASTM D 6931* (2012).

49. AASHTO. *Standard Method of Test for Determining the Creep Compliance and Strength of Hot Mix Asphalt (HMA) Using the Indirect Tensile Test Device Determining the Creep Compliance and Indirect Tensile Test Device*. *AASHTO specifications and test Method* (2011).

50. Cocurullo, A., Airey, G. D., Collop, A. & Sangiorgi, C. Indirect Tensile versus Two-point Bending Fatigue Testing. *Proceedings of the Institution of Civil Engineers* 207–220 (2008). doi:10.1680/tran.2008.161.4.207

51. Khalid, H. a. A comparison between bending and diametral fatigue tests for bituminous materials. *Materials and Structures* 33, 457–465 (2000).

52. Kim, J., Koh, C. & Ph, D. Development of a Predictive System for Estimating Fatigue Life of Asphalt Mixtures Using the Indirect Tensile Test. 138, 1530–1540 (2012).

53. Nguyen, M. T., Lee, H. J., Baek, J. & Moon, J. A New Fatigue Failure Criterion Based on Crack Width of Asphalt Concrete Under Indirect Tensile Mode of Loading. *Journal of Testing and Evaluation* 44, 20130029 (2016).

54. Christensen, D. W., Bonaquist, R. & Jack, D. P. *Evaluation of Triaxial Strength as a Simple Test for Asphalt Concrete Rut Resistance*. (2000).

55. Mihai Marasteanu, William Buttlar, Hussain Bahia, and Christopher Williams, et al. Investigation of Low Temperature Cracking in Asphalt Pavements. 378 (2012).

56. Wen, H. & Kim, Y. Simple Performance Test for Fatigue Cracking and Validation with WesTrack Mixtures. *Transportation Research Record* 1789, 66–72 (2002).

57. Zofka, A. & Braham, A. Comparison of Low-Temperature Field Performance and Laboratory Testing of 10 Test Sections in the Midwestern United States. *Transportation Research Record: Journal of the Transportation Research Board* 2127, 107–114 (2009).

58. Wen, H. & Bhusal, S. A Laboratory Study to Predict the Rutting and Fatigue Behavior of Asphalt Concrete Using the Indirect Tensile Test. *Journal of Testing and Evaluation* 41, 20120004 (2013).

59. West, R. C., Van Winkle, C., Maghsoodloo, S. & Dixon, S. Relationships between simple asphalt mixture cracking tests using ndesign specimens and fatigue cracking at FHWA's accelerated loading facility. *Road Materials and Pavement Design* 86, 579–602 (2017).

60. Idaho Transportation Department (ITD DOT). *Standard Specifications for Highway Construction*. (2012).

61. Idaho Transportation Department (ITD). *Standard Specification for Highway Construction*. (2017).

62. Poorbaugh, J. Idaho Transportation System Pavement Performance-2017 Report. (2017).

63. PathWay Services Incorporated Companies. Pavement profiler information- the PathRunner. (2019). Available at: http://www.pathwayservices.com/equipment-1/.

64. Kercher Engineering. *AgileAssets Pavement Management System Engineering Configuration*.

(2015).

65. AASHTO. *Standard practice for mixture conditioning of Hot Mix Asphalt (AASHTO R30)*. *AASHTO specifications and test Method* (2015).

66. AASHTO. *Standard Method for Preparing and Determining the Density of Hot Mix Asphalt (HMA) Specimens By Means of the SHRP Gyratory Compactor (AASHTO T 312)*. *AASHTO specifications and test Method* (2015).

67. American Society for Testing and Materials (ASTM). *Standard Test Method for Bulk Specific Gravity and Density of Non-Absorptive Compacted Bituminous Mixtures*. *ASTM D2726* (2005). doi:10.1520/D2726

68. American Society for Testing and Materials (ASTM). *Standard Test Method for Maximum Specific Gravity and Density of Asphalt Mixtures Using Automatic Vacuum Sealing Method*. *ASTM D6857 / D6857M - 18* (2018).

69. National Asphalt Paving Association Educatio foundation. *Hot Mix Asphalt Materials, Mixture Design, and Construction*. (1996).

70. Zhou, F. *et al. Field Validation of Laboratory Tests to Assess Cracking Resistance of Asphalt Mixtures: An Experimental Design*. *National Cooperative Highway Research Program (NCHRP)* (2016). doi:10.17226/23608

71. American Society for Testing and Materials (ASTM). *Standard Test Method for Evaluation of Asphalt Mixture Cracking Resistance using the Semi-Circular Bend Test (SCB) at Intermediate Temperatures*. *ASTM D8044-16* (2015). doi:10.1145/3132847.3132886

72. American Association of State Highway and Transportation (AASHTO). *Determining the Fracture Energy of Asphalt Mixtures Using the Semicircular Bend Geometry (SCB) (AASHTO TP 105)*. *AASHTO specifications and test Method* (2013).

73. Zhou, F., Im, S., Sun, L. & Scullion, T. Development of an IDEAL cracking test for asphalt mix design and QC/QA. *Asphalt Paving Technology: Association of Asphalt Paving Technologists-Proceedings of the Technical Sessions* 86, 549–577 (2017).

74. Zhu, Y., Dave, E. V., Rahbar-Rastegar, R., Daniel, J. S. & Zofka, A. Comprehensive evaluation of low temperature fracture indices for asphalt mixtures. *Asphalt Paving Technology: Association of Asphalt Paving Technologists-Proceedings of the Technical Sessions* 86, 629–658 (2017).

75. Chen, X. & Solaimanian, M. Simple Indexes to Identify Fatigue Performance of Asphalt Concrete. *Journal of Testing and Evaluation* 48, 20170722 (2018).

76. Buttlar, W. G., Roque, R. & Kim, N. Accurate Asphalt Mixture Tensile Strength. in *Proceedings of the Materials Engineering Conference* (1996).

77. Molenaar, A. A. A., Scarpas, A., Liu, X. & Erkens, S. M. J. G. SEMI-CIRCULAR BENDING TEST; SIMPLE BUT USEFUL. *Asphalt Paving Technology: Association of Asphalt Paving Technologists* (2002).

78. Huang, L., Cao, K. & Zeng, M. Evaluation of semicircular bending test for determining tensile strength and stiffness modulus of asphalt mixtures. *Journal of Testing and Evaluation* 37, 122–128

(2009).

79. Hofman, R., Oosterbaan, B., Erkens, S. M. J. G. & Van der Kooij, J. Semi-Circular Bending Test to Assess the Resistance Against Crack Growth. *6th International Rilem Symposium* 257–263 (2003).

80. Walubita, L. F. *et al. New Generation Mix-Designs: Laboratory Testing and Construction of the APT Test Section*. *Texas Department of Transportation* (2010).

81. West, R. C. & Copeland, A. High RAP Asphalt Pavements: Japan practice-lessons learned. *National Asphalt Pavement Association* 139, 62 (2015).

82. Ozer, H. *et al.* Development of the fracture-based flexibility index for asphalt concrete cracking potential using modified semi-circle bending test parameters. *Construction and Building Materials* 115, 390–401 (2016).

83. Hanz, A., Dukatz, E. & Reinke, G. Use of performance-based testing for high RAP mix design and production monitoring. *Road Materials and Pavement Design* 0629, (2017).

84. Kim, S. S., Yang, J. J. & Etheridge, R. A. Effects of mix design variables on flexibility index of asphalt concrete mixtures. *International Journal of Pavement Engineering* 0, 1–6 (2018).

85. Rivera-Perez, J., Ozer, H. & Al-Qadi, I. L. Impact of Specimen Configuration and Characteristics on Illinois Flexibility Index. *Transportation Research Record* 2672, 383–393 (2018).

86. Barry, M. AN ANALYSIS OF IMPACT FACTORS ON THE ILLINOIS FLEXIBILITY INDEX TEST. (2016).

87. Rivera, J. Effects of speciemn geometry and test configuration on the fracture process zone for asphalt materials. (2017).

88. Dong, W. & Charmot, S. Proposed Tests for Cold Recycling Balanced Mixture Design with Measured Impact of Varying Emulsion and Cement Contents. *Journal of Materials in Civil Engineering* 2, 1–8 (2019).

89. Bennert, T., Haas, E. & Wass, E. Indirect Tensile Test (IDT) to Determine Asphalt Mixture Performance Indicators during Quality Control Testing in New Jersey. *Transportation Research Record* 2672, 394–403 (2018).

90. ASTM D8225-19. *Standard Test Method for Determination of Cracking Tolerance Index of Asphalt Mixture Using the Indirect Tensile Cracking Test at Intermediate Temperature*. (2019).

91. Yin, F., Garita, J., Taylor, A. & West, R. Refining the indirect tensile (IDT) Nflex Factor test to evaluate cracking resistance of asphalt mixtures for mix design and quality assurance. *Construction and Building Materials* 172, 396–405 (2018).

92. Bayomy, F., Ahmad, A. abdo & Ann Mull, M. Evaluation of Hot Mix Asphalt (HMA) Fracture Resistance Using the Critical Strain Energy Release Rate , J c. (2006).

93. Elseifi, M. A., Mohammad, L. N., Ying, H. & Iii, S. C. Modeling and Evaluation of the Cracking Resistance of Asphalt Mixtures Using the Semi-Circular Bending Test at Intermediate Temperatures. X, 1–23 (2005).

94. Cao, W., Mohammad, L., Elseifi, M., Cooper, S. B. & Saadeh, S. Fatigue Performance Prediction of

Asphalt Pavement Based on Semicircular Bending Test at Intermediate Temperature. *Journal of Materials in Civil Engineering* 30, 1–8 (2018).

95. Weibull, W. & Sweden, S. A Statistical Distribution Function of Wide Applicability. *Journal of Applied Mechanics* 18, 293–297 (1951).

96. Brown, A. M. A step-by-step guide to non-linear regression analysis of experimental data using a Microsoft Excel spreadsheet. *Computer Methods and Programs in Biomedicine* 65, 191–200 (2001).

97. Anderson, T. L. *Fracture Mechanics: Fundamentals and Applications*. (2005).

98. Lim, I. L., Johnston, I. W. & Choi, S. K. Stress intensity factors for semi-circular specimens under three-point bending. *Engineering Fracture Mechanics* 44, 363–382 (1993).

99. Hassan, M. M. & Khalid, H. A. Fracture Characteristics of Asphalt Bottom Ash Aggregate. 1–8 (2005). doi:10.3141/2180-01

100. Artamendi, I. & Khalid, H. A. A comparison between beam and semi-circular bending fracture tests for asphalt. *Road Materials and Pavement Design* 7, 163–180 (2006).

101. Biligiri, K. P., Said, S. & Hakim, H. Asphalt Mixtures ' Crack Propagation Assessment using Semi - Circular Bending Tests Sixteen Mixes with Three Replicates Each. *Chinese Society of Pavement Engineering* 5, 209–217 (2012).

102. Pszczola, M. & Szydlowski, C. Influence of bitumen type and asphalt mixture composition on low-temperature strength properties according to various test methods. *Materials* 11, 1–18 (2018).

103. Khalid, H. A. & Monney, O. K. Moisture damage potential of cold asphalt. *International Journal of Pavement Engineering* 10, 311–318 (2009).

104. Paris, P., Director, A. & Erdogan, F. A Critical Analysis of Crack Propagation Laws. *Journal of Basic Engineering* 85, 528–533 (1963).

105. Bilir, O. G. Crack propagation in a commercial steel. 80, 73–80 (1988).

106. Bilir, Ö. G. The relationship between the parameters and of Paris' law for fatigue crack growth in a SAE 1010 steel. *Engineering Fracture Mechanics Vol.* 36, 361–364 (1990).

107. American Association of State Highway and Transportation (AASHTO). *Standard Method of Test for Hamburg Wheel-Track Testing of Compacted Hot Mix Asphalt (HMA) (AASHTO T324-14)*. *AASHTO specifications and test Method* 3, (2015).

108. American Association of State Highway and Transportation (AASHTO). *Standard Method of Test for Determining the Rutting Susceptibility of Asphalt Paving Mixtures Using the Asphalt Pavement Analyzer (APA) (AASHTO T340)*. *AASHTO specifications and test Method* (2015).

109. Bairgi, B. K., Syed, I. A. & Tarefder, R. A. Evaluation of Rutting and Stripping Potential of WMA with Different Additives. 201–212 (2017). doi:10.1061/9780784481219.018

110. Zaumanis, M., Poulikakos, L. D. & Partl, M. N. Performance-based design of asphalt mixtures and review of key parameters. *Materials and Design* 141, 185–201 (2018).

111. AWu, R., Harvey, J., Buscheck, J. & Mateos, A. *Mechanistic-Empirical (ME) Design: Mix Design Guidance for Use with Asphalt Concrete Performance-Related Specifications*. (2018).

112. Barros, L. Influence of Mix Design Parameters on Performance of Balanced Asphalt Concrete. (University of Texas at El Paso, 2018).

113. Rooijen, R. C. Van & Bondt, A. H. De. Crack propagation performance evaluation of asphaltic mixes using a new procedure based on cyclic semi-circular bending tests. 437–450 (2008).

114. Linden, R. N., Mahoney, J. & Jackson, N. C. Effect of Compaction on Asphalt Concrete Performance. *Transportation Research Board* (1989).

115. Tran, N., Turner, P. & Shambley, J. *ENHANCED COMPACTION TO IMPROVE DURABILITY AND EXTEND PAVEMENT SERVICE LIFE : A LITERATURE REVIEW (NCAT Report 16-02R)*. (2016).

116. Al-Qadi, I., Ozer, H., Lambros, J., El Khatib, A. & Singhvi, D. *Testing Protocols to Ensure Performance of High Asphalt Binder Replacement Mixes Using RAP and RAS*. (2020).

117. Diefenderfer, S. D. & Bowers, B. F. Initial Approach to Performance (Balanced) Mix Design : The Virginia Experience. *Transportation Research Board* (2019). doi:10.1177/0361198118823732

118. Salkind, N. J. *Encyclopedia of research design*. (2010).

119. Sreedhar, S., Coleri, E. & Haddadi, S. S. Selection of a performance test to assess the cracking resistance of asphalt concrete materials. *Construction and Building Materials* 179, 285–293 (2018).

120. Washington State Department of Transportation (WSDOT). *Standard Specifications for Road, Bridge, and Municipal Construction*. (2018).

Appendix A
PMLC Mix Design Summary Sheet

Table 31 Mixture D1L1 Mix Design Summary Sheet

Laboratory Values	Target			Spec.
Total Asphalt by Weight of Mix % (Pb)	5.3			
Total Aspalt by Weight of Aggregate	5.6			
Air Voids % (Va)	4.0			3.0-5.0
Voids in Mineral Aggregate (VMA)	14.7			14.0 min
Voids Filled with Asphalt (VFA)	72.8			65-75
Bulk Specific Gravity (Gmb)	2.383			
Unit Weight lb./cuft.	148.3			
Theo Max Spec Gravity (Gmm)	2.483			
Theo Max Spec Gravity lb./cuft.	154.6			
Effective Specific Gravity of Blend (Gse)	2.696			
Effect of Water on Compressive Strength *(AllWest)*	94			85 min
Ninitial (8 Gyrations)	88.6			≤ 89.0
Ndesign SP-5 (100 Gyrations)	96.0			= 96.0
Nmax (160 Gyrations)	97.7			≤ 98.0
NCAT Asphalt Correction Factor	0.10			
Dust to Asphalt	1.4			0.8-1.6
Laboratory Mixing Temperature(deg in F)	325			
Laboratory Compaction Temperature(deg in F)	300			
Plant Mixing Temperature(deg in F)**	317	-	326	
Field Compaction Temperature(deg in F)**	295	-	303	
Superpave Design Sample Wt. in grams	4735			

**Field mixing and compaction may be adjusted +/- 25 degrees per Viscosity Graph*

Aggregate Gradation Data

Sieve Size		Kt-213c B Rock 32.0%	Kt-213c C Rock 17.0%	Kt-213c Wash C 11.0%	Br-2c Dover Sand 5.5%	RAP 34.0%	Break Down 0.5%	JMF Blended Gradation
1" / 25mm		100	100	100	100	100	100	100
3/4" / 19mm		100	100	100	100	100	100	100
1/2" / 12.5mm		87	100	100	100	98	100	95
3/8" / 9.5mm		57	100	100	100	89	100	83
No. 4 / 4.75mm		6	87	86	98	63	100	53
No. 8 / 2.36mm		3	57	54	86	42	100	36
No.16 / 1.18mm		2	38	31	72	29	100	25
No. 30 / 600um		2	26	17	48	21	100	17
No. 50 / 300um		2	19	9	21	16	100	12
No. 100 / 150um		2	14	4	5	12	96	8
No. 200 / 75um		1.5	10.9	2.0	1.9	9.4	86.0	6.3

** Aggregate breakdown will be controlled by the Hot Plant dust control system.*

Table 32 Mixture D2L1 Mix Design Summary Sheet

Mix Design Summary

Project	US.12 Arrow Br to Big Canyon Creek Br
Mix Producer	Knife River
SPMDT (print)	Justin Drye
JMF Mix ID NO	17008-19187-12 5mmSP3-R45

Mix Class	12.5mm SP3(1-<10 Design ESALs)
Specified Asphalt Grade	PG 70-28
*Adjusted Binder Grade	PG 64-34
Project Number	A018(792) A019 (187)(751)
Key Number	19187, 18792 & 19751

Aggregate & (Gravel) Other Constituents (RAP, Blend Sand, Lime, ETC.)							
Stock Pile	B	C	C2	P. Millings			
Stock Pile Percentage (Psp)	33	17	5	45			
Stock Pile Source Number	NP168c	NP168c	NP168c				
Design developed with "dry back" Gmm			Yes		No	X	

Mixture at Design Asphalt Content	
Maximum Specific Gravity (Gmm)	2.528
Gyratory Bulk Specific Gravity (Gmb)	2.428
Combined Aggregate (Gsb)	2.672
Effective Specific Gravity (Gse)	2.771
Combined Apparent Gravity (Gsa)	2.715
Absorbtion	2.0
Bulk Specific Gravity Rap (Gsb)	2.750
Absorbed Asphalt, % (Pba)	1.38
Effective Asphalt Content, % (Pbe)	4.398
P200 / Pbe Ratio	1.50
Air Voids, % (Va)	4.0
VMA %	14.6
VFA %	72
Rap oil content	6.30
Percent Rap by Binder	50
Relative Density %gmm @ Nmax	97.6
Ncat Correlation Factor @538C	0.39
Laboratory Compaction Temp	295
Gmb sample weight @ JMF	4730
Number of Gyrations	75
Aggregate Properties	
Uncompacted Void Content Fines	50
Sand Equivalent	63
Fracture Face (1 Face / 2 Face)	100/100
Flat and Elongated Particles	1
Fine Aggregate Gsb	2.572

Job Mix Formula		
Aggregate Gradation Sieve	Blend	Spec. Limits
1" (25 mm)	100	100
3/4" (19 mm)	100	100
1/2" (12.5 mm)	93	90-100
3/8" (9.5 mm)	81	90max
No. 4 (4.75 mm)	50	
No. 8 (2.36 mm)	35	28-58
No. 16 (1.18 mm)	25	
No. 30 (0.60 mm)	19	
No. 50 (0.30 mm)	13	
No. 100 (0.150 mm)	9	
No. 200 (0.075 mm)	6.6	2-10

Asphalt content, % (Pb)	5.7
Rap % AC contributed	2.8
Asphalt content added	2.9
Asphalt content by weight of agg	6.0
Asphalt content by agg added	3.2
Antistrip, %	0.75%
Asphalt Brand	Idaho Asphalt
Asphalt Grade	PG 70-28
Mix temp. range	324-338
Compaction temp. range	295-309
Asphalt specific gravity (Gb) 77 F	1.026
Asphalt specific gravity (Gb) 60 F	1.030

Min/Max Properties	Min	Target	Max	Spec Limits
Asphalt content, % (Pb)	5.4	5.7	6.1	
Air Voids, % (Va)	5.0	4.0	3.0	3.0-5.0
VMA %	14.6	14.3	14.4	14 min.
Maximum Specific Gravity (Gmm)	2.539	2.528	2.512	
Bulk Specific Gravity (Gmb)	2.413	2.428	2.437	
P200 / Pbe Ratio	1.6	1.5	1.4	0.8-1.6

Breakdown will be controlled by means of our baghouse.

Table 33 Mixture D2L2 Mix Design Summary Sheet

Mix Design Summary

Project	Top of Bear Ridge Grade to Pine Cr Latah Co
Mix Producer	Knife River
SPMDT (print)	Justin Drye
JMF Mix ID NO.	18020-19640-12 5mmSP3-R27

Mix Class	12 5mm SP3(1-<10 Design ESALs)
Specified Asphalt Grade	PG 64-28
*Adjusted Binder Grade	PG 58-34
Project Number	A019 (640)
Key Number	19640

Aggregate & (Gravel) Other Constituents (RAP, Blend Sand, Lime, ETC.)							
Stock Pile	B	C	C3	Basalt B	RAP		
Stock Pile Percentage (Psp)	22	26	10	15	27		
Stock Pile Source Number	NP168c	NP168c	NP168c	NP168c	NP168c		
Design developed with "dry back" Gmm			Yes		No	X	

Mixture at Design Asphalt Content	
Maximum Specific Gravity (Gmm)	2.521
Gyratory Bulk Specific Gravity (Gmb)	2.420
Combined Aggregate (Gsb)	2.719
Effective Specific Gravity (Gse)	2 762
Combined Apparent Gravity (Gsa)	2 802
Absorbtion	1 6
Bulk Specific Gravity Rap (Gsb)	2 799
Absorbed Asphalt, % (Pba)	0 59
Effective Asphalt Content, % (Pbe)	5 143
P200 / Pbe Ratio	1 19
Air Voids, % (Va)	4 0
VMA %	16.1
VFA %	75
Rap oil content	5 84
Percent Rap by Binder	30
Relative Density %gmm @ Nmax	97.1
Ncat Correlation Factor @538C	0.51
Laboratory Compaction Temp	290
Gmb sample weight @ JMF	4750
Number of Gyrations	75
Aggregate Properties	
Uncompacted Void Content Fines	60
Sand Equivalent	83
Fracture Face (1 Face / 2 Face)	100/100
Flat and Elongated Particles	1
Fine Aggregate Gsb	2 656

Job Mix Formula		
Aggregate Gradation Sieve	Blend	Spec Limits
1" (25 mm)	100	100
3/4" (19 mm)	100	100
1/2" (12 5 mm)	93	90-100
3/8" (9.5 mm)	80	90max
No. 4 (4.75 mm)	51	
No. 8 (2 36 mm)	34	28-58
No. 16 (1.18 mm)	24	
No. 30 (0 60 mm)	17	
No. 50 (0 30 mm)	12	
No. 100 (0 150 mm)	9	
No. 200 (0 075 mm)	6.1	2-10

Asphalt content, % (Pb)	5.7
Rap % AC contributed	1 6
Asphalt content added	4.1
Asphalt content by weight of agg	6.0
Asphalt content by agg added	4 5
Antistrip, %	0 75%
Asphalt Brand	Idaho Asphalt
Asphalt Grade	PG 64-28
Mix temp. range	313-327
Compaction temp range	282-298
Asphalt specific gravity (Gb) 77 F	1.029
Asphalt specific gravity (Gb) 60 F	1.033

Min/Max Properties	Min	Target	Max	Spec Limits
Asphalt content, % (Pb)	5 3	5 7	6 0	
Air Voids, % (Va)	5.0	4 0	3 0	3 0-5 0
VMA %	16 1	16 1	15 9	14 min
Maximum Specific Gravity (Gmm)	2.536	2.521	2.510	
Bulk Specific Gravity (Gmb)	2.410	2.420	2.434	
P200 / Pbe Ratio	1 3	1 2	1 1	0 8-1 6

Breakdown will be controlled by means of our baghouse

Table 34 Mixture D3L1 Mix Design Summary Sheet

Laboratory Values	Target			Spec.
Total Asphalt by Weight of Mix % (Pb)	5.2			
Total Aspalt by Weight of Aggregate	5.52			
Air Voids % (Va)	4.0			4.0
Voids in Mineral Aggregate (VMA)	14.5			14.0 min
Voids Filled with Asphalt (VFA)	72			65-75
Bulk Specific Gravity (Gmb)	2.324			
Unit Weight lb./cuft.	144.7			
Theo Max Spec Gravity (Gmm)	2.422			
Theo Max Spec Gravity lb./cuft.	150.8			
Effective Specific Gravity of Blend (Gse)	2.617			
Effect of Water on Compressive Strength *(AllWest)*	91			85 min
Ninitial (7 Gyrations)	88.6			≤ 89.0
Ndesign SP-3 (75 Gyrations)	96.0			= 96.0
Nmax (115 Gyrations)	97.3			≤ 98.0
NCAT Asphalt Correction Factor	0.28			
Dust to Asphalt	1.2			0.6-1.2
Laboratory Mixing Temperature(deg in F)	324			
Laboratory Compaction Temperature(deg in F)	298			
Plant Mixing Temperature(deg in F)**	290	-	324	
Field Compaction Temperature(deg in F)**	280	-	303	
Superpave Design Sample Wt. in grams	4645			

**Field mixing and compaction may be adjusted +/- 25 degrees per Viscosity Graph*

Aggregate Gradation Data

Sieve Size	1/2" Chips 8.0%	#4 Chips 6.0%	C-Pile 3.0%	Washed C-Pile 16.0%	Sand 12.0%	RAP 54.0%	Break Down 1.0%	JMF Blended Gradation
1" / 25mm	100	100	100	100	100	100	100	100
3/4" / 19mm	100	100	100	100	100	100	100	100
1/2" / 12.5mm	74	100	100	100	100	94	100	95
3/8" / 9.5mm	24	79	100	100	100	85	100	85
No. 4 / 4.75mm	2	3	76	86	97	65	100	64
No. 8 / 2.36mm	1	1	51	55	85	51	100	49
No.16 / 1.18mm	1	1	35	34	73	41	100	39
No. 30 / 600um	1	1	26	20	45	31	100	27
No. 50 / 300um	1	1	17	10	14	19	100	15
No. 100 / 150um	1	1	12	3	2	12	100	9
No. 200 / 75um	0.9	0.4	8.2	1.2	0.8	7.7	90.0	5.7

** Aggregate breakdown will be controlled by the Hot Plant dust control system.*

Table 35 Mixture D3L2 Mix Design Summary Sheet

Laboratory Values	Target			Spec.
Total Asphalt by Weight of Mix % (Pb)	5.2			
Total Aspalt by Weight of Aggregate	5.49			
Air Voids % (Va)	4.0			4.0
Voids in Mineral Aggregate (VMA)	14.3			14.0 min
Voids Filled with Asphalt (VFA)	72			65-75
Bulk Specific Gravity (Gmb)	2.316			
Unit Weight lb./cuft.	144.2			
Theo Max Spec Gravity (Gmm)	2.413			
Theo Max Spec Gravity lb./cuft.	150.2			
Effective Specific Gravity of Blend (Gse)	2.605			
Effect of Water on Compressive Strength *(AllWest)*	91			85 min
Ninitial (7 Gyrations)	88.6			≤ 89.0
Ndesign SP-3 (75 Gyrations)	96.0			= 96.0
Nmax (115 Gyrations)	97.2			≤ 98.0
NCAT Asphalt Correction Factor	0.16			
Dust to Asphalt	1.2			0.6-1.2
Laboratory Mixing Temperature(deg in F)	324			
Laboratory Compaction Temperature(deg in F)	298			
Plant Mixing Temperature(deg in F)**	290	-	324	
Field Compaction Temperature(deg in F)**	280	-	303	
Superpave Design Sample Wt. in grams	4640			

**Field mixing and compaction may be adjusted +/- 25 degrees per Viscosity Graph*

Aggregate Gradation Data

Sieve Size	1/2" Chips 16.0%	#4 Chips 11.0%	C-Pile 18.5%	Washed C-Pile 10.0%	Sand 10.0%	RAP 34.0%	Break Down 0.5%	JMF Blended Gradation
1" / 25mm	100	100	100	100	100	100	100	100
3/4" / 19mm	100	100	100	100	100	100	100	100
1/2" / 12.5mm	74	100	100	100	100	95	100	94
3/8" / 9.5mm	24	79	100	100	100	87	100	81
No. 4 / 4.75mm	2	3	76	86	97	66	100	56
No. 8 / 2.36mm	1	1	51	55	85	50	100	41
No.16 / 1.18mm	1	1	35	34	73	40	100	32
No. 30 / 600um	1	1	26	20	45	30	100	22
No. 50 / 300um	1	1	17	10	14	20	100	13
No. 100 / 150um	1	1	12	3	2	13	100	8
No. 200 / 75um	0.9	0.4	8.2	1.2	0.8	8.7	90.0	5.3

** Aggregate breakdown will be controlled by the Hot Plant dust control system.*

Table 36 Mixture D3L3 Mix Design Summary Sheet

Design Specifications: Blend 1 / 75 Gyrations @ N Design PG 64-28 (58-34 Adjusted Binder)

Gyratory Compactor: Model # AFG2AS, Serial # 8436

	Job Mix Formula	Spec
Percent Asphalt by Weight of Total Mix	5.3	--
Percent Asphalt by Weight of Aggregate	5.6	--
Virgin Asphalt by Weight of Mix	3.8	--
Percent Air Voids (Va)	4.0	4.0
Voids in Mineral Aggregate (VMA)	14.6	14 min
Compacted Unit Weight Gmb, pcf	2.330 145.0	--
Theoretical Maximum Density Gmm, pcf	2.427 151.1	--
Percent Absorbed Asphalt, Pba	0.7	--
Specific Gravity of Binder (Gb)	1.028	--
Percent Gmm @ N Initial (7 Gyrations)	87.1	≤ 89.0
Percent Gmm @ N Design (75 Gyrations)	96.0	96.0
Percent Gmm @ N Max (115 Gyrations)	97.2	≤ 98.0
Dust to Asphalt Ratio (D/A)	1.2	0.8-1.6
Percent Passing #200 Sieve	5.4	2.0-10.0
Voids Filled w/ Asphalt (VFA)	73	65-75
Laboratory Mixing Temperature for Design (°F)	307	302-311
Laboratory Compaction Temperature for Design (°F)	284	280-288
Laboratory Sample Weight for Volumetric Testing (g)	4675	--
(L5-134) Ignition Oven (NCAT) Correction Factor @ 538 °F	0.33	--
*Los Angeles Abrasion (LAR) (%)	27	30 max
*Idaho Degradation Δ % -200	4.2	5.0 max
Sand Equivalent	68	40 min
*Fracture Face Count (%)	100/99	75/60
Fine Aggregate Angularity (%)	46.5	40 min
*Flat and Elongated Particles in Coarse Aggregates (%)	0.0	10 max
Recycled Asphalt Pavement (RAP) Properties		
Percentage of Asphalt in RAP (Wt. of Mix)	4.03	--
Percentage of RAP by Total Weight of Aggregate	38	--
Percent of RAP Binder by Weight of Total Binder	29	30 max
RAP Contribution by Mix	1.53	--
RAP NCAT Correction Factor	0.36	--

*Composite blend including RAP

Table 37 Mixture D3L4 Mix Design Summary Sheet

Percent Asphalt by Weight of Total Mix	5.3	--
Percent Asphalt by Weight of Aggregate	5.6	--
Agg = 3.95 Virgin Asphalt by Weight of Mix	3.8	--
Percent Air Voids (Va)	4.0	4.0
Voids in Mineral Aggregate (VMA)	14.6	14 min
Compacted Unit Weight Gmb, pcf	2.305 143.5	--
Theoretical Maximum Density Gmm, pcf	2.401 149.5	--
Percent Absorbed Asphalt, Pba	0.6	--
Specific Gravity of Binder (Gb)	1.030	--
Percent Gmm @ N Initial (7 Gyrations)	88.1	≤ 89.0
Percent Gmm @ N Design (75 Gyrations)	96.0	96.0
Percent Gmm @ N Max (115 Gyrations)	97.6	≤ 98.0
Dust to Asphalt Ratio (D/A)	1.2	0.6-1.2
Percent Passing #200 Sieve	5.4	2.0-10.0
Voids Filled w/ Asphalt (VFA)	72	65-75
Laboratory Mixing Temperature for Design (°F)	**285	**281-289
Laboratory Compaction Temperature for Design (°F)	**264	**260-268
Laboratory Sample Weight for Volumetric Testing (g)	4660	--
Ignition Oven (NCAT L5-134) Correction Factor @ 538 °F	0.33	--
*Los Angeles Abrasion (LAR) (%)	27	30 max
*Idaho Degradation Δ % -200	3.7	5.0 max
Sand Equivalent	68	40 min
*Fracture Face Count (%)	99/97	75/60
Fine Aggregate Angularity (%)	46.9	40 min
*Flat and Elongated Particles in Coarse Aggregates (%)	0.0	10 max
Recycled Asphalt Pavement (RAP) Properties		
Percentage of Asphalt in RAP (Wt. of Mix)	5.4	--
Percentage of RAP by Total Weight of Aggregate	28	--
Percent of RAP Binder by Weight of Total Binder	29	30 max
RAP Contribution by Mix	1.51	--
RAP NCAT Correction Factor	0.36	--

*Composite blend including RAP

**Temperatures decreased by 35° F due to the introduction of EVOTHERM M1 warm mix additive.

Table 38 Mixture D3L5 Mix Design Summary Sheet

Percent Asphalt by Weight of Total Mix	5.3	--
Percent Asphalt by Weight of Aggregate	5.6	--
Agg = 3.95 Virgin Asphalt by Weight of Mix	3.8	--
Percent Air Voids (Va)	4.0	4.0
Voids in Mineral Aggregate (VMA)	14.6	14 min
Compacted Unit Weight Gmb, pcf	2.305 143.5	--
Theoretical Maximum Density Gmm, pcf	2.401 149.5	--
Percent Absorbed Asphalt, Pba	0.6	--
Specific Gravity of Binder (Gb)	1.030	--
Percent Gmm @ N Initial (7 Gyrations)	88.1	≤ 89.0
Percent Gmm @ N Design (75 Gyrations)	96.0	96.0
Percent Gmm @ N Max (115 Gyrations)	97.6	≤ 98.0
Dust to Asphalt Ratio (D/A)	1.2	0.6-1.2
Percent Passing #200 Sieve	5.4	2.0-10.0
Voids Filled w/ Asphalt (VFA)	72	65-75
Laboratory Mixing Temperature for Design (°F)	**285	**281-289
Laboratory Compaction Temperature for Design (°F)	**264	**260-268
Laboratory Sample Weight for Volumetric Testing (g)	4660	--
Ignition Oven (NCAT L5-134) Correction Factor @ 538 °F	0.33	--
*Los Angeles Abrasion (LAR) (%)	27	30 max
*Idaho Degradation Δ % -200	3.7	5.0 max
Sand Equivalent	68	40 min
*Fracture Face Count (%)	99/97	75/60
Fine Aggregate Angularity (%)	46.9	40 min
*Flat and Elongated Particles in Coarse Aggregates (%)	0.0	10 max
Recycled Asphalt Pavement (RAP) Properties		
Percentage of Asphalt in RAP (Wt. of Mix)	5.4	--
Percentage of RAP by Total Weight of Aggregate	28	--
Percent of RAP Binder by Weight of Total Binder	29	30 max
RAP Contribution by Mix	1.51	--
RAP NCAT Correction Factor	0.36	--
*Composite blend including RAP **Temperatures decreased by 35° F due to the introduction of EVOTHERM M1 warm mix additive.		

Table 39 Mixture D5L1 Mix Design Summary Sheet

PROPOSED JOB MIX FORMULA

Laboratory Gyratory Values	Min	Target	Max	Spec.
Total Asphalt by Weight of Mix % (Pb)		4.80		
Virgin Asphalt by Weight of Mix Hot Plant		3.38		
Rap Binder Replacement 29.5%		1.42		
Air Voids % (Va)		4.0		4.0
Voids in Mineral Aggregate (VMA)		14.5		13.0
Voids Filled with Asphalt (VFA)		72.5%		65-75
Dust Ratio(PCS 45% passing #4 / 0.8%-1.6%,MS2)		1.15		0.8-1.6
Bulk Specific Gravity (Gmb)		2.386		
Unit Weight lb./cuft.		148.5		
Theo Max Spec Gravity (Gmm)		2.485		
Theo Max Spec Gravity lb./cuft.		154.7		
% Gmm @ Nini(8 gyrations)		88.0%		89% max
% Gmm @ Ndes(100 gyrations)		96.0%		96%max
% Gmm @ Nmax(160 gyrations)		97.2%		98% Max
Effective Specific Gravity of Blend (Gse)		2.677		
Specific Gravity of Aggregate (Gsb provided by ITD)		2.656		
Immersion Compression Dose 0.50% by weight		89%		85 Min
Fine Aggregate Angularity		47%		45.0%
NCAT Asphalt Correction Factor(538 deg C)		-0.20		
Sand Equivalency (SE)		75%		45% min
Flat and Elongation		4%		10% max
Percent Fracture 1 Face		97%		95.0%
Percent Fracture 2 Face		95%		90.0%
Laboratory Mixing Temperature(deg in F)		280 deg		
Laboratory Compaction Temperature(deg in F)		260 deg		
Plant Mixing Temperature(deg in F)	277 deg		285 deg	
Field Compaction Temperature(deg in F)	257 deg		265 deg	
Super pave Design Sample Wt. in grams		4750 g		

AGGREGATE GRADATION DATA

Sieve Size	A Rock 20%	B Rock 27%	Clean C 28.5%		Cat 1 Rap 24%	Bag House Use 0.5%	Break Down 0.0%	JMF Blended Gradation	ITD Specification
1" / 25mm	100	100	100		100	100	100	100	100 - 100
3/4" / 19mm	100	100	100		100	100	100	100	95 - 100
1/2" / 12.5mm	28	98	100		97	100	100	84	79 - 90
3/8" / 9.5mm	5	55	100		93	100	100	67	62 - 72
No. 4 / 4.75mm	2	3	76		73	100	100	41	36 - 46
No. 8 / 2.36mm	2	2	50		55	100	100	29	25 - 33
No.16 / 1.18mm	1	2	35		38	100	100	21	17 - 25
No. 30 / 600um	1	2	26		29	100	100	16	12 - 20
No. 50 / 300um	1	2	18		22	-99	100	11	8 - 14
No. 100 / 150um	1	2	12		17	-95	100	8	5 - 11
No. 200 / 75um	1.1	1.3	8.1		11.0	-90	100	5.0	3.5 - 6.5

Table 40 Mixture D6L1 Mix Design Summary Sheet

	AASHTO	JMF	Requirements
1 Asphalt by Weight of Total Mix, %	R 35	**5.4%**	
2 Asphalt by Weight of Aggregates, %		5.7%	
3 Air Voids (Va), %	T 269	4.0%	3.0-5.0
4 Voids in Mineral Aggregate (VMA), %	R 35	15.1%	14 min
5 Bulk Specific Gravity @ Ndes (Gmb) (100 Gyrations)	T 166	2.347	146.1 pcf
6 Theoretical Maximum Specific Gravity (Gmm)	T 209	**2.444**	152.1 pcf
7 Relative Density %Gmm @ Nini (8 Gyrations)	R 35	87.0	≤ 89.0
8 Relative Density %Gmm @ Nmax (160 Gyrations)	R 35	97.1	≤ 98.0
9 Voids Filled w/ Asphalt (VFA), %	R 35	73.3%	65-75
10 Film thickness, microns		7	
11 Absorbed Asphalt (Pba) by Weight of Aggregate, %	R 35	0.50%	
12 Effective Asphalt Content (Pbe) by Total Wt of Mixture, %	R 35	4.9%	
13 Specific Gravity of Asphalt		**1.032**	
14 Laboratory Mixing Temp, °C/°F		327	
15 Laboratory Compaction Temp, °C/°F		295	
16 Recommended Plant Mixing Temp, °F		313-327	
17 Compaction Temp Range, °F		286-300	
18 NCAT Ignition Oven Correlation Factor @ 538° C	T 308	**0.06**	
19 Dust to Asphalt Ratio	R 35	0.9	0.8-1.6
20 Immersion Compression Retained Strength, %	T 165	91%	85% min
21 Gyratory Gmb specimen weight, grams		4670	
22 Combined Bulk Dry Specific Gravity of Aggregate (Gsb)	T 85 / IT 144	**2.614**	

AGGREGATE STOCKPILE GRADATION

		SM A	B-Pile	C-Pile			Blended	Mix Design Tolerances	
		12%	36%	52%			Gradation		
25.0 mm (1")		100%	100%	100%			**100%**	100	100
19.0 mm (3/4")		100%	100%	100%			**100%**	100	100
12.5 mm (1/2")		42%	100%	100%			**93%**	90	99
9.5 mm (3/8")		6%	72%	100%			**79%**	73	85
4.75 mm (No.4)		2%	4%	86%			**46%**	40	52
2.36 mm (No.8)		2%	2%	56%			**30%**	28	35
1.18 mm (No.16)		2%	2%	40%			**22%**	17	27
600 um (No.30)		2%	2%	31%			**17%**	12	22
300 um (No.50)		1%	2%	23%			**13%**	9	17
150 um (No.100)		1%	1%	15%			**8%**	4	12
75 um (No.200)		0.9%	1.0%	9.4%			**4.2%**	2.2	6.4

Appendix B
Field Projects Mix Design Summary Sheet

Table 41 Mix Design Summary Sheet for Project D2C4

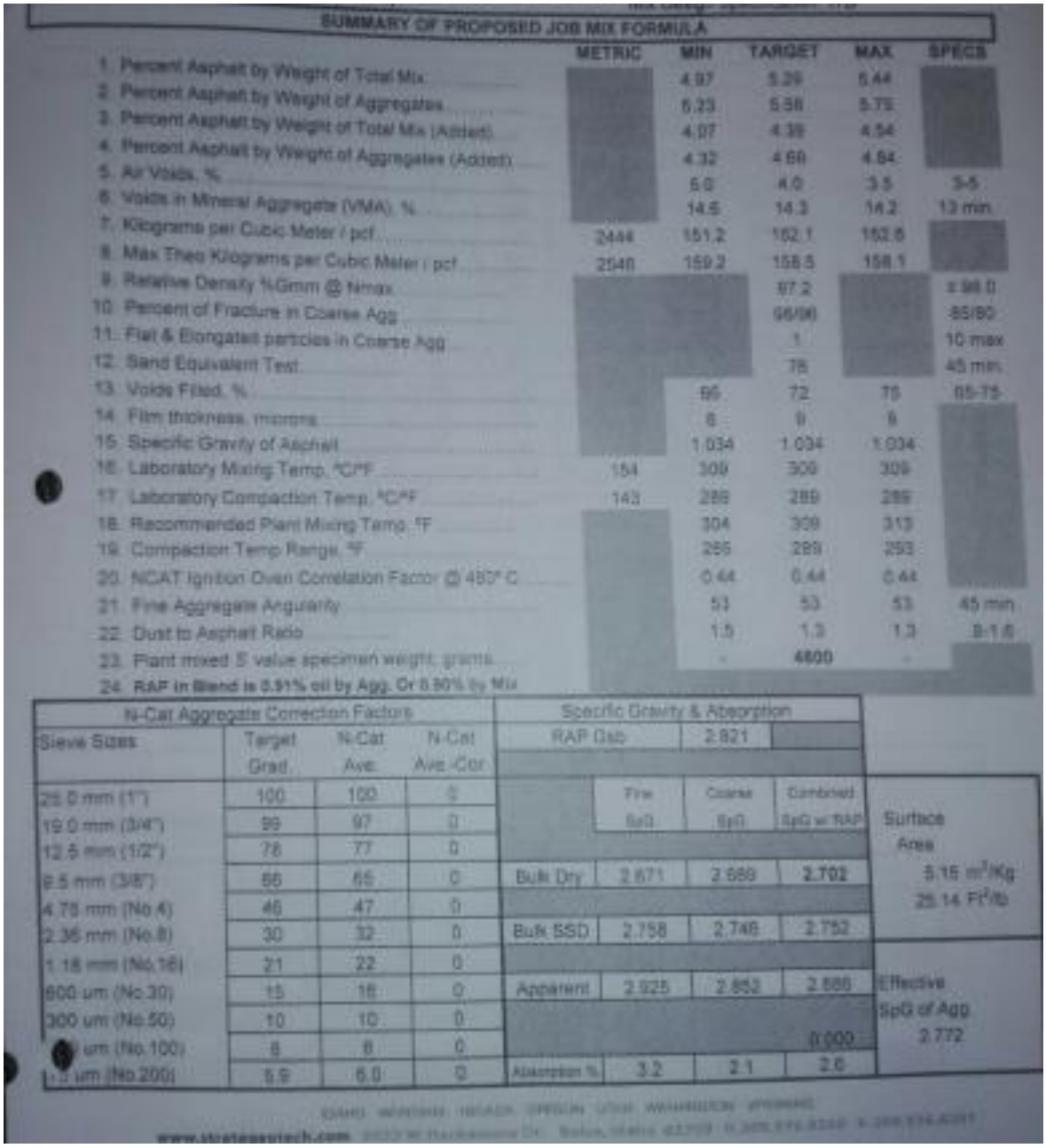

SUMMARY OF PROPOSED JOB MIX FORMULA

	METRIC	MIN	TARGET	MAX	SPECS
1. Percent Asphalt by Weight of Total Mix		4.97	5.29	5.44	
2. Percent Asphalt by Weight of Aggregates		5.23	5.58	5.75	
3. Percent Asphalt by Weight of Total Mix (Added)		4.07	4.39	4.54	
4. Percent Asphalt by Weight of Aggregates (Added)		4.32	4.68	4.84	
5. Air Voids, %		5.0	4.0	3.5	3-5
6. Voids in Mineral Aggregate (VMA), %		14.5	14.3	14.2	13 min
7. Kilograms per Cubic Meter / pcf	2444	151.2	152.1	152.6	
8. Max Theo Kilograms per Cubic Meter / pcf	2548	159.2	158.5	158.1	
9. Relative Density %Gmm @ Nmax			97.2		≤ 98.0
10. Percent of Fracture in Coarse Agg			96/90		85/80
11. Flat & Elongated particles in Coarse Agg			1		10 max
12. Sand Equivalent Test			78		45 min.
13. Voids Filled, %		66	72	75	65-75
14. Film thickness, microns		8	9	9	
15. Specific Gravity of Asphalt		1.034	1.034	1.034	
16. Laboratory Mixing Temp. °C/°F	154	309	309	309	
17. Laboratory Compaction Temp. °C/°F	143	289	289	289	
18. Recommended Plant Mixing Temp. °F		304	309	313	
19. Compaction Temp Range, °F		285	289	293	
20. NCAT Ignition Oven Correlation Factor @ 480° C		0.44	0.44	0.44	
21. Fine Aggregate Angularity		53	53	53	45 min
22. Dust to Asphalt Ratio		1.5	1.3	1.3	0.6-1.6
23. Plant mixed S value specimen weight, grams		-	4600	-	
24. RAP in Blend is 0.91% oil by Agg. Or 0.90% by Mix					

N-Cal Aggregate Correction Factors

Sieve Sizes	Target Grad.	N-Cal Ave.	N-Cal Ave.-Cor.
25.0 mm (1")	100	100	0
19.0 mm (3/4")	99	97	0
12.5 mm (1/2")	78	77	0
9.5 mm (3/8")	66	66	0
4.75 mm (No.4)	46	47	0
2.36 mm (No.8)	30	32	0
1.18 mm (No.16)	21	22	0
600 um (No.30)	15	16	0
300 um (No.50)	10	10	0
um (No.100)	6	6	0
um (No.200)	5.9	6.0	0

Specific Gravity & Absorption

RAP Gsb 2.821

	Fine SpG	Coarse SpG	Combined SpG w/ RAP
Bulk Dry	2.671	2.689	2.703
Bulk SSD	2.758	2.746	2.752
Apparent	2.925	2.852	2.886
			0.000
Absorption %	3.2	2.1	2.6

Surface Area 5.15 m²/kg 25.14 Ft²/lb

Effective SpG of Agg 2.772

Table 42 Mix Design Summary Sheet for Project D2C5

SUMMARY OF PROPOSED JOB MIX FORMULA		
	STANDARD	SPECS
1. Percent Asphalt by Weight of Total Mix	5.0	4.7-5.3
2. Percent Asphalt by Weight of Aggregates	5.3	
3. Air Voids (VA), %	4.0	4.0
4. Voids in Mineral Aggregate (VMA), %	14.2	13 min.
5. Compacted Unit Weight (Gmb), pcf	154.5	
6. Maximum Theoretical (Rice) (Gmm), pcf	161.0	
7. % Gmm @ Ninitial	86.1	89 max.
8. % Gmm @ Nmax	97.1	98 max.
9. Dust/Asphalt Ratio	1.2	0.6-1.2
10. Percent Passing #200 Screen	5.0	
11. Voids Filled (VFA), %	71.8	65-75
12. NCAT Ignition Oven Correlation Factor	0.15	
13. Specific Gravity of Asphalt (Gb)	1.034	
14. Laboratory Mixing Temp, °F	325	
15. Laboratory Compaction Temp, °F	280	
16. Recommended Plant Mixing Temp, °F	313-334	
17. Compaction Temp Range, °F	280-298	
18. Index of Retained Strength	90	85 min.
19. Laboratory Sample Compaction Weight, gm	4600	

Sieve Sizes	*Target Value	Correction Factor	Spec
25.4 mm (1")	100		100
19.0 mm (3/4")	98		93-100
12.5 mm (1/2")	82		77-87
9.5 mm (3/8")	69		64-74
4.75 mm (No.4)	53		48-58
2.36 mm (No.8)	33		29-37
1.18 mm (No.16)	19		15-23
600 um (No.30)	13		9-17
300 um (No.50)	9		6-12
150 um (No.100)	7		4-10
75 um (No.200)	5.0	-0.7	3.5-6.5

Specific Gravity & Absorption				
		Combined Sp Gr		
Bulk SpG		2.747		
Apparent SpG		2.888		
Absorption %		1.8		
* 53% C-Pile				
27% B-Pile		1% Breakdown		
19% A-Pile				

Effective Specific Gravity of Agg. (Gse) 2.810

Table 43 Mix Design Summary Sheet for Project D2C8

SUMMARY OF PROPOSED JOB MIX FORMULA		
	STANDARD	SPECS
1. Percent Asphalt by Weight of Total Mix	5.0	4.7-5.3
2. Percent Asphalt by Weight of Aggregates	5.3	
3. Air Voids (VA), %	4.0	4.0
4. Voids in Mineral Aggregate (VMA), %	14.2	13 min.
5. Compacted Unit Weight (Gmb), pcf	154.5	
6. Maximum Theoretical (Rice) (Gmm), pcf	161.0	
7. % Gmm @ Ninitial	88.1	89 max.
8. % Gmm @ Nmax	97.1	98 max.
9. Dust/Asphalt Ratio	1.2	0.6-1.2
10. Percent Passing #200 Screen	5.0	
11. Voids Filled (VFA), %	71.8	65-75
12. NCAT Ignition Oven Correlation Factor	0.15	
13. Specific Gravity of Asphalt (Gb)	1.034	
14. Laboratory Mixing Temp, °F	325	
15. Laboratory Compaction Temp, °F	280	
16. Recommended Plant Mixing Temp, °F	315-334	
17. Compaction Temp Range, °F	280-298	
18. Index of Retained Strength	90	85 min.
19. Laboratory Sample Compaction Weight, gm	4800	

Sieve Sizes	*Target Value	Correction Factor	Spec
25.4 mm (1")	100		100
19.0 mm (3/4")	98		93-100
12.5 mm (1/2")	82		77-87
9.5 mm (3/8")	69		64-74
4.75 mm (No.4)	53		48-58
2.36 mm (No.8)	33		29-37
1.18 mm (No.16)	19		15-23
600 um (No.30)	13		9-17
300 um (No.50)	9		8-12
150 um (No.100)	7		4-10
75 um (No.200)	5.0	-0.7	3.5-6.5

Specific Gravity & Absorption				
		Combined Sp Gr		
Bulk SpG		2.747		
Apparent SpG		2.888		
Absorption %		1.8		
* 53% C-Pile				
27% B-Pile		1% Breakdown		
19% A-Pile				

Effective Specific Gravity of Agg. (Gse) 2.810

Table 44 Mix Design Summary Sheet for Project D2C12

ASPHALT CONCRETE MIX DESIGN

Project:	Lawyer's Creek to Lauer Rd. ST-4110 (884)	Date:	7/5/2007
Paving Contractor:	Valley Paving	Class of Mixture:	SP 5 (3 to <30)
Asphalt Supplier:	Idaho Asphalt	Grade of Asphalt:	PG 64-28ER
Stripping Agents:	Unichem 8185w	Testing Performed By:	Justin Drye
Aggregate Sources:	Brandt Quarry	Mix Design Specification:	ITD

SUMMARY OF PROPOSED JOB MIX FORMULA

	METRIC	MIN	DESIGN TARGET	MAX	SPECS
1. Percent Asphalt by Weight of Total Mix		5.32	5.53	5.75	
2. Percent Asphalt by Weight of Aggregates		5.62	5.85	6.10	
3. Air Voids, %		4.7	4.0	3.3	3-5
4. Voids in Mineral Aggregate (VMA), %		13.6	13.4	13.3	13 min.
5. Kilograms per Cubic Meter / pcf	2402	148.8	149.5	150.1	
6. Max Theo Kilograms per Cubic Meter / pcf	2502	156.2	155.7	155.2	
7. % GMM @ Nmax			97.2		<98
8. Percent of Fracture in Coarse Agg.		100/100	100/100	100/100	85/80
9. Flat & Elongated particles in Coarse Agg.		2	2	2	10max
10. Sand Equivalent Test		59	59	59	45min
11. Voids Filled, %		65	70	75	65-75
12. Film thickness, microns		7	8	8	6 min.
13. Specific Gravity of Asphalt		1.032	1.032	1.032	
14. Laboratory Mixing Temp, °C/°F	160	320	320	320	
15. Laboratory Compaction Temp, °C/°F	143	290	290	290	
16. Recommended Plant Mixing Temp, °F		309-327	309-327	309-327	
17. Compaction Temp Range, °F		277-297	277-297	277-297	
18. Dust to Asphalt Ratio		1.6	1.6	1.5	.8-1.6
19. Fine Aggregate Angularity		51	51	51	45 min.
20. Recommended plant mixed AC specimen weight		-	**4850**	-	

N-Cat Aggregate Correction Factors				Specific Gravity & Absorption				
Sieve Sizes	Blank Grad.	N-Cat Ave.	N-Cat Ave.-Cor.		Fine SpG	Coarse SpG	Combined SpG	
25.0 mm (1")	100	100	0					
19.0 mm (3/4")	100	100	0	Bulk SpG	2.622	2.620	2.621	Surface Area: 5.31 m^2/Kg 25.90 Ft^2/lb
12.5 mm (1/2")	86	86	0					
9.5 mm (3/8")	68	69	0					
4.75 mm (No.4)	41	43	0	Bulk SSD SpG	2.696	2.689	2.693	
2.36 mm (No.8)	27	28	0					
1.18 mm (No.16)	19	19	0					
600 um (No.30)	13	14	0	Apparent SpG	2.837	2.814	2.823	Effective SpG of Agg. 2.730
300 um (No.50)	11	11	0					
150 um (No.100)	8	9	0					
75 um (No.200)	6.6	7.3	-0.7	Absorption %	2.9	2.6	2.7	

Table 45 Mix Design Summary Sheet for Project D2C13

SUMMARY OF PROPOSED JOB MIX FORMULA

	MIN	TARGET	MAX	SPECS
1. Percent Asphalt by Weight of Total Mix	6.10	6.35	6.80	
2. Percent Asphalt by Weight of Aggregates	6.50	6.78	7.30	
3. Percent Asphalt by Weight of Total Mix (Added)	4.98	5.23	5.68	
4. Percent Asphalt by Weight of Aggregates (Added)	5.39	5.67	6.20	
5. Air Voids, %	5.0	4.0	3.0	3-5
6. Voids in Mineral Aggregate (VMA), %	16.5	16.2	16.2	14 min.
7. Lab Compacted Unit Weight pcf	149.7	150.6	151.3	
8. Maximum Theoretical (Rice) pcf	157.6	157.0	155.9	
9. Relative Density %Gmm @ Nmax		96.6		≤ 98.0
10. Percent of Fracture in Coarse Agg		100/100		75/60
11. Flat & Elongated particles in Coarse Agg		1		10 max
12. Sand Equivalent Test		74		40 min.
13. Voids Filled, %	70	75	82	65-75
14. Film thickness, microns	9	10	11	6 min
15. Specific Gravity of Asphalt	1.034	1.034	1.034	
16. Laboratory Mixing Temp, °F	300	300	300	
17. Laboratory Compaction Temp, °F	290	290	290	
18. Recommended Plant Mixing Temp, °F	295	300	305	
19. Compaction Temp Range, °F	275	290	283	
20. NCAT Ignition Oven Correlation Factor @ 480° C	0.82	0.82	0.82	
21. Fine Aggregate Angularity	48	48	48	40 min.
22. Dust to Asphalt Ratio	1.2	1.1	1.0	0.8-1.6
23. Plant mixed *S* value specimen weight, grams	-	**4600**	-	
24. RAP Correction Factor		0.59		
25. **RAP in Blend is 1.12% oil by Agg. Or 1.11% by Mix**				

N-Cat Aggregate Correction Factors			
Sieve Sizes	Target Grad.	N-Cat Ave.	N-Cat Ave.-Cor.
25.0 mm (1")	100	100	0
19.0 mm (3/4")	100	100	0
12.5 mm (1/2")	96	96	0
9.5 mm (3/8")	80	82	0
4.75 mm (No.4)	52	56	0
2.36 mm (No.8)	37	40	0
1.18 mm (No.16)	24	27	0
600 um (No.30)	17	20	0
300 um (No.50)	11	13	0
150 um (No.100)	8	8	0
75 um (No.200)	5.9	5.7	0

Specific Gravity & Absorption			
RAP	Fine	Coarse	Combined
Bulk Specific Gravity			
2.819	2.631	2.698	2.704
Bulk SSD Specific Gravity			
	2.721	2.752	
Apparent Specific Gravity			
	2.894	2.853	
Percent Absorption			
	3.5	2.0	0.9

Surface Area
5.40 m^2/Kg
26.36 Ft^2/lb

Effective SpG of Agg.
2.795

Table 46 Mix Design Summary Sheet for Project D3C2

Laboratory Values	Target			Spec.
Total Asphalt by Weight of Mix % (Pb)	5.2			
Total Aspalt by Weight of Aggregate	5.49			
Air Voids % (Va)	4.0			4.0
Voids in Mineral Aggregate (VMA)	14.8			14.0 min
Voids Filled with Asphalt (VFA)	73.0			65-75
Bulk Specific Gravity (Gmb)	2.314			
Unit Weight lb./cuft.	144.0			
Theo Max Spec Gravity (Gmm)	2.411			
Theo Max Spec Gravity lb./cuft.	150.1			
Effective Specific Gravity of Blend (Gse)	2.601			
Effect of Water on Compressive Strength *(AllWest)*	103			85 min
Ninitial (7 Gyrations)	88.6			≤ 89.0
Ndesign SP-3 (75 Gyrations)	96.0			= 96.0
Nmax (115 Gyrations)	97.2			≤ 98.0
NCAT Asphalt Correction Factor	0.29			
Dust to Asphalt	1.2			0.6-1.2
Laboratory Mixing Temperature(deg in F)	330			
Laboratory Compaction Temperature(deg in F)	302			
Plant Mixing Temperature(deg in F)**	286	-	335	
Field Compaction Temperature(deg in F)**	262	-	311	
Superpave Design Sample Wt. in grams	4645			

**Field mixing and compaction may be adjusted +/- 25 degrees per Viscosity Graph*

Aggregate Gradation Data

Sieve Size	1/2" Chips 10.0%	#4 Chips 9.0%	C-Pile 7.0%	Washed C-Pile 10.0%	Sand 9.5%	RAP 54.0%	Break Down 0.5%	JMF Blended Gradation
1" / 25mm	100	100	100	100	100	100	100	100
3/4" / 19mm	100	100	100	100	100	100	100	100
1/2" / 12.5mm	74	100	100	100	100	93	100	94
3/8" / 9.5mm	24	79	100	100	100	85	100	82
No. 4 / 4.75mm	2	3	76	86	97	66	100	60
No. 8 / 2.36mm	1	1	51	55	85	52	100	46
No.16 / 1.18mm	1	1	35	34	73	41	100	36
No. 30 / 600um	1	1	26	20	45	31	100	26
No. 50 / 300um	1	1	17	10	14	20	100	15
No. 100 / 150um	1	1	12	3	2	13	100	9
No. 200 / 75um	0.9	0.4	8.2	1.2	0.8	8.5	90.0	5.9

** Aggregate breakdown will be controlled by the Hot Plant dust control system.*

Table 47 Mix Design Summary Sheet for Project D3C3

SUMMARY OF PROPOSED JOB MIX FORMULA

	METRIC	MIN	TARGET	MAX	SPECS
1. Percent Asphalt by Weight of Total Mix		5.13	5.49	5.63	
2. Percent Asphalt by Weight of Aggregates		5.41	5.81	5.97	
3. Percent Asphalt by Weight of Total Mix (Added)		4.50	4.86	5.00	
4. Percent Asphalt by Weight of Aggregates (Added)		4.75	5.15	5.31	
5. Air Voids, %		5.0	4.0	3.6	3-5
6. Voids in Mineral Aggregate (VMA), %		14.7	14.5	14.4	14 min.
7. Kilograms per Cubic Meter / pcf	2298	142.2	143.0	143.4	
8. Max Theo Kilograms per Cubic Meter / pcf	2394	149.7	149.0	148.8	
9. Relative Density %Gmm @ Nmax			97.4		≤ 98.0
10. Percent of Fracture in Coarse Agg			99/96		85/80
11. Flat & Elongated particles in Coarse Agg.			1		10 max
12. Sand Equivalent Test			70		45 min
13. Voids Filled, %		68	72	75	65-75
14. Film thickness, microns		8	9	9	
15. Specific Gravity of Asphalt		1.032	1.032	1.032	
16. Laboratory Mixing Temp, °C/°F	160	320	320	320	
17. Laboratory Compaction Temp, °C/°F	144	292	292	292	
18. Recommended Plant Mixing Temp, °F		313-329	313-329	313-329	
19. Compaction Temp Range, °F		280-298	280-298	280-298	
20. NCAT Ignition Oven Correlation Factor @ 538° C		0.33	0.33	0.33	
21. Fine Aggregate Angularity		46	46	46	45 min.
22. Dust to Asphalt Ratio		1.0	0.9	0.9	.6-1.2
23. Plant mixed *S* value specimen weight, grams		-	4625	-	
24. **RAP in Blend is .66% oil by Agg. Or .63% by Mix**					

N-Cat Aggregate Correction Factors				Specific Gravity & Absorption				
Sieve Sizes	Target Grad.	N-Cat Ave.	N-Cat Ave.-Cor.		Fine SpG	Coarse SpG	Combined SpG	
25.0 mm (1")	100	100	0					
19.0 mm (3/4")	100	100	0	Bulk SpG	2.541	2.538	2.540	Surface Area
12.5 mm (1/2")	96	97	0					5.42 m^2/Kg
9.5 mm (3/8")	85	86	0					26.44 Ft^2/lb
4.75 mm (No.4)	61	63	0	Bulk SSD SpG	2.577	2.576	2.577	
2.36 mm (No.8)	46	48	0					
1.18 mm (No.16)	34	36	0					
600 um (No.30)	23	24	0	Apparent SpG	2.635	2.639	2.637	Effective SpG of Agg.
300 um (No.50)	14	15	0					2.593
150 um (No.100)	7	8	0					
75 um (No.200)	4.4	4.7	0	Absorption %	1.4	1.5	1.4	

Table 48 Mix Design Summary Sheet for Project D3C4

SUMMARY OF PROPOSED JOB MIX FORMULA

	METRIC	MIN	TARGET	MAX	SPECS
1. Percent Asphalt by Weight of Total Mix		5.18	5.56	5.70	
2. Percent Asphalt by Weight of Aggregates		5.46	5.89	6.04	
3. Percent Asphalt by Weight of Total Mix (Added)		4.68	5.06	5.20	
4. Percent Asphalt by Weight of Aggregates (Added)		4.95	5.38	5.53	
5. Air Voids, %		5.0	4.0	3.7	3-5
6. Voids in Mineral Aggregate (VMA), %		14.9	14.9	14.9	14 min.
7. Kilograms per Cubic Meter / pcf	2336	144.7	145.4	145.6	
8. Max Theo Kilograms per Cubic Meter / pcf	2434	152.4	151.5	151.2	
9. Relative Density %Gmm @ Nmax			97.2		≤ 98.0
10. Percent of Fracture in Coarse Agg			96/87		85/80
11. Flat & Elongated particles in Coarse Agg			1		10 max
12. Sand Equivalent Test			62		45 min
13. Voids Filled, %		66	73	75	65-75
14. Film thickness, microns		9	10	10	
15. Specific Gravity of Asphalt		1.032	1.032	1.032	
16. Laboratory Mixing Temp, °C/°F	163	325	325	325	
17. Laboratory Compaction Temp, °C/°F	143	290	290	290	
18. Recommended Plant Mixing Temp, °F		313-329	313-329	313-329	
19. Compaction Temp Range, °F		280-298	280-298	280-298	
20. NCAT Ignition Oven Correlation Factor @ 538° C		0.23	0.23	0.23	
21. Fine Aggregate Angularity		46	46	46	45 min.
22. Dust to Asphalt Ratio		1.1	1.0	1.0	.8-1.6
23. Plant mixed *S* value specimen weight, grams		-	**4685**	-	
24. **RAP in Blend is .51% oil by Agg. Or .50% by Mix**					

N-Cat Aggregate Correction Factors				Specific Gravity & Absorption				
Sieve Sizes	Target Grad.	N-Cat Ave.	N-Cat Ave.-Cor.		Fine SpG	Coarse SpG	Combined SpG	
25.0 mm (1")	100	100	0					
19.0 mm (3/4")	100	100	0	Bulk SpG	2.571	2.610	2.591	Surface Area
12.5 mm (1/2")	98	98	0					
9.5 mm (3/8")	85	86	0					5.05 m^2/Kg
4.75 mm (No.4)	54	56	0	Bulk SSD	2.606	2.641	2.624	24.66 Ft^2/lb
2.36 mm (No.8)	37	39	0	SpG				
1.18 mm (No.16)	26	27	0					
600 um (No.30)	18	19	0	Apparent	2.664	2.694	2.679	Effective
300 um (No.50)	11	13	0	SpG				SpG of Agg.
150 um (No.100)	7	9	0					2.646
75 um (No.200)	5.0	5.3	0	Absorption %	1.4	1.2	1.3	

Table 49 Mix Design Summary Sheet for Project D3C5

ASPHALT CONCRETE MIX DESIGN

		Date:	3/28/2013
Project:	SH-44, Linder Rd to Ballantyne Lane	Class of Mixture:	3/4" SP4 (3 < 10)
Paving Contractor:	Central Paving	Blended Grade of Asphalt:	PG 64-28
Asphalt Supplier:	Western States Asphalt	Virgin Grade of Asphalt:	PG 58-34
Stripping Agents:	MORLIFE 5000	Testing Performed By:	D. Kilmer
Aggregate Sources:	Ad-136c	Mix Design Specification:	ITD

SUMMARY OF PROPOSED JOB MIX FORMULA

	METRIC	MIN	TARGET	MAX	SPECS
1. Percent Asphalt by Weight of Total Mix		4.40	4.72	5.12	
2. Percent Asphalt by Weight of Aggregates		4.60	4.95	5.40	
3. Percent Asphalt by Weight of Total Mix (Added)		3.06	3.38	3.78	
4. Percent Asphalt by Weight of Aggregates (Added)		3.19	3.54	3.99	
5. Air Voids, %		5.0	4.0	3.0	3-5
6. Voids in Mineral Aggregate (VMA), %		13.9	13.8	13.6	13 min
7. Kilograms per Cubic Meter / pcf	2346	145.3	146.0	146.8	
8. Max Theo Kilograms per Cubic Meter / pcf	2445	152.9	152.2	151.3	
9. Relative Density %Gmm @ Nmax			97.2		≤ 98.0
10. Percent of Fracture in Coarse Agg			99/96		85/80
11. Flat & Elongated particles in Coarse Agg			0		10 max
12. Sand Equivalent Test			66		45 min
13. Voids Filled, %		64	71	78	60-80
14. Film thickness, microns		8	9	10	
15. Specific Gravity of Asphalt		1.027	1.027	1.027	
16. Laboratory Mixing Temp, °C/°F	161	322	322	322	
17. Laboratory Compaction Temp, °C/°F	148	299	299	299	
18. Recommended Plant Mixing Temp, °F		317-326	317-326	317-326	
19. Compaction Temp Range, °F		295-303	295-303	295-303	
20. NCAT Ignition Oven Correlation Factor @ 538° C		0.22	0.22	0.22	
21. Fine Aggregate Angularity		47	47	47	45 min
22. Dust to Asphalt Ratio		1.2	1.2	1.1	0.7-1.7
23. Plant mixed *S* value specimen weight, grams		-	**4725**	-	
24. **RAP in Blend is 1.41% oil by Agg. Or 1.34% by Mix**					

N-Cat Aggregate Correction Factors				Specific Gravity & Absorption				
Sieve Sizes	Target Grad.	N-Cat Ave.	N-Cat Ave.-Cor.	RAP Gsb		2.590		
25.0 mm (1")	100	100	0		Fine SpG	Coarse SpG	Combined SpG w/ RAP	
19.0 mm (3/4")	100	100	0					Surface Area
12.5 mm (1/2")	84	84	0					
9.5 mm (3/8")	70	71	0	Bulk Dry	2.602	2.587	**2.592**	4.89 m^2/Kg
4.75 mm (No.4)	46	48	0					23.84 Ft^2/lb
2.36 mm (No.8)	32	34	0	Bulk SSD	2.623	2.615	2.619	
1.18 mm (No.16)	24	25	0					
600 um (No.30)	17	19	0	Apparent	2.657	2.662	2.660	Effective SpG of Agg.
300 um (No.50)	11	12	0					
150 um (No.100)	7	8	0					2.625
75 um (No.200)	4.9	5.3	0	Absorption %	0.8	1.1	1.0	

Table 50 Mix Design Summary Sheet for Project D6C1

Aggregate Data

Sieve Sizes	Stockpile RAP 15%	Stockpile A 20%	Stockpile B 25%	Stockpile C 40%	Blended Stockpile Gradation	CJMF Limits
1"	100	100	100	100	100	
3/4"	100	93	100	100	99	
1/2"	93	18	91	100	80	
3/8"	85	3	45	100	65	
#4	61	1	2	78	41	
#8	43	1	1	54	29	
#16	33	1	1	40	21	
#30	28	1	1	28	16	
#50	23	1	1	19	12	
#100	15	1	1	12	8	
#200	7.9	0.7	0.5	6.0	3.9	

Agg. Data	Combined
Bulk Sp. G	2.613

Mix Data

AC Content (Wt. Of Mix)	3.8	4.3	4.8	5.2
Bulk Specific Gravity	2.332	2.345	2.369	2.382
Bulk Density (lb/ft^3)	145.1	146.0	147.4	148.3
Maximum Specific Gravity	2.484	2.466	2.448	2.434
Maximum Density (lb/ft^3)	154.6	153.5	152.4	151.5
% Air Voids	6.1	4.9	3.2	2.1
VMA %	14.1	14.1	13.7	13.6

Design Values	**Min**	**Target**	**Max**	Job Specs
Oil Content by Weight of Mix %	4.26	4.55	4.74	
Oil Content by Weight of Aggregate %	4.45	4.77	4.98	
Oil Content by Wt of Mix % (Added) 0.90	3.36	3.65	3.84	
Oil Content by Wt of Agg % (Added) 0.91	3.54	3.86	4.07	
Air Voids %	5.0	4.0	3.4	3-5
Bulk Density (lb/ft^3)	145.9	146.8	147.3	
Maximum Density (lb/ft^3)	153.5	152.9	152.5	
VMA %	14.1	13.8	13.7	13 min
VFA %	65	71	75	65-75
DP		0.9		0.6-1.2
% GMM @ Nmax		97.1		98.0
Stripping Evaluation		99		85 min
Mixing Temperature (°F)		320		316-329
Compaction Temperature (°F)		290		284-302
Ignition Oven Correction Factor (%) 538		0.09		

Appendix C
Sensitivity of Monotonic Indicators to Binder Content and PG

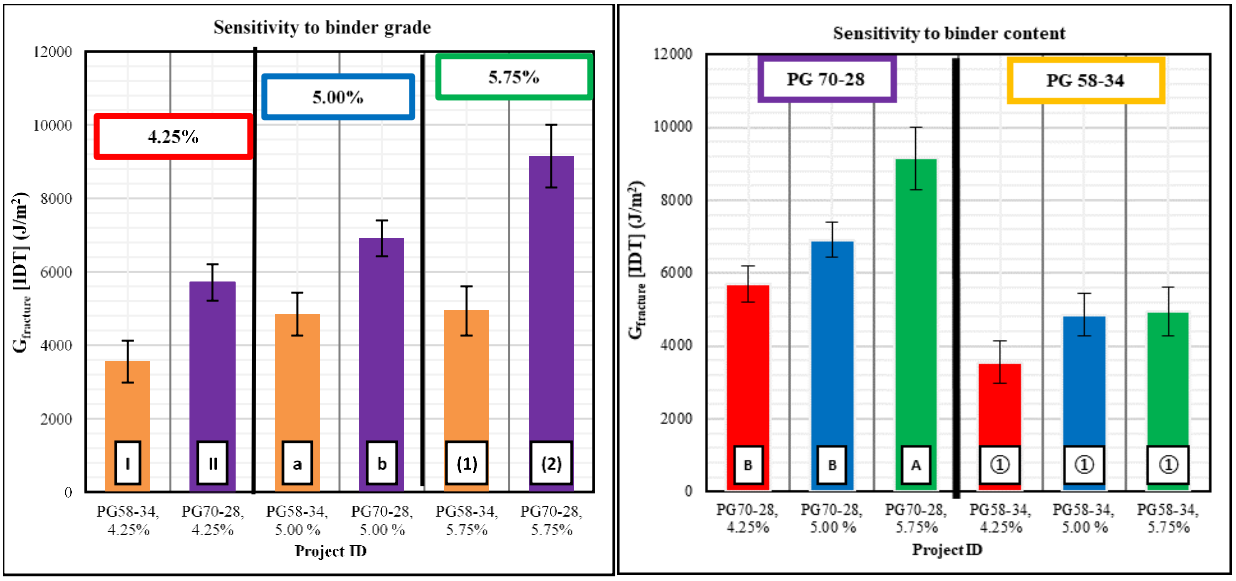

Figure 138 Sensitivity of Total Fracture Energy from IDT Test for PG and Binder Content $G_{fracture}$ (IDT)

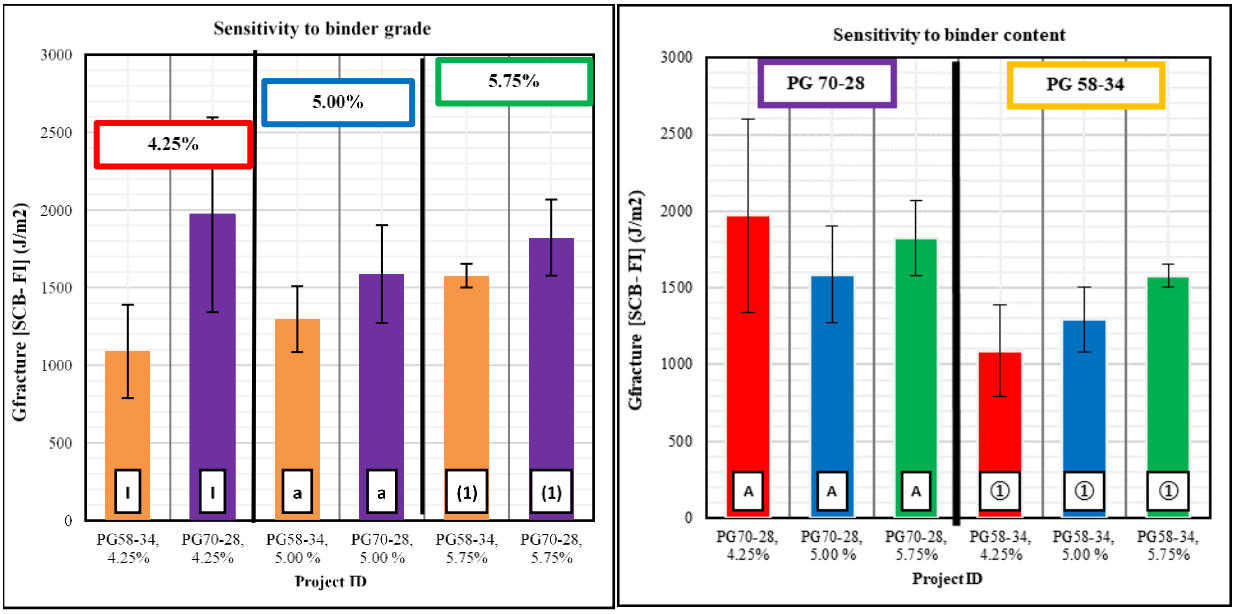

Figure 139 Sensitivity of Total Fracture Energy from SCB-FI Test for PG and Binder Content

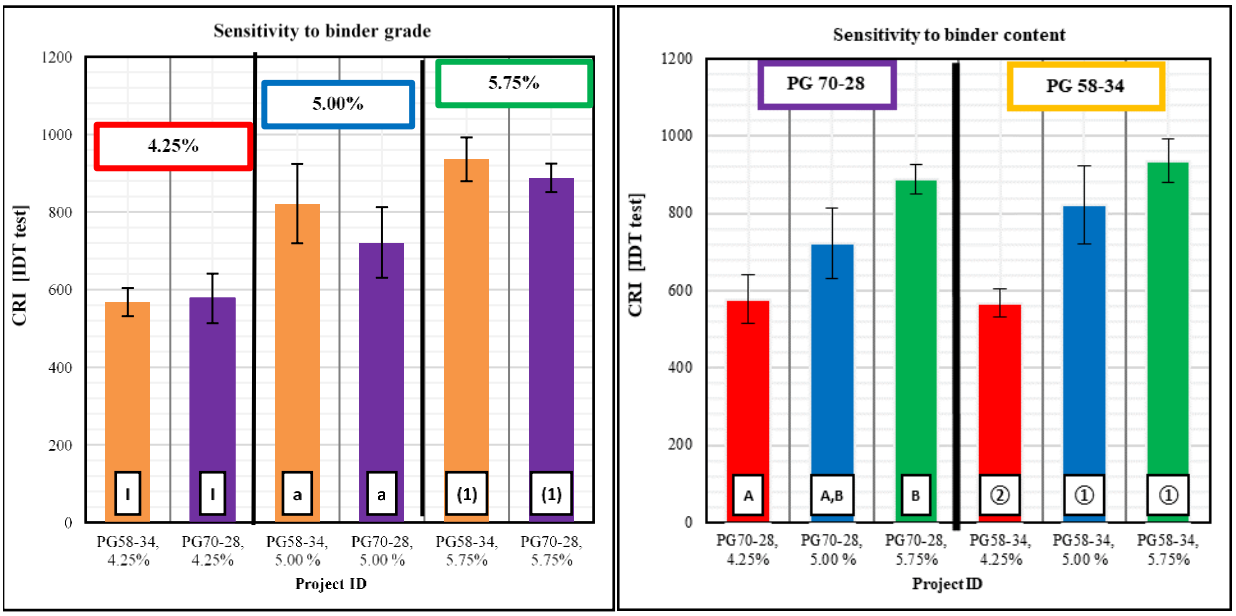

Figure 140 Sensitivity of CRI from IDT Test for Binder Grade

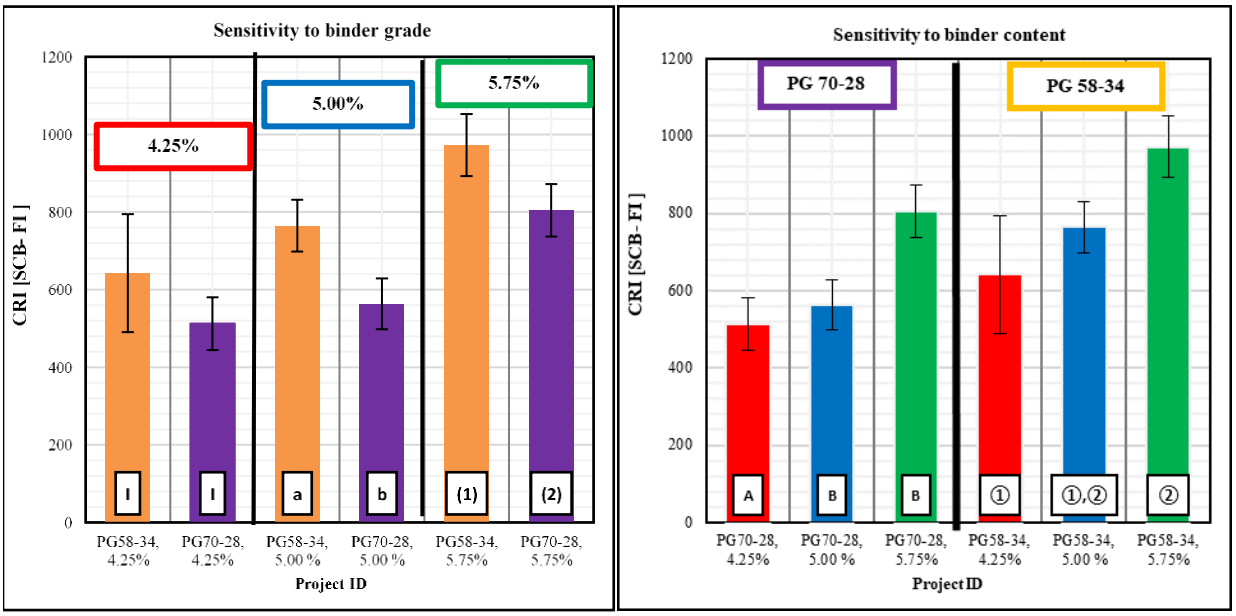

Figure 141 Sensitivity of CRI from SCB-FI Test for PG and Binder Content

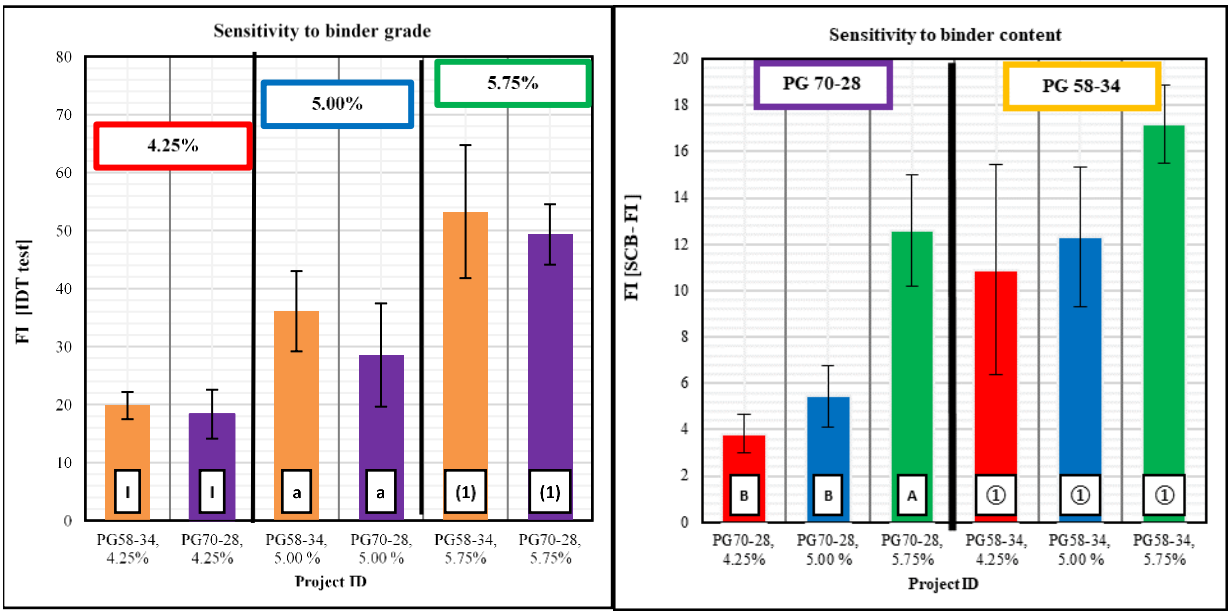

Figure 142 Sensitivity of FI from IDT Test for PG and Binder Content

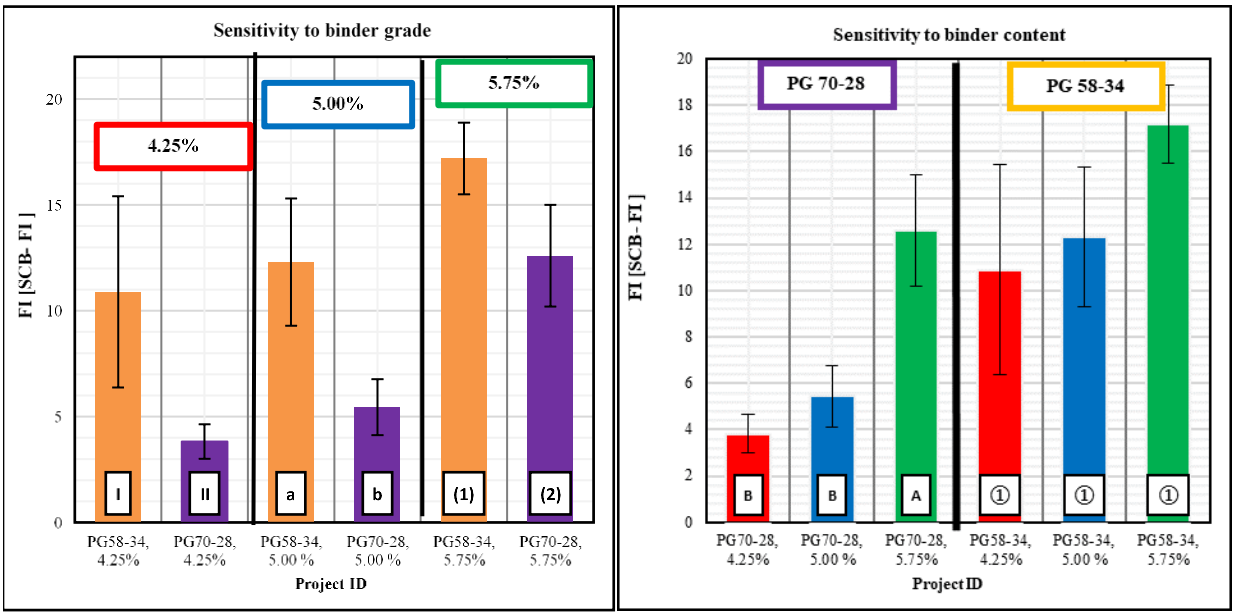

Figure 143 Sensitivity of FI from SCB-FI Test for PG and Binder Content

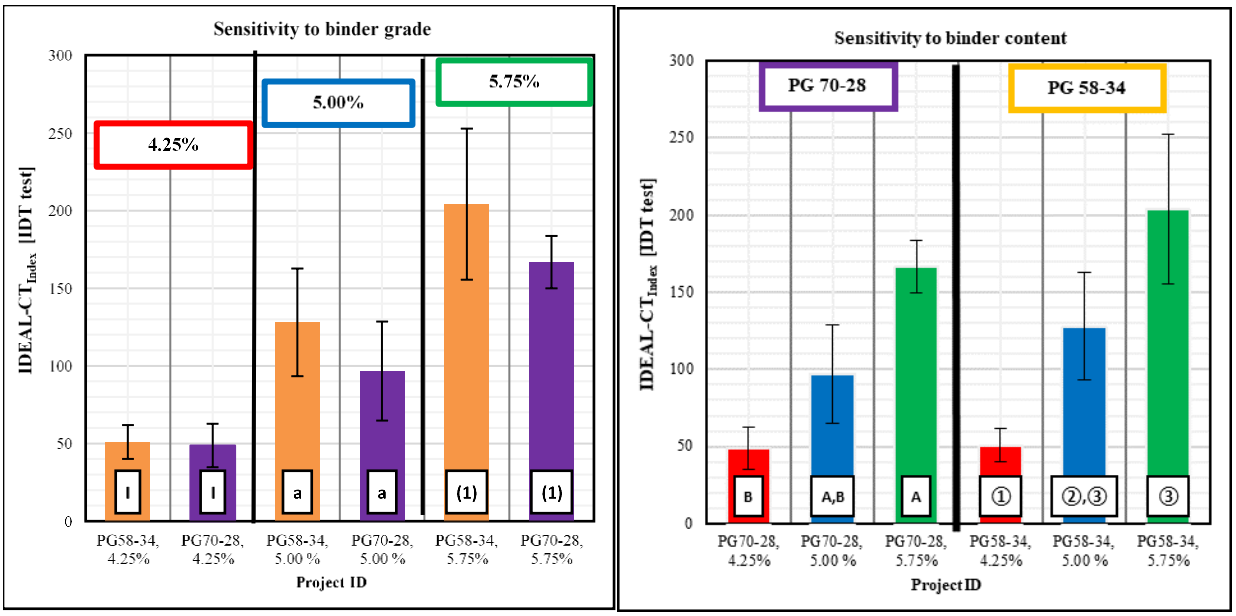

Figure 144 Sensitivity of IDEAL-CT$_{Index}$ from IDT Test for PG and Binder Content

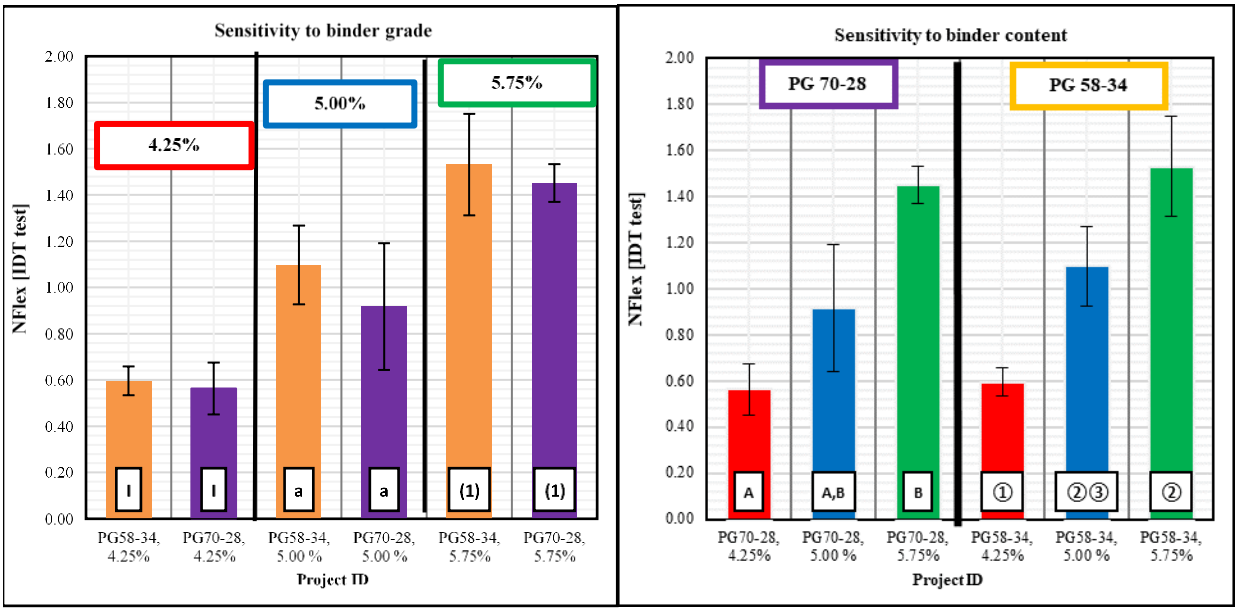

Figure 145 Sensitivity of Nflex from IDT Test for PG and Binder Content

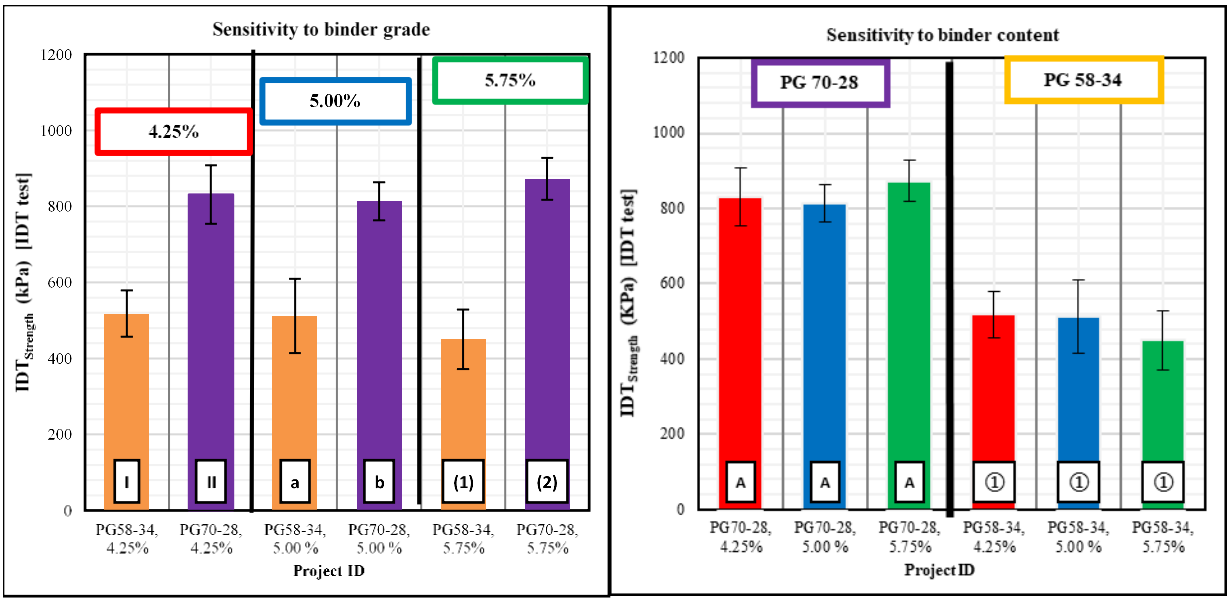

Figure 146 Sensitivity of $IDT_{strength}$ from IDT Test for PG and Binder Content

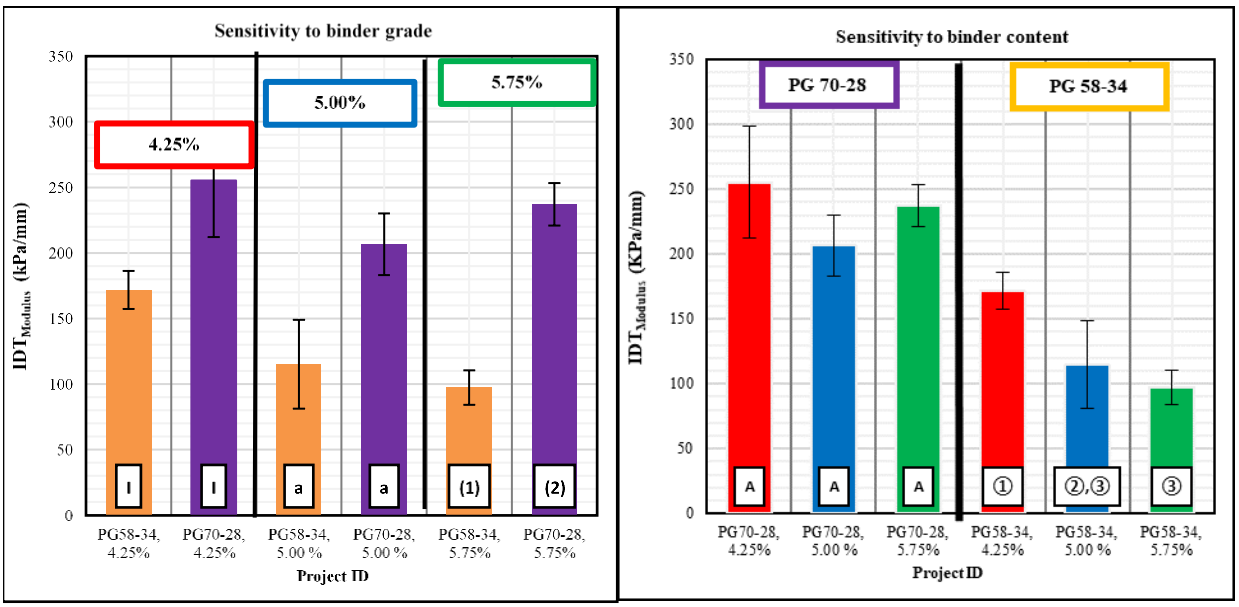

Figure 147 Sensitivity of $IDT_{Modulus}$ from IDT Test for PG and Binder Content

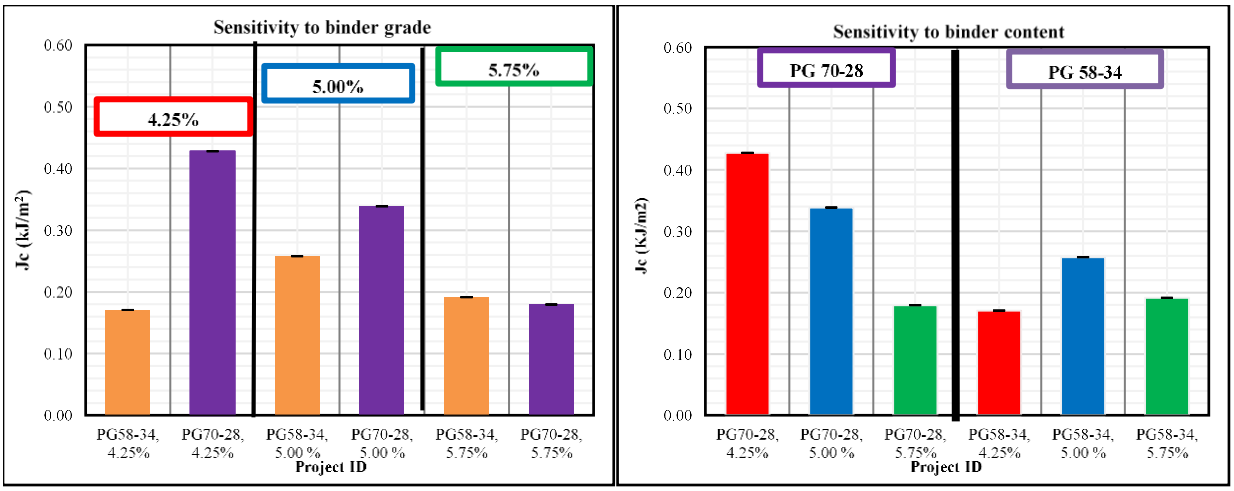

Figure 148 Sensitivity of J_c from IDT Test for PG and Binder Content

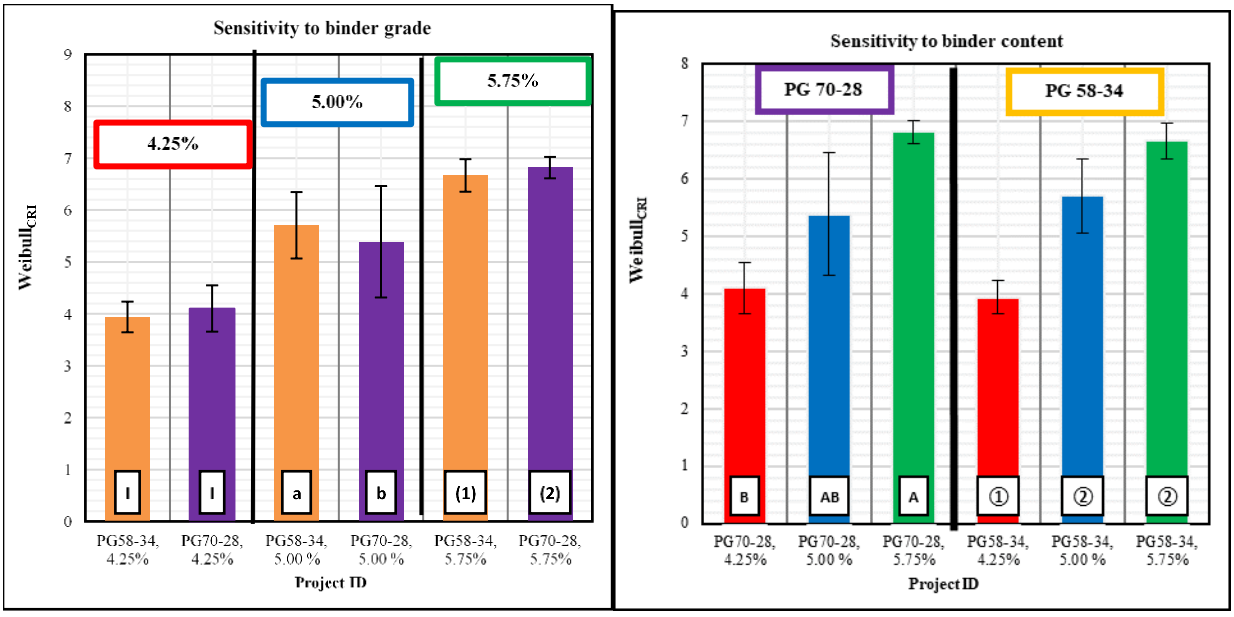

Figure 149 Sensitivity of Weibull$_{CRI}$ from IDT Test for PG and Binder Content

Appendix D
Correlation between Field Cracking Resistance and Monotonic Indicators

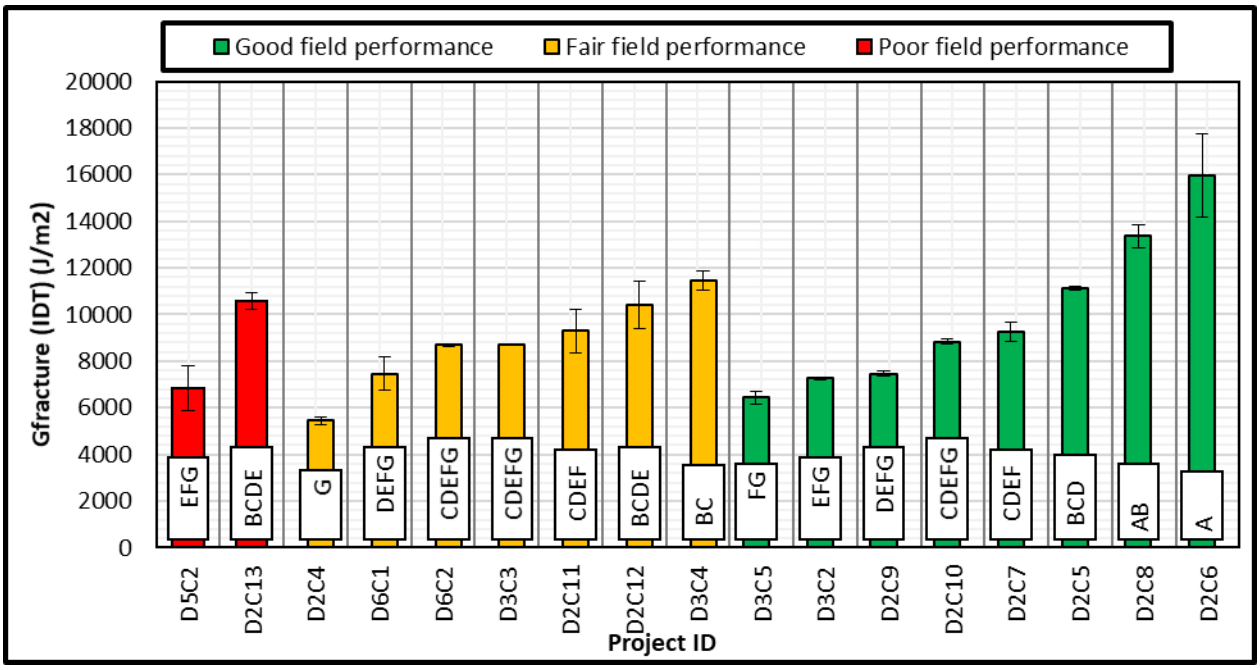

Figure 150 Correlation between Total Fracture Energy from IDT Test with Field Project Performance ($G_{fracture}$ [IDT])

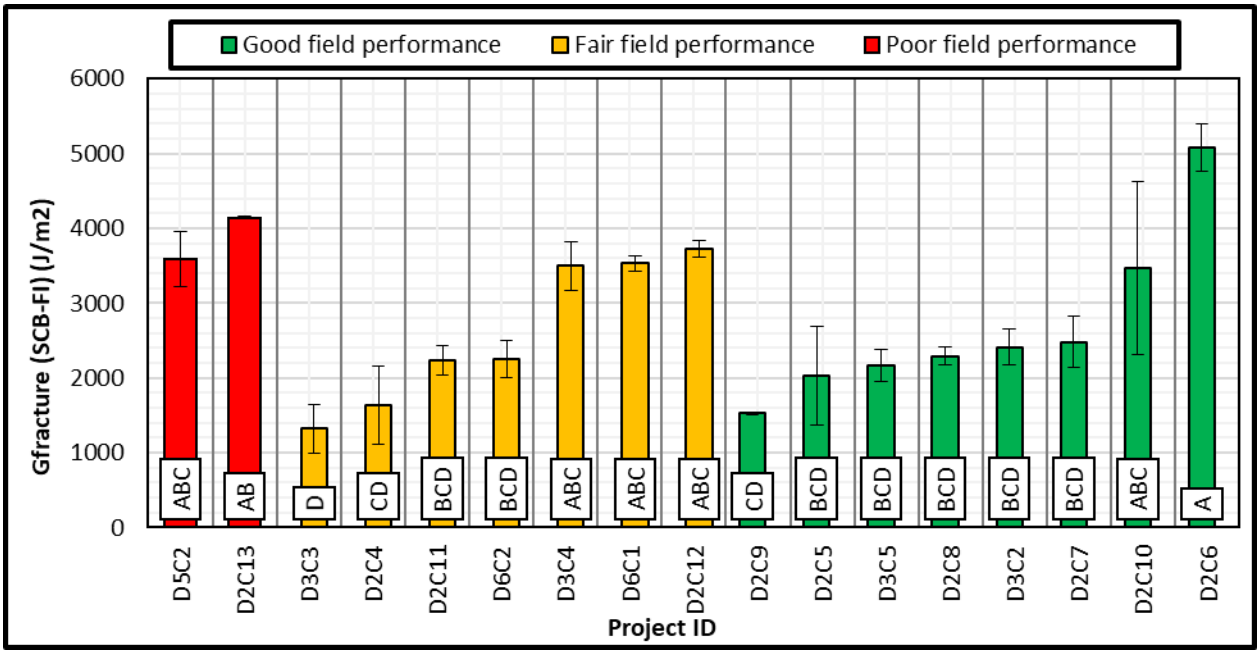

Figure 151 Correlation between $G_{fracture}$ (SCB) with Field Project Performance

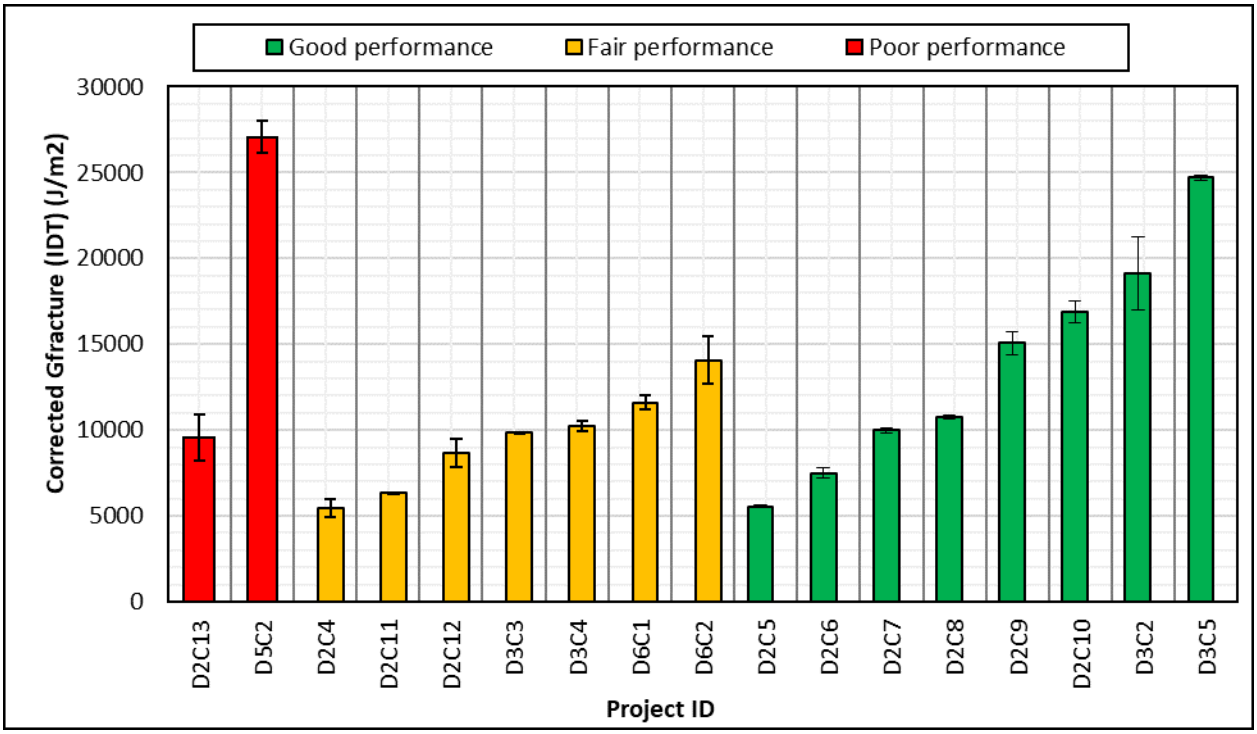

Figure 152 Correlation between Corrected Total Fracture Energy from IDT Test with Field Project Performance ($G_{fracture}$ [IDT]

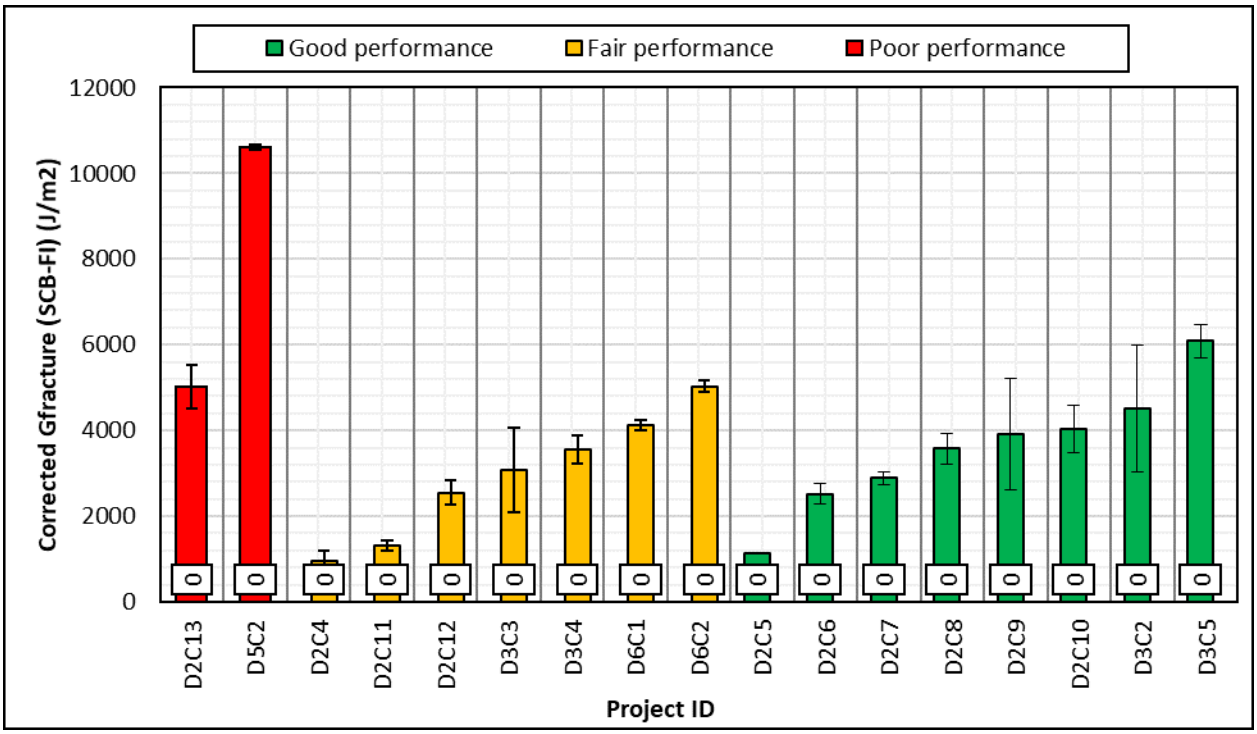

Figure 153 Correlation between Corrected Total Fracture Energy from SCB Test with Field Project Performance ($G_{fracture}$ [SCB])

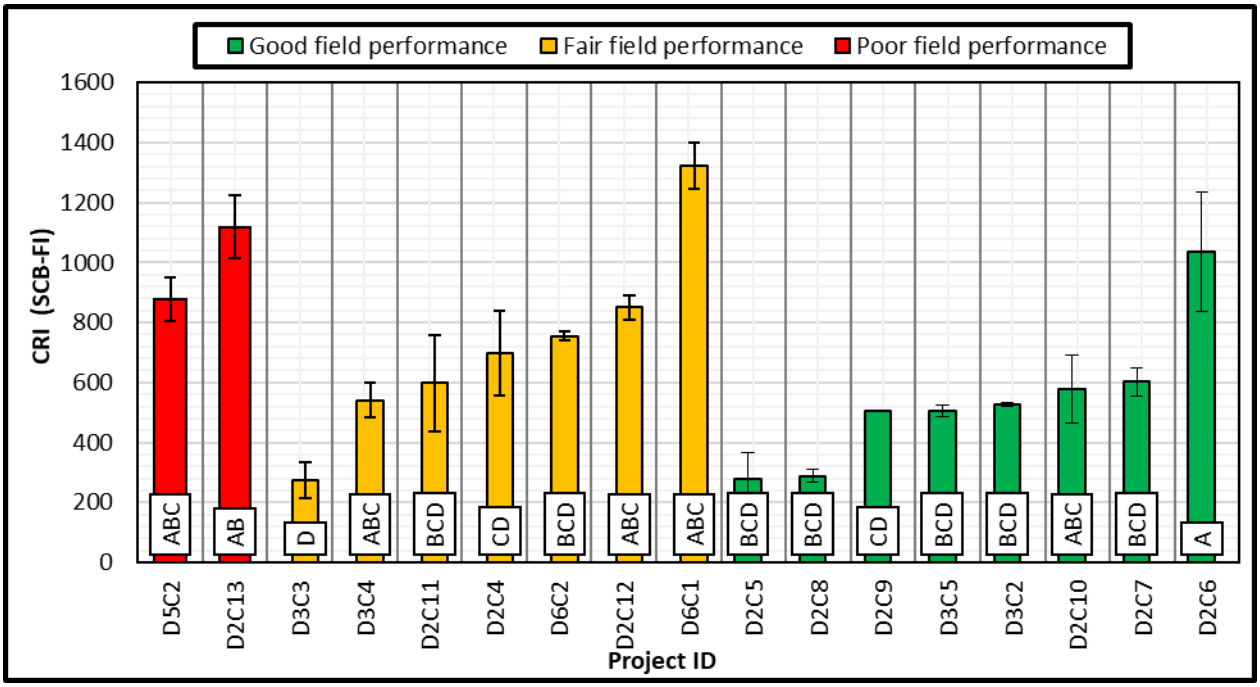

Figure 154 Correlation between CRI from Computed from SCB Test with Field Project Performance

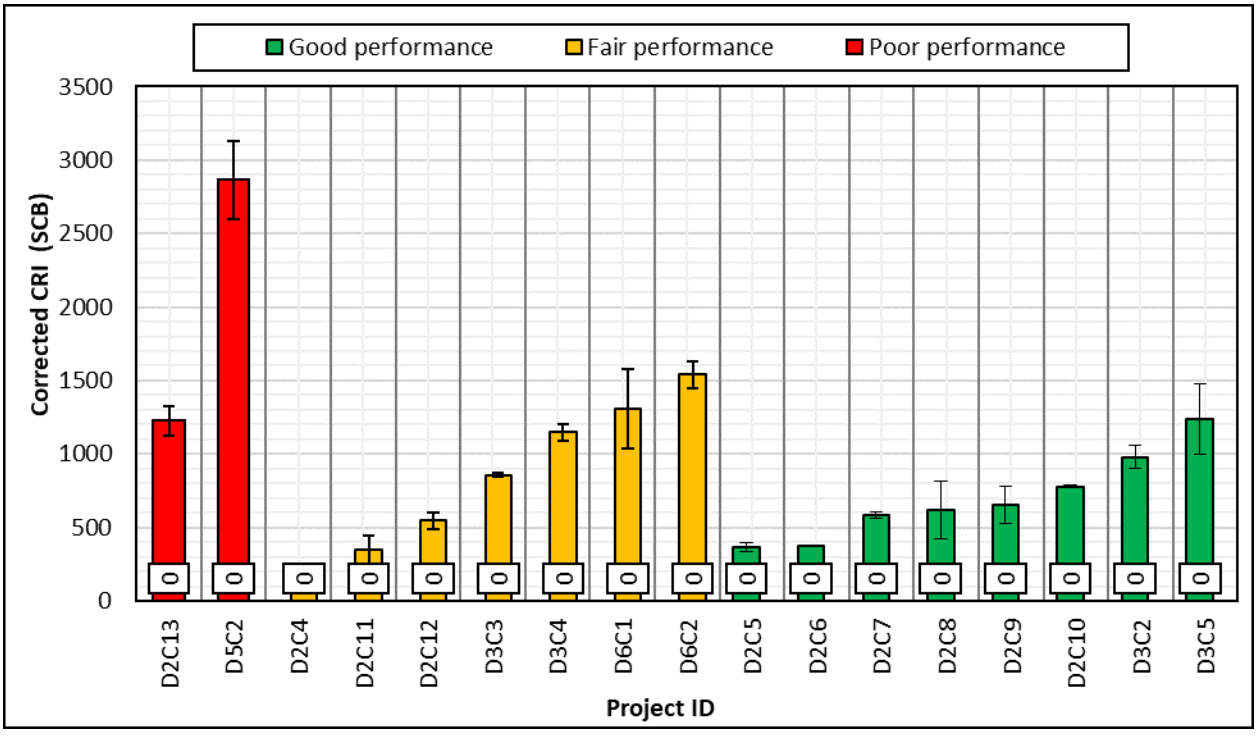

Figure 155 Correlation between Corrected CRI Computed from IDT Test with Field Project Performance

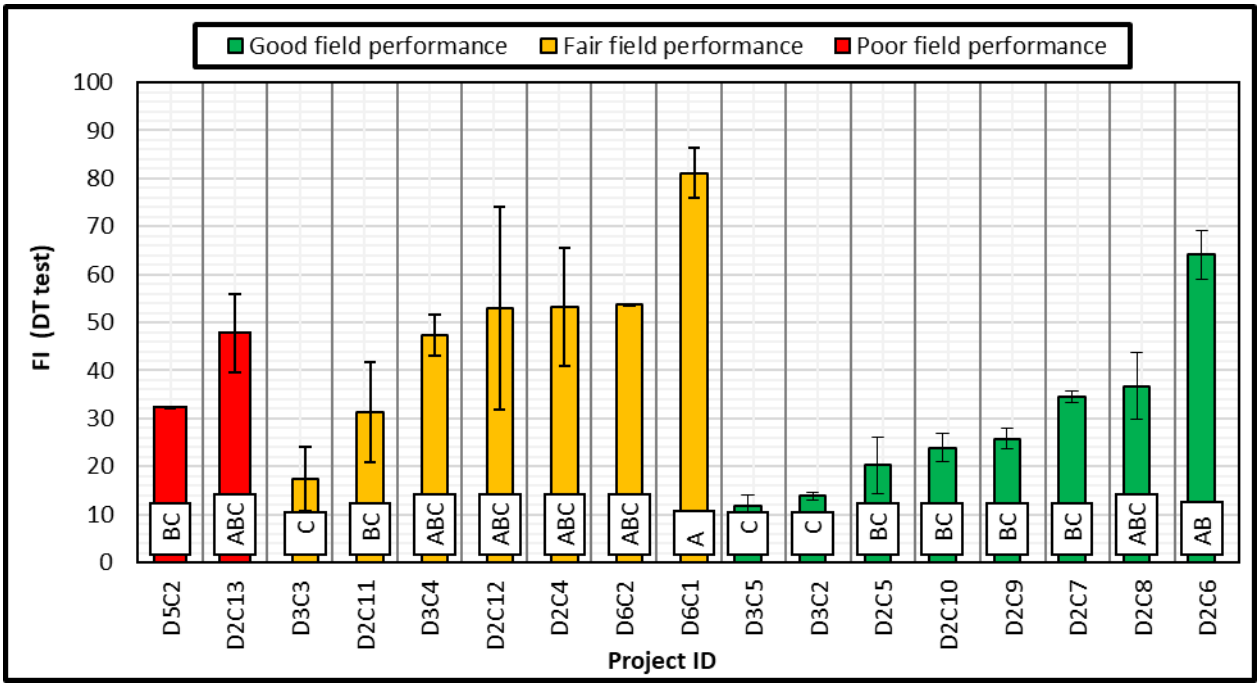

Figure 156 Correlation between FI Computed from IDT Test with Field Project Performance

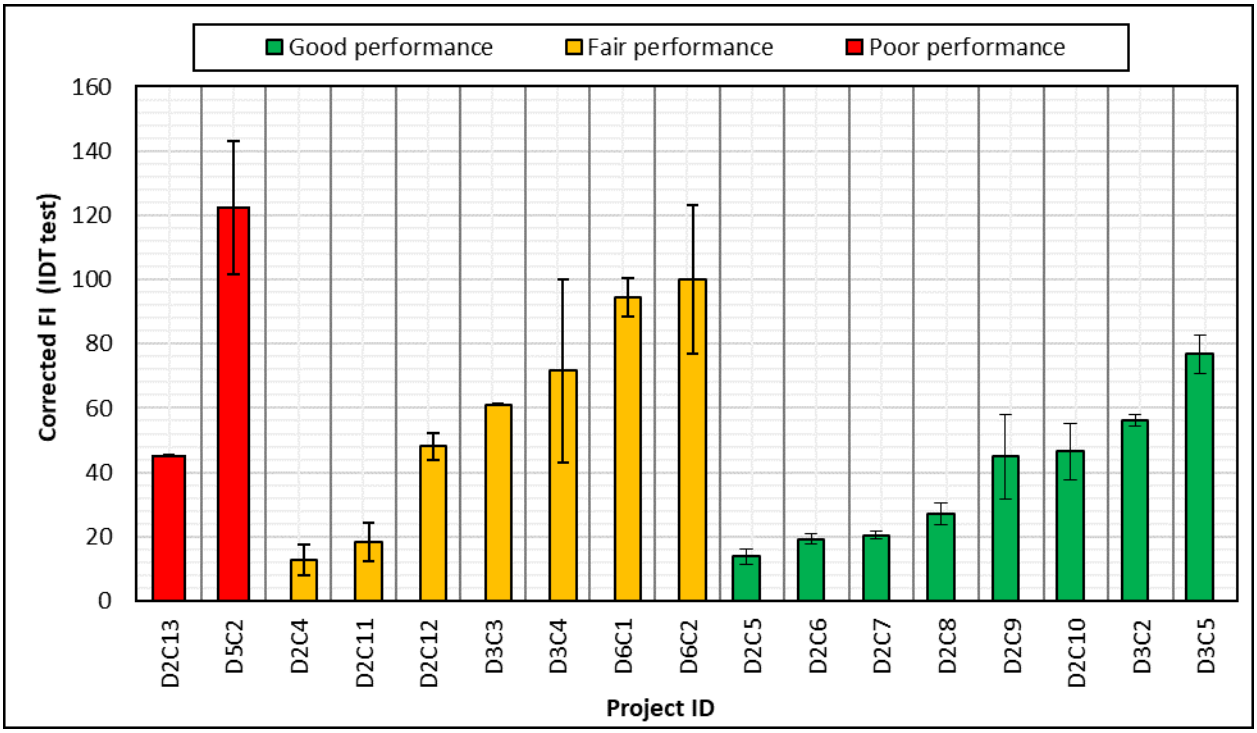

Figure 157 Correlation between FI from Computed from SCB Test with Field Project Performance

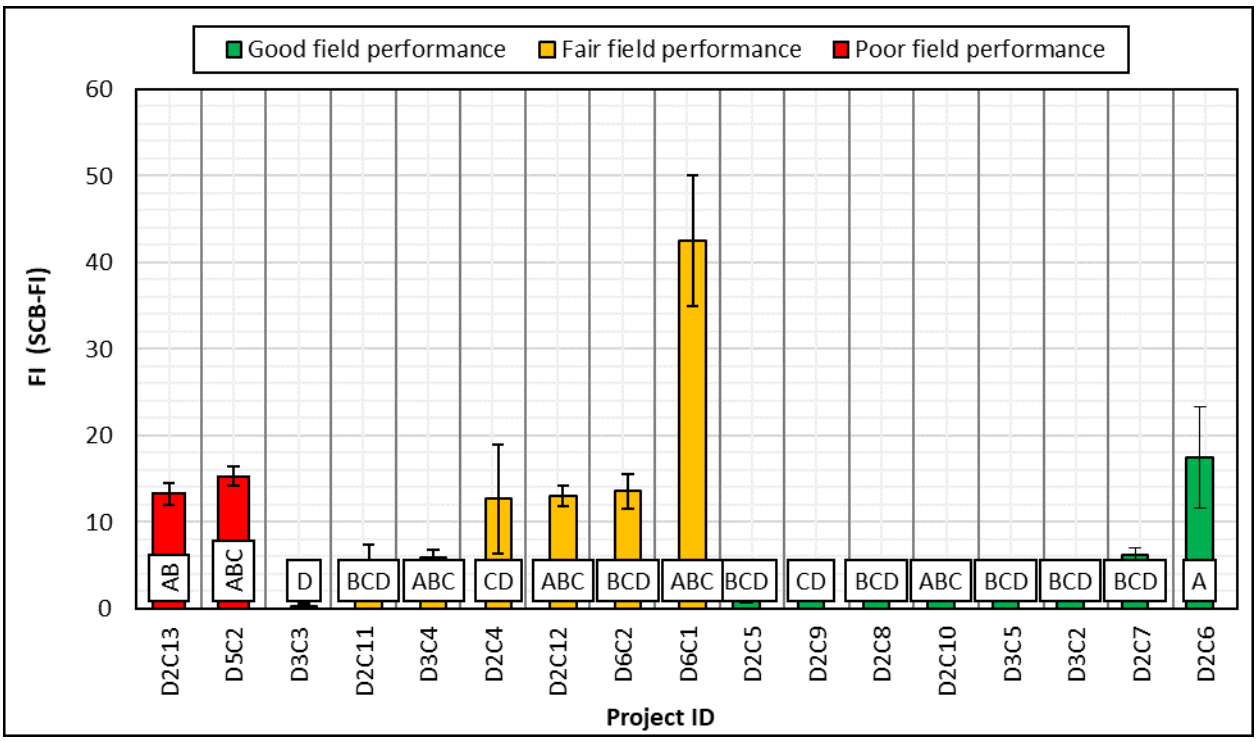

Figure 158 Correlation between Corrected FI Computed from IDT Test with Field Project Performance

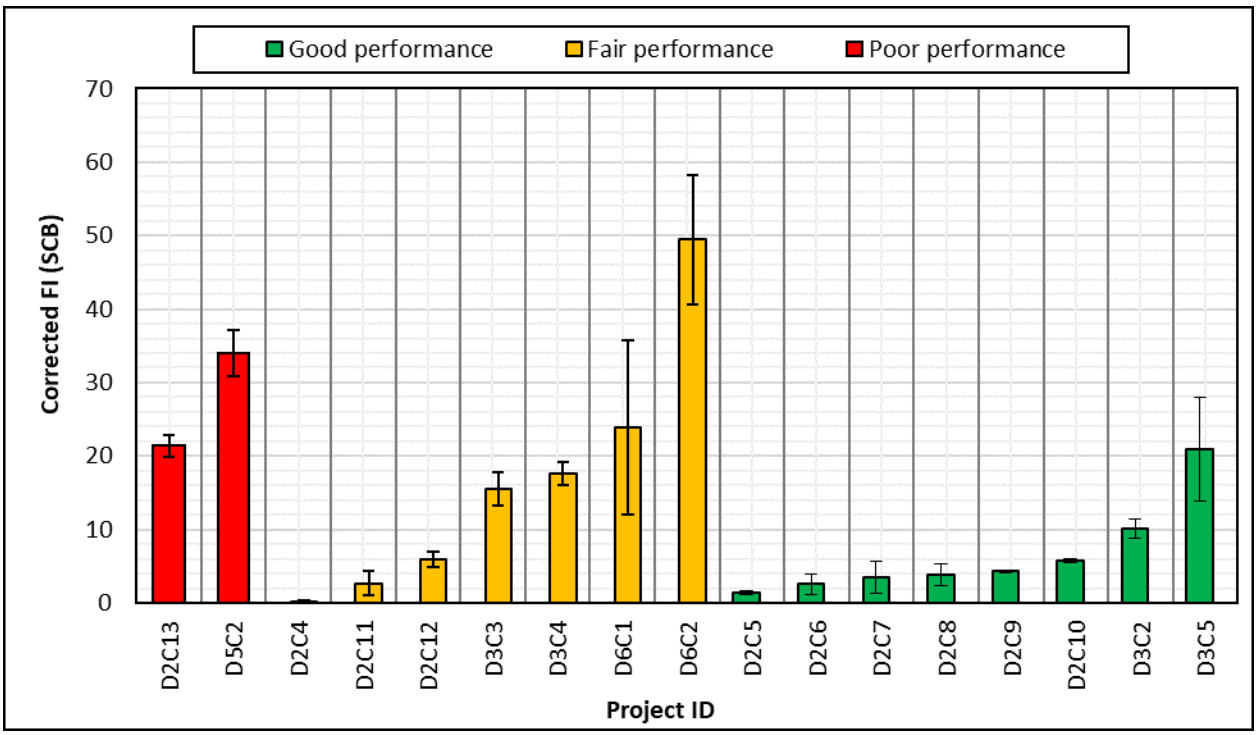

Figure 159 Correlation between Corrected FI from Computed from SCB Test with Field Project Performance

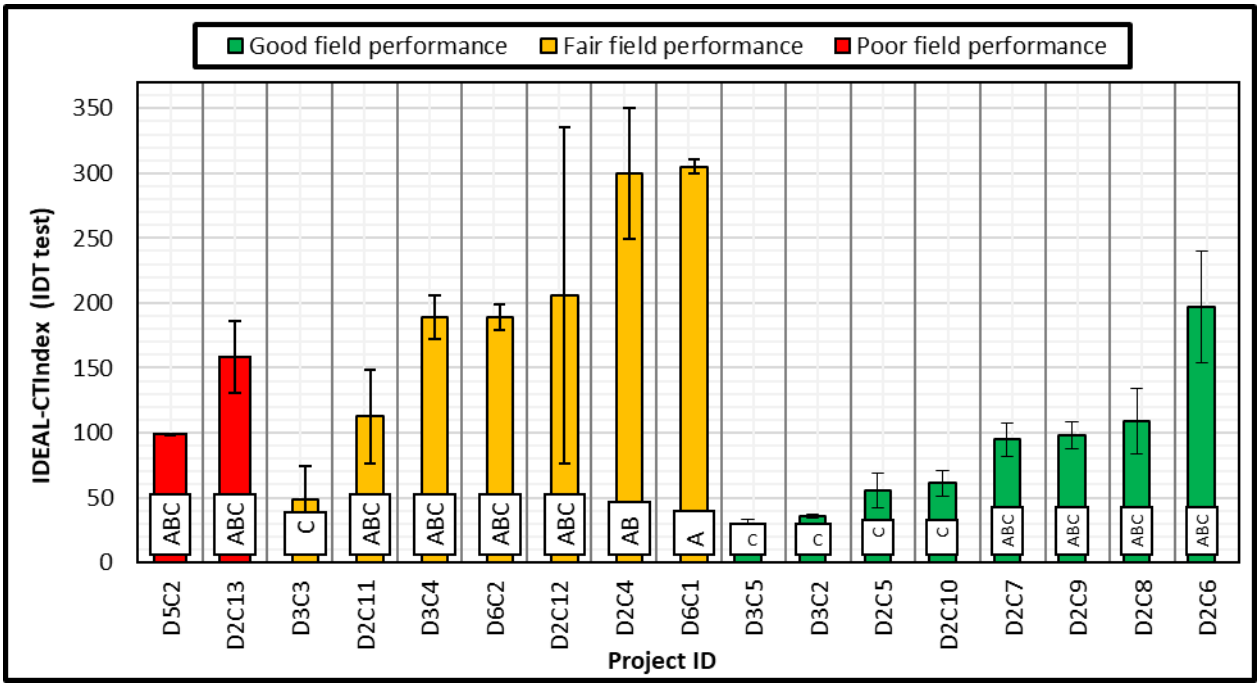

Figure 160 Correlation between IDEAL-CT$_{Index}$ from Computed from SCB Test with Field Project Performance

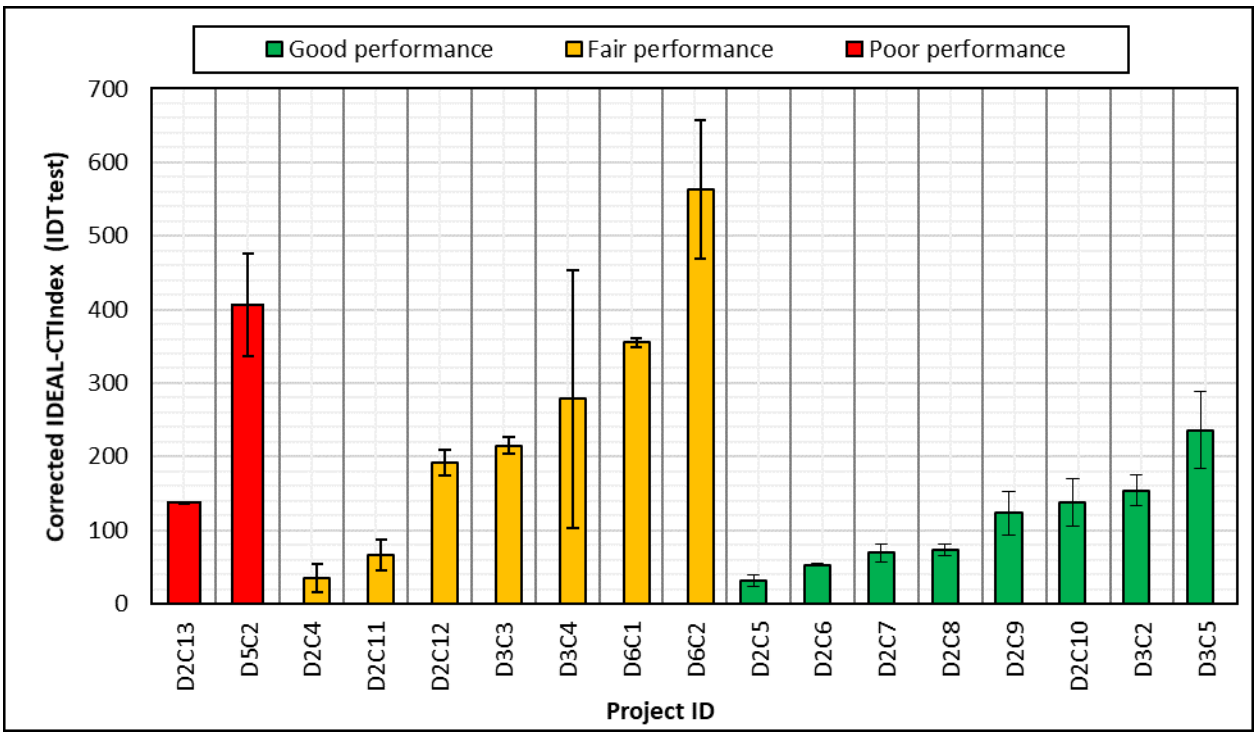

Figure 161 Correlation between Corrected IDEAL-CT$_{Index}$ from Computed from SCB Test with Field Project Performance

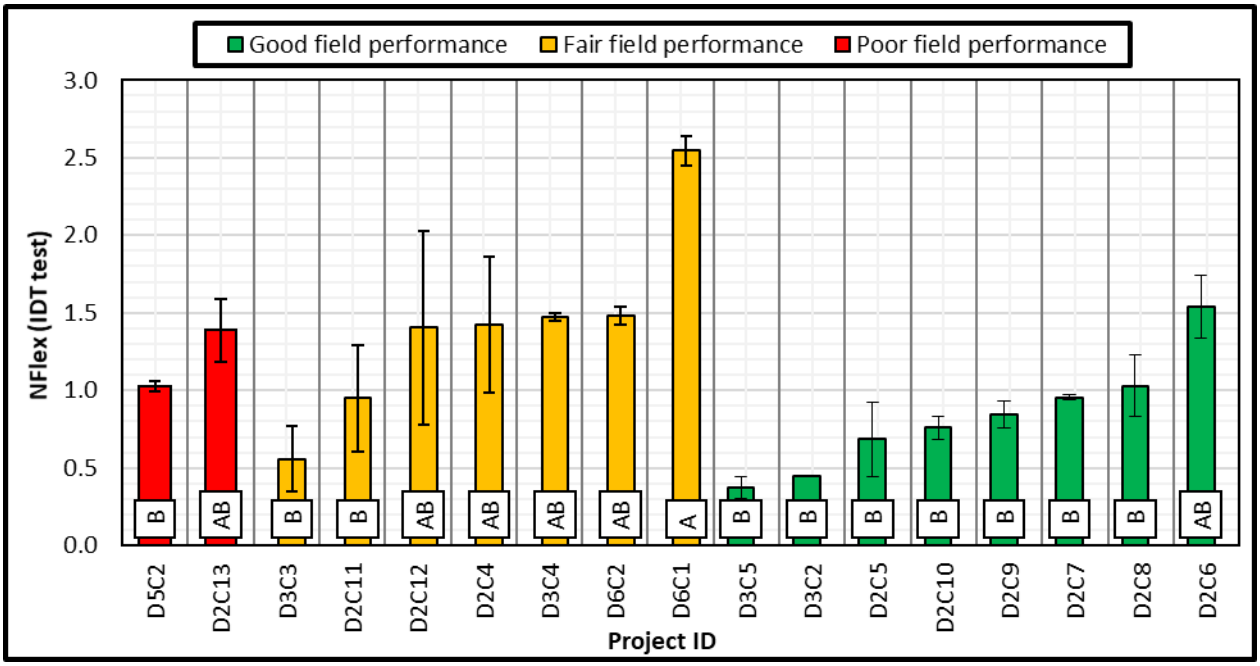

Figure 162 Correlation between Nflex from Computed from SCB Test with Field Project Performance

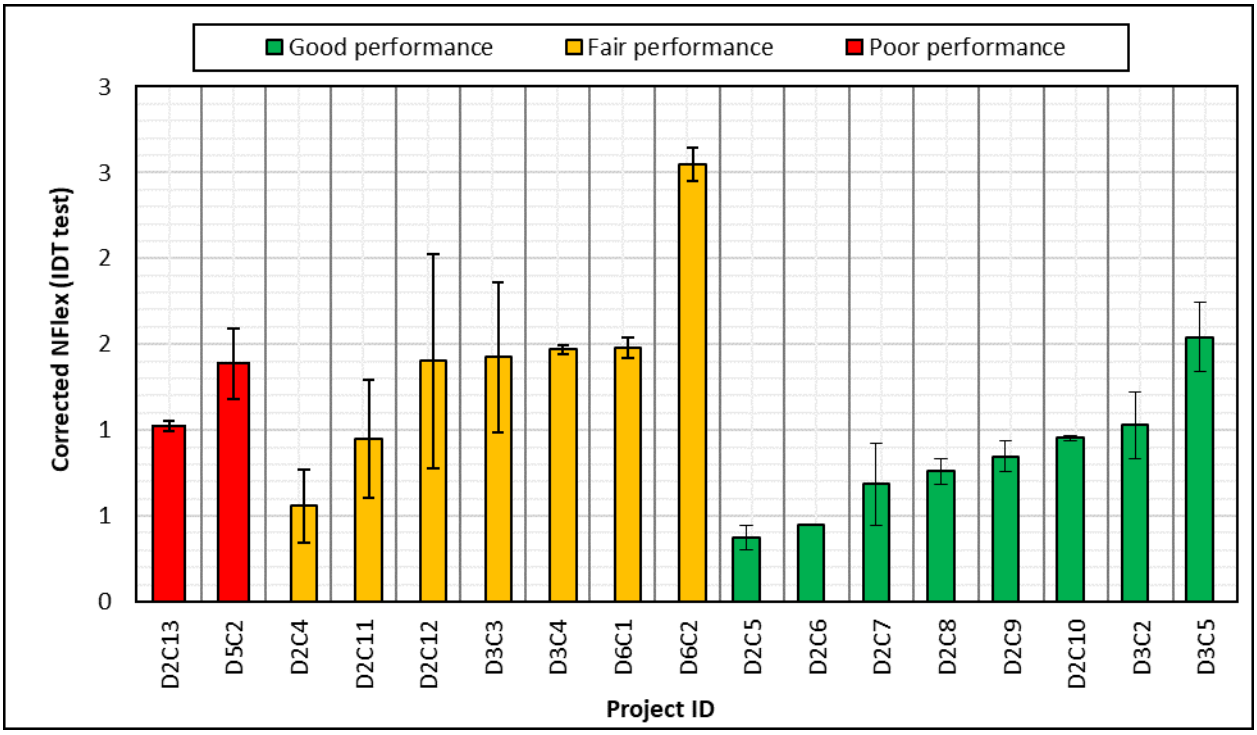

Figure 163 Correlation between Corrected Nflex from Computed from SCB Test with Field Project Performance

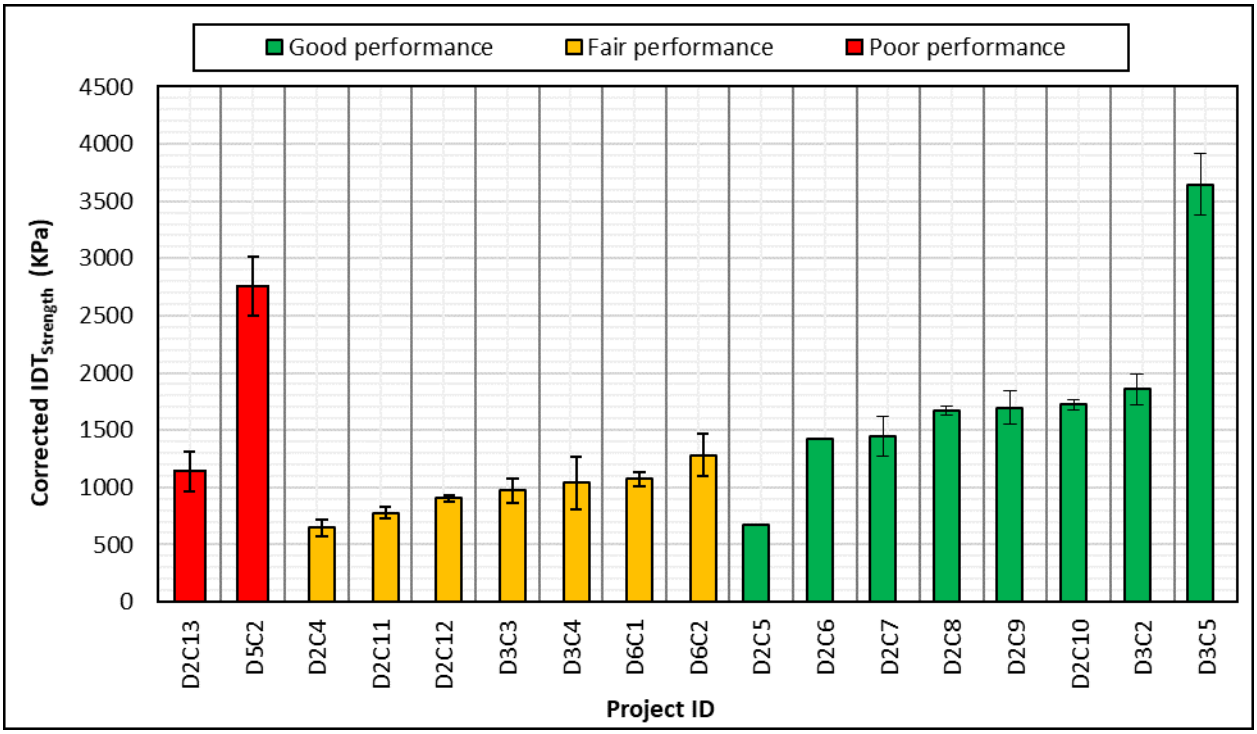

Figure 164 Correlation between Corrected IDT$_{strength}$ from Computed with Field Project Performance

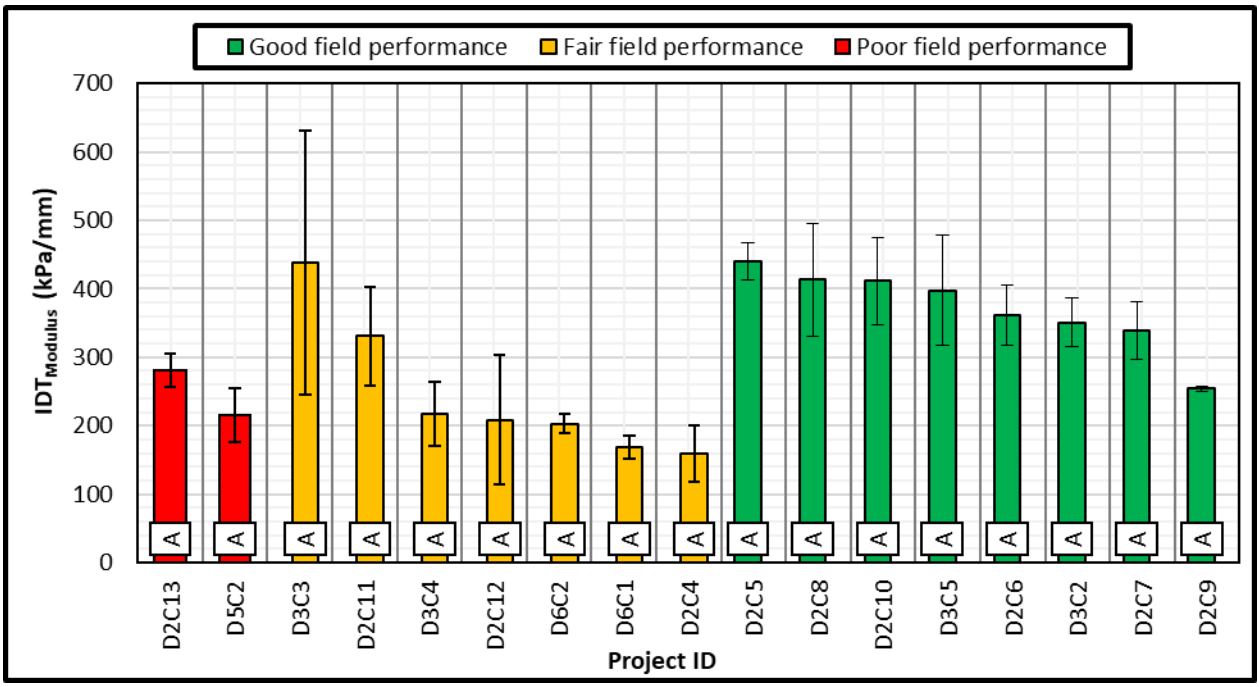

Figure 165 Correlation between IDT$_{Modulus}$ from Computed with Field Project Performance

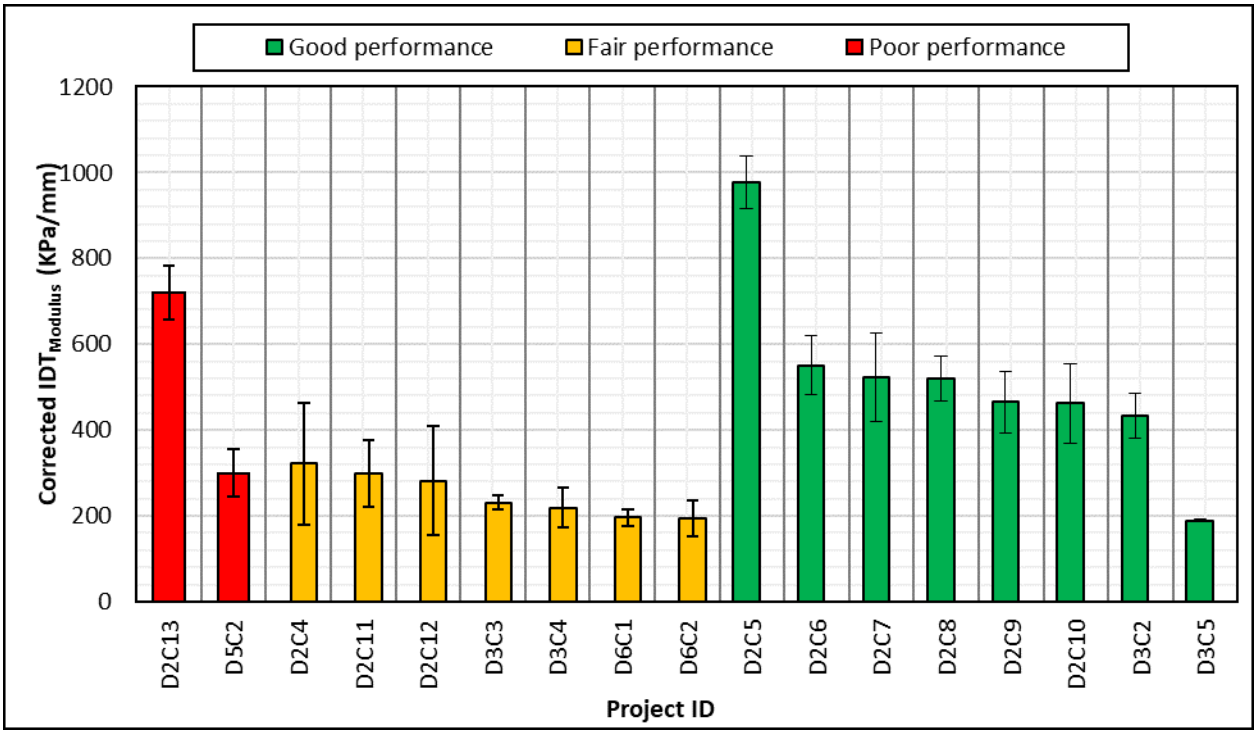

Figure 166 Correlation between Corrected $IDT_{Modulus}$ from Computed with Field Project Performance

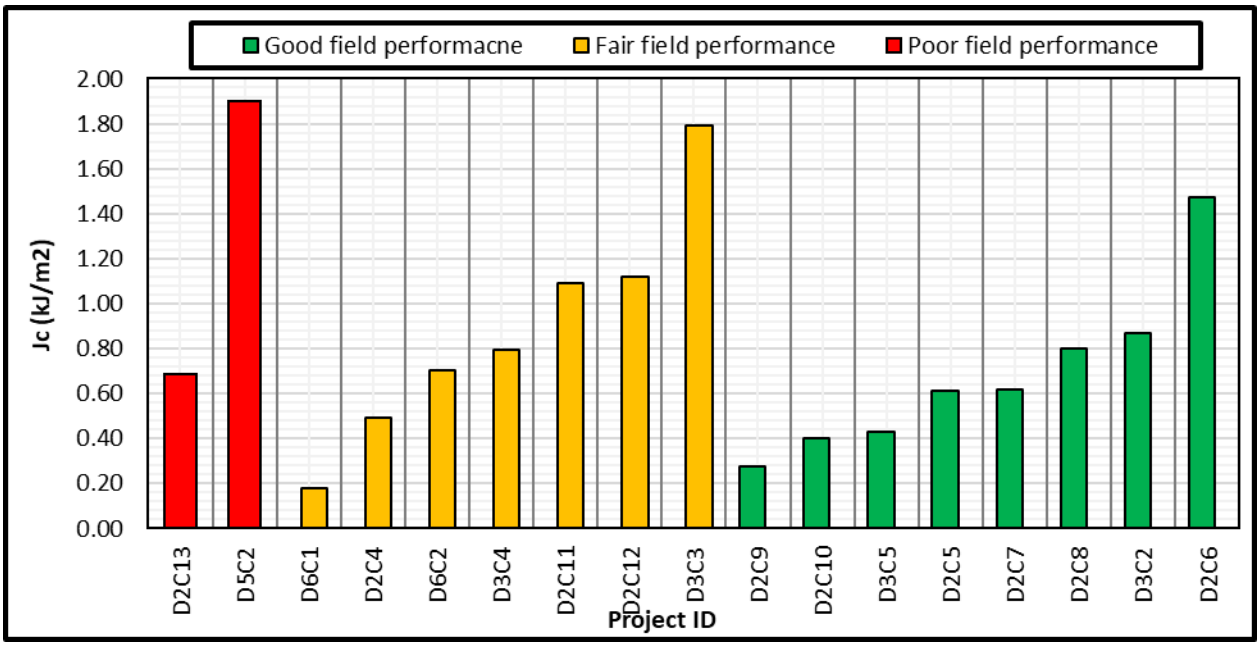

Figure 167 Correlation between J_c with Field Project Performance

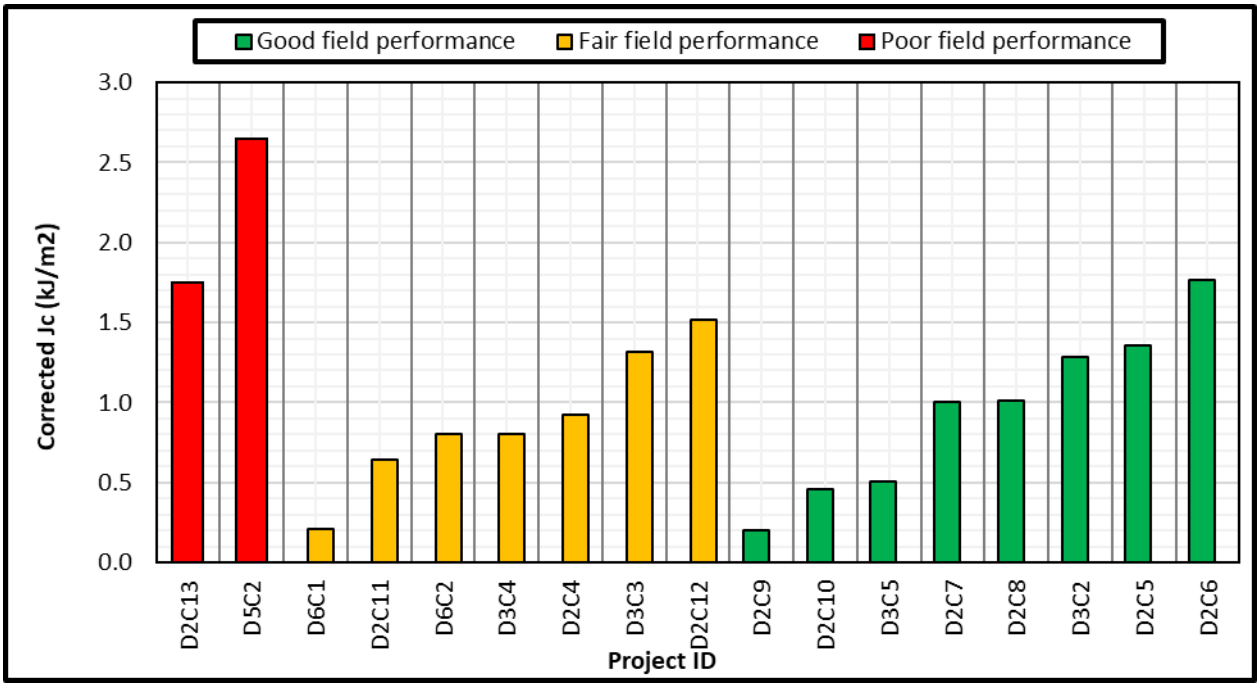

Figure 168 Correlation between Corrected J_c with Field Project Performance

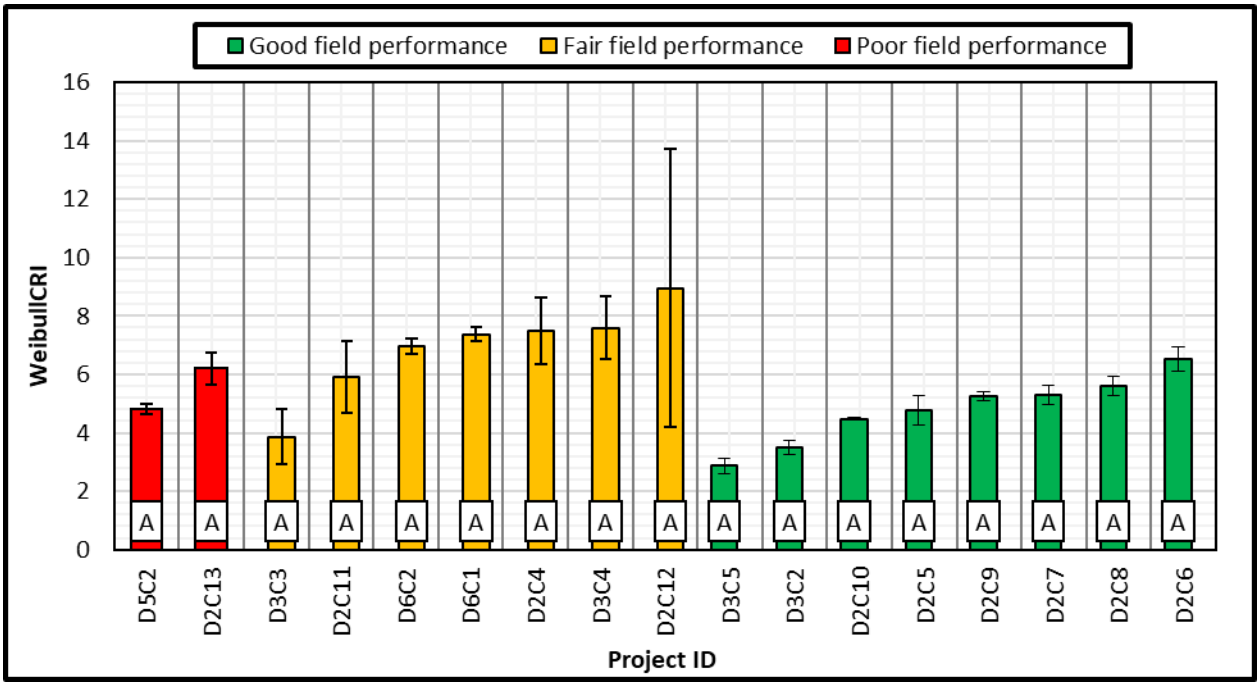

Figure 169 Correlation between $Weibull_{CRI}$ with Field Project Performance

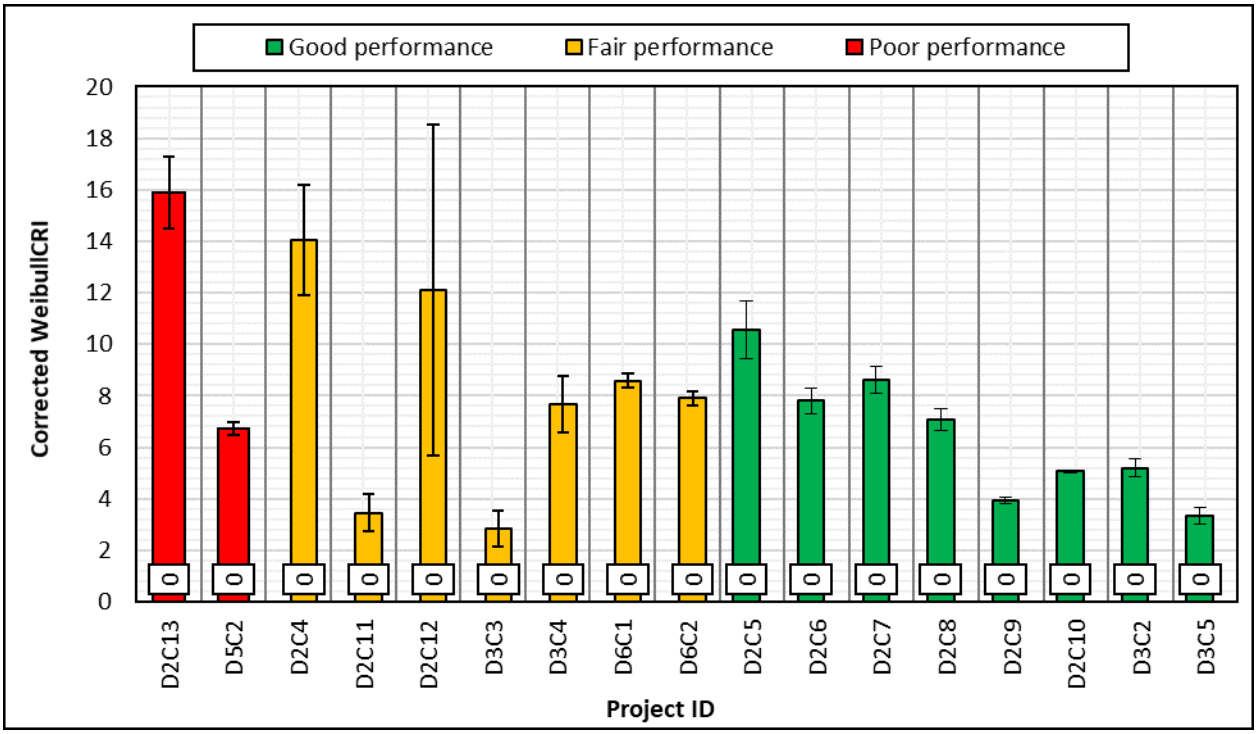

Figure 170 Correlation between Corrected Weibull$_{CRI}$ with Field Project Performance

Appendix E
Correlation between Monotonic and MSSD Indicators

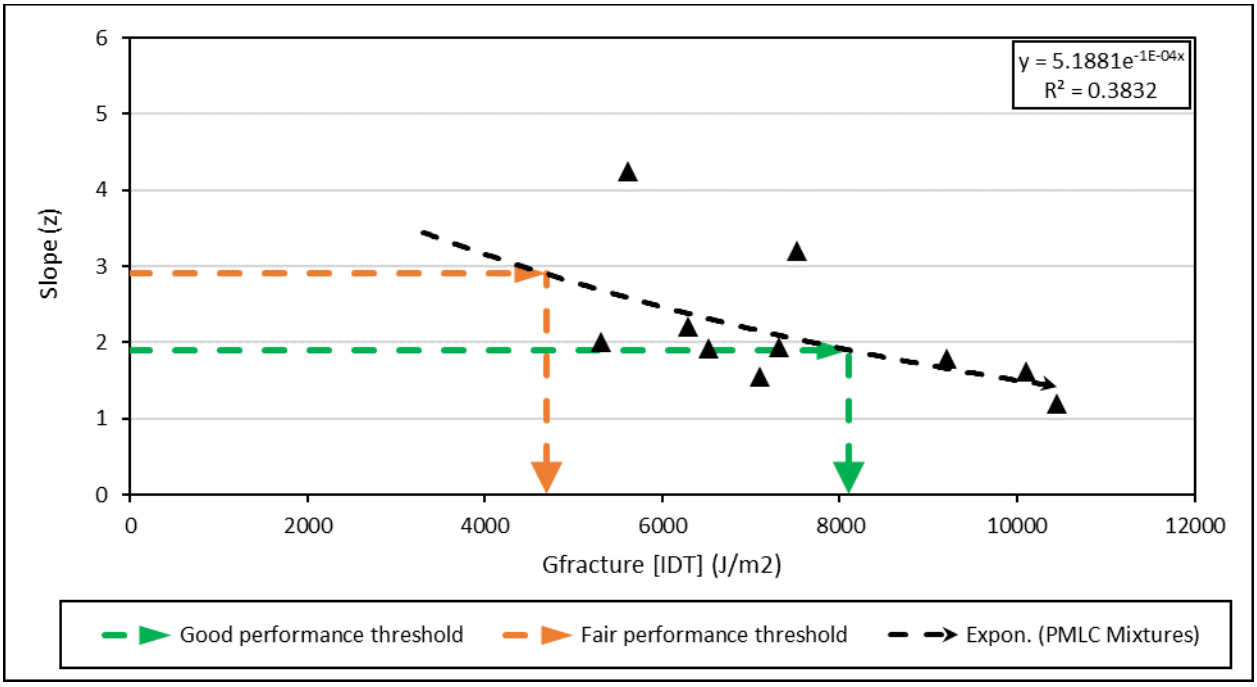

Figure 171 Correlation between $G_{fracture}$ (IDT) and the Slope (*z*) Parameter

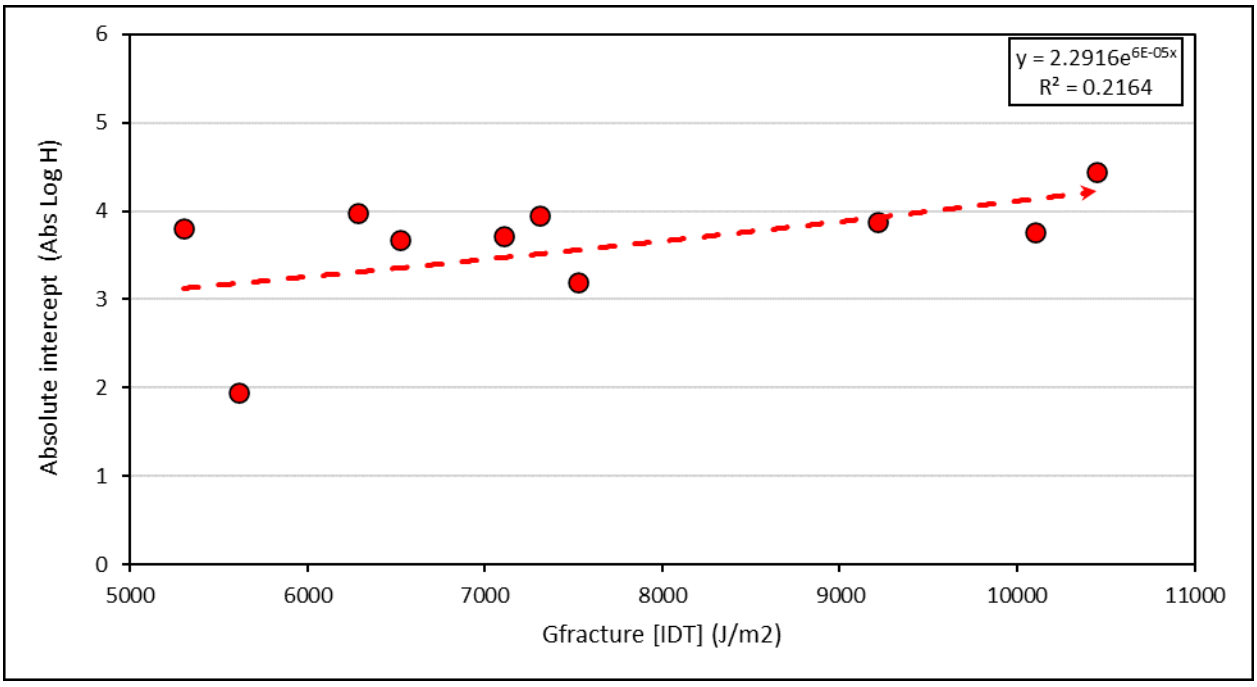

Figure 172 Correlation between $G_{fracture}$ (IDT) and Abs (log *H*) Parameter

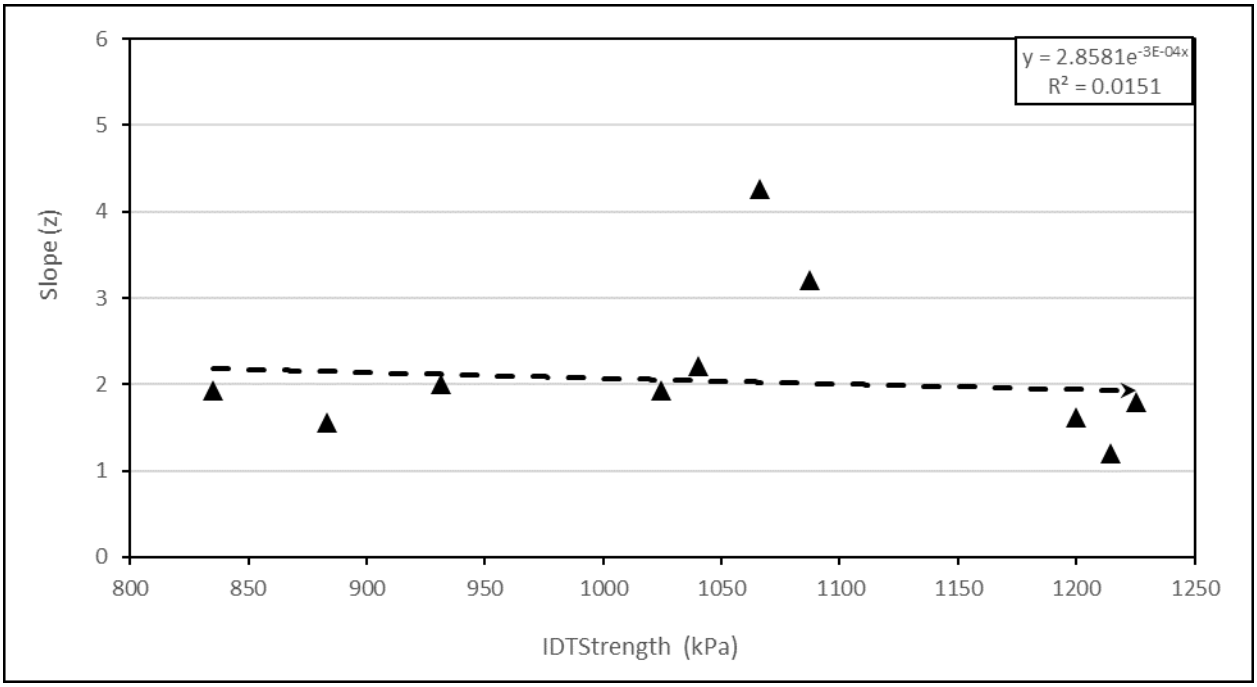

Figure 173 Correlation between $IDT_{Strength}$ and the Slope (z) Parameter

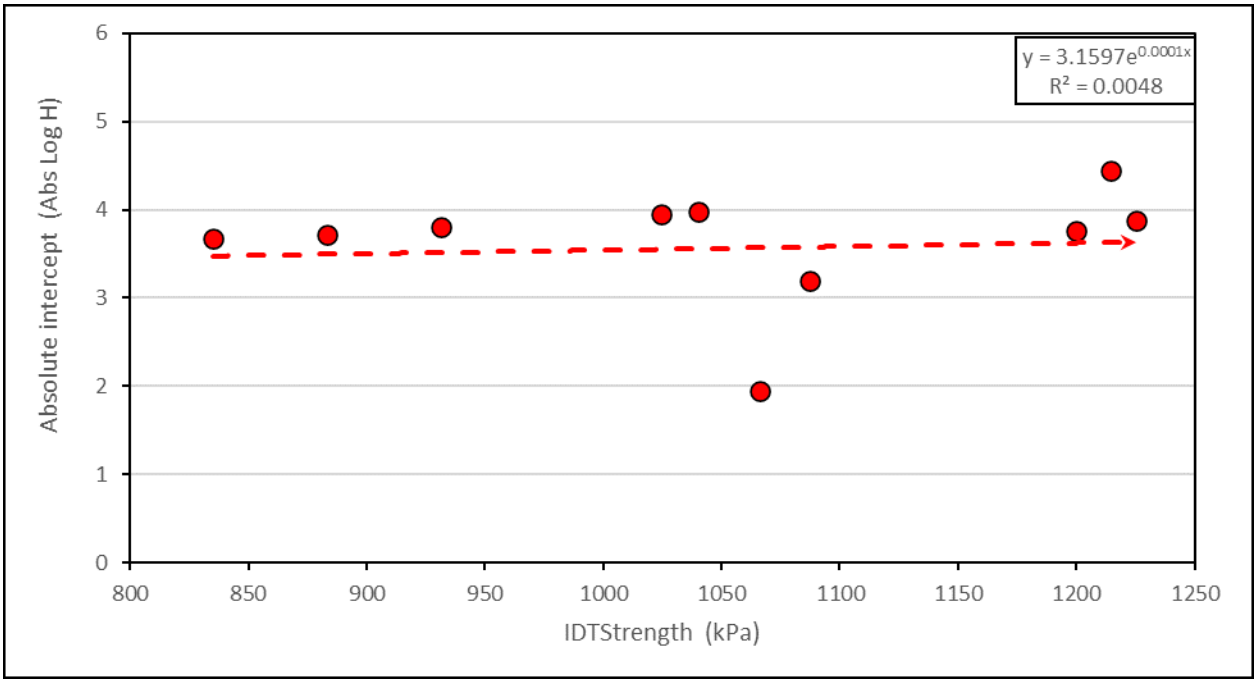

Figure 174 Correlation between $IDT_{Strength}$ and Abs (log *H*) Parameter

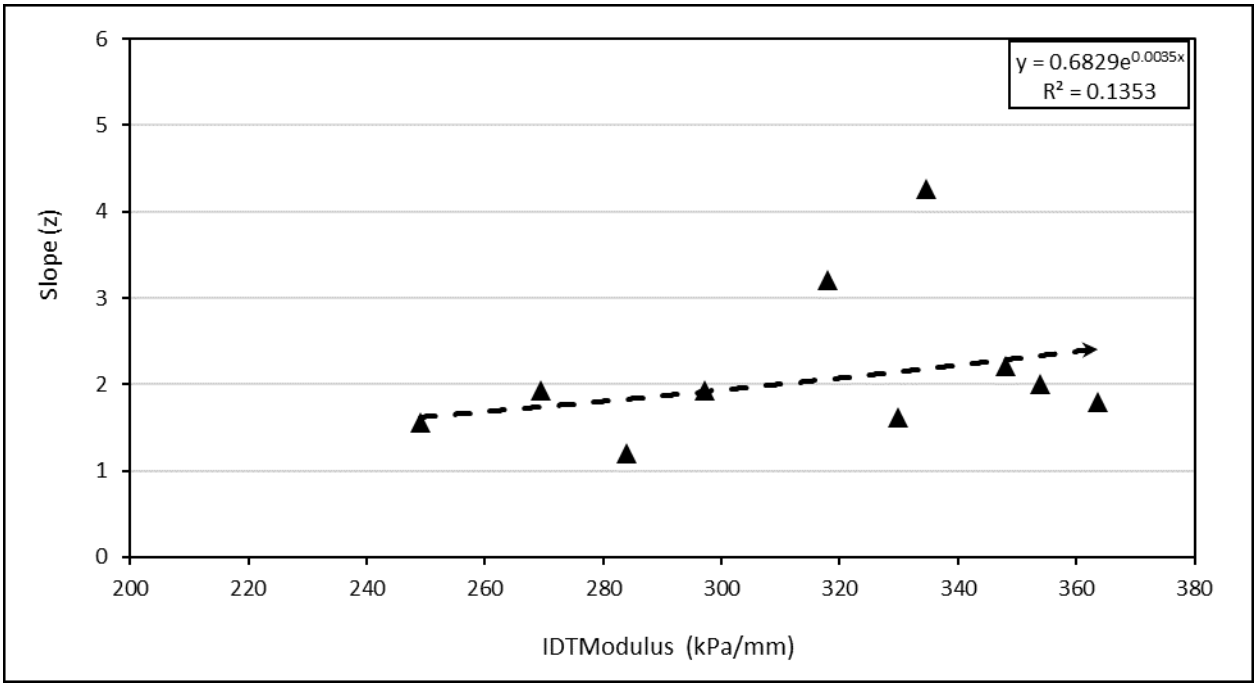

Figure 175 Correlation between $IDT_{Modulus}$ and the Slope (*z*) Parameter

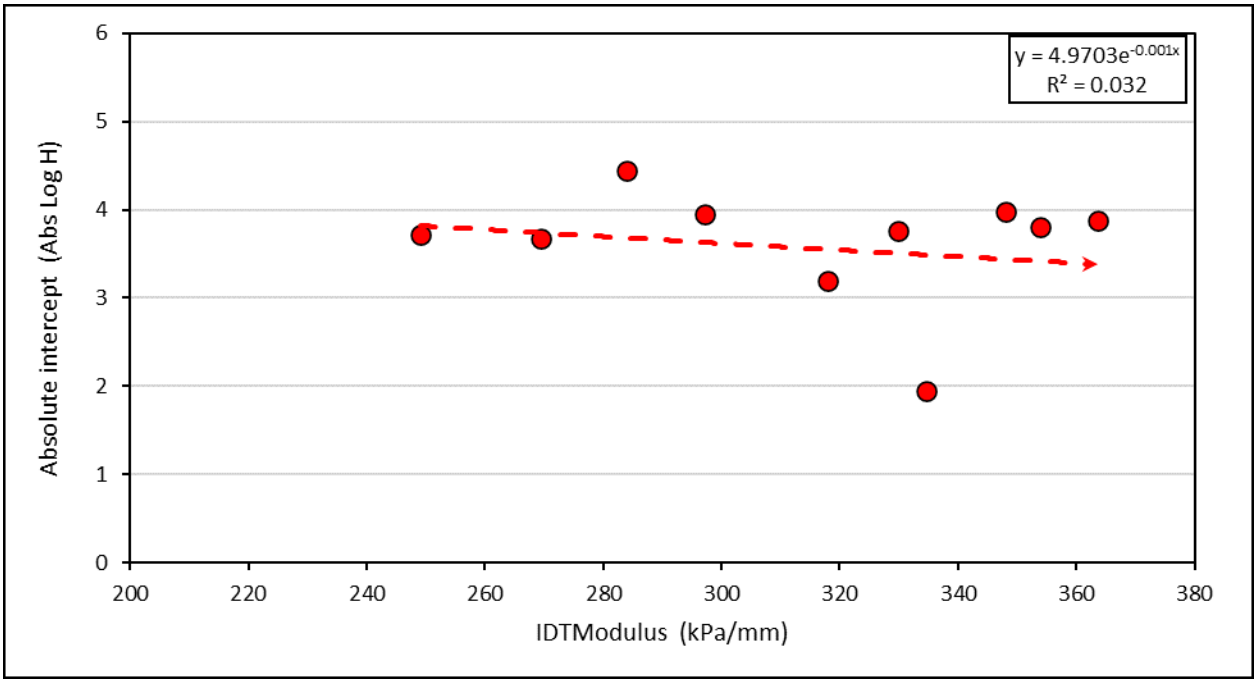

Figure 176 Correlation between $IDT_{Modulus}$ and Abs (log *H*) Parameter

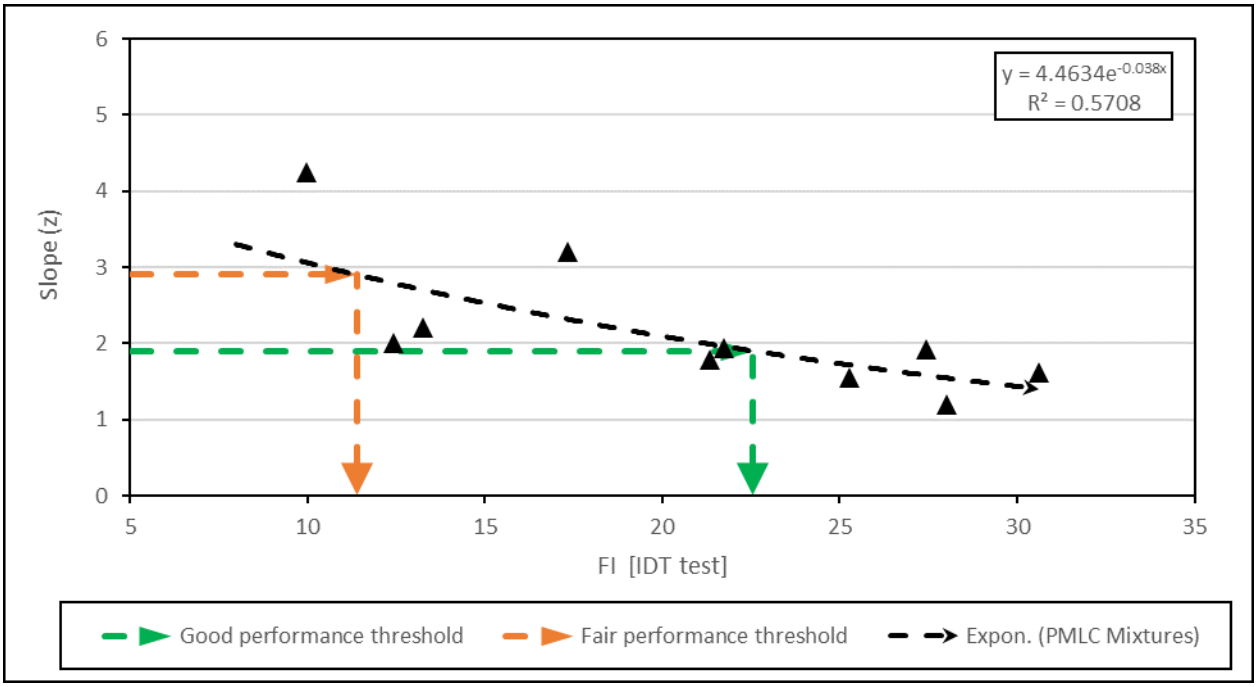

Figure 177 Correlation between FI [IDT test] and the Slope (*z*) Parameter

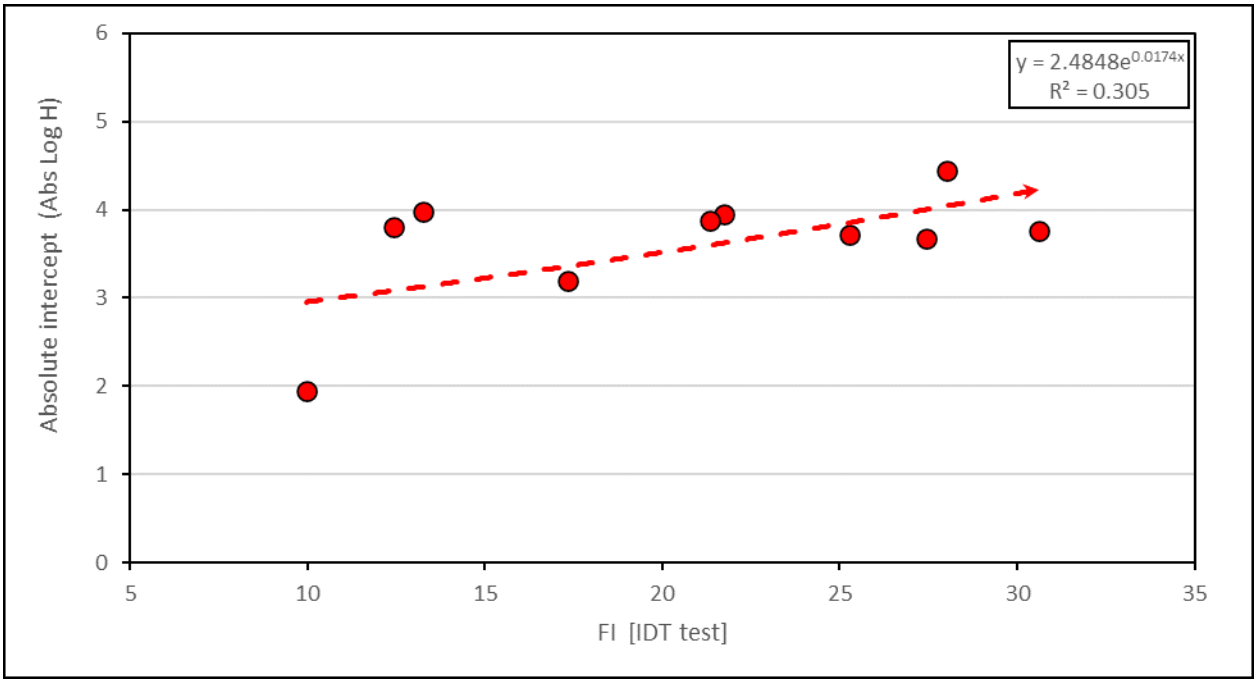

Figure 178 Correlation between FI [IDT test] and Abs (log *H*) Parameter

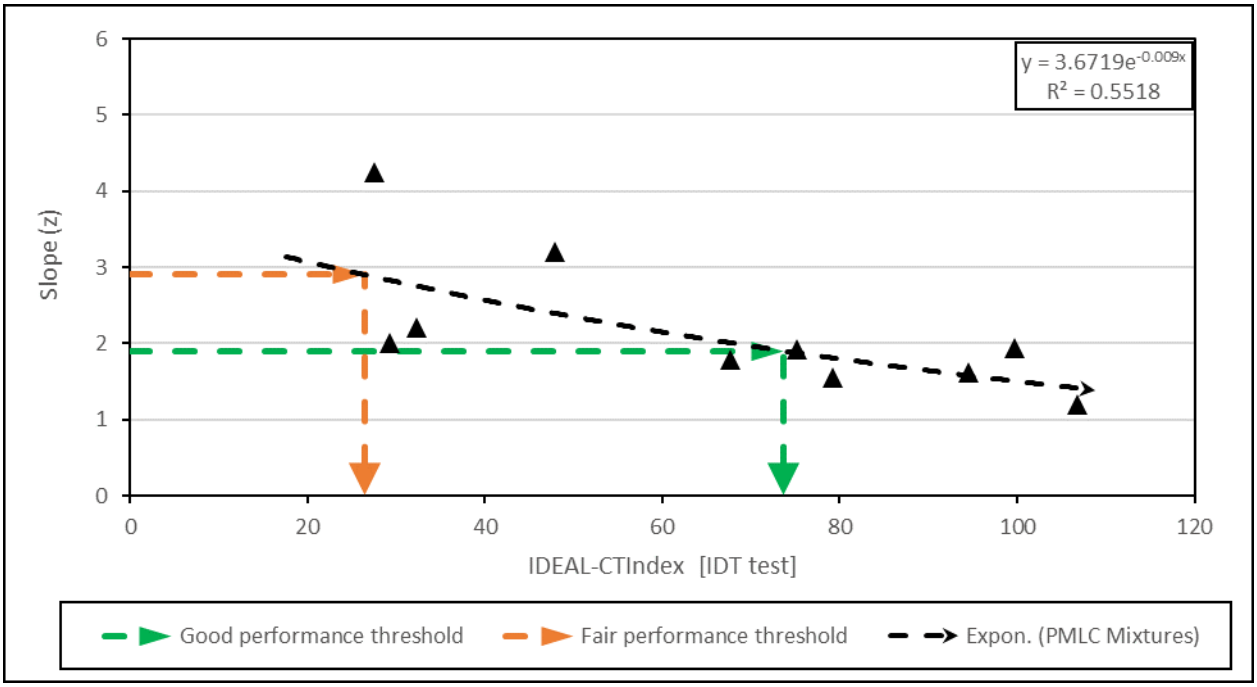

Figure 179 Correlation between IDEAL-CT$_{Index}$ [IDT test] and the Slope (*z*) Parameter

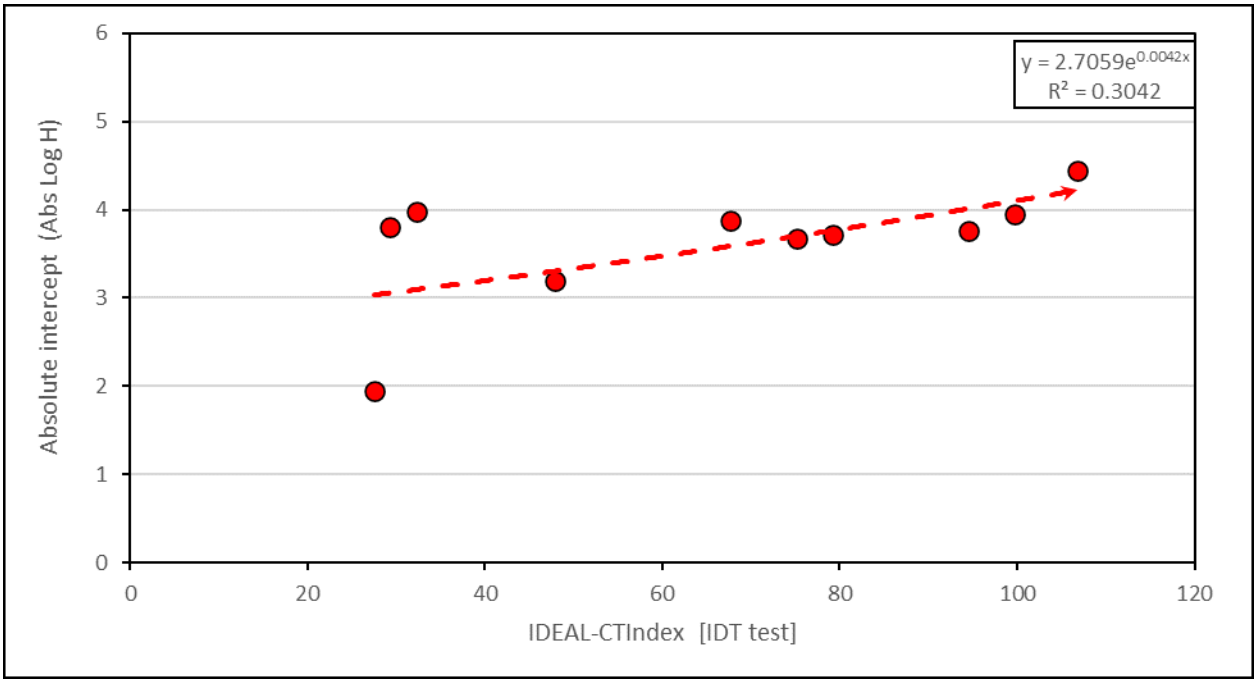

Figure 180 Correlation between IDEAL-CT$_{Index}$ (IDT test) and Abs (log *H*) Parameter

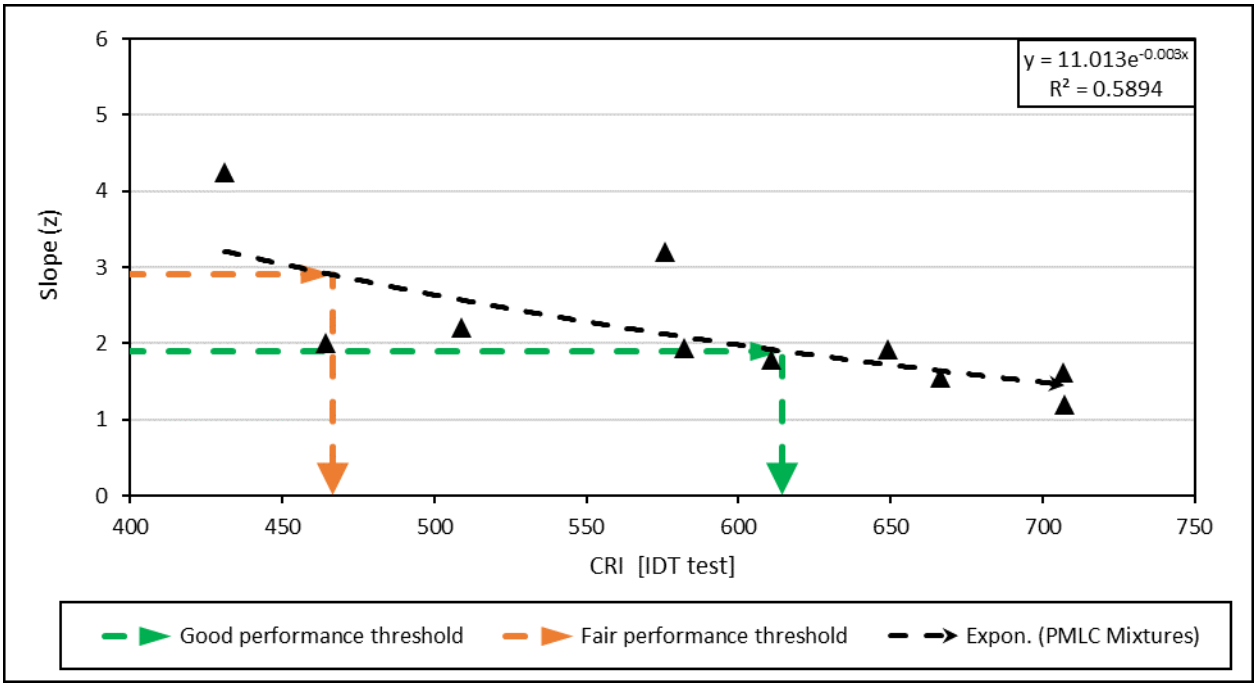

Figure 181 Correlation between CRI (IDT test) and the Slope (*z*) Parameter

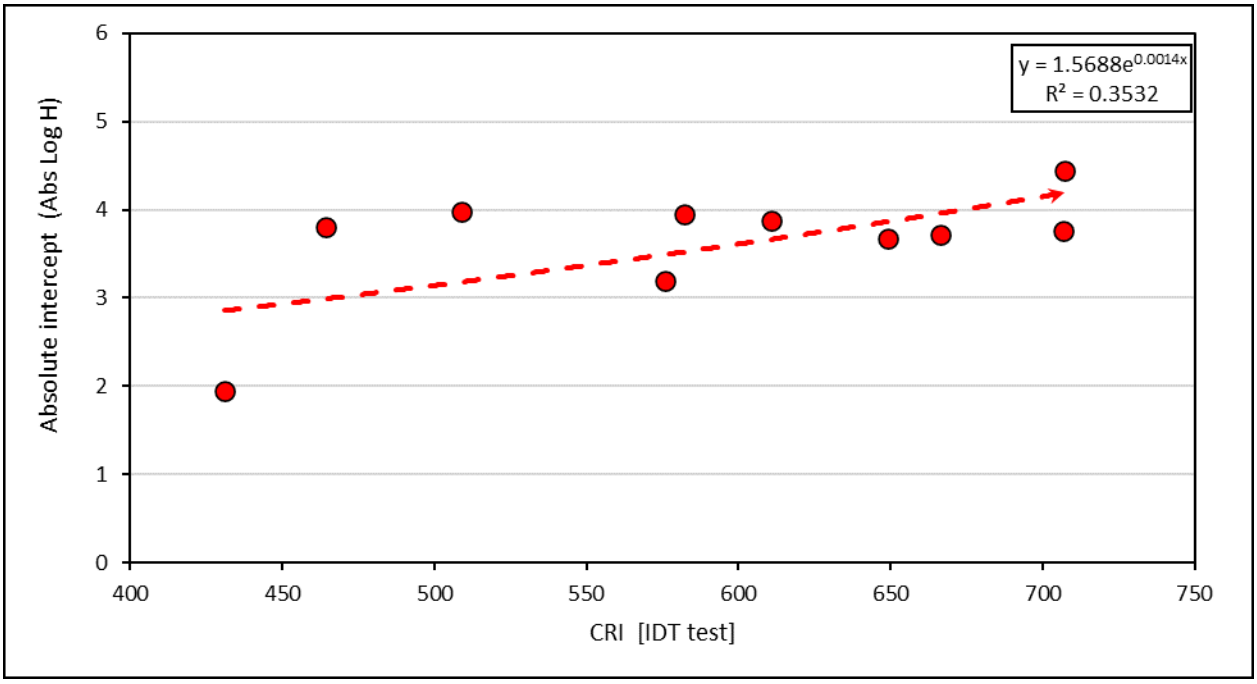

Figure 182 Correlation between CRI (IDT test) and Abs (log *H*) Parameter

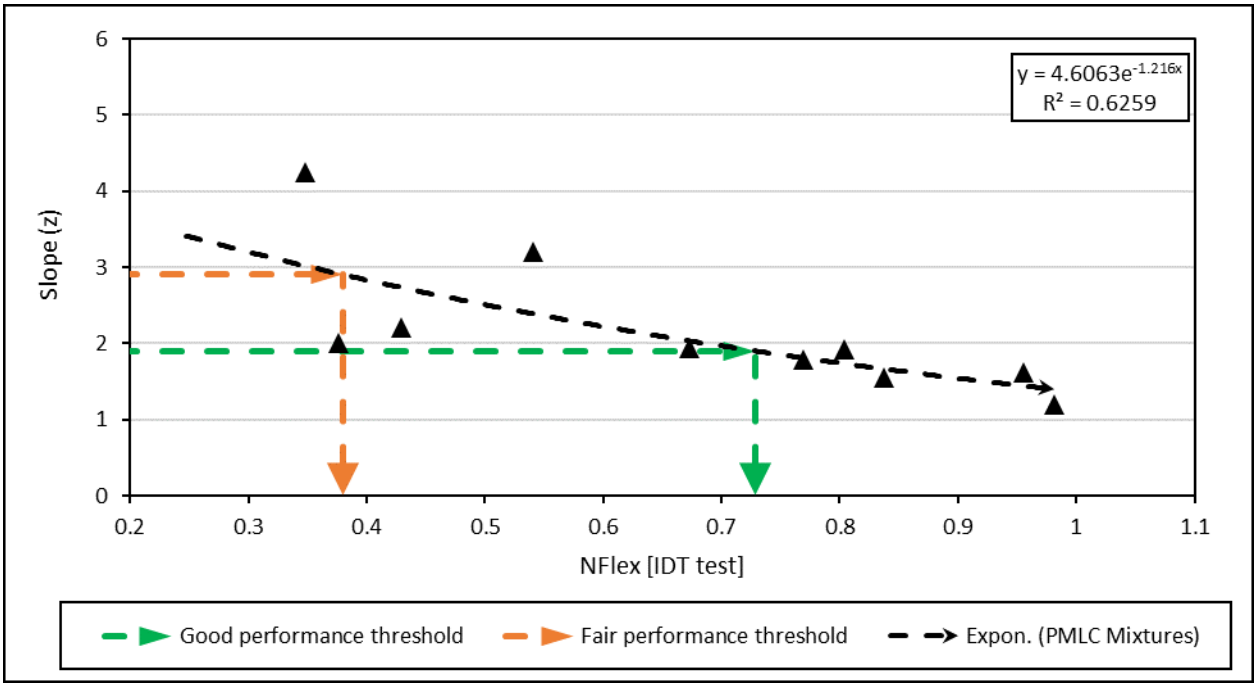

Figure 183 Correlation between NFlex (IDT test) and the Slope (*z*) Parameter

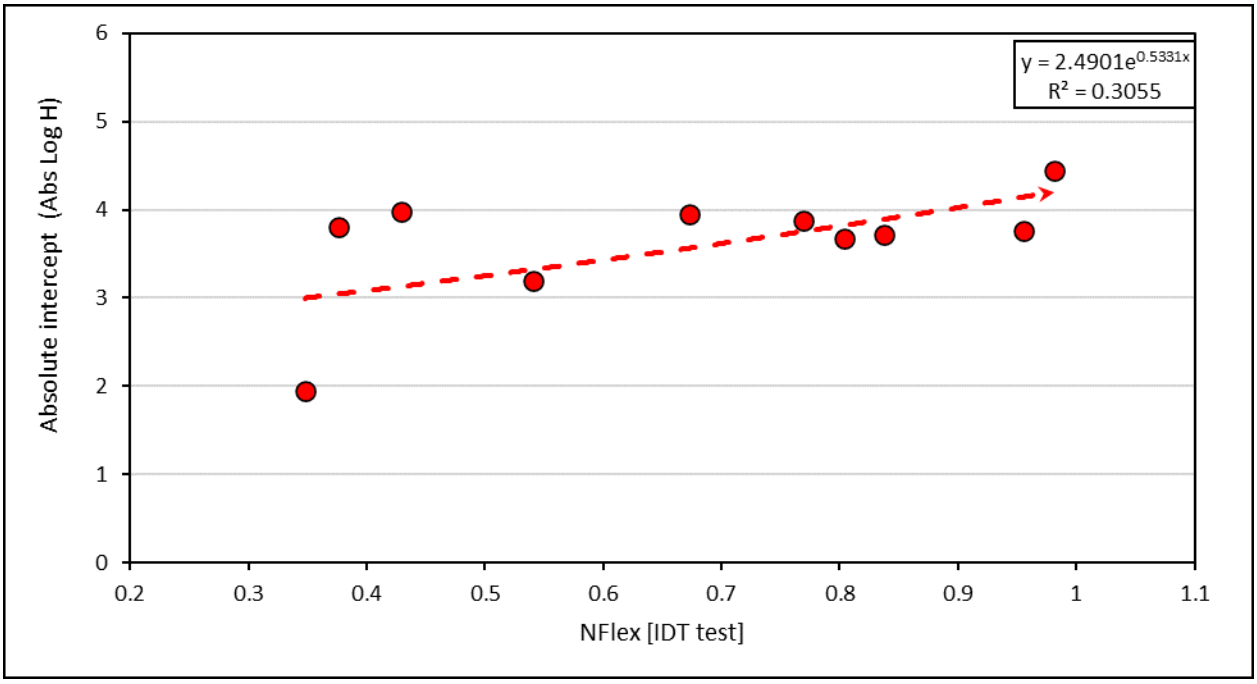

Figure 184 Correlation between NFlex (IDT test) and Abs (log *H*) Parameter

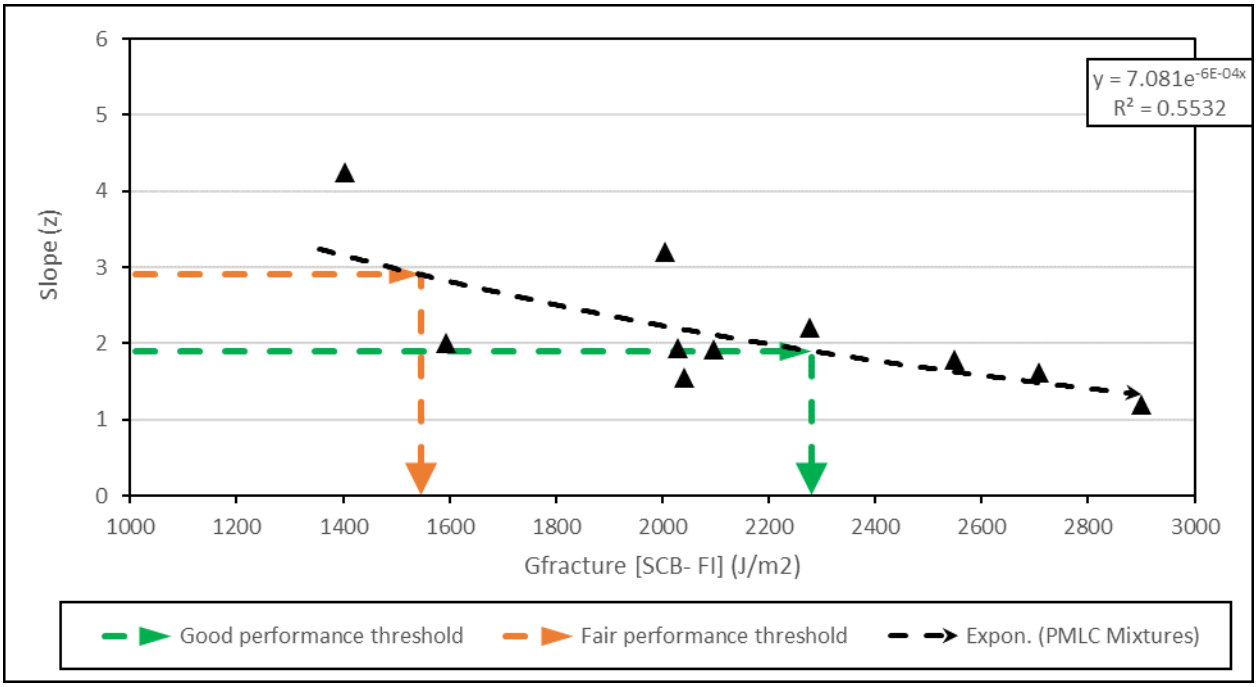

Figure 185 Correlation between $G_{fracture}$ (SCB- FI) and the Slope (*z*) Parameter

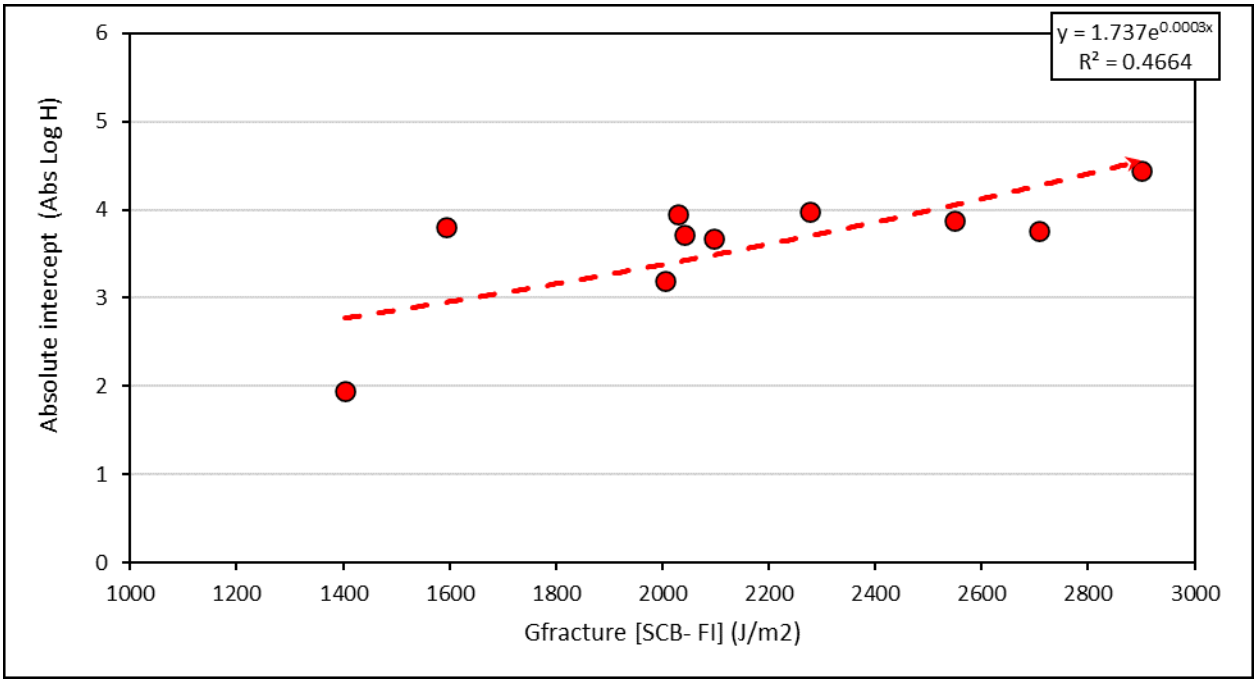

Figure 186 Correlation between $G_{fracture}$ (SCB- FI) and Abs (log *H*) Parameter

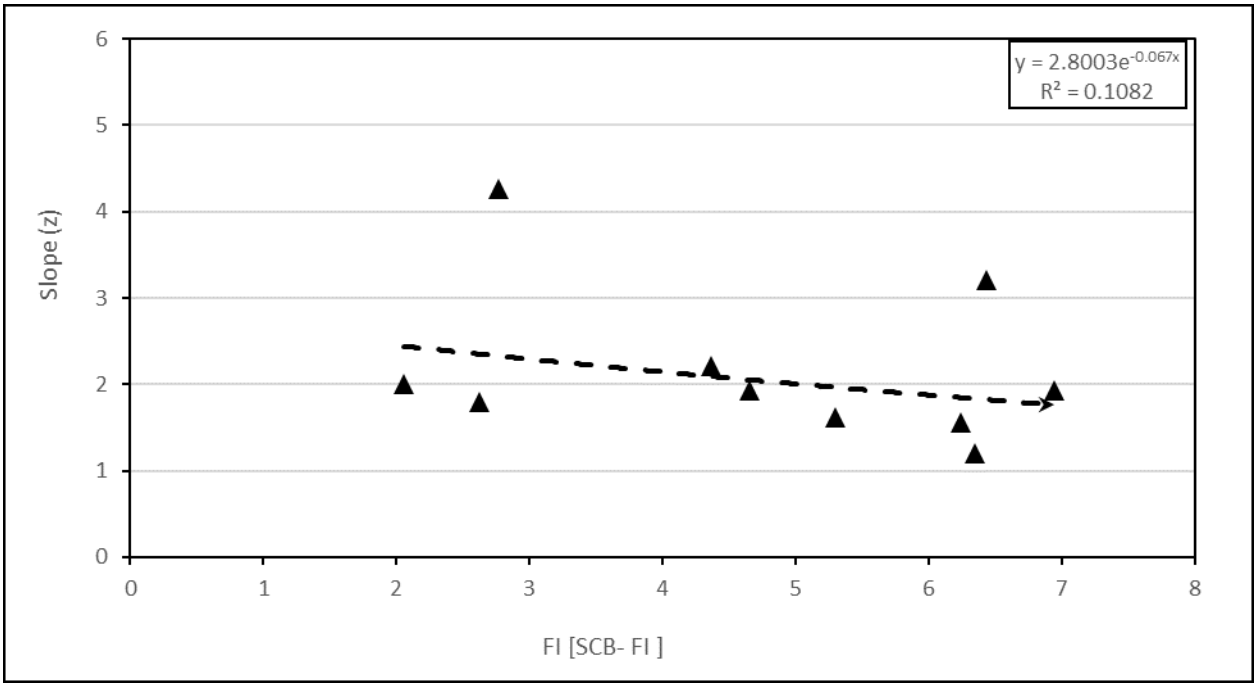

Figure 187 Correlation between FI (SCB- FI) and the Slope (*z*) Parameter

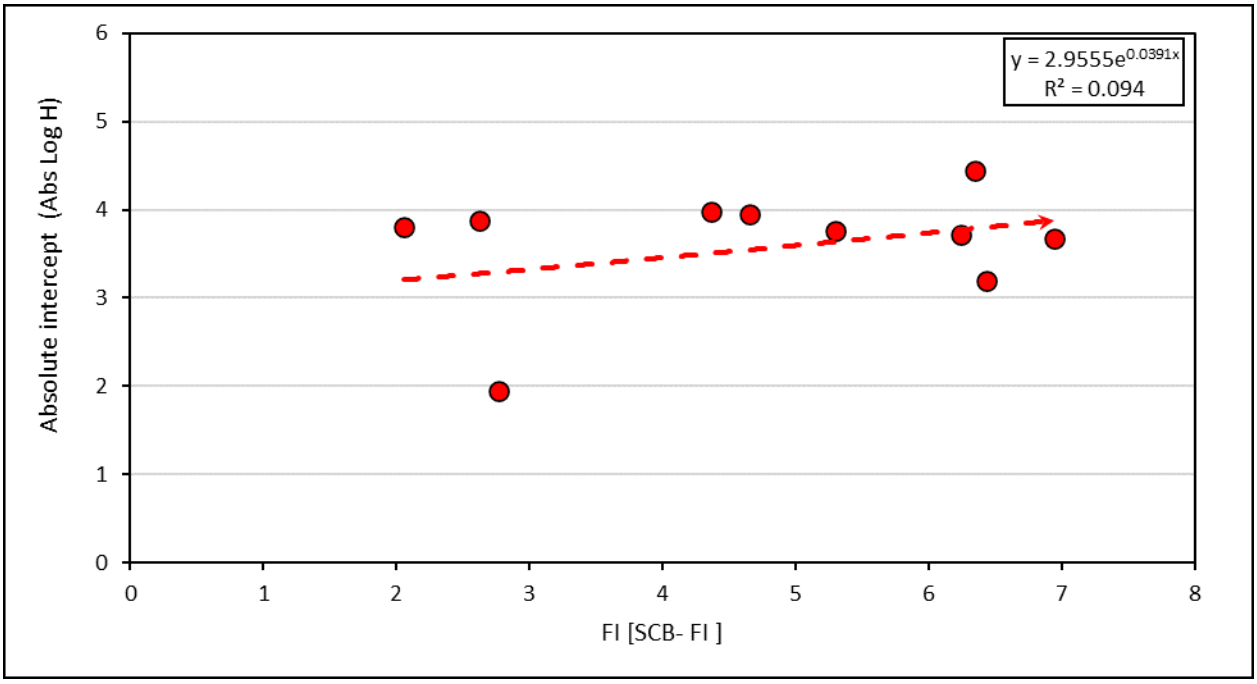

Figure 188 Correlation between FI (SCB- FI) and Abs (log *H*) Parameter

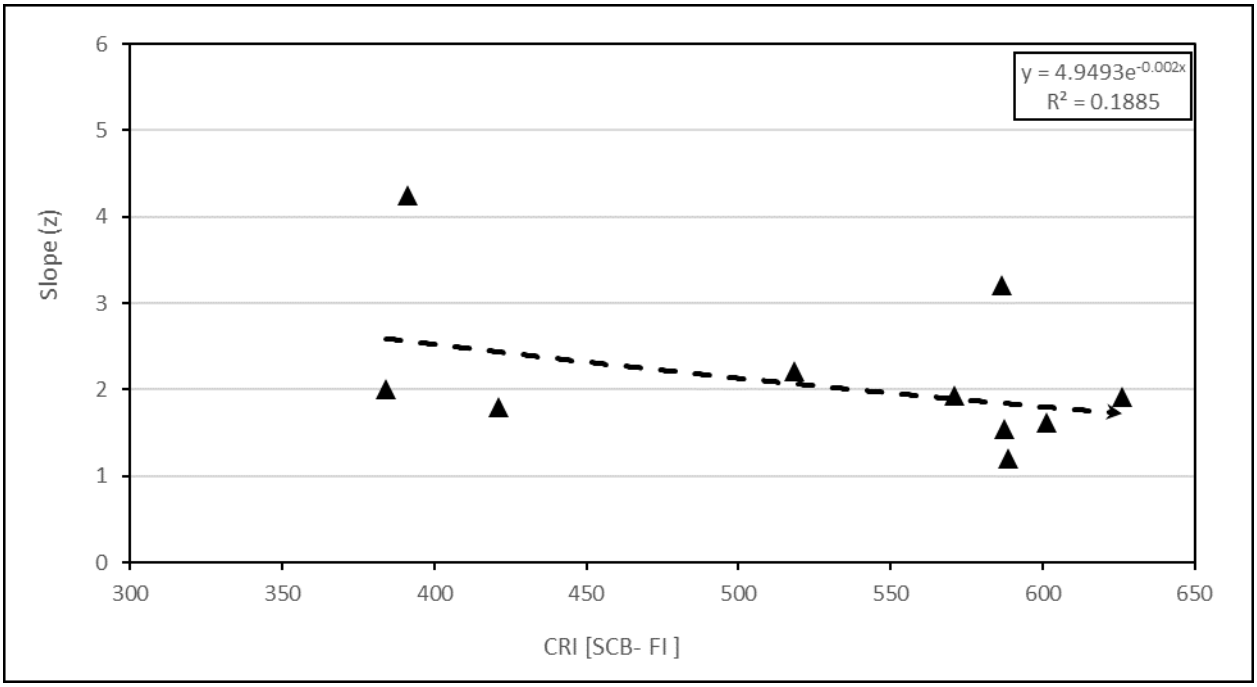

Figure 189 Correlation between CRI (SCB- FI) and the Slope (*z*) Parameter

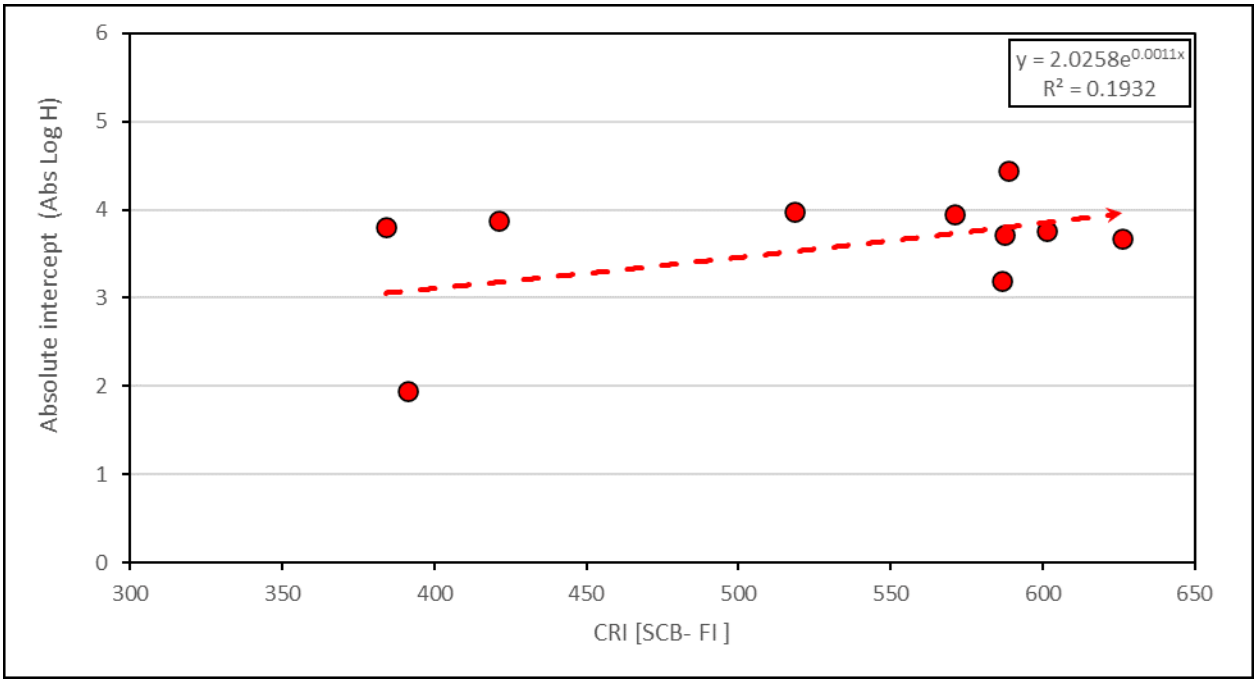

Figure 190 Correlation between CRI (SCB- FI) and Abs (log *H*) Parameter

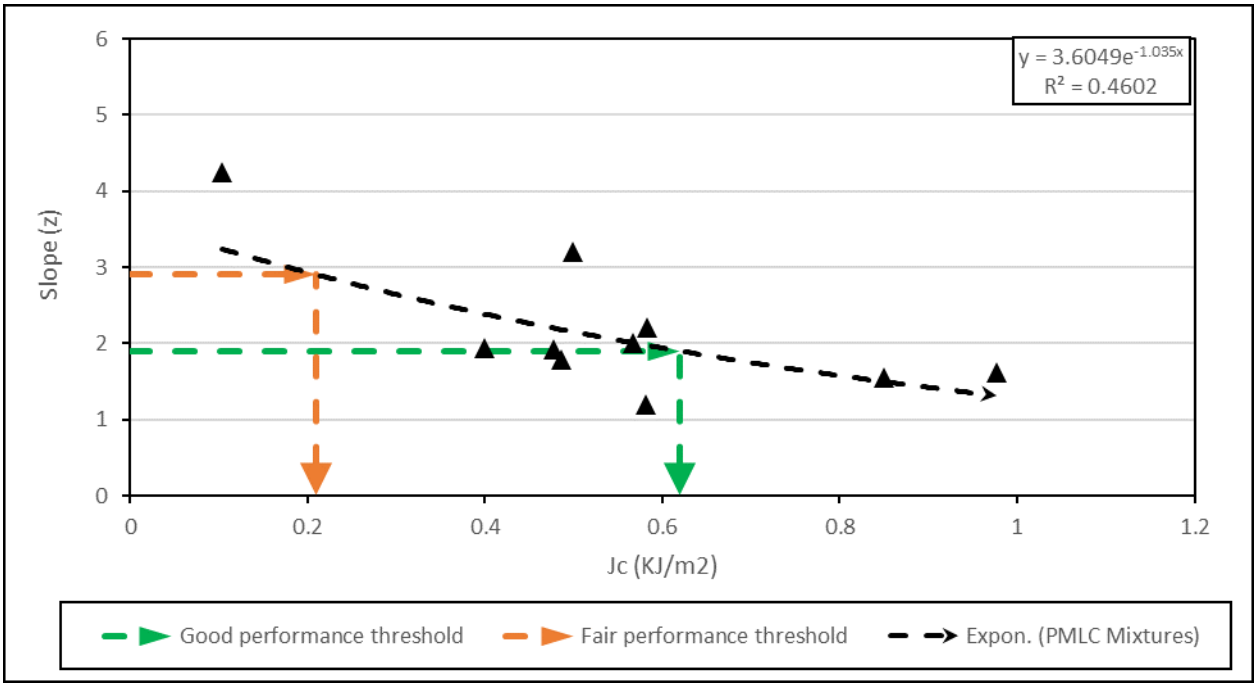

Figure 191 Correlation between J_c and the Slope (*z*) Parameter

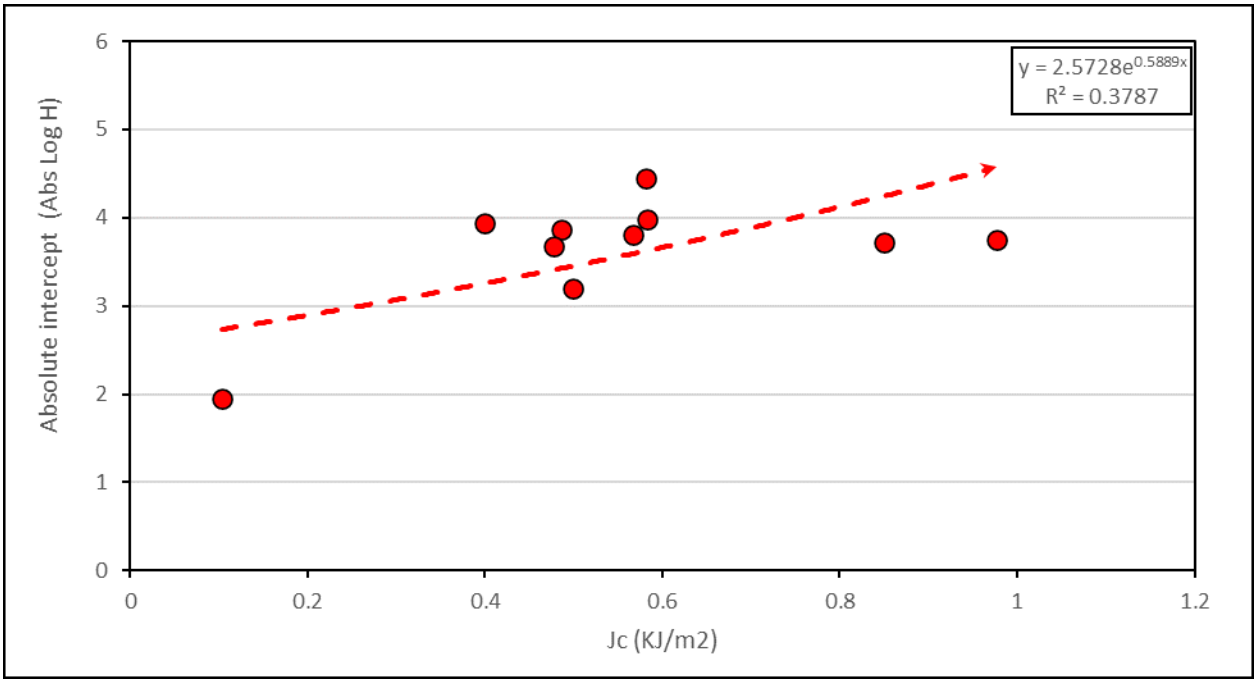

Figure 192 Correlation between J_c and Abs (log *H*) Parameter

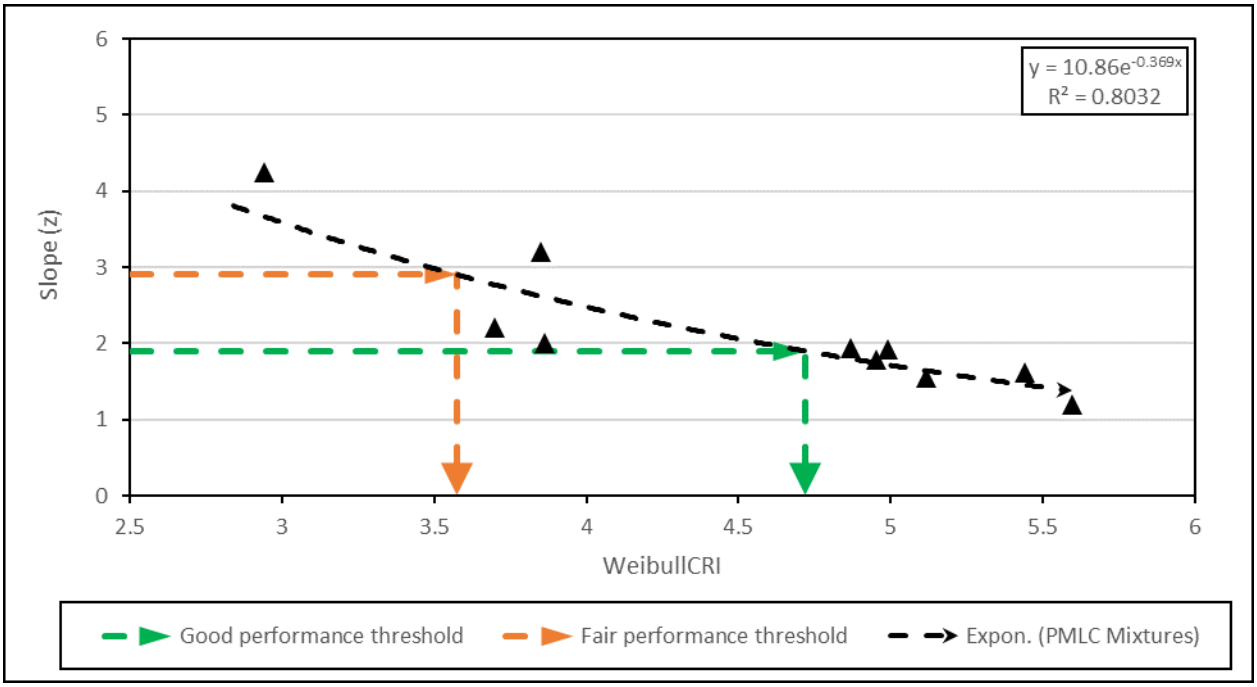

Figure 193 Correlation between Weibull$_{CRI}$ and the Slope (*z*) Parameter

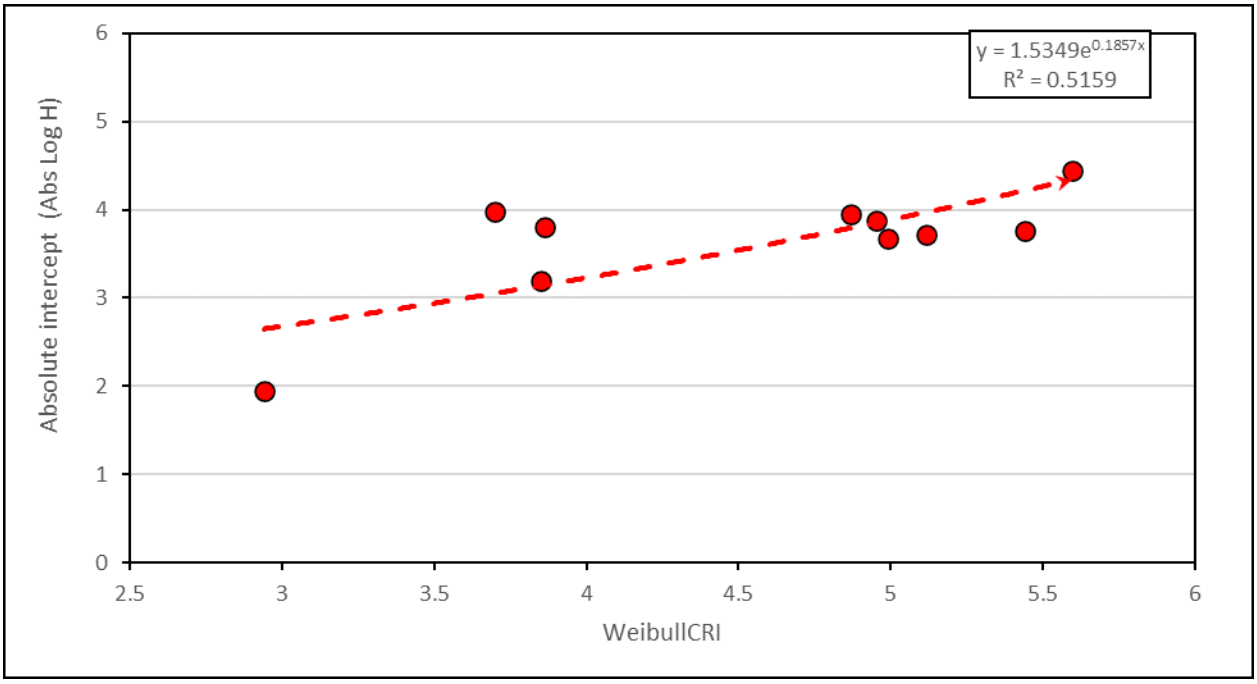

Figure 194 Correlation between Weibull$_{CRI}$ and Abs (log *H*) Parameter